COMPUTATION OF OPEN-CHANNEL DISCONTINUOUS FLOWS USING THE MODIFIED GODUNOV METHOD

by

Ljubodrag Savic

An Abstract

Of a thesis submitted in partial fulfillment
of the requirements for the Doctor of
Philosophy degree in Civil and Environmental Engineering
in the Graduate College of
The University of Iowa

May 1991

Thesis supervisor: Professor Forrest M. Holly, Jr

ABSTRACT

In this work the Godunov method, modified by Colella and Woodward for gas-dynamics discontinuous flows, is adapted to discontinuous open-channel flow problems, in particular to instantaneous dambreaks. Some of the most commonly used numerical methods for discontinuous problems are reviewed, showing the need for a new type of algorithm which would be able to cope efficiently with mixed flow regimes and very strong shocks in non-prismatic channels.

The proposed Godunov method is introduced through application to two scalar problems: the linear advection equation and Burgers' equation. The one-dimensional open-channel flow equations (the de St.Venant equations) are then solved with two variants of the Godunov method: one based on linear interpolation, the other on Colella and Woodward's piecewise parabolic interpolation (PPM). The latter approach is first applied to open-channel flow problems in this work. To evaluate the utility of the proposed Godunov methods (linear and PPM) comparisons with the analytical solution, the shock-fitting method of characteristics, the Preissmann, Lax-Wendroff and MacCormack methods are presented. Both Godunov methods agree well with the

analytical solutions, and perform significantly better then the other compared methods, in solving discontinuous problems.

Guidance for generalization of the Godunov method to two-dimensional open-channel flow problems is also presented, as well as some suggestions for the possible future applications of the one-dimensional algorithm in an industrial code.

Abstract approved: Forrest M. Holly Jr.
Thesis supervisor

Prof. of Civil and Env. Engr.
Title and department

5 Feb 1991
Date

COMPUTATION OF OPEN-CHANNEL DISCONTINUOUS FLOWS USING THE MODIFIED GODUNOV METHOD

by

Ljubodrag Savic

A thesis submitted in partial fulfillment
of the requirements for the Doctor of
Philosophy degree in Civil and Environmental Engineering
in the Graduate College of
The University of Iowa

May 1991

Thesis supervisor: Professor Forrest M. Holly, Jr

Graduate College
The University of Iowa
Iowa City, Iowa

CERTIFICATE OF APPROVAL

PH.D. THESIS

This is to certify that the Ph.D. thesis of

Ljubodrag Savic

has been approved by the Examining Committee for the thesis requirement for the Doctor of Philosophy degree in Civil and Environmental Engineering at the May 1991 graduation.

Thesis committee: Jowt M. Holly Jr.
Thesis supervisor

Member

Member

Member

Member

TABLE OF CONTENTS

LIST OF FIGURES

CHAPTER I. INTRODUCTION

I.1 Discontinuous flows in hydraulic practice

Flows with discontinuities are often encountered in hydraulic practice. The most common of such flows is certainly the hydraulic jump, a more-or-less stationary roller of water through which the change from supercritical to subcritical flow occurs. A discontinuity of the flow variables (depths and velocities) occurs between the two sections separated by the jump.

In addition to a stationary hydraulic jump in steady flow, there are also unsteady flows which are characterized by discontinuities of the same type. The difference is that now the discontinuity is moving through the channel and is constantly changing as a result of the evolution of the forces acting upon it. The phenomenon is known as a moving hydraulic jump, a surge, a shock or a bore. Flows with moving jumps occur in some operations of hydropower canals, in tidal flows, in flows resulting from the collapse of a dam, and in other flows where sudden increase of depth and/or discharge (or sudden decrease of discharge) is likely to occur.

Accurate prediction of the flow variables in all of

these cases is of great importance. In designing a hydropower channel, one needs to know the maximum depth of water at the sections for all possible operating conditions of the plant. (Spillage over the levees may not only flood the protected area, but also damage the canal itself.)

Dam failures, though not common events, are by no means impossible. The consequences of such disasters are not only huge material damage, but the loss of human lives. There are two means of protection from such catastrophes: first to increase and enhance the maintenance of dams and spillways, second to predict accurately the area endangered by the possible failure, and to develop a system of efficient alarm and evacuation of the population in an emergency.

In all these flows, the most important quantities needed for design/prediction are maximum depths, and the time of their occurrence, along the waterway.

I.2 Current state-of-the-art

For unsteady flows without discontinuities reliable methods exist for computing the temporal and spatial evolution of the flow variables. Usually, the one-dimensional (de St. Venant) or, if needed, the two-dimensional partial-differential equations, based on the mass and momentum (or energy) conservation laws are used for the mathematical description of the flow. But these

differential equations suppose that the variables are continuous, and such an assumption fails in the case of flows with moving hydraulic jumps, i.e., for discontinuous flows. Here an integral approach should be exploited as an appropriate mathematical representation obviating the problems of discontinuities. It has been proven by Lax(1954) that the differential equations derived directly from the integral form preserve the properties of discontinuous flows (so called weak solutions). This form of the differential equations is commonly called the conservative (or divergent) form, due to its ability to conserve mass and momentum. Unfortunately, the theory can be strictly applied only to the homogeneous set of equations, i.e. for the idealized case of a frictionless flow in a prismatic horizontal channel. Nevertheless, real discontinuous flows in natural channels, described by the full (non-homogeneous) equations, are also treated in practice (more or less successfully) by the conservative differential equations. Such an approach, commonly called the "through" approach, is one way of dealing with discontinuous flows. Its disadvantage is that one cannot totally rely on the results of the computations, due to the above-mentioned violation of the assumption of homogeneous equations. Also, one cannot expect to be able to obtain a good resolution of the discontinuity (shock) itself, though

this is usually not important for practical purposes. If a non-conservative scheme is used for discontinuous flows the results are completely unreliable; mass and momentum are not preserved, and the numerical loss of mass may well exceed 50 %.

The other commonly used approach in dealing with discontinuous flows is the shock-fitting method, whereby the discontinuity (shock) is isolated from the rest of the flow domain, and handled separately by an integral approach. The flow outside of the shock is treated with the usual differential equations (either conservative or non-conservative). The shock-fitting method is a theoretically correct way of dealing with shocks. In practical applications, however, large difficulties arise in tracking the shocks, especially in natural channels where, due to irregular topography, one can expect a large number of shocks surging and reflecting, both upstream and downstream.

Finally, methods based on simplified equations of motion - so called hydrological methods - are also used. In such approaches, inertial terms are neglected (sometimes the depth gradient also is omitted). For highly unsteady flows, such as those resulting from an instantaneous dambreak, or a shutdown of hydropower plant turbines, the inertial terms are very important and must be included to obtain a correct solution.

The consequence of the above-mentioned issues is that at the present time all available methods used in industrial codes for computing discontinuous flows are either unreliable and overly sensitive to changes of the cross-sections and occurrence of mixed sub/supercritical flow regimes, or very difficult to implement for practical applications.

I.3 Statement of purpose and overview of investigation

The need exists for a new type of algorithm which should be based on highly conservative schemes, have the capability of dealing with discontinuities and mixed regimes, and at the same time be robust and not so elaborate as to exclude implementation for real-world problems.

One possible candidate for a new algorithm is the Godunov scheme. Its main advantage is its conservative property. The Godunov method was first introduced in 1959 and applied in aerodynamics (see Godunov,1959). Some applications have been made in computational hydraulics, but they were not generally satisfactory. It has been in gas dynamics that Godunov's method, modified by Van-Leer, Colella and Woodward, and other authors, has been successfully applied since about 1980. Particularly effective implementations have been reported for the computation of shocks (discontinuities).

The objective of the present work is to analyze the possibility of application of the modified Godunov method to computational hydraulics problems, in particular to flows with discontinuities. The main goal is to asses the capability of the scheme for coping with the problems of one-dimensional flow in non-prismatic channels, and hence to provide a basis for possible further development of an algorithm capable of being incorporated in industrial codes which would be used for computations of flows with strong shocks, especially for dam-break flows. A secondary goal is to get some insight into, and experience with, the scheme for possible further two-dimensional generalization.

A literature review, presented in chapter II, surveys and evaluates state-of-the-art methods for open-channel discontinuous flows, thus showing the need for an investigation of a new method. Then follows a brief presentation of the modified Godunov method, which is successfully used for gas-dynamics discontinuous flows, and therefore is proposed in the present work for application to open-channel flow.

In chapter III, the modified Godunov scheme is applied to the one-dimensional linear advection equation as a test, or model, equation because of its simplicity in an analytical sense, so that the results can easily be verified and interpreted. Subsequently, in the same chapter III,

Burgers' equation is solved as an appropriate, but simplified, model of the nonlinear flow equations.

In chapters IV and V the full de St. Venant one-dimensional equations are dealt with; first in homogeneous, and then non-homogenous, form. The algorithm is developed in chapter IV, and the tests and interpretation of the results are given in chapter V. These chapters contain the original contributions of this work to the solution of discontinuous open-channel flow problems.

Guidance for generalization of the Godunov method to two-dimensional free-surface problems is presented in chapter VI.

Finally, in chapter VII conclusions, and the most important results of this work, are summarized.

I.4 Criteria for assessing the quality of simulation

Objective quantitative evaluation of the quality of solution is difficult in computational hydraulics. The only important aspect of the solution which can be (and usually is) explicitly quantified is the mass-conservation error. (It is defined as a ratio of the total error in the mass conservation equation (computed for the entire computational reach and the entire computational time) and the initial mass of water for the entire reach.) The computational time and memory requirements can be compared quantitatively,

also. However, these latter comparisons are not entirely appropriate for the present work, since the effort was not directed to produce an efficient code, but to explore a new scheme which may be applied industrially in the future.

Visual examination and comparison are most commonly used in computational hydraulics to judge the quality of simulated results as one aspect of the performance of the investigated schemes. The amplitude ratio between the numerical and analytical solution (concentration, depths, velocities, etc.) is one of the indicators which can be expressed quantitatively, but in most cases there is no analytical solution to compare with. Comparison between alternative numerical solutions can be done, but one must be alert to the extent of reliability of such a comparison (i.e. none of the solutions may be correct). The comparison of wave speeds can be even more difficult to quantify, since determining the wavespeed of the front, in case of a numerical method which diffuses the wave front over several computational points, is a very delicate and subjective procedure.

The important features of the solution that suggest good performance of the method, or conversely indicate a problem, are usually not quantified. One observes, for example, that numerical diffusion (or oscillations, overshoots and undershoots etc.) occur, and then tries to

judge if this behavior has a significant influence on reliability of the simulation in a particular application; however, quantitative evaluation of these phenomena is seldom performed. As a rough measure of preservation (or smearing) of the steep front resolution for discontinuous flows, one can use the number of spatial steps within which the steep front is confined at the end of the computation; however, this is also subjective, since one has to define how steep the front should be without recourse to an analytical solution.

Therefore, in this work quantitative comparisons of amplitude are provided when the analytical solution is available, and in some cases between numerical solutions when such a comparison seems to provide significant and reliable information. The resolution of the front is evaluated comparing the solution of the considered method with the analytical one, where it exists (or with the shock-fitting method of characteristics for the de St.Venant equations). For all cases the relative mass conservation error is the only reliable quantitative indication of the behavior of the numerical solution.

CHAPTER II. REVIEW OF LITERATURE

II.1 Physical description of the phenomenon

Unsteady flow in open channels is characterized by the constant temporal and spatial evolution of the flow variables. Density is considered constant in such flows, so the variables are the properties that describe the quantity of water (such as the depth, area, or water surface elevation) and its motion (the velocity or the discharge). Those variables may have so-called discontinuities in some of the flow regions, while they are continuous for the rest of the flow domain. These "discontinuities" are not real physical discontinuities, but the rate of change of flow variables over the "discontinuous" regions is orders of magnitudes greater than in the regions of continuous flow. The terms "discontinuous flows" and "shocks" come from the analogy with gas-dynamics shock phenomena (Stoker,1957; Terzidis and Strelkoff,1970).

Discontinuities are not exclusively characteristics of unsteady flows. They are the moving counterparts of their steady-flow relative - the well known hydraulic jump (Henderson, 1966). The discontinuity is characterized by a fairly rapid change of the flow properties (depths and

velocities) over a very short region. The transition occurs within the roller comprising huge, powerful eddies, where considerable energy is dissipated. The roller might be absent in cases of very small discontinuities when weak, so-called undular, jumps form. A thorough survey of hydraulic jumps from both theoretical and practical points of view is given by Peterka, (1964).

In unsteady flow, discontinuities (shocks) usually form as a result of the successive superposition of elementary positive waves, as described by Stoker (1957) and Henderson (1966). A positive elementary wave is one in which the depth increases in the direction of the wave propagation. As the celerity of the wave is proportional to its depth (see Stoker,1957), the disturbances (waves) of larger depth will eventually overtake those initiated earlier (and accordingly having smaller depths and celerities). The result is a formation of an initially steep front, which grows in height by the arrival of successive waves, and finally curls over and breaks forming the turbulent roller of a hydraulic jump. The effect of resistance, however, may postpone, or even make impossible, the formation of shocks initiated as a result of superposition of small waves (Henderson,1966), and also diffuse those created by a sudden increase of depth and/or discharge (for example dam-break waves).

Another aspect of dam-break flow is the possibility of a dry bed, where the trough downstream of the surge is empty. This situation might arise in some applications, and is an especially delicate one for numerical modelling.

II.2 Mathematical models for open-channel flow

To obtain any kind of prediction of the flow variables one needs to apply appropriate physical laws, and to put them into quantitative--mathematical form, describing the relationships among the variables in question. Fluid flow is described by conservation laws applied to the mass of fluid in a fixed or moving control volume: the conservation of mass, momentum and energy. The equations which precisely describe those laws are available in the literature (Hajdin,1977; or Sclichting,1979).

Analytical solution of the full equations is possible only for a few idealized cases (see White,1974), and at this time even numerical solutions of the full equations are practically feasible only for a very narrow range of real-life problems. Consequently, one must limit oneself to a less comprehensive set of equations, yet one which provides a sufficiently accurate description of flow, and therefore permits a good prediction of the relevant variables. The usual simplifications of the full flow equations comprise neglecting minor influences (such as surface tension effects

and the variation in density of water in flood propagation), and averaging the variables and their products in time and/or space.

In current hydraulic practice for open-channel flow computations, the most common mathematical models are based on a one-dimensional flow approximation (the de St.Venant equations), though the two-dimensional approach is being increasingly exploited due to the rapid development of computational facilities, and the greater demand for more accurate flow predictions (Strelkoff,1989). These models are often called dynamic models. In addition, so-called hydrological models, which utilize a simplified momentum (or energy) equation, are used. In a one-dimensional approach the depth and velocity are averaged over the cross section. The flow is considered to be in one direction, so there are no velocity components in the directions normal to the flow (vertically and laterally). In a two-dimensional approach averaging is done over the depth only, allowing for variations along the width of the cross-section; the velocity is expressed by two vector components, both being in the plane of flow.

The velocity component in the vertical direction, and consequently the possibility of a non-hydrostatic pressure distribution, are neglected in both approaches. In a flow region where a hydraulic jump occurs (moving or stationary),

huge vertical accelerations result, and the pressure distribution is certainly not hydrostatic. On the other hand a discontinuity (jump) occurs over a short region of the flow, and can be successfully treated by the use of a momentum approach, provided that the boundary sections of the control volume are far enough from the discontinuity to permit the assumption of a hydrostatic pressure distribution. The computational consequence is that, although there is no real physical discontinuity of flow in the jump, the mathematical description treats it as a discontinuity in flow variables. Another situation in which an extremely non-hydrostatic pressure distribution occurs is for the dam-break problem at the instant of the removal of the dam (Strelkoff,1989; Basco,1989). Numerical solution of the equations which take into account the vertical acceleration (so-called Boussinesq equations) shows that the duration of non-hydrostatic pressure conditions is short, so that for practical applications, it does not need to be taken into account (see Basco,1989).

In addition to the assumption of hydrostatic pressure distribution, assumptions of the validity of the steady-flow resistance evaluation for unsteady conditions, and small bed slopes (so that the cosine of the angle between the bed and the horizontal plane can be taken as a unity) for both one- and two-dimensional dynamic models are applied (see Cunge

et al.,1980; Liggett,1975; and Strelkoff,1969).

II.2.1 Mathematical 1-D models (de St.Venant equations)

First derived by Barre de St.Venant in the nineteenth century, these one-dimensional equations are still the most commonly used mathematical tool for describing unsteady flow problems in open channels. The assumption of one-dimensional flow means that the depth and the velocity are averaged over the whole cross-section, implying that the non-uniformity of the velocity and the depth across the section must not be such as to affect significantly the wave propagation. (For example, the one-dimensional assumption fails for the case of supercritical flow in a sharp bend.) The other important limitation of the one-dimensional approach, which stems from the previous one, is that the rate of change of the cross-sectional area must not be severe. In the case of an abrupt expansion, the main body of flow will not fill the boundaries of the channel and the flow will become essentially two-dimensional.

In the one-dimensional approach, the number of unknown variables reduces to two, since the density is assumed constant, and there is only one component of velocity. The two independent variables must be chosen such that one of them represents the quantity of water at the section (depth, wetted area or water-surface elevation), and the other the

flow motion at the section (the mean velocity or the discharge). To solve for those two variables two equations are needed. One equation is always the mass conservation equation, and the other is either the momentum or energy equation. If the flow variables are continuous, both approaches are appropriate; when discontinuities appear only the momentum principle is valid, since the energy losses in the roller cannot be properly estimated. A rigorous mathematical explanation of this is given by Abbott (1979).

One can obtain the one-dimensional equations by integrating the Reynolds differential equations and introducing appropriate averaging following the one-dimensional flow assumptions (Strelkoff,1969). Another way of deriving the equations is based on an integral approach for a control volume between two cross-sections of the channel (Cunge et al.,1980 and Liggett,1975).
The mass conservation, or continuity, equation is:

$$(2.1): \int_{x_1}^{x_2} [A(x,t_2) - A(x,t_1)]\,dx + \int_{t_1}^{t_2} [Q(x_2,t) - Q(x_1,t)]\,dt = 0,$$

and the momentum, or dynamic equation is:

$$(2.2): \quad \int_{x_1}^{x_2} [Q(x,t_2) - Q(x,t_1)]\,dx +$$

$$+ \int_{t_1}^{t_2} [Q(x_2,t)\,u(x_2,t) - Q(x_1,t)\,u(x_1,t)]\,dt =$$

$$= g\int_{t_1}^{t_2} [I_1(x_1,t) - I_1(x_2,t)]\,dt + g\int_{t_1}^{t_2}\int_{x_1}^{x_2} I_2(x,t)\,dx\,dt +$$

$$+ g\int_{t_1}^{t_2}\int_{x_1}^{x_2} A(x,t)\,[S_o(x) - S_f(x,t)]\,dx\,dt\,,$$

where A is the wetted area, Q is the discharge, g is the gravitational acceleration, I_1 and I_2 are the centroid moment and the rate of its change due to the variation of cross-sectional geometry, So is the bottom slope, and Sf is the friction slope. The first term in the continuity Eq.(2.1) represents the mass accumulation in the control volume, and the second one the net flux of mass out of the volume in an incremental time. An additional term can be included to describe the contribution of lateral inflow. Similarly, the first and the second terms in the dynamic Eq.(2.2) represent the accumulation of momentum in the control volume and its net flux. These are commonly called inertial terms. The right-hand side terms represent the impulse of forces, acting on the control volume, during the incremental time (t^2-t^1). The first term describes the

pressure forces acting on the upstream and downstream boundaries of the control volume, the second one the contour force from the non-prismatic boundary, and the last one the difference between the body force (component of the weight of water along the direction of flow) and friction forces.

After obtaining the equations in integral form, one can use Taylor-series expansion and the mean value theorem to obtain the differential form if the variables are continuous (Wylie,1960):

(2.3): $$\frac{\partial A}{\partial t} + \frac{\partial Q}{\partial x} = 0,$$

(2.4): $$\frac{\partial Q}{\partial t} + \frac{\partial}{\partial x}(Qu+gI_1) = gA(S_o-S_f) + gI_2.$$

The Eqs.(2.3) and (2.4) can be compactly expressed in matrix form as:

(2.5): $$\frac{\partial U}{\partial t} + \frac{\partial}{\partial x}[F(u)] = G(U,x,t),$$

where:

(2.5a): $$U=[A,Q]^T,\ F(U)=[Q,Qu+gI_1]^T,$$
$$G(U,x,t)=[0,gA(S_o-S_f)+gI_2]^T.$$

To compensate for the non-uniform velocity distribution over the cross section, a correction term may be added in the momentum Eq.(2.4) (see Strelkoff,1969; Cunge et.al.,1980).

Eqs.(2.3) and (2.4) comprise a system of two hyperbolic, non-linear (or, in some references quasi-linear) partial-differential equations of the first order. Such a system requires one initial condition for each variable and two boundary conditions to be properly posed. The initial condition is the known value of the flow variables at the initial time, and the boundary conditions depend on the type of the problem and the type of flow.

As shown by Lax (1954) the above formulation of the differential equations (the ones derived directly from the integral equations) has the property of preserving the discontinuous solution of the integral equations for the case of a homogeneous system of Eqs.(2.3) and (2.4). The solution obtained in such a way is called a weak solution, and it is commonly used for the full set of Eqs.(2.3) and (2.4) to compute unsteady flows with discontinuities; numerical experiments have confirmed good agreement with

analytical solutions or shock-fitting solutions (Cunge,1975). This approach is called the "through" method (Cunge.et.al.,1980; Cunge and Liggett,1975; Terzidis and Strelkoff, 1970).

When one wants to isolate the discontinuity and treat it separately from the rest of the continuous flow (shock-fitting method), the equations based on a control volume moving at the speed of the discontinuity are used (Stoker,1957; Terzidis and Strelkoff,1970).
The continuity equation is:

(2.6): $$A_1(u_1-w) = A_2(u_2-w),$$

and the momentum equations is:

(2.7): $$gI_1 + A_1(u_1-w)^2 = gI_2 + A_2(u_2-w)^2,$$

where u is the mean cross-sectional velocity and w is the speed of shock propagation.

II.2.2 Mathematical 2-D models

In a two-dimensional approach, the variation of variables along the width of the cross-section is accommodated, since the averaging is performed only in the

vertical direction. Here appears a new variable, the second component of the velocity vector in the plane of flow. Accordingly, three equations must be provided to solve for the three variables (the depth h, and the two velocity components, u in the x-direction, and v in the y-direction). The equations are based on the mass-conservation law, and the momentum conservation expressed for the x- and y-directions (Liggett,1975; Radojkovic,1980).

The continuity equation is:

$$(2.8): \quad \frac{\partial h}{\partial t} + \frac{\partial}{\partial x}(uh) + \frac{\partial}{\partial y}(vh) = 0,$$

the momentum equation in the x-direction is:

$$(2.9): \quad \frac{\partial (uh)}{\partial t} + \frac{\partial}{\partial x}(u^2 h) + \frac{\partial}{\partial y}(vuh) + \frac{\partial}{\partial x}\left(\frac{h^2}{2}\right) = gh(S_{ox} - S_{fx}),$$

and the momentum equation in the y-direction is:

$$(2.10): \quad \frac{\partial (vh)}{\partial t} + \frac{\partial}{\partial x}(uvh) + \frac{\partial}{\partial y}(v^2 h) + \frac{\partial}{\partial y}\left(\frac{h^2}{2}\right) = gh(S_{oy} - S_{fy}),$$

In the x-momentum Eq.(2.9) a new term appears,

describing the transfer of x-direction momentum by the velocity in the y-direction. There are no terms due to non-prismatic contours, since a prismatic control volume is chosen.

The matrix form of the Eqs.(2.8)-(2.10) is:

$$(2.11): \quad \frac{\partial U}{\partial t} + \frac{\partial}{\partial x}[F(u)] + \frac{\partial}{\partial y}[G(U)] = H(U,x,y,t),$$

where:

$$(2.11a): \quad U=[h, uh, vh]^T,\ F(U)=[uh, u^2h+\frac{gh^2}{2}]^T,$$

$$G(U)=[vh, uvh, v^2h+\frac{gh^2}{2}]^T,$$

$$H(U,x,y,t)=[0, gh(S_{ox}-S_{fx}), gh(S_{oy}-S_{fy})]^T.$$

As in the one-dimensional approach, appropriate initial and boundary conditions are required to solve the system of partial-differential Eqs.(2.8)-(2.10).

The advantage of the two-dimensional approach over the one-dimensional is not merely in that the flow field is represented more realistically, but in the capability to treat any kind of topography (abrupt expansions and/or contractions) without restriction. On the other hand,

solving the system of three equations with three variables is a more difficult task than is the case for the one-dimensional approach. Difficulties also arise from the constant change of the boundaries of flow, which complicates handling the boundary conditions (dry-bed problems occur in almost all applications).

II.2.3 Mathematical models based on simplified equations

Since the one/two-dimensional systems of non-linear partial-differential equations cannot easily be solved, in some cases even with a digital computer, simplifications may be introduced to obtain equations that can be handled more easily (see Miller and Cunge,1975; or Cunge et al.,1980). In using simplified methods, one must be careful not to sacrifice the properties of the equations which are important in the problem under study.

Many different procedures are used to simplify the equations, beginning with the linearization of the equations or particular terms, neglecting some of the terms, and finally omitting the whole equation. In all such applications the acceleration components (inertial terms) are neglected.

In the initial stage of the instantaneous dam-break problem the inertial terms are extremely important, and cannot be neglected (Strelkoff et.al.,1977; Savic,1988).

For the case of a partial and gradual dambreak, the inertial terms can be neglected without significant loss of accuracy.

The methods based on the continuity equation alone are very unsafe to use for rapidly varied flows with discontinuities. The very popular Muskingum flood-routing method is reported to introduce errors of several orders of magnitude for dam-break computations (Wurbs,1987).

II.3 Analytical solutions for discontinuous flows

There is no general analytical solution for the flow Eqs.(2.5) and (2.11). A few existing analytical solutions have been obtained for simplified cases based on the assumption of a rectangular, frictionless channel (ideal fluid), with horizontal bottom slope (see Henderson,1966; or Stoker,1957). The case of a sudden instantaneous dambreak with either a dry or wetted downstream channel has been analyzed by Stoker (1957), using the method of characteristics, and the approximate effect of resistance on the dry-bed solution has been studied by Dressler (1952) and Whitham (1955).

Though the above-mentioned analytical solutions have very little applicability in solution of real-life problems, they are regularly used for assessment of the performance of numerical solutions.

II.4 Numerical methods for discontinuous flows in computational hydraulics

Numerous numerical methods have been used in computational hydraulics to solve the one/two-dimensional flow equations, but no method has proven to be superior for a broad range of real-life problems. In this review only some of the methods used for the computation of discontinuous flows are presented. The methods upon which the algorithm proposed in the present work is based, and those used for comparison, are given in more detail.

There are presently three major classes of methods that are most commonly used for solving the open-channel flow equations:

1. The method of characteristics,
2. The finite-difference method, and
3. The finite-element method.

The method of characteristics is theoretically the most accurate one, but it is very difficult to implement, since it requires shock-fitting for the treatment of discontinuities. In an idealized prismatic channel this is not a difficult problem, but for any discontinuous flow in a real (non-prismatic) channel, this means detecting and computing all reflected waves that form during the evolution of the unsteady flow event - an almost impossible task (Cunge,1975). Accordingly, the method of characteristics is

seldom utilized for solution of the open-channel flow equations, though there have been some numerical experiments for the two-dimensional equations (Katopodes and Strelkoff,1978). The method of characteristics is widely exploited for the computation of the boundary conditions within other methods (finite-difference methods in particular). In the present work the method of characteristics is used in the first (predictive) step of the solution.

The finite-difference method is the most common numerical method for solving both the one- and two-dimensional equations (Liggett and Cunge,1975; Cunge et.al.,1980). The method is capable of solving a wide range of practical problems, and at the same time is very easy to implement. The implementation for curvilinear coordinates, first used in fluid mechanics (see for example Thompson et.al.,1985), has greatly increased the potential of the method for the solution of two-dimensional problems, though it complicates the implementation to some extent. Some of the finite-difference schemes that have been used for the computation of discontinuous open-channel flows are described in more detail later.

The finite-element method is less widely used in computational hydraulics. For one-dimensional flow, the finite-element method is inferior to the finite-difference

method (Cunge et.al.,1980); it is much more difficult to implement, and lacks the capability to adjust to mixed-flow regimes, and to handle various hydraulic structures which are described by laws different from the equations for the rest of the flow. Since in two-dimensional applications the finite-element method has a major advantage over finite-difference in being able to represent the topography in much more detail and much more naturally, efforts have been made to overcome some of the above-mentioned shortcomings (treatment of mixed regimes, in particular). Aknabi and Katopodes (1988) developed a moving-grid finite-element method, which is very complicated and not easy to implement. The method is tested on an idealized hypothetical flow - no practical application has been reported.

It is worth recalling that most of the numerical methods reported in the literature perform very well for the ideal case of a (frictionless), prismatic, horizontal channel, while in solving practical problems they fail to give even physically meaningful results. The most difficult problem seems to arise from the topography, especially from sudden changes of the channel width (Strelkoff,1989).

II.4.1 Method of characteristics

Since the method of characteristics is used in the initial step of the algorithm proposed in the present work,

as well as for comparison with the proposed method, it is presented here in some detail. The description follows closely the derivation by Stoker (1957), using the fixed-grid method of characteristics. (See also Henderson (1966) for a brief account, and Courant et.al.(1948) for the original application of the method in gas dynamics.)

The method of characteristics is based on the fact that the hyperbolic partial-differential equations posses characteristic paths - characteristics - in the space of independent variables, along which the dependent variables are expressed in terms of their total differentials. (The resulting expressions, valid along the characteristics and comprising the total differentials, are often called compatibility conditions.) For practical computations, this enables transferring the problem of solving two partial-differential equations into a problem of solving four ordinary differential equations (two characteristics equations and two compatibility conditions), which is a much easier task.

To obtain the characteristic relations one must work with the non-conservative form of the flow equations. By appropriate transformations (see Cunge et.al.,1980) the mass and momentum conservation Eqs.(2.3) and (2.4) can be expressed as:

$$(2.12): \quad B\frac{\partial h}{\partial t} + uB\frac{\partial h}{\partial x} + A\frac{\partial u}{\partial x} + u\left(\frac{\partial A}{\partial x}\right)_{h=const} = 0,$$

$$(2.13): \quad \frac{\partial u}{\partial t} + u\frac{\partial u}{\partial x} + g\frac{\partial h}{\partial x} = g(S_o - S_f),$$

where B-is the top width at the cross-section and, $\left(\frac{\partial A}{\partial x}\right)_{h=const}$ is the derivative of the area with respect to x, at constant depth. Introducing the celerity of an elementary wave:

$$(2.14): \quad c = \sqrt{\frac{gA}{B}},$$

together with its derivatives into flow Eqs.(2.12) and (2.13), and first adding, and then subtracting the resulting equations, one obtains the characteristics form. In the case of a rectangular, but non-prismatic, cross-section this finally yields:

$$(2.15): \quad \frac{D}{Dt}(u+2c) = g(S_o - S_f) - \frac{uc}{B}\frac{\partial B}{\partial x},$$

along the positive characteristics (C+):

$$(2.16): \quad \frac{dx}{dt} = u+c,$$

and

$$(2.17): \quad \frac{D}{Dt}(u-2c) = g(S_o-S_f) + \frac{uc}{B}\frac{\partial B}{\partial x},$$

along the negative characteristics (C-):

$$(2.18): \quad \frac{dx}{dt} = u-c.$$

The compatibility conditions Eqs.(2.15) and (2.17) are valid only along the characteristic paths Eqs (2.16) and (2.18) (given as lines LA and RA in Fig.(2.1)). At point A, an intersection of the characteristics LA and RA, both compatibility conditions are valid, and given known conditions at the points L and R (the "feet" of the characteristics), the solution can be found. This requires solving all four equations simultaneously, since the paths themselves are the functions of dependent variables. The

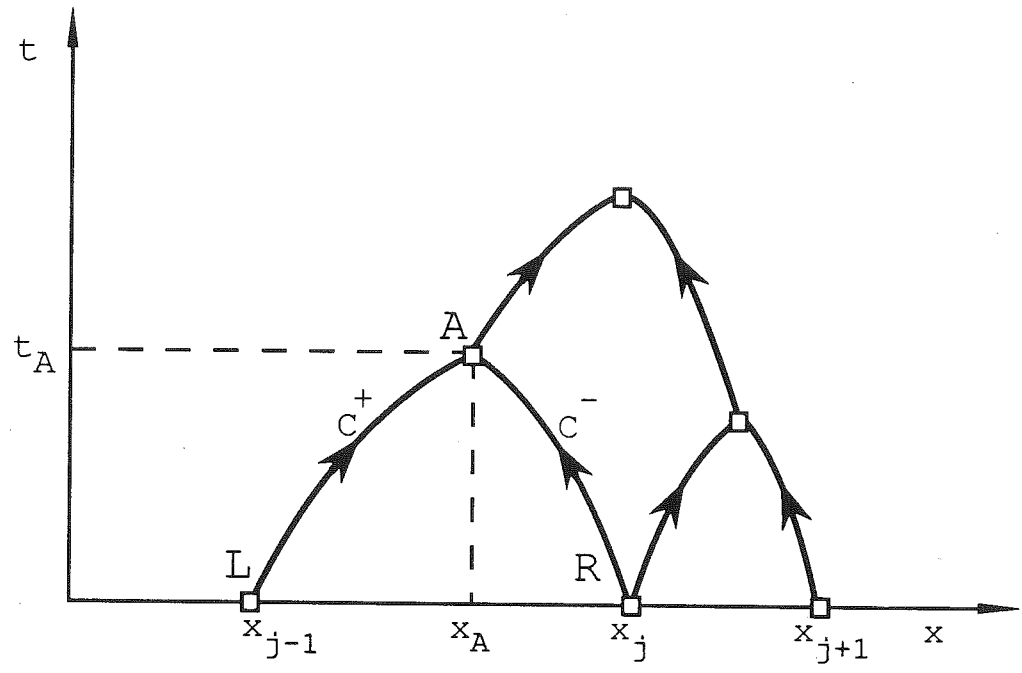

Figure 2.1 The characteristic grid method

problem becomes somewhat easier when the right-hand side of the compatibility conditions is equal to zero (the case of a horizontal, prismatic and frictionless channel). The expressions under the differential operator, which are constant along the characteristic paths, are then called Riemann invariants. If in addition, the initial state is a uniform flow, the exact analytical solution can be found (Stoker,1957). In a general case, however the system of ordinary differential equations must be integrated numerically, and the accuracy of the integration determines the accuracy of the whole method, since the original equations have not been compromised to this point. Two general approaches are used to solve the problem (Liggett and Cunge,1975): the characteristic-grid method, and the fixed-grid method.

In the characteristic-grid method, one starts from the known time level t^n (Fig.2.1) and solves the system of Eqs.(2.15-2.18) for the position X_A and time t_A, and the velocity u_A and celerity c_A.

In the fixed-grid method the solution is obtained at the points of the finite-difference-grid in the x-t plane, i.e. for a known values of the independent variables (Fig.2.2). Here, in addition to the unknown velocity and celerity at point A, the positions (and therefore the velocities and celerities) of the feet of characteristics LA

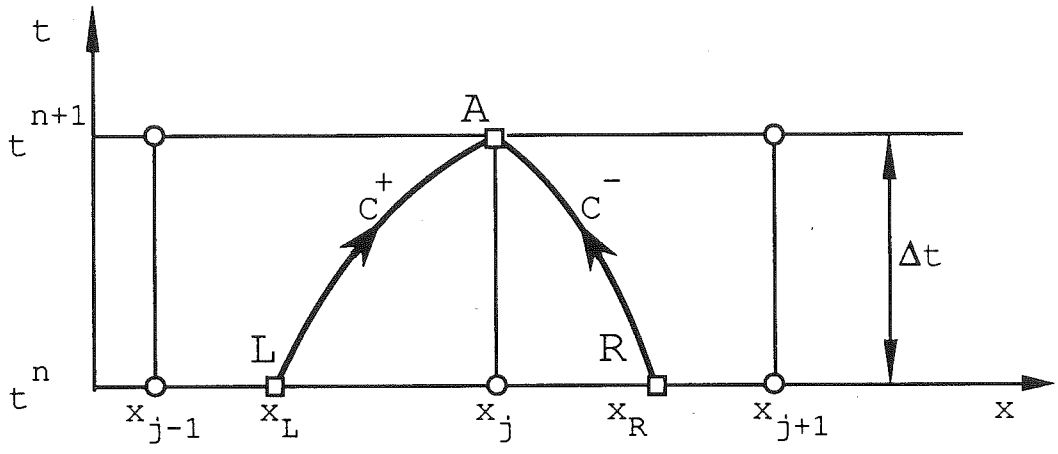

Figure 2.2 The fixed-grid method of characteristics

and RA are also unknown. They must be obtained from interpolation between the points at the known time level t^n. The type of interpolation greatly influences the accuracy of the method. In addition to the most simple linear interpolation, various types of parabolic interpolation have been used. Higher-order interpolation procedures involve the use of a greater number of points, complicating the method. In order to obtain a method which uses only two points for the interpolation, Toda and Holly (1988) applied the Holly-Preissmann method (Holly and Preissmann, 1977), which is successfully used for contaminant transport problems, to Burgers' equation (a model equation for the flow equations). The results were not entirely satisfactory, due to the problem of unique determinacy of the foot of the trajectory (characteristic path), and difficulties in obtaining reliable guidance for the parameters of computation.

The characteristics-grid method is potentially more accurate, since no interpolation error is introduced. However, after a few computational steps the solution points become "randomly" dispersed all over the computational domain, and a projection of the results onto a fixed grid is necessary, at least to obtain a reasonable interpretation of the calculations.

Regardless of the approach (fixed-grid

vscharacteristic-grid) the method of characteristics fails to yield a solution when the characteristics of the same family (C+, or C-) intersect (see Stoker,1957 or Cunge,1975), as given in Fig.(2.3). Physically, this means that at time t^{n+1} the particle L2 will be overtaken by the particle L1, which is behind L2 at the time t^n, but has a larger celerity (due to its larger depth - see Eq.2.14). The resulting steep front (surge) moves at a speed different from the speed of either of the particles before they met. The speed of the surge is lower than the speed of the perturbation behind it, but larger than the speed of the particles downstream of it (Stoker,1957).

This problem of shocks is solved by the shock-fitting technique (Cunge et.al.,1980; and Cunge,1975). The conservation Eqs.(2.6) and (2.7) for the moving control volume are applied to the shock (whose path is designated as the line SP in Fig.2.4), in addition to the equation of the trajectory of the shock:

$$(2.19): \qquad \frac{dx}{dt} = w,$$

and the equation of the characteristics and compatibility condition issuing from the point P. Again, when the fixed-

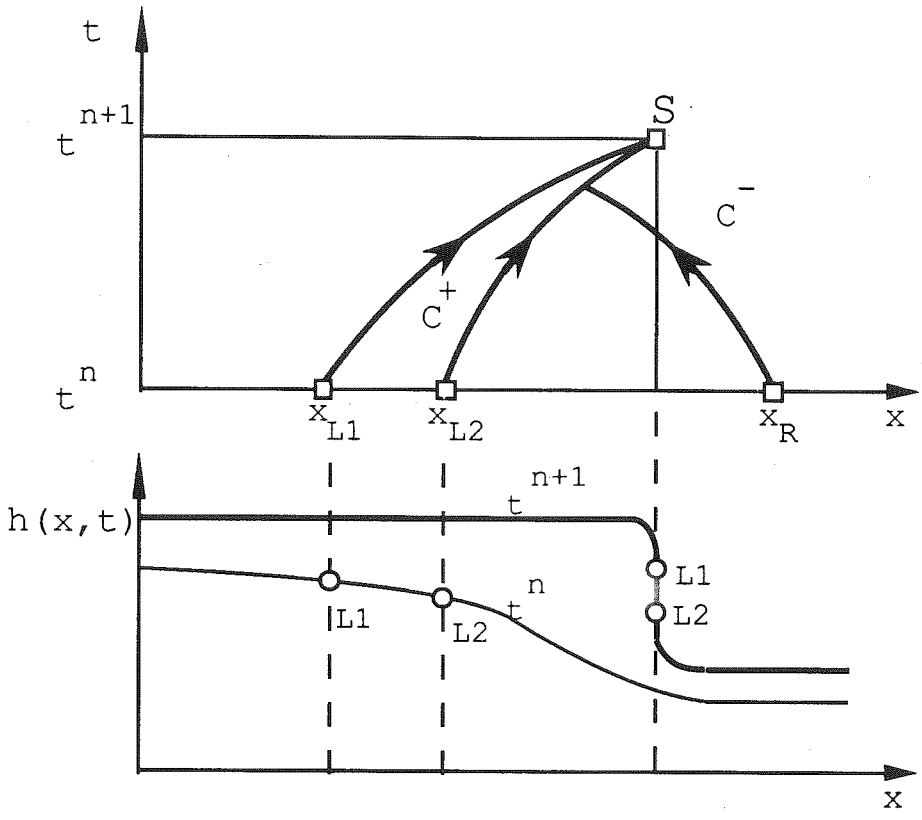

Figure 2.3 Inception of the shock

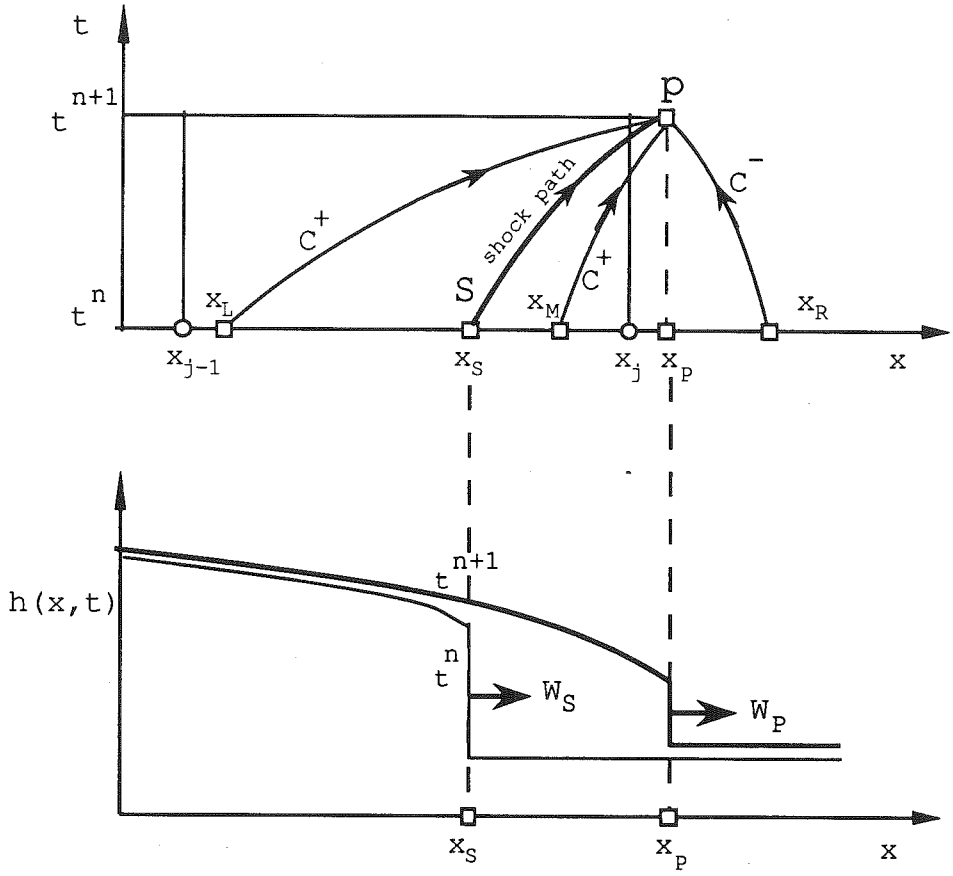

Figure 2.4 The shock-fitting method

grid method is used, interpolation is necessary to obtain the values of the variables at the feet of the trajectories (characteristics). The problem then becomes a system of fifteen nonlinear equations in fifteen variables, and is usually solved by a combination of a simple iteration and the Newton-Raphson method.

The method of characteristics also has been applied to the two-dimensional equations - the so-called bicharacteristics method (Katopodes and Strelkoff,1978).

II.4.2 Finite-difference methods

The finite-difference method is the most commonly used numerical tool for the solution of the partial-differential equations for flow problems, not only in computational hydraulics, but also in fluid mechanics and aerodynamics.

The basis for all finite-difference methods is in approximation of (normally) continuous functions with discrete values on particular grid points of the x-t plane, and approximation of derivatives with divided differences. Hence, the differential equations are approximated with difference equations. The method and the order of approximation is what makes a particular scheme attractive for the solution of a given problem. Two major groups of finite-difference schemes exist: explicit schemes, in which the variables from only one of the "unknown points" appear

in each of the difference equations (so that the solution can be obtained explicitly), and implicit schemes, where at least two unknown points appear in the equations (which requires solving a system of equations).

To achieve convergence of the numerical solution to the solution of the differential equations every finite-difference scheme must satisfy two requirements: the consistency condition, and the stability condition (Richtmeyer and Morton,1957). While the consistency condition is in general easy to fulfil, the stability condition may require a limitation of the ratio of the time step and the spatial step, usually expressed through the Courant-Friedrichs-Lewy condition (or, less formally, the Courant condition):

$$(2.20): \qquad Cr = |u+c| \frac{\Delta t}{\Delta x} \leq 1.0.$$

The limitation typically affects only explicit schemes; most implicit schemes are unconditionally stable, regardless of the value of the Courant number.

In addition to stability considerations, problems of numerical diffusion and numerical oscillations also occur in finite-difference methods. Both problems arise since the

solution of the difference equations is equivalent to the solution to some slightly modified form of the original differential equations (Warming and Hyett,1974). For first-order methods, where the truncation error has a leading term containing the second derivative, the modified equation is of a diffusion type, with the consequence of artificial smearing, of diffusion of the solution. Numerical oscillations characterize second-order methods, for which the leading term in the truncation error is usually a third derivative.

A broad survey of different schemes used in fluid mechanics is given by Anderson et.al.(1984) and Patankar (1980). In the following some of the schemes used for dam-break computations, and in particular those used for comparison with the method proposed in the present work, are presented. Schemes upon which the proposed new algorithm is constructed are also explained in more detail.

II.4.2.1 Preissmann method

The Preissmann (or Sogreah, or four-point) scheme is probably the most exploited of all methods for the solution of the one-dimensional (de St.Venant) equations. The DAMBRK model, presently the most widely used industrial code for the calculation of dam-break waves, uses the Preissmann scheme (Fread,1977).

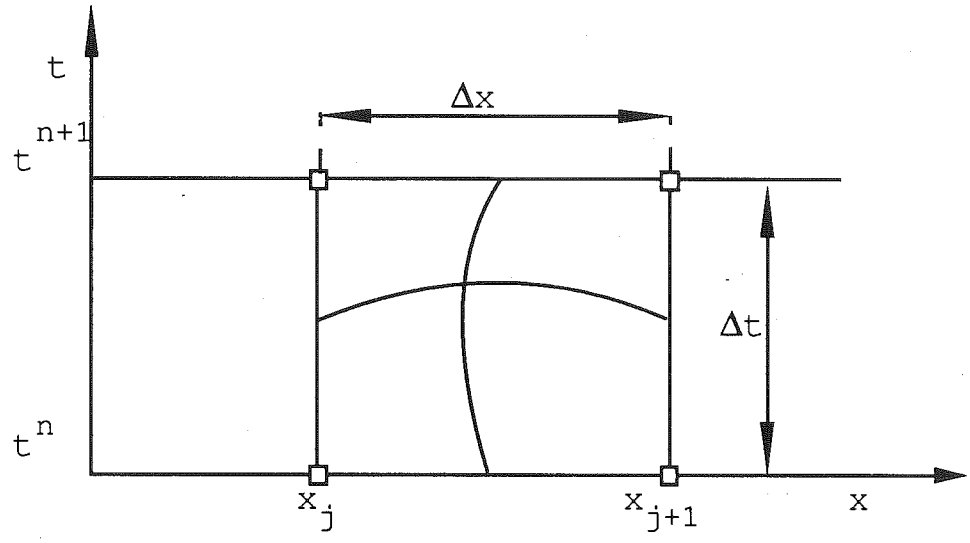

Figure 2.5 The finite-difference grid for the Preissmann scheme

In the Preissmann scheme all functions and derivatives are expressed using only four point values in the x-t plane (see Fig.2.5):

(2.21a): $$f(x,t) \doteq \frac{\theta}{2}(f_j^{n+1}+f_{j+1}^{n+1}) + \frac{1-\theta}{2}(f_j^n+f_{j+1}^n),$$

(2.21b): $$\frac{\partial f}{\partial x} \doteq \theta\frac{f_{j+1}^{n+1}-f_j^{n+1}}{\Delta x} + (1-\theta)\frac{f_{j+1}^n-f_j^n}{\Delta x},$$

(2.21c): $$\frac{\partial f}{\partial t} \doteq \frac{f_{j+1}^{n+1}-f_{j+1}^n + f_j^{n+1}-f_j^n}{2\Delta t},$$

where f(x,t) is any function to be approximated and θ is a temporal-weighting coefficient that can in principle be assigned any value between zero and unity, though $\Theta \leq 0.5$ is required for unconditional stability. Application of the above approximations to the de St.Venant Eqs.(2.3 and 2.4), with careful treatment of nonlinear terms and coefficients, results in a system of non-linear algebraic equations, which can be solved by a Newton-Raphson method. (Of course, the boundary conditions must be added to close the system.) This leads to a system of linear algebraic equations, which

form a tri-diagonal matrix, and can be solved by a double-sweep algorithm in order to reduce computer time and memory requirements. It can be shown (see Cunge et.al.,1980) that the Preissmann scheme applied to the homogeneous differential equations in conservation form, also satisfies the appropriate integral equations, which makes it especially attractive for "through" computations. Unfortunately, the double-sweep algorithm is very awkward and unnatural to apply for mixed-regime flows, which usually occur in dam-break computations.

For a uniformly spaced grid the Preissmann scheme is second-order accurate in space, and first/second-order accurate in time. (The accuracy in time depends on the value of weighting coefficient θ.) As an implicit scheme, it has no theoretical stability limitation on the Courant number (and accordingly on the time step). However, in application to discontinuous problems, rather small time steps are required, to avoid excessive diffusion (smearing) of the wave front. The recommended value of the Courant number for discontinuous calculations is around unity (Fennema and Chaudhry,1986).

II.4.2.2 Lax-Wendroff method

The Lax-Wendroff method (Lax and Wendroff,1960) is used

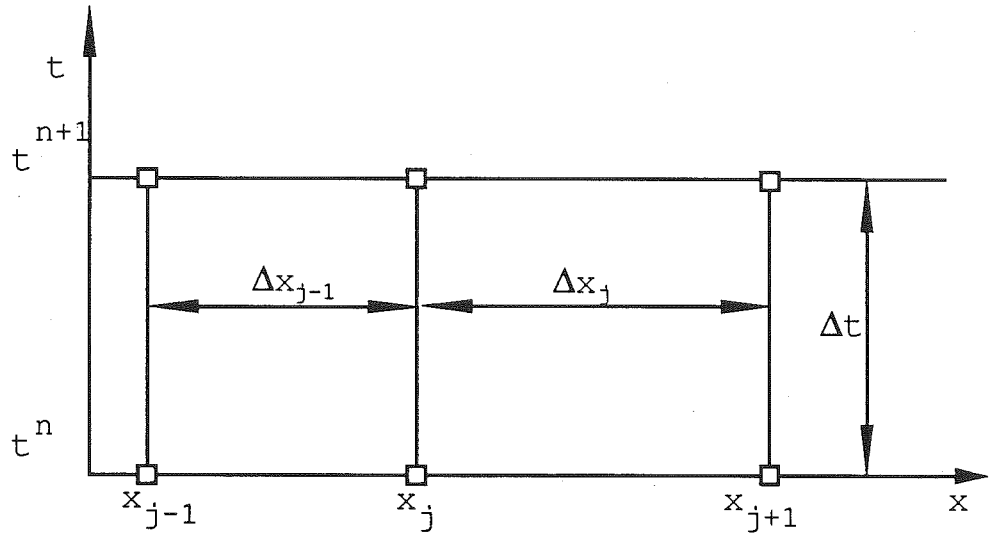

Figure 2.6 The finite-difference grid for the Lax-Wendroff scheme

for solving conservative equations in gas-dynamics problems involving discontinuities. The scheme has also been applied to some open-channel flow problems by Houghton and Kasahara (1968).

The method is based on the capability of the conservative equations to express the time derivative through the spatial derivative, thus leading to an explicit scheme with second-order accuracy in time, using only two time levels to construct the grid (Fig.2.6). The approximation of time derivatives by spatial derivatives is obtained through Taylor-series expansion around the grid point (x_j, t^{n+1}), and then replacement of the time derivatives by spatial derivatives, using the conservation equations themselves. Applied to the conservative system Eq.(2.5), this results in:

$$(2.22): \quad U_j^{n+1} = U_j^n - \frac{\Delta t}{2} F_j^{n'} \frac{U_{j+1}^n - U_{j-1}^n}{\Delta x} + \frac{\Delta t^2}{2}$$

$$\left\{ \frac{1}{\Delta x} \left(\left[(F^{n'}_{j+\frac{1}{2}})^2 \frac{U_{j+1}^n - U_j^n}{\Delta x} + G^n_{j+\frac{1}{2}} \right] - \left[(F^{n'}_{j-\frac{1}{2}})^2 \frac{U_j^n - U_{j-1}^n}{\Delta x} + G^n_{j-\frac{1}{2}} \right] \right) + \right.$$

$$\left. + G_j^{n'} \left[F_j^{n'} \frac{U^n_{j+\frac{1}{2}} - U^n_{j-\frac{1}{2}}}{\Delta x} + G_j^n \right] \right\},$$

where $F_j^{n'}$ and $G_j^{n'}$ are the jacobians of the column matrices F_j^n and G_j^n at the point j+1, and $F_{j+\frac{1}{2}}^{n'}$ and $G_{j+\frac{1}{2}}^{n'}$ are the jacobians at the midpoint j+½.

As do most of the (potentially) second-order accurate methods, the Lax-Wendroff method suffers from numerical oscillations, which sometimes must be controlled by adding artificial viscosity.

To avoid computation of the jacobians, Richtmyer (1964) reformulated the scheme as a two-step procedure, which was implemented by Terzidis and Strelkoff (1970) for open-channel discontinuous calculations. The algorithm performs well for the cases of prismatic channels and flows with mild discontinuities, but needs artificial viscosity (damping), and extremely small time steps to produce a stable computation for severely non-prismatic channels and very strong shocks.

II.4.2.3 MacCormack method

The MacCormack scheme also originated in aerodynamics (MacCormack,1969), and is a very frequently used method for discontinuous problems in fluid mechanics (Anderson et al.,1984). It is a second-order accurate, explicit predictor-corrector scheme. In the first (predictor) step a

backward type of spatial differencing is used:

$$(2.23): \qquad \bar{U}_j^{n+1} = U_j^n - \frac{\Delta t}{\Delta x}(F_j^n - F_{j-1}^n) + \Delta t G_j^n,$$

while for the final (corrector) step forward differences are exploited for the spatial derivatives:

$$(2.24): \qquad U_j^{n+1} = \frac{1}{2}\left[U_j^n + \bar{U}_j^{n+1} - \frac{\Delta t}{\Delta x}(\bar{F}_{j+1}^n - \bar{F}_j^n) + \Delta t \bar{G}_j^n\right].$$

The order of differencing can be reversed depending on the particular case.

The scheme is very simple and easy to implement, though it usually requires addition of artificial viscosity for damping numerical oscillations.

Fennema and Chaudhry (1986) applied the MacCormack scheme to the de St.Venant Eqs.(2.5) for the computation of flows with discontinuities. The results, obtained for a prismatic channel and shocks less severe than those of dam-break waves, were good. However, to obtain a stable solution for very strong discontinuities in non-prismatic channels, artificial damping (with significant smearing of the results) must be added, and time steps (the Courant

number) must be reduced. Fennema and Chaudhry (1990) also used the MacCormack scheme for the solution of the two-dimensional equations, with not entirely satisfactory results.

II.5 Summary assessment of state-of-the-art and needs

All the above-mentioned finite-difference methods, when applied to nonhomogeneous equations, are based on schemes that are not truly conservative, since the Lax theorem can be strictly applied only to the homogeneous (ideal) system of differential equations. Consequently, they are able to produce satisfactory results only for moderately strong surges (discontinuities) in prismatic and/or nearly prismatic channels. However, the majority of them cannot handle mixed-regime flow well (most finite-difference schemes cannot handle it at all), though a mixed regime is very likely to occur, at least in the earlier stages of dam-break flow (Strelkoff,1989). (Not infrequently the practice is to increase the roughness artificially, and so avoid supercritical flow entirely (Wurbs,1987)). In addition, the presently used schemes are very sensitive to abrupt changes of cross-sectional geometry and to the presence of very strong shocks.

Consequently, there is a need for a new method, based on a conservative scheme, and able to treat well both

discontinuities and mixed regime. Ideas for a new method can be taken from other fields dealing with hyperbolic equations with discontinuities, in particular from gas-dynamics.

II.6 Numerical methods for discontinuous flows used in other disciplines

Three general approaches are currently used for solving the hyperbolic conservation laws for discontinuous flows in gas-dynamics (Roe,1980): random-choice methods, methods based on linearized Riemann problems, and Godunov methods. Each of those general groups has numerous variations, depending on the application.

The finite-difference method for the gas-dynamics equations, based on the linearized Riemann problem, has been developed by Roe (1980 and 1981) and further improved by Glaister (1988a). Glaister (1988b) applied the method to the homogeneous de St.Venant Eqs.(2.5) . The test results of the application agree well with the Stoker (1957) analytical solution, but it is not quite clear how the generalization to the full equations, and in particular to non-prismatic natural channels, is possible, without significant modification of the algorithm.

The random-choice method, developed by Glimm (1965), preserves the structure of the shocks with the uncertainty

in their location. It is successfully applied to one-dimensional porous-media flows, especially for petroleum exploitation (Colella et al.,1983).

The Godunov method has an advantage over the previous two methods in that it does not use any approximations concerning the non-linearity of the Riemann problem and the position of the shock. The method was first presented by Godunov (1959) as a first-order conservative finite-difference scheme with a monotonicity property. (The scheme has the monotonicity property if it does not produce artificial extremums (see Godunov,1959).) Both Lagrangian and Eulerian descriptions of the method have been presented. It is a two-step (predictor-corrector) method, in which the conservative property is provided for by the conservative (corrector) step, where the flow Eqs.(2.5) are integrated between the times t^n and t^{n+1}, and midpoints $x_{j-½}$ and $x_{j+½}$ (see Fig.2.7):

$$(2.25): \qquad \langle U\rangle_j^{n+1} = \langle U\rangle_j^n - \frac{\Delta t}{\Delta x}\left(\overline{F}_{j+\frac{1}{2}}^{n+\frac{1}{2}} - \overline{F}_{j-\frac{1}{2}}^{n+\frac{1}{2}}\right) + \Delta t\,\overline{G}_j^{n+\frac{1}{2}},$$

where $\langle U\rangle_j^n$ and $\langle U\rangle_j^{n+1}$ are space-averaged values of the independent-variable vector U at times t^n and t^{n+1}, while

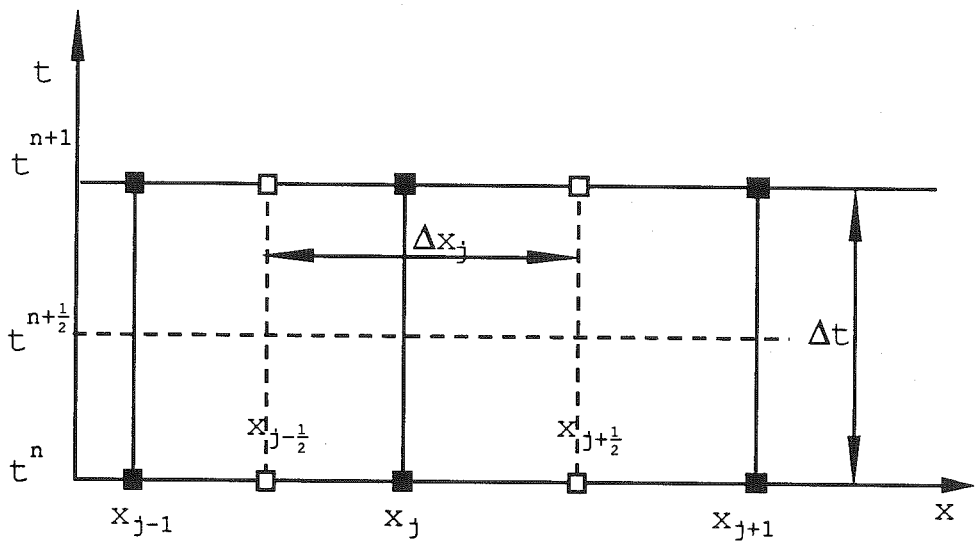

Figure 2.7 The grid for the Godunov scheme

$\overline{F}^{n+1/2}_{j+1/2}$ and $\overline{F}^{n+1/2}_{j-1/2}$ are the time-averaged fluxes at the midpoints $x_{j+1/2}$ and $x^{j-1/2}$, respectively, while the $\overline{G}^{n+1/2}_{j}$ is the time-averaged source term. The most important part of the problem is to obtain approximate values for the fluxes. Many different procedures have been developed (and are still being developed) to compute the fluxes since that is where the potential of the method is gained, or lost. The way in which the flow variables (vector U of Eqs.2.5) are recovered as piecewise functions from the averages $\langle U \rangle^{n+1}_{j}$, is extremely important for the accurate approximation of the fluxes $\overline{F}^{n+1/2}_{j+1/2}$ and $\overline{F}^{n+1/2}_{j-1/2}$, and the source term $\overline{G}^{n+1/2}_{j}$. The original Godunov method uses constant values, i.e. a uniform distribution of the functions, which can be shown to lead to the upwind scheme.

The Godunov method was first applied to some discontinuous gas-dynamics problems, but not with especially good results due to the dispersive properties of the upwind scheme.

One of the first applications of the Godunov-type methods in computational hydraulics (i.e. for solving the de St.Venant equations) was the Vasiliev method of isolating discontinuities (Vasiliev,1970). It is a predictor-corrector moving-grid type method, where the flow is divided

into the zone of disturbance and the zone of initial state. The moving boundary between the two zones is computed using the method of characteristics at the upstream end, and the shock Eqs.(2.6 and 2.7) at the downstream end of the disturbed zone. The position of the grid within the zone of disturbance, and the variables at the intermediate time steps (predictor step), are computed by a modification of the method of characteristics, while the conservative (corrector) step is used to ensure the conservative property of the method. A special device is incorporated to handle the dry-bed problem.

Although preserving the resolution of the shock (it is a kind of shock-fitting method), and being able to deal efficiently with the dry-bed problem, the Vasiliev method of isolating discontinuities has many shortcomings for successful application in practice. The constant expanding of the grid diffuses the solution significantly, there is no possibility of mixed-regime simulation, and certainly the most important weakness of the method is its practical incapability to treat reflected shocks. In order to cope with a reflected wave one must construct another "sub-zone", by which eventually the algorithm takes on the complexity of a shock-fitting method, if not worse.

The Godunov method was rediscovered in the late seventies, in particular in the work of Van-Leer described

in a series of papers, and finalized by him through proposal of a new variant of the scheme for compressible flow (Van-Leer,1979). A Lagrangian step, based on the solution of the Riemann problem (see Courant and Friedrichs,1948), is used to obtain the fluxes, while the final results are obtained from an Eulerian conservative step. This differs from the original Godunov schemes, which was either Lagrangian or Eulerian. Van-Leer used a sloped (linear) distribution to obtain piecewise functions from the averages, which greatly contributed to the accuracy of the results (see also Colella et al.,1983 and Vila,1988). The requirement for monotonic functions is provided for by a "monotonicity algorithm", a device almost unanimously adopted in subsequent developments.

The Godunov scheme has been further improved by Colella and Woodward (1984) (see also Woodward and Colella,1984). They developed a special interpolation procedure (piecewise parabolic interpolation PPM) which produces third-order accurate schemes. In addition to the Lagrangian-Eulerian scheme, they created a purely Eulerian scheme for the full compressible flow equations with very good results.

The implicit variation of the Godunov scheme is presented by Fryxell et al.(1986). A new procedure for the computation of fluxes, using an alternative interpolation, removed the Courant number restrictions, but the accuracy of

the method is now reduced to second-order.

Bell et al.(1988) introduced a characteristics-based approach for flux computation (predictor step), and applied it to the two-dimensional advection-diffusion equation. For recovering the distribution of the averaged functions they used a two-dimensional equivalent of the Colella-Woodward PPM method. Although the results of the test computations show even better agreement with analytical results than the Colella-Woodward method, the authors claim that the generalization to the flow equations would be impossible without introducing considerable difficulties in an already complicated scheme.

Some other possibilities for recovering distributions for the reach-averaged functions are described by Woodward (1986).

Vila (1986) presented a thorough theoretical evaluation of Godunov-type schemes and introduced a new solution for the predictor step (flux determination) based on Riemann solvers. Vila (1987) applied his second-order scheme (based on linear interpolation) to the one-dimensional and two-dimensional open-channel flow equations. Though the scheme is intended for the full equations, only the results for a prismatic frictionless channel are presented.

In the computation of discontinuous compressible flow problems the major difficulty is very strong shocks. For

computational hydraulics, most of the difficulties come from non-prismatic channel geometry and mixed-regime flows (though mixed regime presents a problem in aerodynamics, also). The method proposed in this work for computing unsteady open-channel flow with strong discontinuities is based on a Godunov type scheme. It uses an Eulerian-explicit approach, and Colella-Woodward piecewise-parabolic interpolation for recovering the distribution of functions from the reach-averaged values. For the computation of fluxes several options of the characteristic-based procedures in combination with a Riemann problem solver are considered. The goal is to obtain a stable, oscillation-free scheme capable of handling strong discontinuities in mixed regimes and for non-prismatic, frictional channels.

CHAPTER III. MODIFIED GODUNOV SCHEME APPLIED TO LINEAR ADVECTION EQUATION AND BURGERS' EQUATION

The modified Godunov scheme is first applied to the one-dimensional linear advection equation as a model equation because of its simplicity in an analytical sense, so that the results can easily be verified and interpreted. In addition, the numerical damping (diffusion) problems associated with advection equation make it ideal for assessment of some of the capabilities of the scheme. An objective was to get thoroughly familiar with the method, to learn its good features and to try to improve those that seem to be less satisfactory, and thus lay the foundations for implementation of the method for the de St.Venant equations.

Subsequently, another scalar equation - Burgers' equation - is solved as an appropriate, but simplified, model of the non-linear flow equations.

First, the idea of the method is explained through a detailed presentation of the two major computational steps: 1) conservative step based on the integral equations, 2) flux predictor step based on the method of characteristics. The interpolation procedure used for recovering the spatial

distribution of reach averages, is then presented. Then follows the implementation of the interpolation procedure in explicit and implicit schemes for the linear advection equation, and Von-Neumann stability analysis. Test computations for the advection equation, and comparison of the results with the Holly-Preissmann scheme, are then presented.

The modifications needed to implement the scheme for Burgers' equation, appropriate test computations, and conclusions on the performance of the Godunov scheme for the scalar equations are given at the end of the chapter.

III.1 Conceptual basis

The one-dimensional linear advection equation is written herein as:

$$(3.1): \qquad \frac{\partial \rho}{\partial t} + \frac{\partial}{\partial x}[\psi(\rho)] = 0,$$

where ρ is a dependent variable and $\psi(\rho)$ is a function of this variable. One can recognize the above equation as an equation of mass conservation, where ψ is then the product of the density ρ and velocity u in the x direction.

Equation (3.1) can also describe one-dimensional contaminant advection, in which case ρ is either the contaminant point concentration, or depth averaged concentration multiplied by the depth of the channel.

Whatever Eq.(3.1) represents, it can be integrated between times t^n and t^{n+1}, and spatial reaches $X_{j-½}$ and $X_{j+½}$, Fig.(3.1):

$$(3.2): \quad \int_{t^n}^{t^{n+1}} \int_{X_{j-½}}^{X_{j+½}} \left\{ \frac{\partial \rho}{\partial t} + \frac{\partial}{\partial x} [\psi(\rho)] \right\} dx dt = 0,$$

Using the divergence theorem (from which arise the conservation properties) the integral Eq.(3.1) is now rewritten as:

$$(3.3): \quad \int_{X_{j-½}}^{X_{j+½}} \rho(t^{n+1}, x)\, dx - \int_{X_{j-½}}^{X_{j+½}} \rho(t^n, x)\, dx + \int_{t^n}^{t^{n+1}} \{\psi[\rho(x_{j+½}, t)] - \psi[\rho(x_{j-½}, t)]\} dt = 0$$

or if one introduces the notation:

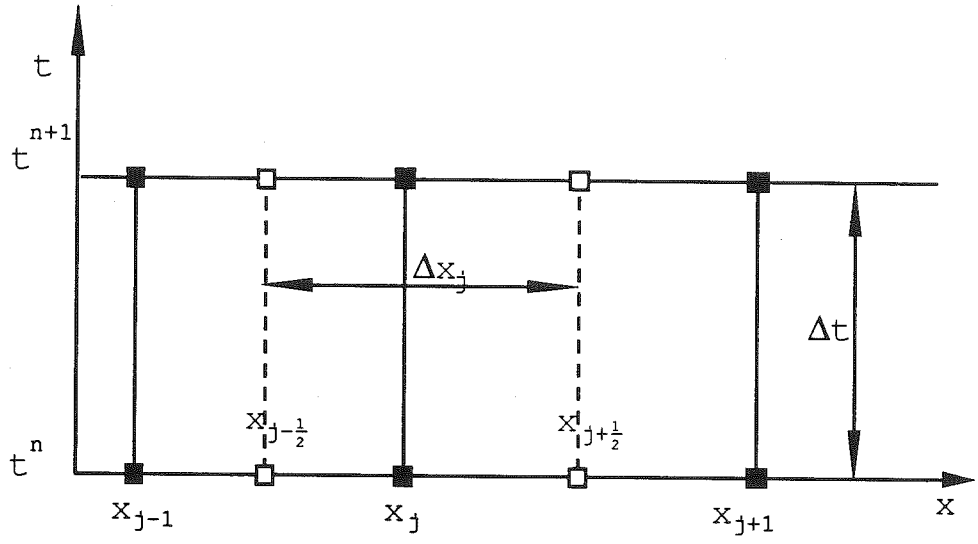

Figure 3.1 The staggered grid for the Godunov scheme

$$(3.4): \qquad \langle\rho\rangle_j^n = \frac{1}{\Delta x_j} \int_{x_{j-\frac{1}{2}}}^{x_{j+\frac{1}{2}}} \rho(t^n, x)\, dx\,, \qquad \Delta x_j = x_{j+\frac{1}{2}} - x_{j-\frac{1}{2}},$$

Eq.(3.3) becomes:

$$(3.5): \qquad \langle\rho\rangle_j^{n+1} - \langle\rho\rangle_j^n + \frac{1}{\Delta x_j} \int_{t^n}^{t^{n+1}} \{\psi[\rho(x_{j+\frac{1}{2}}, t)] - \psi[\rho(x_{j-\frac{1}{2}}, t)]\} dt = 0$$

The space averaged values $\langle\rho\rangle_j^n$ of the variable ρ resemble a grid function in the finite-difference sense. Once the time integrals of "fluxes" $\psi[\rho(x_{j\pm\frac{1}{2}}, t)]$ are obtained, the difference Eq.(3.5) can be solved for the grid function $\langle\rho\rangle_j^{n+1}$.

Note that one actually solves an integral equation, which offers the conservation properties of the integral approach even if the variables are not continuous. (For the case of discontinuous variables, Eq.(3.5) has to be derived directly from the integral conservation equations.) Note, also, that so far no approximation has been made, and if one could evaluate the flux integral exactly, one would have the

exact solution. This is, of course, impossible for the general case, but at least the source of an error is known - it is always introduced through the evaluation of the flux integral.

The computation is performed in two steps, the algorithm being of a predictor-corrector type.

In the first (predictor) step the flux integrals at the midpoints $X_{j-½}$ and $X_{j+½}$ are approximated. In the second (corrector or, conservative) step the reach-averaged values of $\langle\rho\rangle_j^{n+1}$ are computed at the grid points X_j (therefore a staggered grid must be used).

III.1.1 Approximation of fluxes

Approximation of fluxes is of the utmost importance in the Godunov method. How must one evaluate the integral for the time "reach" ($t^{n+1} - t^n$)? Godunov's idea was to use the method of characteristics to transform the temporal integration problem to a spatial integration problem at the previous time step t^n.

The case of uniform, steady water flow is considered, so that the velocity u is constant in the entire X,t plane, and thus can be taken out of the X derivative in Eq.(3.1):

(3.1a): $$\frac{\partial \rho}{\partial t} + u\frac{\partial \rho}{\partial x} = 0,$$

which can be readily cast in the form of the characteristics approach:

(3.6): $$\rho = \text{const},$$

along the characteristic (path) u = dx/dt.

It should be observed that Eq.(3.1a) is in non-conservative form (as required for the method of characteristics), and hence the computation of the fluxes is based on the non-conservative equations. However, in the final step, the grid-averaged function $\langle\rho\rangle_j^{n+1}$ is computed from Eq.(3.5), which is based on the conservative form (Eq.3.1).

In the case of a constant velocity the flux $\psi = \rho u$ is also constant along the characteristics. Therefore, for each value of the flux $\psi[\rho(x_{j+1/2}, t)]$ at the variable time t and fixed spatial point $X_{j+1/2}$, there exits some point X at the previous time level t^n (see Fig.3.2), such that:

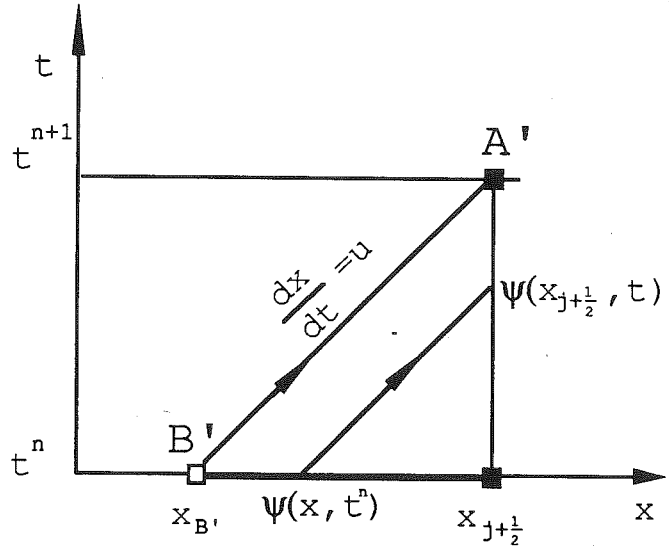

Figure 3.2 Characteristics for linear advection

(3.7): $\psi[\rho(x_{j+1/2}, t)] = \psi\{\rho[x_{j+1/2}-u(t-t^n),\ t^n]\} = \psi[\rho(x, t^n)]$.

For a uniform velocity field all characteristics are parallel straight lines, as shown in Fig.(3.2). Hence, the integral along the X axis for constant time t^n can be expressed by the integral along the t axis for fixed position $X_{j+1/2}$, using a simple change of variables :

$$(3.8): \quad \int_{t^n}^{t^{n+1}} \psi(x_{j+1/2}, t)\, dt = \begin{bmatrix} x = x_{j+1/2}-u(t-t^n) \\ dx = -u\,dt \end{bmatrix} =$$

$$= \frac{\Delta t}{x_{j+1/2}-x_{B'}} \int_{x_{B'}}^{x_{j+1/2}=x_{A'}} \psi(x, t^n)\, dx.$$

In a more general case of a non-uniform velocity field (either in time, in space, or both), the characteristics will not be parallel straight lines, so that Eq.(3.8) is not strictly applicable. Nevertheless, the characteristics are approximated as both straight and parallel, supposing that the time step is small enough to allow for this assumption.

The flux problem has not yet been solved. Since the final task is to integrate the fluxes of Eq.(3.8) over the interval $X_{B'}, X_{j+1/2}$, one needs to know the values of the

continuous function $\psi(\rho(x,t^n)) = \psi(x)$ on the interval (which is, for the case of a uniform velocity field, equivalent to knowing the function $\rho(x,t^n)$). Consequently, one has to reconstruct the distribution of the function $\rho(x,t^n)$ from the known grid-averaged values $\langle\rho\rangle_j^n$.

Recovery of the function $\rho(x,t^n)$ from its previously computed interval average $\langle\rho\rangle_j^n$ is extremely important; it is the point where the accuracy of the method is obtained, or lost.

Originally, Godunov used a constant function i.e. $\psi(x,t^n) = \langle\psi\rangle_j^n$, leading to an upwind difference scheme which is unsatisfactory with regard to numerical damping. Van Leer (1979) introduced linear interpolation, which yields a second-order accurate scheme. Finally, Woodward and Colella (1984) introduced a piecewise parabolic interpolation (PPM) which proved to be third-order accurate and showed very good behavior, in particular for the treatment of discontinuities.

III.2 Interpolation procedure (PPM)

To obtain the continuous function on the interval $X_{j-½} < X < X_{j+½}$ which is needed for the integration of fluxes,

a piecewise parabolic interpolation (PPM) is used. In what follows, a brief account of the PPM, which is necessary for understanding further development of the method, is presented. A detailed description of the interpolation procedure is given in Appendix A.

The goal is to obtain a piecewise monotonic function, whose integral over the computational reach ($X_{j-½}$, $X_{j+½}$) equals the known grid-averaged value $\langle\psi\rangle_j^n$ multiplied by the length of the interval. In addition, some modifications are introduced to provide a good representation of discontinuities.

A second-order polynomial, the coefficients of which are obtained through the integral conditions (see Appendix A), is used for approximation. The resulting expression is:

$$(3.9): \qquad \psi(x) \doteq \psi_{L,j} + \frac{x - x_{j-½}}{\Delta x_j}\left[\Delta\psi_j + \psi_{6,j}\left(1 - \frac{x - x_{j-½}}{\Delta x_j}\right)\right],$$

where:

$$(3.10): \qquad \Delta\psi_j = \psi_{R,j} - \psi_{L,j} \quad , \text{ and,}$$

$$(3.11): \qquad \psi_{6,j} = 6\left[\psi_j - \frac{(\psi_{R,j} + \psi_{L,j})}{2}\right].$$

The values at the left and right limits of the reach, $\psi_{L,j}$ and $\psi_{R,j}$, are obtained from another interpolation, based again on the integral condition. An auxiliary integral function of the variable $\psi(x)$ is approximated by a quartic polynomial, and then differentiated at the appropriate point ($X_{j+½}=X_{R,j}$ or $X_{j-½}=X_{L,j}$) to obtain the desired limit values $\psi_{L,j}$ and $\psi_{R,j}$ (Appendix A).

To avoid artificial oscillations of the results, and to improve representation of discontinuities, modifications of the algorithm are introduced, the most important one being Van Leer's monotonicity procedure (see Colella and Woodward, 1984). Monotonicity is obtained by not allowing values at the midpoints $\psi^n_{j+½}$ to overshoot adjacent reach-average values $\langle\psi\rangle^n_j$ and $\langle\psi\rangle^n_{j+1}$. This principle results in a modified expression ($\delta_m\psi_j$) for the differences $\delta\psi^n_j \equiv \delta\psi_j$ (see Appendix A):

$$(3.12): \qquad \delta_m\psi_j = \begin{cases} \min(|\delta\psi_j|, 2|\psi_{j+1}-\psi_j|, 2|\psi_j-\psi_{j-1}|) * \operatorname{sgn}\delta\psi_j, \\ \qquad\qquad if\ (\psi_{j+1}-\psi_j)(\psi_j-\psi_{j-1}) > 0 \\ 0 \qquad\qquad if\ (\psi_{j+1}-\psi_j)(\psi_j-\psi_{j-1}) \le 0 \end{cases},$$

where the factor 2, multiplying the absolute values of $|\psi_{j+1}-\psi_j|$ and $|\psi_j-\psi_{j-1}|$, is adopted to ensure that the modification takes place only when $\langle\psi\rangle_j^n$ is very close to either ψ_{j-1} or ψ_{j+1}.

In the vicinity of shocks the algorithm is further modified to produce a narrower discontinuity profile, without creating overshoots or undershoots.

III.3 Explicit scheme for linear advection

Once the unknown flux functions $\psi(x,t^n)$ have been obtained through interpolation, one can integrate them in Eq.(3.8), and hence solve the conservation Eq.(3.5) for the grid-averaged function $\langle\rho\rangle_j^n$. The following notation is introduced for convenience (see Fig.3.3):

(3.13): $$\overline{\psi}_{j+\frac{1}{2}}^{n+\frac{1}{2}} = \frac{1}{B'F}\int_{XB'}^{X_{j+\frac{1}{2}}} \psi^n(x)\,dx. \quad ,$$

so that the conservation Eq.(3.5) can be rewritten as:

(3.14): $$\langle\rho\rangle_j^{n+1} = \langle\rho\rangle_j^n - \frac{\Delta t}{\Delta X_j}\left(\overline{\psi}_{j+\frac{1}{2}}^{n+\frac{1}{2}} - \overline{\psi}_{j-\frac{1}{2}}^{n+\frac{1}{2}}\right).$$

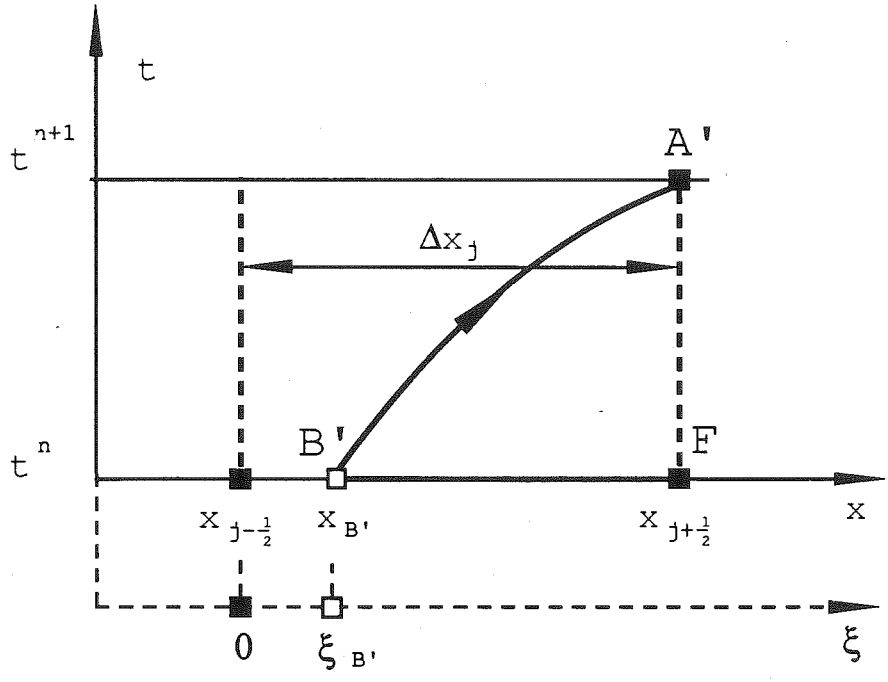

Figure 3.3 Locating the foot of the characteristic

The integrand $\psi(x, t^n)$ in Eq.(3.13) is a known polynomial function Eq.(3.9), obtained through the PPM interpolation (as described in the previous section). Therefore, to obtain the time-averaged flux $\overline{\psi}^{n+1/2}_{j+1/2}$ one needs first to determine the lower limit of integration, that is, to calculate the position $X_{B'}$ of the foot of the characteristic (Fig.3.3), and then to perform the integration in Eq.(3.13).

Determining the location of the foot of the characteristic is a trivial problem for the case of a uniform velocity field, but when velocities change in time or in space (or both) one needs to integrate the trajectories u(x,t)=dx/dt in order to obtain the point of an intersection (the foot B'):

$$(3.15): \qquad X_{j+1/2} - X_{B'} = \int_{t^n}^{t^{n+1}} u(x, t)\, dx.$$

To evaluate the integral of Eq.(3.15) the trapezoidal rule is used:

$$(3.16): \qquad X_{j+1/2} - X_{B'} = \frac{\Delta t}{2} \left(u_{B'} + u^{n+1/2}_{j+1/2}\right),$$

where $u_{j+1/2}$ is known and $u_{B'}$ is to be obtained through linear interpolation as:

$$(3.17): \qquad u_{B'} = u_j^n + \frac{X_{B'} - X_j}{\Delta X_j} \delta u_j$$

where the velocity difference δu_j is computed by the same monotonicity procedure used for $\delta_m \psi_j$ Eq.(3.12). Finally, the value of $X_{B'}$ is expressed from Eqs.(3.16) and (3.17) as:

$$(3.18): \qquad X_{B'} = \frac{1}{1 + \frac{\Delta t}{\Delta X_j} \frac{\delta u_j}{2}} \left\{ X_{j+1/2} + \frac{\Delta t}{\Delta X_j} \frac{\delta u_j}{2} X_j - \frac{\Delta t}{2} \left(u_{j+1/2}^{n+1/2} + u_j^n \right) \right\}$$

After locating the foot of the characteristic $X_{B'}$, one can easily integrate Eq.(3.13). A change of variables is used to facilitate the integration:

$$(3.19): \qquad \xi = X - X_{j-1/2}.$$

With this, the interpolation function for $\psi(x)$ (Eq.3.9) is substituted into Eq.(3.13), yielding the flux

integral:

$$(3.20): \qquad \overline{\Psi}^{n+1/2}_{j+1/2} = \frac{1}{\Delta X_j - \xi_{B'}} \left\{ \Psi^n_{L,j} (\Delta X_j - \xi_{B'}) + \right.$$
$$\left. + \frac{\Delta\Psi^n_j + \Psi^n_{6,j}}{2\Delta X_j} (\Delta X_j^2 - \xi_{B'}^2) - \frac{\Psi_{6,j}{}^n}{3} \frac{\delta X_j^3 - \xi_{B'}^3}{\Delta X_j^2} \right\}.$$

To summarize the entire procedure:

1. First the velocity gradients $\delta u_j \equiv \delta u_j^n$ and δu_j^{n+1} are computed, using a monotonicity procedure equivalent to Eq.(3.12), and the velocity $u^{n+1}_{j+1/2}$ is linearly interpolated between the points "j" and "j+1";
2. Then $X_{B'}$ is computed using Eq.(3.18);
3. The time-averaged flux $\overline{\Psi}^{n+1/2}_{j+1/2}$ at the midpoint $X_{j+1/2}$ is obtained from Eq.(3.20);
4. The flux $\overline{\Psi}^{n+1/2}_{j-1/2}$ at the midpoint $X_{j-1/2}$ is retrieved (since it has been already computed for the previous interval); and
5. The reach-averaged $\langle\rho\rangle^{n+1/2}_j$ is finally computed from the conservation Eq.(3.14).

III.4 Von-Neumann stability analysis

A Von Neumann stability analysis has been performed for the case of uniform flow velocity (u=const) and uniform spatial step ΔX_j = const. With u and ΔX_j constant, and the Courant number Cr defined as $Cr = u\frac{\Delta t}{\Delta x}$, the expression for $\langle\rho\rangle_j^{n+1}$ becomes:

$$
\begin{aligned}
(3.21): \quad \langle\rho\rangle_j^{n+1} = {} & \rho_{j-3}\left\{-\frac{Cr}{12}(Cr-1)\right\} + \\
& + \rho_{j-2}\left\{\frac{2}{3}Cr^2(Cr-1) - \frac{Cr}{12}[Cr(Cr-2)]\right\} + \\
& + \rho_{j-1}\left\{\frac{2}{3}Cr[1+Cr(Cr-2)] + 3Cr^2\left(1-\frac{2}{3}Cr\right)\right\} + \\
& + \rho_j\left\{1 - \left[\frac{2}{3}Cr^2(Cr-1) + 3Cr^2\left(1-\frac{2}{3}Cr\right)\right]\right\} + \\
& + \rho_{j+1}\left\{\frac{Cr^2}{12}(Cr-1) - \frac{2}{3}Cr[1+Cr(Cr-2)]\right\} + \\
& + \rho_{j+1\frac{1}{2}}\left\{\frac{Cr}{12}[1+Cr(Cr-2)]\right\},
\end{aligned}
$$

where $\langle\rho\rangle_j^n \equiv \rho_j$ are concentrations at the previous time step t_n (refer to Fig.3.1). The numerical solution is then expressed in terms of a Fourier series:

$$
(3.22): \qquad \rho_j^{n+1} = \sum_m A_m \, e^{-i\beta_m(n+1)\Delta t} \; e^{i\vartheta_m(j)\Delta x},
$$

where A_m is an amplitude, and β_m and σ_m are time and spatial frequencies of m-th Fourier component. Since Eq.(3.21) is linear, stability analysis can be focused on one component only, $(\rho_j^n)_m$:

$$(3.23): \quad (\rho_j^n)_m = A_m \, e^{-i\beta_m (n)\Delta t} \; e^{i\hat{\sigma}_m (j)\Delta x}$$

After introducing Eq.(3.23) into Eq.(3.21) and rearranging one obtains:

$$(3.24): \quad e^{-i\beta_m \Delta t} = e^{-3i\alpha}\left\{-\frac{Cr^2}{12}(Cr-1)\right\} + e^{-2i\alpha}\left\{\frac{Cr(Cr-1)}{12}(7Cr+1)\right\} +$$
$$+ e^{-i\alpha}\left\{\frac{Cr}{3}(2+5Cr-4Cr^2)\right\} + \left\{1-\frac{Cr^2}{3}(7-4Cr)\right\} +$$
$$+ e^{i\alpha}\left\{\frac{Cr(Cr-1)}{12}(8-7Cr)\right\} + e^{2i\alpha}\left\{\frac{Cr}{12}(Cr-1)^2\right\},$$

where:

$$\alpha = \hat{\sigma}_m \Delta x$$

The amplification factor and the phase error, and consequently amplitude and phase portraits R1 and R2, are obtained from Eq.(3.24). (The R1 and R2 coefficients are the ratios of amplification factor and celerities between the

numerical and analytical solutions for a particular Fourier component (Eq.3.23). For detailed explanation see Abbott,1979 or Cunge et al.,1980.) Plots of those useful indicators of stability, numerical damping and phase error for the Godunov and the Holly-Preissmann (fourth-order) schemes are compared in Fig.(3.4).

As for most explicit schemes, stability requires limitation of the value of the Courant Number. For the explicit Godunov scheme the critical Courant number is Cr=1.5, which is a larger value than the usual one of unity (Cr=1.0). This is the result of using a larger number of points in the PPM interpolation, which, for the case of larger Courant numbers (but not larger than Cr=1.5), enables successful extrapolation, when the feet of the characteristics fall outside of the interpolation domain.

Amplitude and phase portraits (Fig.3.4a) show good behavior of the Godunov scheme, though the Holly-Preissmann method has significantly better performance for dimensionless wavelengths (wavenumbers $L_m/\Delta x$, where L_m is a wavelength) less then five. For wavenumbers above six (and Courant number below unity) numerical damping is insignificant for both schemes. Similar Godunov scheme behavior can be observed for the phase-error (Fig.3.4b). For the Holly-Preissmann scheme the phase-error is

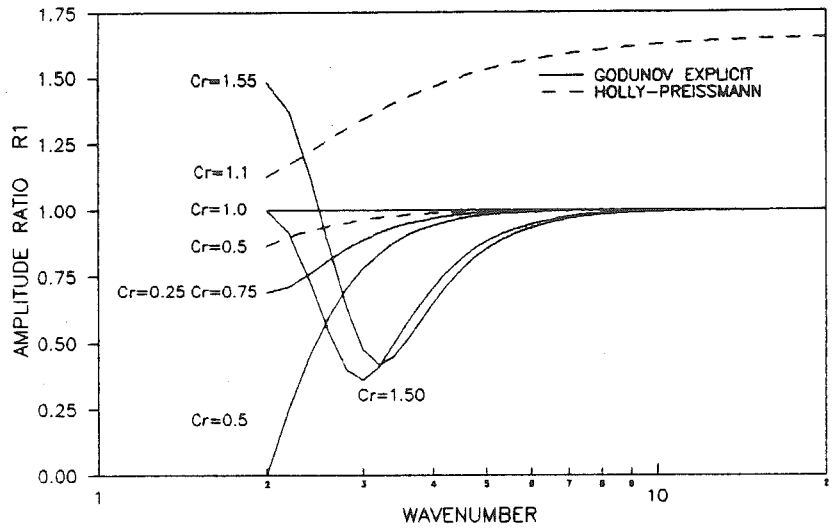

a. Amplitude portrait

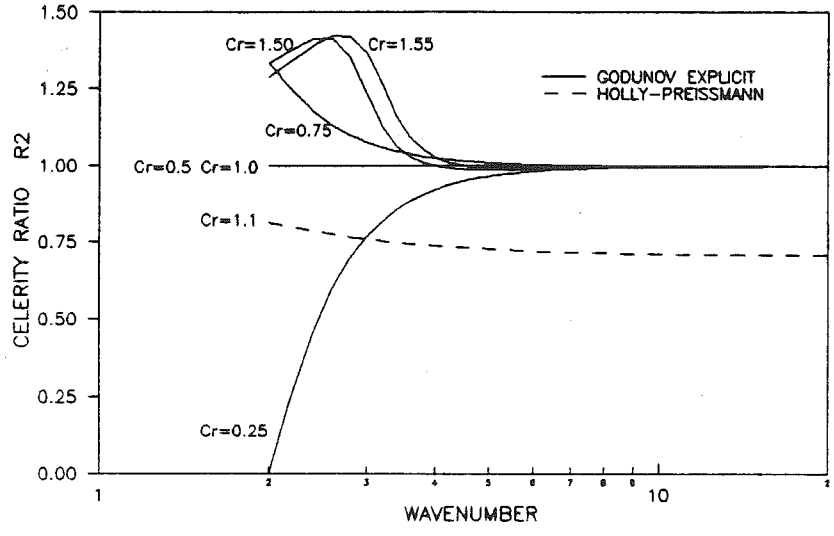

b. Phase portrait

Figure 3.4 Amplitude and phase portraits for the explicit Godunov and Holly-Preissmann fourth-order schemes

imperceptible in the stable range.

III.5 Implicit scheme for linear advection

As has been shown by the Von Neumann analysis in the previous section, the explicit Godunov scheme becomes unstable for values of the Courant number greater than 1.5. To be able to compute for values of Courant number greater than 1.5, Fryxell et al. (1986) developed an implicit scheme, requiring an entirely different approach for the approximation of fluxes.

Only the main features of Fryxell's algorithm, applied to the linear advection equation, are presented in this chapter, since it has not been further used in this work for Burgers' and de St.Venant equations. As explained in the previous chapter, the relatively small time steps needed to preserve the resolution for very sharp discontinuities (Fennema and Chaudhry, 1986) compromise the main potential advantage of the implicit scheme. In addition, the results obtained with Fryxell's implicit algorithm show significant numerical diffusion compared with the explicit method (Figs.3.8 - 3.11). Still, the implicit scheme is briefly presented here because of potential future developments, in which it might be implemented to speed up the computation after a sharp discontinuity has already been smeared by resistance effects. A detailed development of the scheme is

presented in Appendix B.

In the Fryxell implicit algorithm characteristics are used to convey information from the grid-point section X_j at some time t to the midpoint section $X_{j+½}$ at time t^{n+1} (see Fig.3.5). To improve the performance of the solution an intermediate time level "n+½" is introduced, and accordingly another characteristic AB (Fig.3.5) issuing from the midpoint level.

In the first step the conservation Eq.(3.5) is used to relate the unknown grid-averaged concentrations $\langle\rho\rangle_j^{n+½}$ and $\langle\rho\rangle_j^{n+1}$ to the fluxes $\overline{\Psi}_{j+½}^{n+½}$ and $\overline{\Psi}_{j+½}^{n+1}$:

$$(3.25): \qquad \langle\rho\rangle_j^{n+1} = \langle\rho\rangle_j^n - \frac{1}{\Delta x_j}\left[\Psi_{j+½}^{n+½} - \overline{\Psi}_{j-½}^{n+½}\right],$$

$$(3.26): \qquad \langle\rho\rangle_j^{n+½} = \langle\rho\rangle_j^n - \frac{1}{\Delta x_j}\left[\frac{3}{4}\left(\Psi_{j+½}^{n+½} - \overline{\Psi}_{j-½}^{n+½}\right) - \frac{1}{4}\left(\overline{\Psi}_{j+½}^{n+1} - \overline{\Psi}_{j+½}^{n+1}\right)\right],$$

where the coefficients 3/4 and 1/4 come from the time interpolation (see Appendix B).

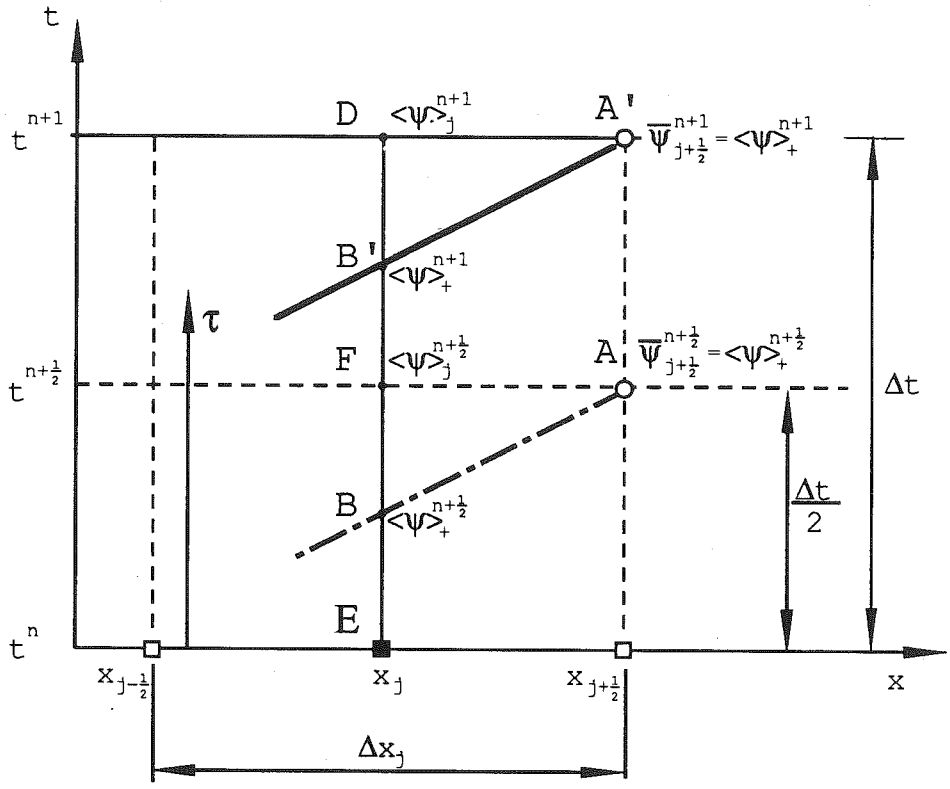

Figure 3.5 Implicit Godunov scheme

In the next stage the flux functions $\overline{\Psi}_{j+\frac{1}{2}}^{n+\frac{1}{2}}$ and $\overline{\Psi}_{j+\frac{1}{2}}^{n+1}$ are expressed in terms of the grid-averaged functions $\langle\psi\rangle_j^n$, $\langle\psi\rangle_j^{n+\frac{1}{2}}$ and $\langle\psi\rangle_j^{n+1}$, using the method of characteristics to transfer information from the line ED to line AA'.

Finally, the expressions for the fluxes are substituted into the relations for the concentrations Eqs.(3.25) and (3.26), which, in the case of uniform flow, results in a system of two linear equations in two unknowns $\langle\rho\rangle_j^{n+\frac{1}{2}}$ and $\langle\rho\rangle_j^{n+1}$.

Stability analysis for the implicit scheme, performed by Fryxell et al (1986), shows that the implicit method is unconditionally stable for Courant numbers greater than unity, while it is unstable for values of the Courant number less than unity (in which case the explicit scheme must be used). The amplitude and phase portraits for the implicit and explicit Godunov schemes are compared in Fig.(3.6). The analytical solution is obtained for both implicit and explicit approaches for a Courant number of unity, since in that case the coefficients R1 and R2 are equal to unity for the entire range of dimensionless wavelengths. Both amplitude and phase errors are much larger for the implicit scheme. The errors increase with the Courant number, and

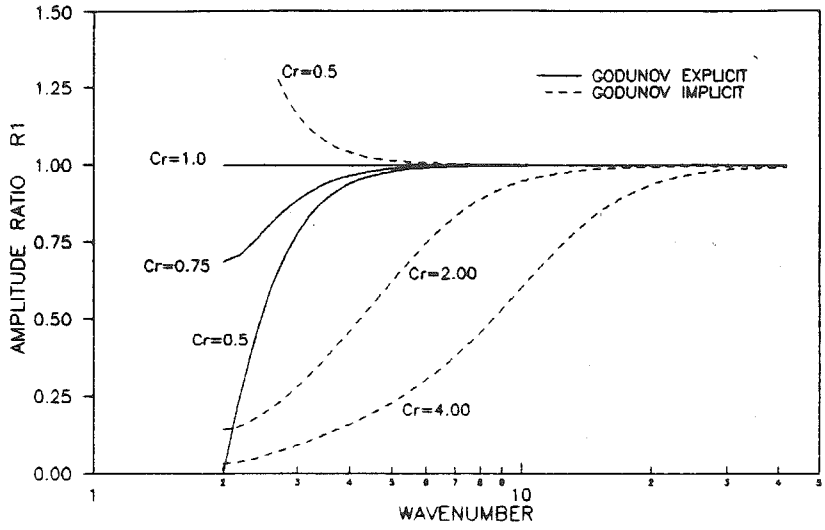

a. Amplitude portrait

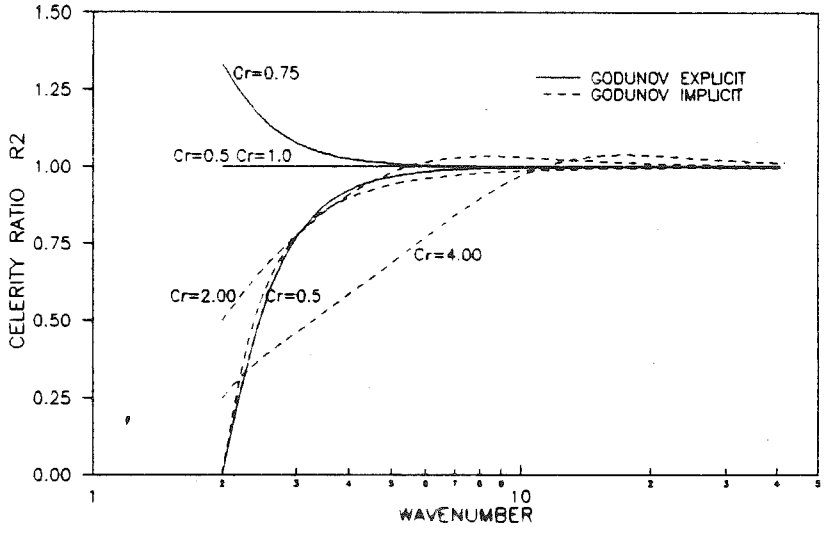

b. Phase portrait

Figure 3.6 Amplitude and phase portraits for the explicit and implicit Godunov schemes

they persist for rather large values of wavenumbers (up to 50 for a Courant number of four). Therefore one can anticipate both large numerical damping and oscillations for the implicit scheme, and this is conformed in test computations described in the following section.

III.6 Test computations for linear advection

The previously described algorithms have been incorporated in a computer code and tests performed in order to assess the performance of the proposed Godunov method, and compare it with methods currently used for pure advection. For comparison the Holly-Preissmann fourth- and sixth-order methods are chosen, both being very accurate methods for advection problems. Particular attention is devoted to examples with steep fronts, because the method is supposed to give good performance for discontinuities, and as such is taken as a possible candidate for a new generation of open-channel steep-front solvers.

Results of the computations are presented in Figures (3.7)-(3.11). First, an example with a continuous initial condition of Gaussian shape, with no influx at the boundary, is considered; then the case of a steep front discontinuity is tested. For all cases, tests for Cr=1 reproduced the exact solution.

The first (continuous) case is taken from Holly and Preissmann (1977). Pure advection in an infinitely long channel of unit width and constant advection velocity u=0.5 m/s is considered. A zero flux of contaminant is introduced through the (upstream) boundary. The initial condition is given as a Gaussian curve with standard deviation σ=264m and a mean concentration of ten units. The computational grid is uniform in space with a spatial step of dx = 200 m. The computational time is t_{END} =9600 s, and the Courant number is varied by changing the time step.

Results of computations for the explicit Godunov method for Courant numbers Cr=0.25 and Cr=0.75 are presented in Fig.(3.7). The peak concentration error is approximately 10% for Cr=0.75, while in case of Cr=0.25 the error increases to about 18%. Phase shift (observed through the location of the peak), though present, does not appear to be significant. This reasonably good amplitude and phase preservation might have been expected from the small damping of the majority of the Fourier components as shown in Fig.(3.4). Negative concentrations are obtained for both tests; in the case of Cr=0.25 they are not insignificant. (The monotonicty algorithm which controls over/undershooting, was not used for this computation in order to preserve the angularity of the solution.) The larger negative concentrations for the Courant number of

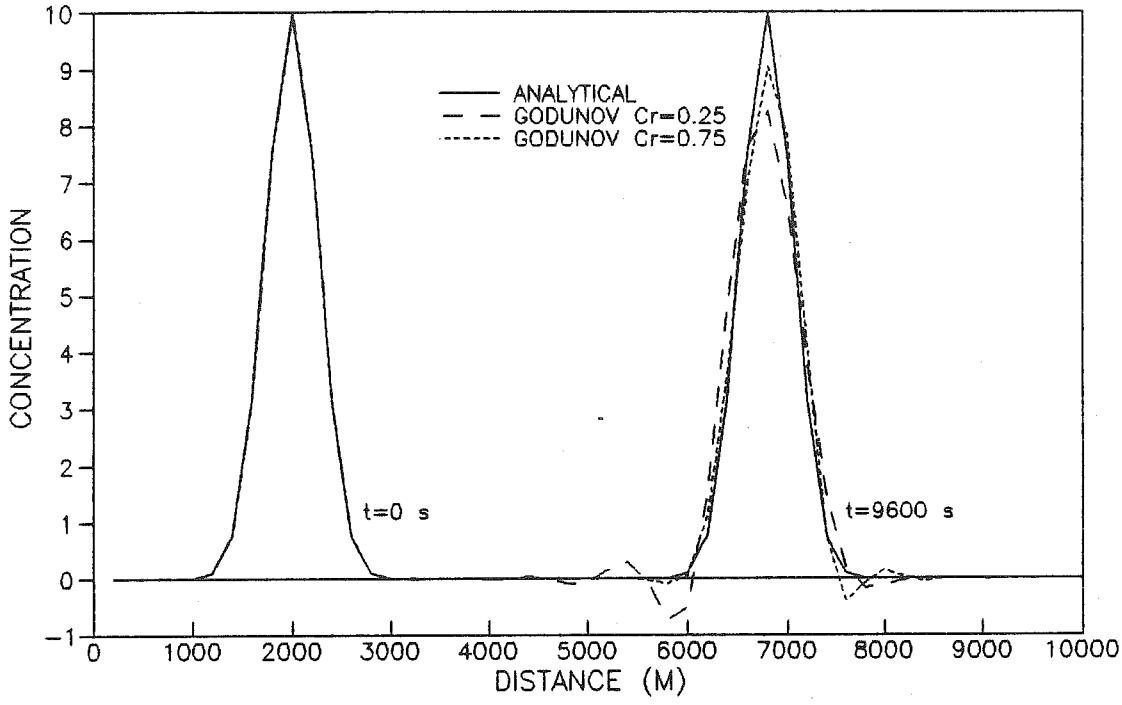

Figure 3.7 Linear-advection equation solved with the explicit Godunov method, Gaussian initial condition; comparison for different Courant numbers

0.25 reflect the larger phase error.

Comparison of the Godunov and Holly-Preissmann fourth-order schemes for Courant number Cr=0.5, given in Fig.(3.8), shows moderate advantages of the latter method. Both amplitude errors and negative concentrations (undershoots) are less in the Holly-Preissmann method, which was expected from the amplitude/phase-error analysis (Fig.3.4). The same trend is observed for other Courant numbers. The sixth-order Holly-Preissmann method gives even better results; the deviations from the exact solution are visually undetectable.

The implicit Godunov scheme was tested for the same data with Courant numbers Cr=2 and Cr=4 (Fig.3.9). The performance worsened significantly compared to the explicit algorithm; for larger values of Courant number numerical diffusion practically ruins the computations - an outcome predicted by the analysis of the amplitude/phase portraits (Fig.3.6).

In the second test case a moving steep discontinuity in concentration is considered. The grid spacing, advection velocity, and computational time are the same as in the first example. The upstream boundary condition is now $\rho(1)=10$ units. The initial condition is given as a steep

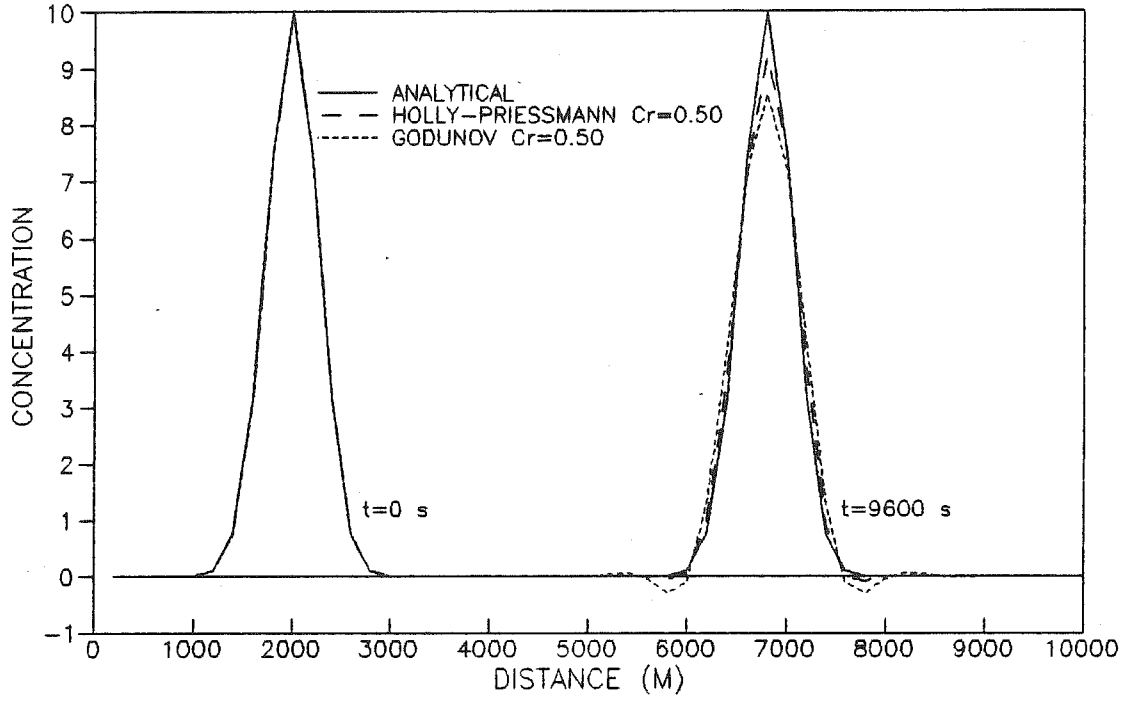

Figure 3.8 Linear-advection equation solved with the explicit Godunov method, Gaussian initial condition; comparison with the Holly-Preissmann fourth order method

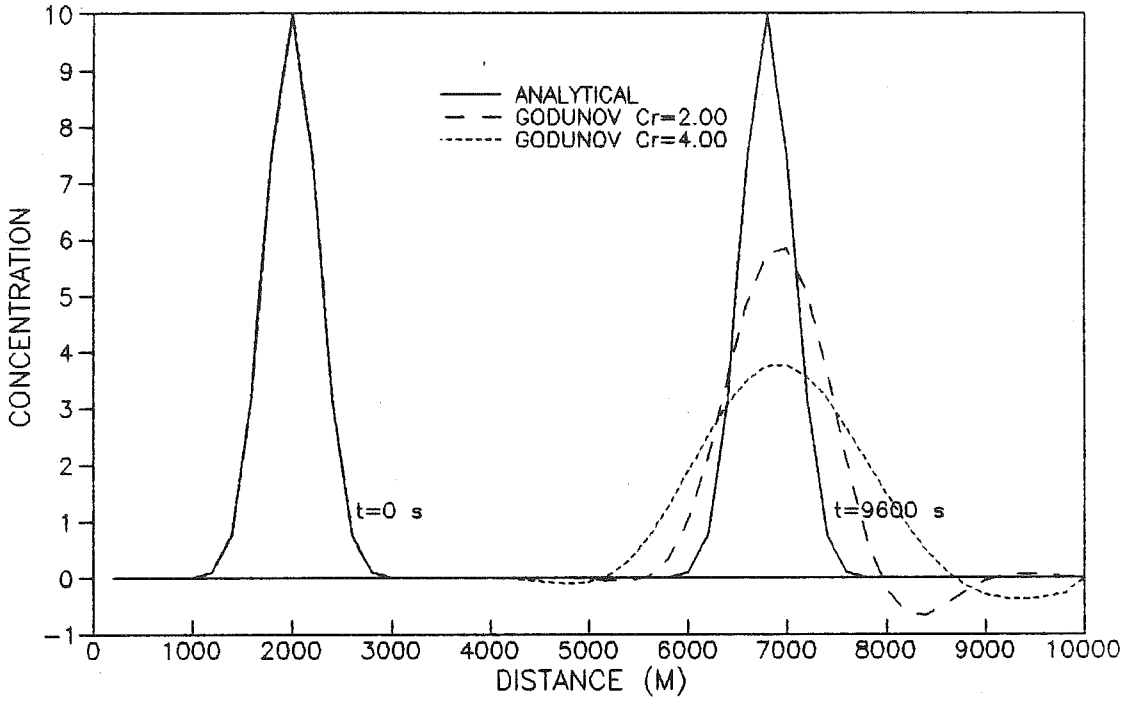

Figure 3.9 Linear-advection equation solved with the implicit Godunov method, Gaussian initial condition; comparison for different Courant numbers

front with the concentration on the upstream side of the front equal to the boundary concentration $\rho=10$ units, and the concentration $\rho=1$ unit on the downstream side.

In Fig.(3.10) the explicit Godunov scheme is compared with the fourth-order Holly-Preissmann scheme for Courant number Cr=0.5. Here the Godunov scheme performs slightly better. The monotonicity algorithm in the Godunov method assures that there is no overshoot and undershoot, and for most of its length the discontinuous front is reproduced well.

Comparison between the Holly-Preissmann and Godunov implicit schemes is shown in Fig.(3.11). The implicit scheme, though performing much better than for the Gaussian example, is still by far the worst. In addition to significant diffusion of the front, large undershoots occur. This is due to the fact that for the implicit method the monotonicity device is not implemented, and the phase-error is significant even for large wavenumbers (Fig.3.6). (The monotonicity algorithm is not developed for the implicit scheme, since the huge numerical damping and phase error have already compromised the approach, and it was considered that the time needed to develop a monotonicity algorithm would not be justified.)

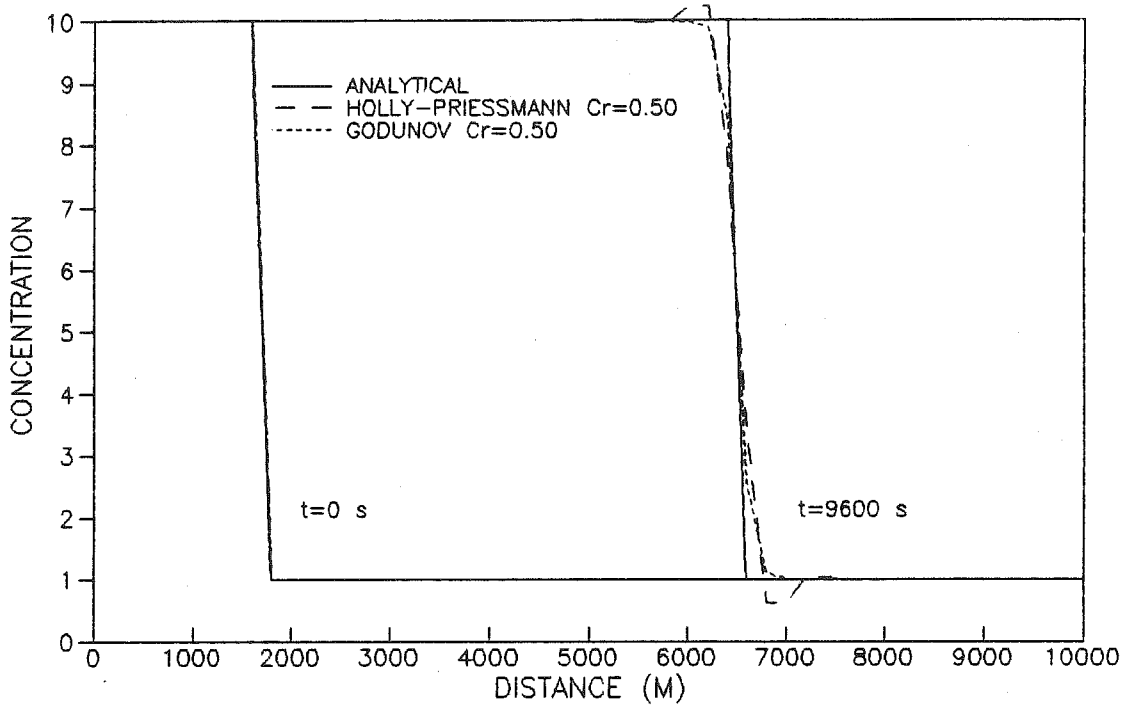

Figure 3.10 Linear-advection equation solved with the explicit Godunov method, Steep-front initial condition; comparison with the Holly-Preissmann fourth-order method

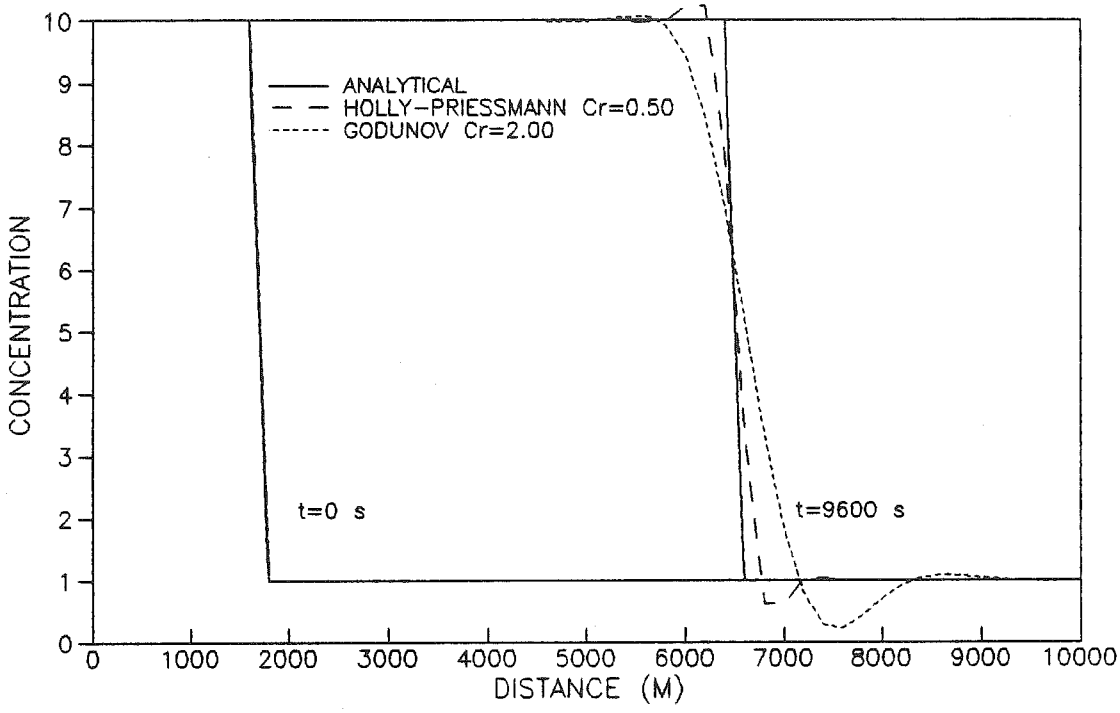

Figure 3.11 Linear-advection equation solved with the implicit Godunov method, Steep-front initial condition; comparison with the Holly-Preissmann fourth-order method

Almost perfect mass conservation is observed for all explicit Godunov computations, relative errors being less then 10^{-13} . The implicit scheme was less conservative, presumably due to errors in the temporal interpolation.

Test cases with variable grid size also have been performed, as well as computations with a nonuniform velocity field. They all showed, in general, the same type of performance (same trend in numerical diffusion, oscillations, stability and conservation properties) as the runs with constant grid size and uniform velocity field.

In summary, the linear-advection test computations have shown that the explicit Godunov scheme gives very good performance, particularly for the case of a steep-front discontinuity. Both conservation properties and spatial resolution of the front were good.

The implicit algorithm, however, gives excessively diffusive and far less conservative results, hence further research is needed to try to improve it's performance. Given the implicit method's large diffusion, complexity of the algorithm, and the fact that relatively small time steps are needed to resolve very sharp discontinuities (Fennema and Chaudhry, 1986), it is not further considered in this work.

III.7 Development of the Godunov algorithm and test computations for Burgers' equation

The goal here is to assess the performance of the Godunov method for nonlinear scalar equations, in particular Burgers' equation (Burgers, 1948). Since the main features of the scheme are the same as for the linear-advection case, in what follows only the important differences are pointed out.

Burgers' equation is a first-order nonlinear (or, in some definitions, quasi-linear) partial-differential advection equation. Its nonlinearity (advection velocity is itself the transported scalar quantity) makes Burgers' equation more similar to the flow equations than to the previously considered linear-advection equation. The homogenous equation is usually written in the form:

$$(3.27): \qquad \frac{\partial u}{\partial t} + u\frac{\partial u}{\partial x} = 0,$$

or in conservative form as:

$$(3.28): \qquad \frac{\partial u}{\partial t} + \frac{\partial}{\partial x}[F(u)] = 0, \quad F=\frac{u^2}{2}$$

As in the case of linear-advection, the conservative Burgers' Eq.(3.28) is integrated in space between the midpoints $X_{j+½}$ and $X_{j-½}$, and in time between levels t^n and t^{n+1} (Fig.3.1):

$$(3.29): \quad \langle u\rangle_j^{n+1} - \langle u\rangle_j^n + \frac{1}{\Delta x_j}\int_{t^n}^{t^{n+1}} [F(u(x_{j+½},t)) - F(u(x_{j-½},t))]\,dt = 0,$$

where $\langle u\rangle_j^n$ and $\langle u\rangle_j^{n+1}$ are grid averages defined as in the case of linear advection. Equation (3.29) is simplified as:

$$(3.30): \quad \langle u\rangle_j^{n+1} = \langle u\rangle_j^n - \frac{\Delta t}{\Delta x_j}(\bar{F}_{j+½}^{n+½} - \bar{F}_{j-½}^{n+½}),$$

where the time-averaged fluxes $\bar{F}_{j\pm½}^{n+½}$ are defined as:

$$(3.31): \quad \bar{F}_{j+½}^{n+½} = \frac{1}{\Delta t}\int_{t^n}^{t^{n+1}} F[u(x_{j+½},t)]\,dt.$$

As in the case of linear advection the flux integral

Eq.(3.31) is approximated using values from the previous time level t^{n+1}, based on the characteristics notion (Fig.3.12):

$$(3.32): \quad \overline{F}^{n+\frac{1}{2}}_{j+\frac{1}{2}} = \frac{1}{\Delta t}\int_{t^n}^{t^{n+1}} F[u(x_{j+\frac{1}{2}}, t)]\,dt = \frac{1}{\overline{BC}}\int_{x_B}^{x_{j+\frac{1}{2}}} F[u(x, t^n)]\,dx \ .$$

The integration in time for a fixed position ($X_{j+\frac{1}{2}}$ in Fig.3.12) is approximated by the integration in space, over the domain of dependence of the point A (at $X_{j+\frac{1}{2}}$ and at time t^{n+1}), for a fixed time (t^n). It should be repeated that since the flow field is not uniform, the characteristics are not straight and parallel. Therefore the Eq.(3.32) is an approximation, not an exact statement as is the case for uniform flow and linear advection.

For Burgers' equation one can analytically integrate the function $F[u(x, t^n)]$ in Eq.(3.32). For the case of the de St.Venant equations, however, such integration is impossible, due to the complexity of the integrand, and therefore the dependent variable (in this case it would be velocity u) is instead averaged:

$$(3.33): \quad \overline{u}^{n+\frac{1}{2}}_{j+\frac{1}{2}} = \frac{1}{\overline{BC}}\int_{x_B}^{x_{j+\frac{1}{2}}} u(x, t^n)\,dx$$

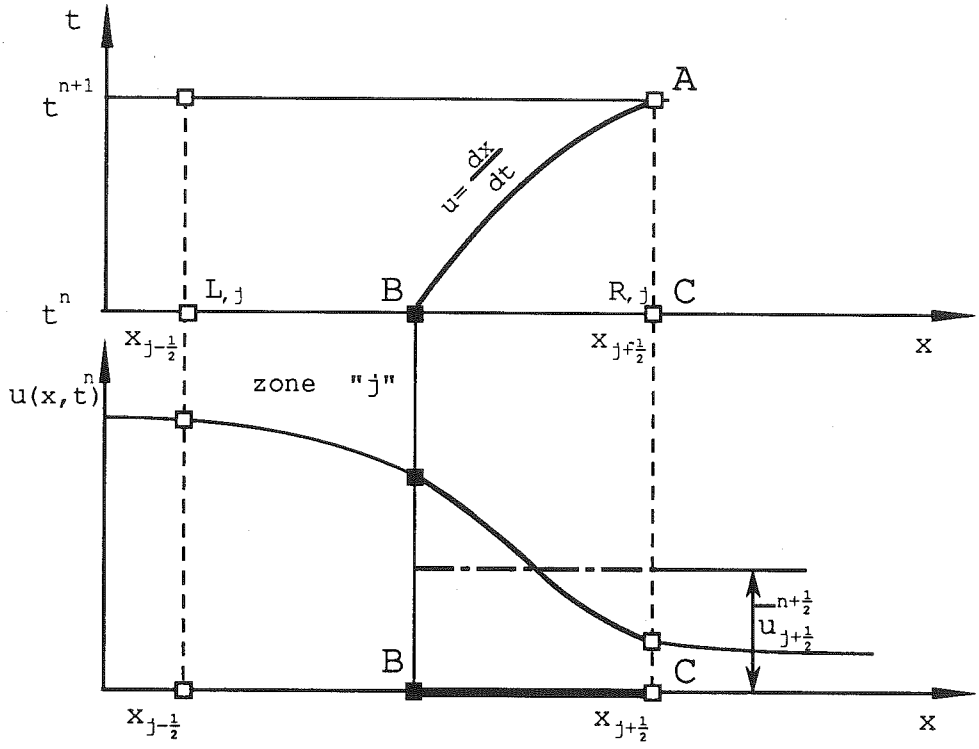

Figure 3.12 The approximation of fluxes for Burgers' equation

and the fluxes approximated as:

$$(3.34): \quad \overline{F}^{n+1/2}_{j+1/2} = F(\overline{u}^{n+1/2}_{j+1/2}) \quad .$$

Since the purpose of investigating Burgers' equation is to provide guidance for further application to the de St.Venant equations, the above procedure for flux approximation (averaging the velocities rather then the flux functions) has been adopted. The PPM interpolation procedure, described in section III.2, is used to recover the piecewise continuous functions from the grid-averages $\langle u \rangle^n_j$:

$$(3.35): \quad u(x, t^n) \equiv u^n(x) \equiv u(x) = u_{L,j} + \frac{x - x_{j-1/2}}{\Delta x_j}\left[\Delta u_j + u_{6,j}\left(1 - \frac{x - x_{j-1/2}}{\Delta x_j}\right)\right],$$

where:

$$(3.36): \quad \Delta u_j = u_{R,j} - u_{L,j}; \quad u_{6,j} = 6\left(u^n_j - \frac{u_{L,j} + u_{R,j}}{2}\right).$$

The polynomial approximation of the velocity (Eq.3.35)

is substituted into the integral Eq.(3.33) to yield the expression for the space-averaged velocity:

$$(3.37): \qquad \overline{u}_{j+\frac{1}{2}}^{n+\frac{1}{2}} = \frac{1}{1\xi_B}\left[u_{L,j}(1-\xi_B) + \frac{\Delta u_j + u_{6,j}}{2}(1-\xi_B^2) - \frac{u_{6,j}}{3}(1-\xi_B^3)\right],$$

where:

$$(3.38) \qquad \xi = \frac{x - x_{j-\frac{1}{2}}}{\Delta x_j} \quad .$$

The time-averaged fluxes $\overline{F}_{j\pm\frac{1}{2}}^{n+\frac{1}{2}}$ are then computed with time-averaged velocities $\overline{u}_{j\pm\frac{1}{2}}^{n+\frac{1}{2}}$, and finally grid-averages $\langle u \rangle_j^{n+1}$ are obtained from the conservation Eq.(3.30).

To obtain the domain of dependence of point A, the foot of the trajectory (point B in Fig.3.12) must be determined. This is accomplished by the method of characteristics. If the velocity u satisfies the characteristic equation:

$$(3.39): \qquad u = \frac{dx}{dt},$$

then the non-conservative Eq.(3.27) becomes a total differential, and consequently the velocity is constant ($u_A = u_B$) along the characteristic path described by Eq.(3.39). The characteristic Eq.(3.39) is approximated as:

$$(3.40): \quad u_B = \frac{x_{j+1/2} - x_B}{\Delta t},$$

and substituted into the polynomial expression (3.35) to yield a quadratic equation which is solved analytically as:

$$(3.41): \quad \xi_B = \frac{\Delta u_j + u_{6,j} + \frac{\Delta x_j}{\Delta t} - \sqrt{(\Delta u_j + u_{6,j} + \frac{\Delta x_j}{\Delta t})^2 - 4u_{6,j}(\frac{\Delta x_j}{\Delta t} - u_{L,j})}}{2u_{6,j}}.$$

To recapitulate the procedure:

1. The foot of the characteristic AB (Fig.3.12) is calculated from Eq.(3.41);
2. The velocity u is averaged over the domain of dependence BC using Eq.(3.37), and the time-averaged fluxes are obtained from (3.34);
3. The conservative Eq.(3.30) is solved for the grid averaged velocity $\langle u \rangle_j^{n+1}$.

Test computations for Burgers' equation show promising behavior. In Fig.(3.13) a test of discontinuous flow is presented. The initial condition is a steep front with a velocity u=10 m/s upstream and with flow at rest (u=0) downstream of the front. The upstream boundary condition is a constant velocity of u=10 m/s. The spatial step of 200 m and time step of 5 seconds yield a Courant number of Cr=0.25. (The computations for other values of the Courant number gave similar results.) After 192 time steps (the computation time was t=960 sec.) the front is still confined within one spatial step and the result is almost identical to the analytical solution (Strang,1986). The conservation of mass is excellent, with a relative error of approximately 10^{-14}. One should bear in mind that the Holly-Preissmann method, applied by Toda to Burgers' equation (Toda and Holly,1988), does not give satisfactory results.

In this chapter the modified Godunov scheme is successfully applied to scalar linear and nonlinear hyperbolic equations for both continuous and discontinuous problems. The results suggest that the method shows promise for solution of the de St.Venant equations when discontinuities are present.

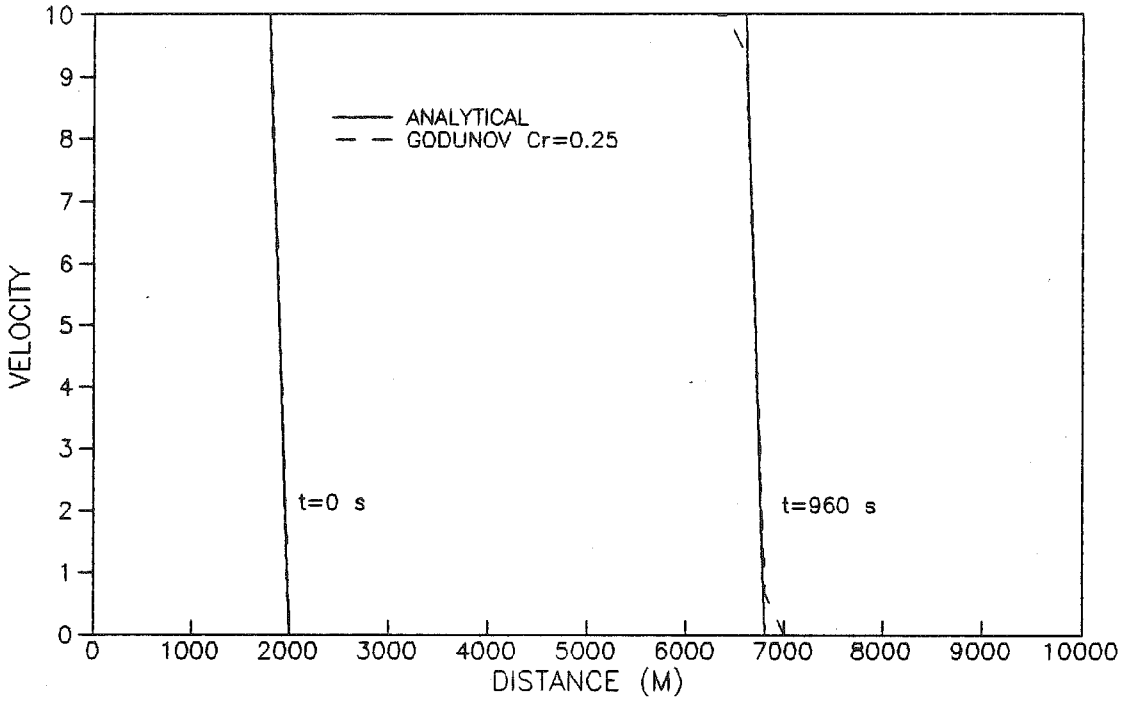

Figure 3.13 Burgers' equation solved with the Godunov method; Steep-front initial condition

CHAPTER IV. MODIFIED GODUNOV SCHEME APPLIED TO DE St.VENANT EQUATIONS

In this chapter the modified Godunov scheme is applied to the full de St.Venant equations. Of the several alternatives developed during the investigation, only two (which are suggested as the best) are presented in detail here; the most important aspects of the other examined alternatives are explained.

First the basis of the method is reviewed in the context of the differences introduced with the de St.Venant equations. Then follows a detailed explanation of the conservative step.

The most delicate issue is approximation of the fluxes. The continuous and discontinuous cases are discussed separately. For both cases the domain of dependence is determined using the characteristics approach, but in two different ways. For the continuous solution, various options of averaging the flux variables in time are considered; those giving good results are presented in more detail. For the discontinuous solution the Riemann solver is applied to the flow equations, with Stoker's solution used for initiation of dam-break type computations.

Finally, treatment of the boundary conditions by the method of characteristics is described, as well as the procedure close to the boundaries where there are not enough points to permit application of the PPM interpolation.

A simplified channel geometry is chosen for the analyses. Again, one should bear in mind that the goal of this work is to develop a method; practical models for natural channel geometry will be developed in the future, provided the method shows promising results.

IV.1 Conceptual basis

There are significant differences in treatment of the scalar equations, considered in the previous chapter, and the de St.Venant equations. New challenges arise from the need to deal with a set of two equations; two streams of information are needed to provide good estimates of the flux functions. This deprives one of the opportunity for exact analytical integration for the computation of fluxes offered by the scalar equations, but in all other respects the ideas of the Godunov method, as explained in the previous chapter, can be successfully implemented.

The de St.Venant equations are presented in the literature review of chapter II. The continuity equation, momentum equation, and the compact matrix form are:

(2.3): $$\frac{\partial A}{\partial t} + \frac{\partial Q}{\partial x} = 0,$$

(2.4): $$\frac{\partial Q}{\partial t} + \frac{\partial}{\partial x}(Qu+gI_1) = gA(S_o-S_f) + gI_2,$$

(2.5): $$\frac{\partial U}{\partial t} + \frac{\partial}{\partial x}[F(u)] = G(U,x,t),$$

where:

(2.5a): $$U=[A,Q]^T,\ F(U)=[Q,Qu+gI_1]^T,$$
$$G(U,x,t)=[0,gA(S_o-S_f)+gI_2]^T.$$

For the case of a rectangular channel, the above equations can be rewritten as:

(4.1): $$\frac{\partial A}{\partial t} + \frac{\partial Q}{\partial x} = 0,$$

(4.2): $$\frac{\partial Q}{\partial t} + \frac{\partial}{\partial x}(Qu+gB\frac{h^2}{2}) = gA(S_o-n^2\frac{u|u|}{R^{4/3}}) + g\frac{\partial B}{\partial x}\frac{h^2}{2},$$

where A is the wetted area, B is the width of the channel, Q is the discharge, h and u are the average depth and velocity of the cross-section, R is the hydraulic radius, g is the gravitational acceleration, n is the Manning roughness coefficient, I_1 and I_2 are the centroidal moment and the rate of its change due to the variation of cross-sectional geometry, So is the bottom slope, and Sf is the friction slope, which is expressed by the Manning equation. The expressions of the matrix Eq.(2.5) are now defined as:

(4.3): $$U=[A,Q]^T,\ F(U)=[Q,Qu+gB\frac{h^2}{2}]^T,$$

$$G(U,x,t)=[0,\ gA(S_o-n^2\frac{u\,|u|}{R^{4/3}})+g\frac{\partial B}{\partial x}\frac{h^2}{2}]^T.$$

The matrix Eq.(2.5) is integrated between times t^{n+1} and t^n, and midpoints $X_{j+½}$ and $X_{j-½}$ (Fig.4.1), as in the case of a scalar equation:

(4.4): $$\int_{t^n}^{t^{n+1}}\int_{X_{j-½}}^{X_{j+½}}\frac{\partial U}{\partial t}\,dt\,dx+\int_{t^n}^{t^{n+1}}\int_{X_{j-½}}^{X_{j+½}}\frac{\partial}{\partial x}[F(U)]\,dx\,dt=$$

$$\int_{t^n}^{t^{n+1}}\int_{X_{j-½}}^{X_{j+½}}G(U,x,t)\,dx\,dt.$$

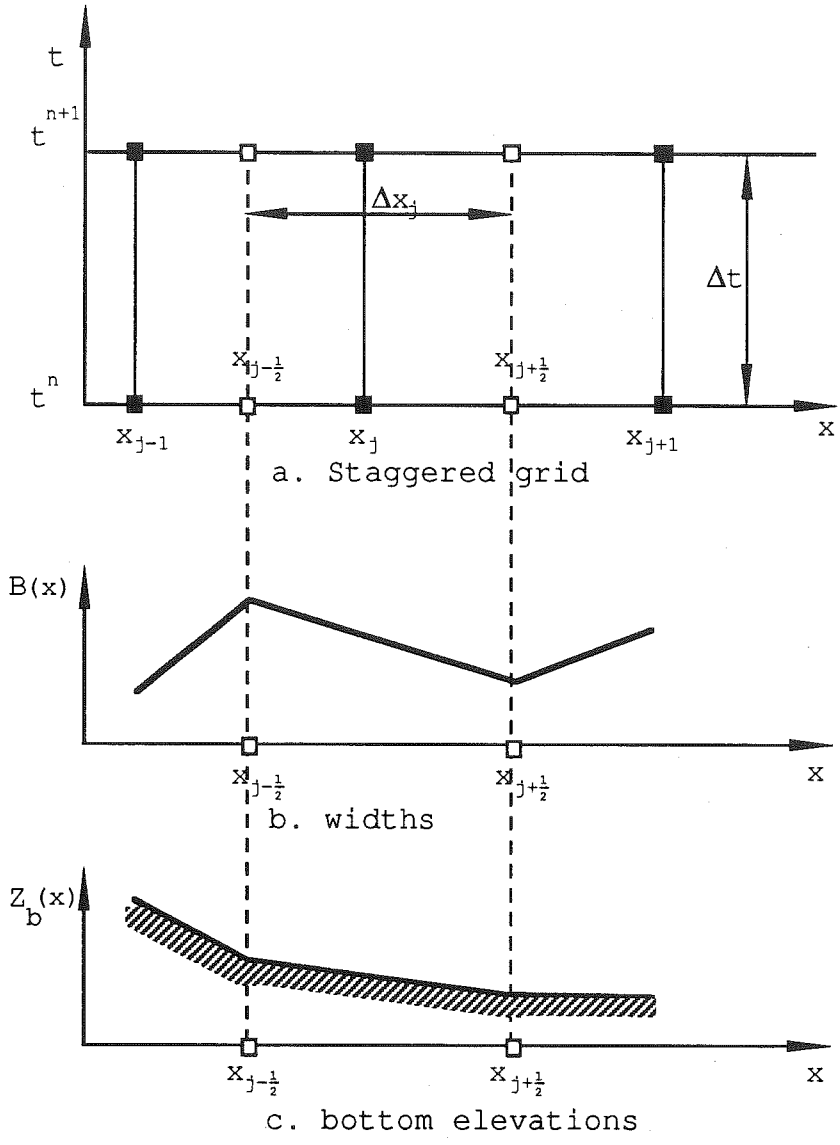

Figure 4.1 Definition sketch for de St.Venant equations

After performing exact integration in time for the first term, and in space for the second term of Eq.(4.4), and averaging the vector variable U over the reach between the midpoints $X_{j+½}$ and $X_{j-½}$, one obtains:

$$(4.5): \quad \langle U\rangle_j^{n+1} = \langle U\rangle_j^n - \frac{1}{\Delta x_j}\int_{t^n}^{t^{n+1}} \{F[U(x_{j+½}, t)] - F[U(x_{j-½}, t]\}dt +$$

$$+ \frac{1}{\Delta x_j}\int_{t^n}^{t^{n+1}}\int_{x_{j-½}}^{x_{j+½}} G(U, x, t)\, dx dt,$$

where the grid average $\langle U\rangle_j^n$ is defined as:

$$(4.6): \quad \langle U\rangle_j^n = \frac{1}{\Delta x_j}\int_{x_{j-½}}^{x_{j+½}} U(x, t^n)\, dx.$$

When the flux terms and source terms of the conservative Eq.(4.5) are expressed as:

$$(4.7): \quad \overline{F}_{j\pm½}^{n+½} = \frac{1}{\Delta t}\int_{t^n}^{t^{n+1}} F[U(x_{j+½}, t)]\, dt \ ,$$

and:

$$(4.8): \qquad \bar{G}_j^{n+1/2} = \frac{1}{\Delta t}\frac{1}{\Delta x_j}\int_{t^n}^{t^{n+1}}\int_{x_{j-1/2}}^{x_{j+1/2}} G(U,x,t)\,dxdt,$$

the grid average $\langle U\rangle_j^{n+1}$ at the time t^{n+1} can be obtained as:

$$(4.9): \qquad \langle U\rangle_j^{n+1} = \langle U\rangle_j^{n} - \frac{\Delta t}{\Delta x_j}\left(\bar{F}_{j+1/2}^{n+1/2} - \bar{F}_{j-1/2}^{n+1/2}\right) + \Delta t\,\bar{G}_j^{n+1/2}.$$

which completes the conservative step.

The approximation of the fluxes Eq.(4.7) and the source term Eq.(4.8), which is the most delicate part of the method, is described in the following section.

Since non-prismatic channels with non-uniform bottom slope are considered, the channel geometry must be defined at discrete computational points. The adopted scheme for defining geometry is presented in Fig.(4.1). The description at the midpoints, which is in spirit of the Godunov method itself, is preferred to the alternative description at the gridpoints, though the former approach introduces additional coding complications.

IV.2 Approximation of fluxes

To solve the conservative Eq.(4.9), for an unknown grid-averaged vector $\langle U \rangle_j^{n+1}$, one needs to approximate the time integral of the flux terms (Eq.4.7), and the double (time and space) integral of the source term (Eq.4.8). The approximation of the time integrals is the most sensitive part of the scheme, and the behavior of the method depends strongly upon it. The spatial integration of the source term presents no special difficulties, hence the following discussion is devoted primarily to the approximation of the time integrals - time averaging - of flux and source terms. The flux term $\overline{F}_{j+\frac{1}{2}}^{n+\frac{1}{2}}$ is taken as a representative one throughout the discussion, but the conclusions are applicable to all terms described by Eqs.(4.7 and 4.8).

Several alternatives have been examined, and those which gave good performance are presented in detail. There are two general approaches for approximation of the time integral (at the point $X_{j+\frac{1}{2}}$).

In the first approach the values of the vector U at the midpoint $X_{j+\frac{1}{2}}$ are first approximated at some point in time $t^n \le t \le t^{n+1}$, where the function F(U) is then evaluated, and numerically integrated. If the trapezium rule is used for integration one obtains:

(4.10): $$\overline{F}^{n+\frac{1}{2}}_{j+\frac{1}{2}} \doteq \frac{1}{2}\left[F(\hat{U}^{n}_{j+\frac{1}{2}}) + F(\hat{U}^{n+1}_{j+\frac{1}{2}})\right],$$

and for the Simpson rule the expression is:

(4.11): $$\overline{F}^{n+\frac{1}{2}}_{j+\frac{1}{2}} \doteq \frac{1}{6}\left[F(\hat{U}^{n}_{j+\frac{1}{2}}) + 4\,F(\hat{U}^{n+\frac{1}{2}}_{j+\frac{1}{2}}) + F(\hat{U}^{n+1}_{j+\frac{1}{2}})\right],$$

where the values with hats ($\hat{U}^{n}_{j+\frac{1}{2}}$, $\hat{U}^{n+\frac{1}{2}}_{j+\frac{1}{2}}$, $\hat{U}^{n+1}_{j+\frac{1}{2}}$) represent the approximations of the vector U at the times t^n, $t^{n+\frac{1}{2}}$, and t^{n+1}, and are computed by the method of characteristics. For both trapezium and Simpson integration this method of averaging showed considerable instability when used for strong shocks in dambreaks, and was accordingly abandoned.

In the second approach the vector U itself is "averaged" , and then the flux function is applied to the averaged vector:

(4.12): $$\overline{F}^{n+\frac{1}{2}}_{j+\frac{1}{2}} \doteq F(\overline{U}^{n+\frac{1}{2}}_{j+\frac{1}{2}}),$$

where $\overline{U}^{n+\frac{1}{2}}_{j+\frac{1}{2}}$ is some representative ("average") value of the vector U along the time of integration. It cannot be strictly thought of as the averaged value of U on the

interval t_n - t_{n+1}, since the integral of a function is not equal to the function of an integral, i.e.:

(4.13): $$\int F(U)\, dt \neq F[\int U dt] .$$

Some attempts of actual time averaging (by the trapezium and Simpson rules) were carried out, the theoretical inaccuracy of Eq.4.13 notwithstanding; it is argued that the averaging in flux-approximation might be corrected in the final conservative step. The results of these attempts were inconsistent. For prismatic channels and expansions they produced proper results, but for the case of a sudden constriction the results were completely senseless.

The approximation of the vector $\bar{U}_{j+½}^{n+½}$ is finally focussed upon as the main problem in flux approximation. Two approaches are presented here. The first approach manipulates the conveying of the Riemann invariants along the characteristics, and originated from the algorithm used by Colella and Woodward (1984) and recommended by Cunge (1988). The second approach, which is a simplified modification of the technique applied by Vila (1987), approximates the vector $\bar{U}_{j+½}^{n+½}$ with the value obtained by the method of characteristics for the mid-time $t^{n+½}$.

Because of the essential difference in treatment of continuous and discontinuous flows, each of the flow regimes is considered separately in the following sub-section.

Regardless of the approach for approximation of the vector U and the type of flow (continuous or discontinuous), once the vector $\overline{U}_{j+\frac{1}{2}}^{n+\frac{1}{2}}$ is obtained, the conservative Eq.(4.9) can be solved for the grid-averaged vector $\langle U \rangle_j^{n+1}$ as:

$$(4.14): \quad \langle U \rangle_j^{n+1} \doteq \langle U \rangle_j^{n} - \frac{\Delta t}{\Delta x_j} \left[F(\overline{U}_{j+\frac{1}{2}}^{n+\frac{1}{2}}) - F(\overline{U}_{j-\frac{1}{2}}^{n+\frac{1}{2}}) \right] + \Delta t G(\overline{U}_j^{n+\frac{1}{2}}, \overline{U}_{j-\frac{1}{2}}^{n+\frac{1}{2}}),$$

or in a developed (scalar) form as:

$$(4.15): \quad \langle A \rangle_j^{n+1} = \langle A \rangle_j^{n} - \frac{\Delta t}{\Delta x_j} \left[(\overline{u}_{j+\frac{1}{2}}^{n+\frac{1}{2}} \overline{h}_{j+\frac{1}{2}}^{n+\frac{1}{2}} B_{j+\frac{1}{2}}) - (\overline{u}_{j-\frac{1}{2}}^{n+\frac{1}{2}} \overline{h}_{j-\frac{1}{2}}^{n+\frac{1}{2}} B_{j-\frac{1}{2}}) \right],$$

for the average area $\langle A \rangle_j^{n+1}$, and:

$$(4.16):\quad \langle Q\rangle_j^{n+1} = \langle Q\rangle_j^{n} - \frac{\Delta t}{\Delta x_j}\left\{\left[(\overline{u}_{j+\frac{1}{2}}^{n+\frac{1}{2}})^2 \overline{h}_{j+\frac{1}{2}}^{n+\frac{1}{2}} B_{j+\frac{1}{2}} + g\frac{(\overline{h}_{j+\frac{1}{2}}^{n+\frac{1}{2}})^2}{2} B_{j+\frac{1}{2}}\right] - \right.$$

$$\left. - \left[(\overline{u}_{j-\frac{1}{2}}^{n+\frac{1}{2}})^2 \overline{h}_{j-\frac{1}{2}}^{n+\frac{1}{2}} B_{j-\frac{1}{2}} + g\frac{(\overline{h}_{j-\frac{1}{2}}^{n+\frac{1}{2}})^2}{2} B_{j-\frac{1}{2}})\right]\right\} +$$

$$+ \frac{g\Delta t}{2}\left[B_{j+\frac{1}{2}}\overline{h}_{j+\frac{1}{2}}^{n+\frac{1}{2}}\left(S_o - n^2\frac{\overline{u}_{j+\frac{1}{2}}^{n+\frac{1}{2}}\left|\overline{u}_{j+\frac{1}{2}}^{n+\frac{1}{2}}\right|}{(\overline{R}_{j+\frac{1}{2}}^{n+\frac{1}{2}})^{4/3}}\right)\right] +$$

$$+ \frac{g\Delta t}{2}\left[B_{j-\frac{1}{2}}\overline{h}_{j-\frac{1}{2}}^{n+\frac{1}{2}}\left(S_o - n^2\frac{\overline{u}_{j-\frac{1}{2}}^{n+\frac{1}{2}}\left|\overline{u}_{j-\frac{1}{2}}^{n+\frac{1}{2}}\right|}{(\overline{R}_{j-\frac{1}{2}}^{n+\frac{1}{2}})^{4/3}}\right)\right] +$$

$$+ \frac{g\Delta t}{2}\,\frac{B_{j+\frac{1}{2}} - B_{j-\frac{1}{2}}}{\Delta x_j}\left(\frac{\overline{h}_{j+\frac{1}{2}}^{n+\frac{1}{2}} + \overline{h}_{j-\frac{1}{2}}^{n+\frac{1}{2}}}{2}\right)^2,$$

for the averaged discharge $\langle Q\rangle_j^{n+1}$. (The bottom slope is approximated as $S_o = (Z_{b_{j+\frac{1}{2}}} - Z_{b_{j-\frac{1}{2}}})/\Delta x_j$.)

IV.2.1 Continuous solution

The procedure for approximation of the flux vector $\overline{U}_{j+\frac{1}{2}}^{n+\frac{1}{2}}$ is now presented. In both approaches for computing the approximate vector $\overline{U}_{j+\frac{1}{2}}^{n+\frac{1}{2}}$, introduced above, (conveying and averaging the Riemann invariants over the domain of dependence, or using the value from the mid-time $t^{n+\frac{1}{2}}$) the problem is based on the method of characteristics, which is therefore described in detail in the following sub-section.

IV.2.1.1 Application of the PPM method to the method of characteristics

Two algorithms for the method of characteristics are used in the present work: one based on piecewise parabolic interpolation (PPM), another on simple linear interpolation. Only the procedure based on the PPM interpolation is presented here, as it is original for open-channel flow computations. The procedure based on linear interpolation can be found in the literature (for example Liggett and Cunge,1975). The variables for interpolation will be referred to, henceforth, as a primary variables. Three combinations of the primary variables have been investigated: the area-discharge (A,Q), the velocity-depth (u,h) and the depth-discharge (h,Q) sets. The (A,Q) and (u,h) sets gave significantly more stable results then the (Q,h) alternative, which is consequently abandoned. The (A,Q) set seems to be the most natural choice, since the grid averages of area $\langle A \rangle_j^n$ and discharge $\langle Q \rangle_j^n$ are the results of the conservative step (Eqs.4.15 and 4.16), and as such are consistent with the method in general. However, for the case of very strong shocks and severe changes of the cross-sectional geometry (width), the (A,Q) combination gives unreasonable results while the (u,h) set performs well. This comes from the unnatural distortions of depths

and velocities in the (A,Q) variant (since areas and discharges are interpolated, and then depths and velocities computed from them), which in cases of sudden expansion leads to unreasonable results.

On the other hand, working with the (u,h) set one must work with further approximations $\langle h\rangle_j^n=\langle A\rangle_j^n/B_j$ and $\langle u\rangle_j^n=\langle Q\rangle_j^n/\langle A\rangle_j^n$, realizing that the integral of a product is not equal to the product of integrals,i.e:

$$(4.17): \quad \Delta x_j \langle A\rangle_j^n = \int_{x_{j-½}}^{x_{j+½}} A(x)\,dx = \int_{x_{j-½}}^{x_{j+½}} B(x)\,h(x)\,dx \neq$$

$$\neq \frac{1}{\Delta x_j} \int_{x_{j-½}}^{x_{j+½}} B(x)\,dx \int_{x_{j-½}}^{x_{j+½}} h(x)\,dx = \langle h\rangle_j^n B_j \Delta x_j,$$

and:

$$(4.18): \quad \Delta x_j \langle Q\rangle_j^n = \int_{x_{j-½}}^{x_{j+½}} Q(x)\,dx = \int_{x_{j-½}}^{x_{j+½}} A(x)\,u(x)\,dx \neq$$

$$\neq \frac{1}{\Delta x_j} \int_{x_{j-½}}^{x_{j+½}} A(x)\,dx \int_{x_{j-½}}^{x_{j+½}} u(x)\,dx = \langle A\rangle_j^n \langle u\rangle_j^n \Delta x_j.$$

Nevertheless, tests have shown that the final conservative step corrects this inaccuracy of the predictor value. Namely, the discrepancy between $\langle A \rangle_j^n$ and $\langle Q \rangle_j^n$, and $\langle h \rangle_j^n$ and $\langle u \rangle_j^n$ in the (u,h) variant can be eliminated by an iteration procedure for obtaining such values for the grid averages of u and h (i.e. $\langle u \rangle_j^n$ and $\langle h \rangle_j^n$), which correspond to the values of grid averages of A and Q ($\langle A \rangle_j^n$ and $\langle Q \rangle_j^n$). The procedure has been tested, but with no significant improvements in results. Apparently the conservative step filters the irregularity.

In the algorithm presented in this chapter the (u,h) variable set is used. The procedure with the (A,Q) set is similar, the only difference being that the areas and discharges are obtained in the interpolation procedure, instead of velocities and depths.

The theoretical development of the fixed-grid method of characteristics is outlined in the literature review. The problem of solving two partial differential equations is transformed into one of solving four ordinary differential equations: two compatibility conditions along the two characteristics. Equations (2.15)-(2.18), valid for a rectangular, but non-prismatic, cross-section, are rewritten here for convenience. The compatibility condition along the

positive characteristic (LA in Fig.4.2) is:

$$(2.15): \quad \frac{D}{Dt}(u+2c) = g(S_o - S_f) - \frac{uc}{B}\frac{\partial B}{\partial x},$$

and the positive characteristic (C+) itself is:

$$(2.16): \quad \frac{dx}{dt} = u+c,$$

while the compatibility condition:

$$(2.17): \quad \frac{D}{Dt}(u-2c) = g(S_o - S_f) + \frac{uc}{B}\frac{\partial B}{\partial x},$$

is valid along the negative characteristic (C-):

$$(2.18): \quad \frac{dx}{dt} = u-c.$$

One can obtain the solution at point A by solving four differential Eqs. (2.15)-(2.18) simultaneously, since at a point of intersection of the characteristics (LA and RA Fig.4.2), both compatibility conditions are valid. The

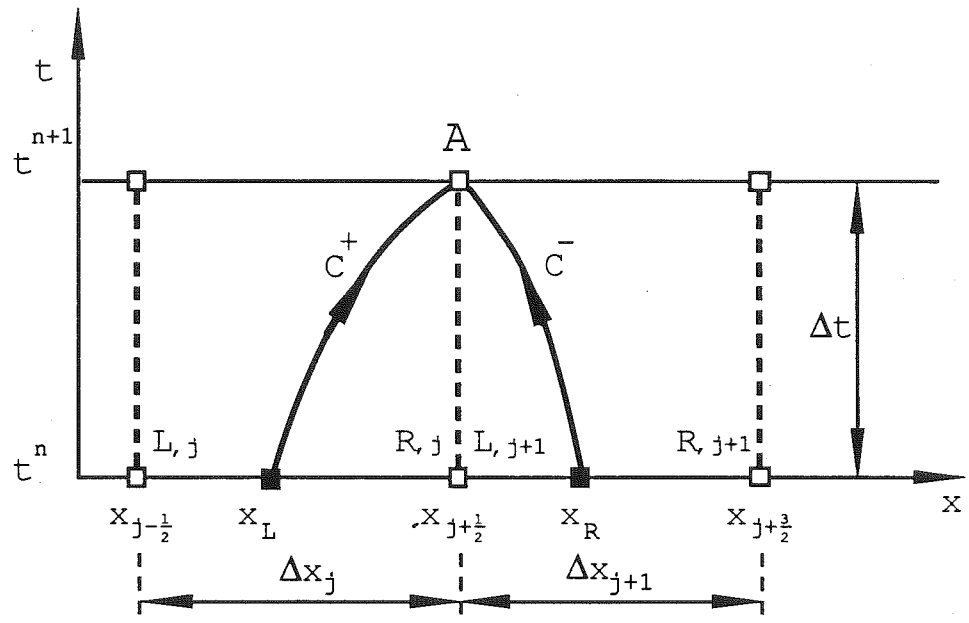

Figure 4.2 Definition sketch for the method of characteristics

second-order approximation of the differential Eqs. (2.15-2.18) according to Fig.(4.2) yields:

$$(4.19): \quad u_A+2c_A = u_L+2c_L+g\frac{\Delta t}{2}\left[\left(S_{oL}-n^2\frac{u_L|u_L|}{R_L^{4/3}}\right)+\left(S_{oL}-n^2\frac{u_A|u_A|}{R_A^{4/3}}\right)\right]-$$
$$-\frac{\Delta t}{2}\left[\frac{u_Lc_L}{B_L}\left(\frac{\partial B}{\partial x}\right)_L+\frac{u_Ac_A}{B_A}\left(\frac{\partial B}{\partial x}\right)_L\right],$$

and :

$$(4.20): \quad u_A-2c_A = u_R-2c_R+g\frac{\Delta t}{2}\left[\left(S_{oR}-n^2\frac{u_R|u_R|}{R_R^{4/3}}\right)+\left(S_{oR}-n^2\frac{u_A|u_A|}{R_A^{4/3}}\right)\right]+$$
$$+\frac{\Delta t}{2}\left[\frac{u_Rc_R}{B_R}\left(\frac{\partial B}{\partial x}\right)_R+\frac{u_Ac_A}{B_A}\left(\frac{\partial B}{\partial x}\right)_R\right].,$$

for the compatibility conditions, and:

$$(4.21): \quad X_L = X_{j+½}-\frac{\Delta t}{2}\,(u_A+c_A+u_L+c_L)\,,$$

and:

$$(4.22): \quad X_R = X_{j+½}-\frac{\Delta t}{2}\,(u_A-c_A+u_R-c_R)\,,$$

for the positive AL and the negative AR characteristic.

Equations (4.19-4.22) are in eight unknown variables: the velocity u_A and depth h_A at the "unknown" point A, and the velocities, depths and the positions of the feet of the characteristics at the points L and R. (The values of celerity c and hydraulic radius R, are obtained from the depth, and are not independent unknowns.) Interpolation relations for the velocities u_L and u_R, and depths h_L and h_R provide the required additional four equations. The piecewise parabolic interpolation, which is explained in detail in Appendix A and applied to the scalar equations in the previous chapter, is used in the algorithm. The only difference with respect to the scalar equation is that now one needs to interpolate not one, but four variables, since both the number of equations and the number of variables for each equation are doubled. If subcritical flow is considered, as in Fig.(4.2), one obtains:

(4.23): $$h_L = h_{L,j} + \xi_L [\Delta h_j + h_{6,j}(1-\xi_L)],$$

and:

(4.24): $$u_L = u_{L,j} + \xi_L [\Delta u_j + u_{6,j}(1-\xi_L)],$$

in the "j" domain of interpolation (between the points $X_{j-½}$ and $X_{j+½}$), and:

(4.25): $$h_R = h_{L,j+1} + \xi_R [\Delta h_{j+1} + h_{6,j+1}(1-\xi_R)],$$

and:

(4.26): $$u_R = u_{L,j+1} + \xi_R [\Delta u_{j+1} + u_{6,j+1}(1-\xi_R)],$$

in the "j+1" zone of interpolation. The dimensionless lengths ξ_L and ξ_R are given as:

(4.27): $$\xi_L = \frac{X_L - X_{j-½}}{\Delta X_j}, \quad \xi_R = \frac{X_R - X_{j+½}}{\Delta X_{j+1}},$$

and for any interpolated variable ψ:

(4.28): $$\Delta\psi_j = \psi_{R,j} - \psi_{L,j}, \quad \psi_{6,j} = 6\left(\langle\psi\rangle_j^n - \frac{\psi_{R,j}+\psi_{L,j}}{2}\right).$$

where $\langle\psi\rangle_j^n$ is a grid point average over the interval (zone) "j", and $\psi_{L,j}$ and $\psi_{R,j}$, the values at the limits of the

zone "j" (Fig.4.2), are obtained by the procedure described in Appendix A.

To obtain the geometric quantities needed for Eqs. (4.19 and 4.20) (the widths B_L , and B_R , width derivatives and bottom slopes) linear interpolation and central differences are used:

(4.29): $$B_L = B_{j-\frac{1}{2}} + \xi_L (B_{j+\frac{1}{2}} - B_{j-\frac{1}{2}}) ,$$

(4.30): $$B_R = B_{j+\frac{1}{2}} + \xi_L (B_{j+3/2} - B_{j+\frac{1}{2}}) ,$$

(4.31): $$\left(\frac{\partial B}{\partial x}\right)_L = \frac{B_{j+1/2} - B_{j-1/2}}{\Delta X_j} ,$$

(4.32): $$\left(\frac{\partial B}{\partial x}\right)_R = \frac{B_{j+3/2} - B_{j+1/2}}{\Delta X_{j+1}} ,$$

(4.33): $$S_{oL} = - \frac{Z_{b_{j+1/2}} - Z_{b_{j-1/2}}}{\Delta X_j} ,$$

(4.34): $$S_{oR} = - \frac{Z_{b_{j+3/2}} - Z_{b_{j+1/2}}}{\Delta X_{j+1}} .$$

The appropriate interpolation zone (domain) for the points L and R must be determined according to the type of flow regime (sub/supercritical, negative/positive direction), in order to obtain the proper stream of information necessary for the correct solution of the problem. The type of flow regime is determined from the relative positions of the feet of the positive and negative characteristics and the computational point A, as described in Fig.(4.3). Therefore for subcritical flow, regardless on the flow direction, zone "j" is used for the positive LA, and zone "j+1" for the negative RA characteristics. In supercritcal flow, however, the feet of both characteristics are in one interpolation zone only: zone "j" for positive, and zone "j+1" for negative (reverse) flow. The possibility of interpolation in adjacent zones "j-1", "j-2", etc., which would allow Courant numbers greater then unity, and consequently larger time steps, is not considered, since this increasing of the Courant number would diffuse the steep-front (see Fennema and Chaudhry, 1986).

At this point all the equations necessary to solve the problem (characteristics/compatibility Eqs. 4.19-4.22, interpolation Eqs. 4.23-4.26, and supplementary geometrical Eqs.4.29-4.34) are available. The system of Eqs. (4.19-4.26) is nonlinear, but can be solved by the Newton-Raphson method. This involves a matrix inversion and additional

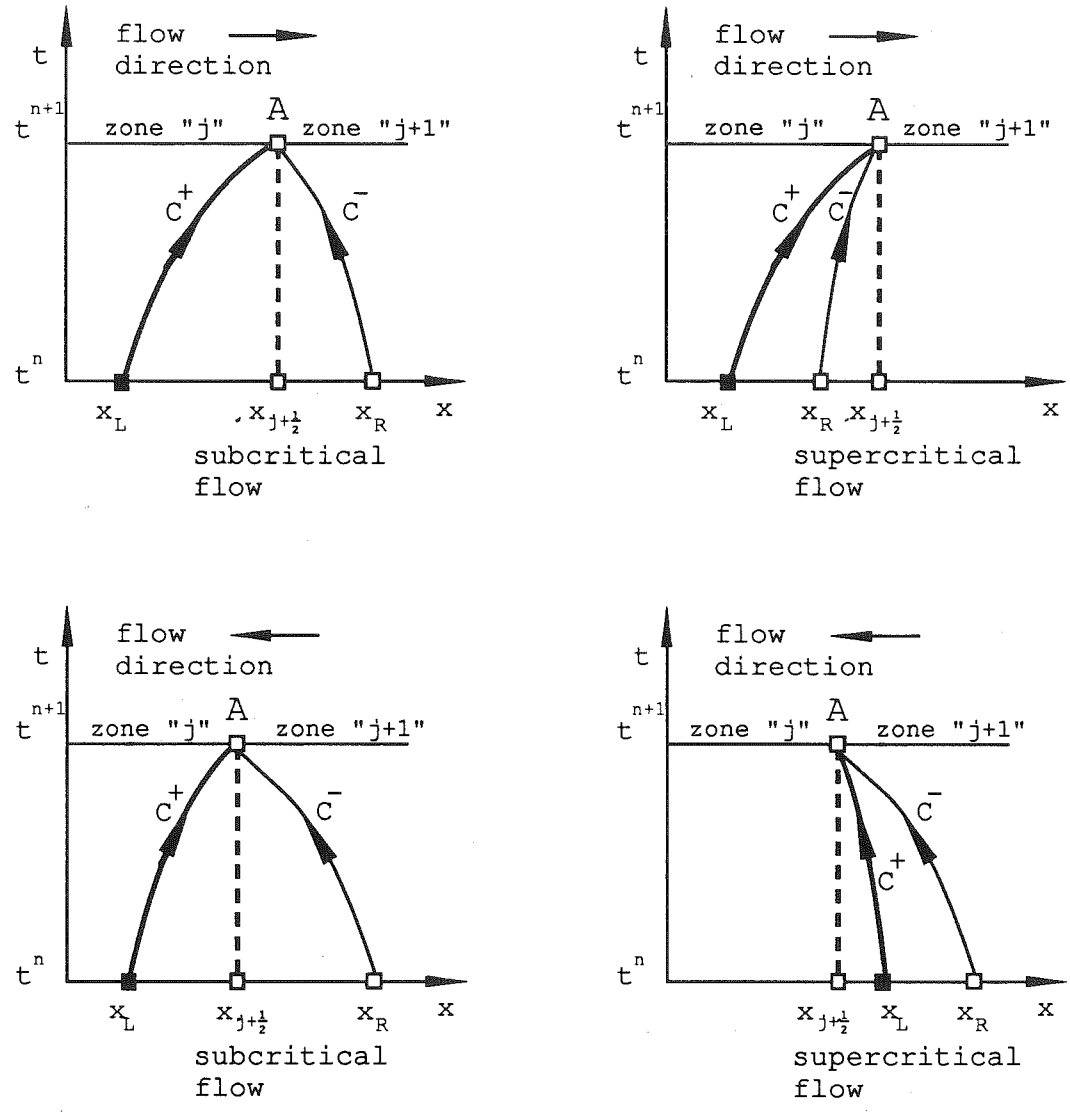

Figure 4.3 Relationship between the flow regime and the position of the feet of the characteristics

complications with location of the zone of interpolation for mixed-regime flows. Therefore an alternative procedure, combining simple iteration and the Newton-Raphson method, is adopted herein.

The initial approximation for the variables at the "unknown" point A (Fig.4.2) is computed as an average between the right boundary of the "j" interpolation zone and the left boundary of the "j+1" interpolation zone ($h_A=½(h_{R,j}+h_{L,j+1})$, etc.). For initial values of variables at the feet of the characteristics L and R the same values are chosen as for the point A ($h_L=h_R=h_A$).

First, the locations of the feet of characteristics X_L and X_R are computed from the characteristics Eqs. (4.21) and (4.22).

The interpolation Eqs. (4.23)-(4.34) are then used to obtain new approximations for the variables at the feet of the characteristics.

An iteration terminates with computation of the velocity u_A and depth h_A at the "unknown" point A, based on use of the Newton-Raphson method to solve the system of compatibility-condition approximations Eqs.(4.19) and (4.20). The procedure for the Newton-Raphson method is explained in detail in Appendix C. If the first-order integration of compatibility conditions (Eqs.2.15 and 2.17)

is used, the following system of linear equations in u_A and h_A results:

$$(4.19a): \quad u_A+2c_A = u_L+2c_L+g\Delta t\left(S_{oL}-n^2\frac{u_L|u_L|}{R_L^{4/3}}\right)-\Delta t\frac{u_Lc_L}{B_L}\left(\frac{\partial B}{\partial x}\right)_L,$$

$$(4.20a): \quad u_A-2c_A = u_R-2c_R+g\Delta t\left(S_{oR}-n^2\frac{u_R|u_R|}{R_R^{4/3}}\right)+\Delta t\frac{u_Rc_R}{B_R}\left(\frac{\partial B}{\partial x}\right)_R,$$

and one does not need to solve the nonlinear system Eqs.(4.19) and (4.20).

To control the convergence of the process, the values of variables u_A and h_A from the new iteration are compared with those from the previous iteration. Iterations are continued until the required accuracy for the variables u_A and h_A is achieved, i.e. until:

$$(4.35): \quad |h_A^{(m+1)}-h_A^{(m)}| \le \varepsilon_h \text{ and } |u_A^{(m+1)}-u_A^{(m)}| \le \varepsilon_u,$$

where $h_A^{(m+1)}$ and $h_A^{(m)}$ are the values of the depth h_A at the m-th and m+1-st iteration, respectively.

The procedure for obtaining the values of the depth and

velocity at the midpoint $X_{j+½}$ and mid-time $t^{n+½}$, used to obtain the approximation vector $\bar{U}^{n+½}_{j+½}$ is the same, the only difference being that now the time step is halved.

IV.2.1.2 Computing approximation vector

Now the values of the flow variables at mid-point $X=X_{j+½}$ (either at time $t=t^{n+1}$, or mid-time $t=t^{n+½}$) are obtained, and one can proceed to compute the approximation vector $\bar{U}^{n+½}_{j+½}$ (time averaged vector), which is the final goal of the predictor step. Two methods, introduced at the beginning of this section, are presented.

The first approach, which follows Vila's method, simply equates the value of the approximation vector $\bar{U}^{n+½}_{j+½}$ (time-averaged vector) with the vector $U^{n+½}_{j+½}$ computed by the method of characteristics at mid-time $t^{n+½}$.

The second approach, based on conveying the Riemann invariants along the characteristics, has its roots in the method exploited for the scalar equations. As with the scalar equations, the idea is to change the problem of an integration in time at the fixed space position $X_{j+½}$, to an integration in space at the fixed and known time level t^n. A simplified variant of this approach (based on the algorithm by Colella and Woodward, 1984) is to average the

flow variables (velocity and depth) over the domain of dependence of point A (Fig.4.4). This produces numerical oscillations for strong dam-break waves, i.e. for large ratios of upstream to downstream depths. However, the procedure is used for the discontinuous part of the flow, where the characteristics approach simply cannot be applied.

An alternative concept is to perform the change from temporal to spatial integration through the characteristics-based approach, which is more natural. Here the Riemann invariants, conveyed by the characteristics, are averaged, and then the averaged velocity and depth (i.e. the components of the approximation vector $\overline{U}_{j+\frac{1}{2}}^{n+\frac{1}{2}}$) are calculated from them.

The Riemann invariants, as presented in chapter II, are:

(4.36): $W_1 = u + 2c,$

and:

(4.37): $W_2 = u - 2c,$

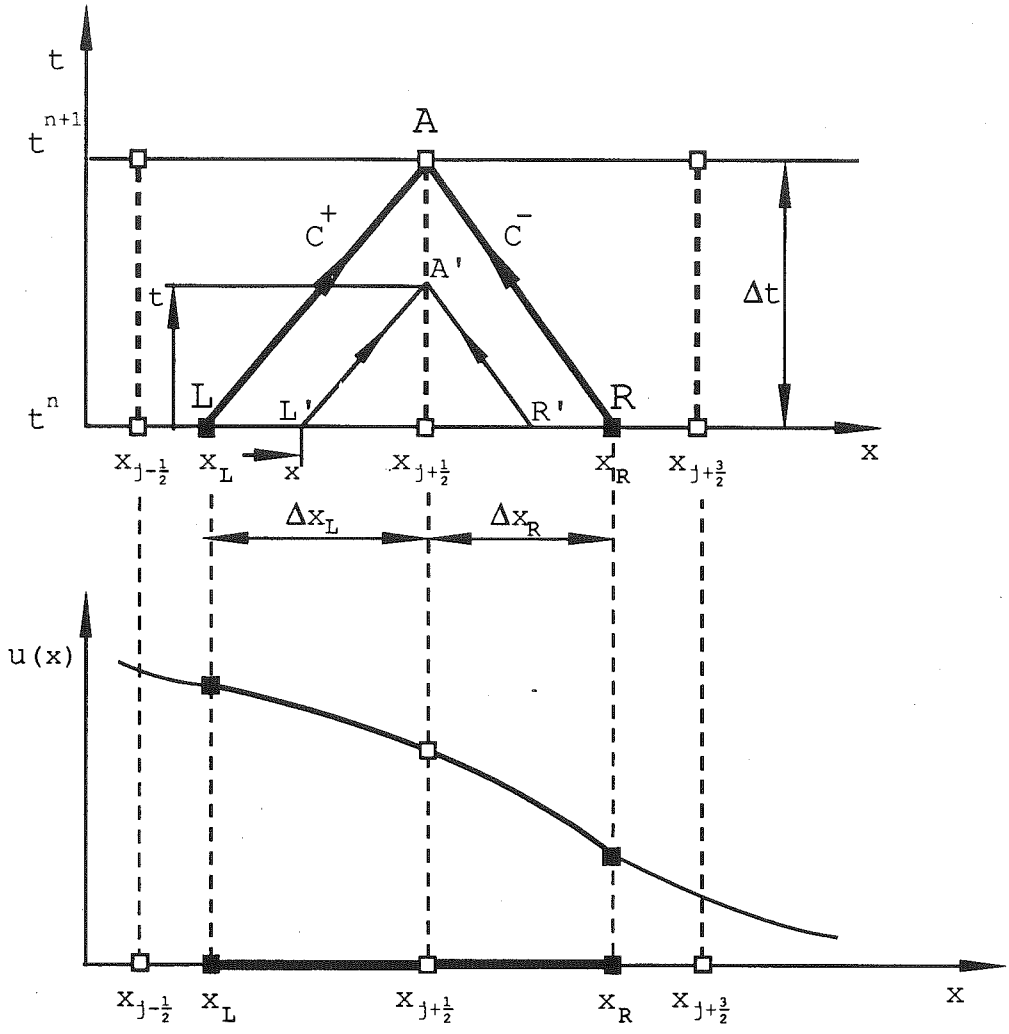

Figure 4.4 Averaging the Riemann invariants: domain of dependence of point A

where W_1 and W_2 are the Riemann invariants along the positive and negative characteristics, respectively. For convenience in subsequent discussion, the expressions Eqs(4.36) and (4.37) are referred to as Riemann "invariants", even for the case of nonhomogeneous compatibility conditions, where "invariants" are by no means invariant.

Compatibility conditions (2.15) and (2.17) along the characteristics A'L', and A'R' (Fig.4.4) can be expressed in terms of Riemann invariants W_1 and W_2 as:

$$(4.38): \quad W_1 = u(t) + 2c(t) = u(x) + 2c(x) + \int_{t^n}^{t} \left[g\left(S_o - n^2 \frac{u(x)\,|u(x)|}{R(x)^{4/3}}\right) - \frac{u(x)\,c(x)}{B(x)} \left(\frac{\partial B}{\partial x}\right)\right] dt$$

$$(4.39): \quad W_2 = u(t) - 2c(t) = u(x) - 2c(x) + \int_{t^n}^{t} \left[g\left(S_o - n^2 \frac{u(x)\,|u(x)|}{R(x)^{4/3}}\right) + \frac{u(x)\,c(x)}{B(x)} \left(\frac{\partial B}{\partial x}\right)\right] dt$$

where u(t) and c(t) designate the values at the point A' (for the fixed spatial position $X_{j+1/2}$), and u(x) and c(x) designate the values at points L'and R'(for the fixed time t^n). If a first-order approximation of the integrals in Eqs.(4.38) and (4.39) is used, one obtains:

$$(4.40): \quad W_1 = u(x) + 2c(x) + \\ + (t-t^n)\left[g\left(S_o - n^2 \frac{u(x)\,|u(x)|}{R(x)^{4/3}}\right) - \frac{u(x)\,c(x)}{B(x)}\left(\frac{\partial B}{\partial x}\right)\right],$$

$$(4.41): \quad W_2 = u(x) - 2c(x) + \\ + (t-t^n)\left[g\left(S_o - n^2 \frac{u(x)\,|u(x)|}{R(x)^{4/3}}\right) + \frac{u(x)\,c(x)}{B(x)}\left(\frac{\partial B}{\partial x}\right)\right].$$

(A second-order approximation of Eqs.(3.38) and (3.39) has also been used without improvement of the behavior of the method; indeed, artificial oscillations were introduced.)

The Riemann invariant W_1 is integrated between times t^n and t^{n+1}:

$$(4.42): \quad \overline{W_1} = \frac{1}{\Delta t}\int_{t^n}^{t^{n+1}} [u(t) + 2c(t)]\,dt = \frac{1}{\Delta t}\int_{t^n}^{t^{n+1}} [u(x) + 2c(x)]\,dt + \\ + \frac{1}{\Delta t}\int_{t^n}^{t^{n+1}} (t-t^n)\left[g\left(S_o - n^2 \frac{u(x)\,|u(x)|}{R(x)^{4/3}}\right) - \frac{u(x)\,c(x)}{B(x)}\left(\frac{\partial B}{\partial x}\right)\right] dt.$$

A change of variables, motivated by the equation of the characteristic LA , is then introduced (see Fig.4.4):

$$(4.43):\quad \left\{ \begin{array}{l} X = X_{j+½} - \dfrac{\Delta X_L}{\Delta t}(t-t^n), \\ \Delta X_L = X_{j+½} - X_L = \dfrac{1}{2}(u_A + c_A + u_L + c_L), \\ dX = -\dfrac{\Delta X_L}{\Delta t}\,dt, \\ X = X_{j+½} \text{ for } t=t^n; \quad X=X_L \text{ for } t=t^{n+1}. \end{array} \right\},$$

leading to:

$$(4.44):\quad \overline{W}_1 = \frac{1}{\Delta t}\int_{t^n}^{t^{n+1}} [u(t)+2c(t)]\,dt = \frac{1}{\Delta X_L}\int_{X_L}^{X_{j+½}} [u(x)+2c(x)]\,dx +$$

$$+\frac{\Delta t}{\Delta X_L{}^2}\int_{X_L}^{X^{j+½}} (X_{j+½}-x)\left[g\left(S_o - n^2\frac{u(x)\,|u(x)|}{R(x)^{4/3}}\right) - \frac{u(x)\,c(x)}{B(x)}\left(\frac{\partial B}{\partial x}\right)\right]dx.$$

It is worth noting that in the integral expression (4.42) the values of u(t), h(t) at different times "t" are related with those of u(x) and c(x) at different locations "x" always by a particular characteristic which corresponds to only one time and spatial position. Since the velocity and depth (and accordingly celerity) differ in time, those characteristics differ in slope - they are not parallel. Consequently, the change of variables Eq.(4.43), though

mathematically correct, introduces another approximation by assuming that the slope for all characteristics (of one family) is the same and equal to the slope of the characteristic issuing from the point A.

By a similar argument, the expression for the averaged W_2 invariant can be obtained as:

$$(4.45): \quad \overline{W}_2 = \frac{1}{\Delta t}\int_{t^n}^{t^{n+1}} [u(t) - 2c(t)]\, dt = \frac{1}{\Delta X_R}\int_{X_{j+1/2}}^{X_R} [u(x) - 2c(x)]\, dx +$$

$$+ \frac{1}{\Delta X_R}\int_{X_{j+1/2}}^{X_R} (x - X_{j+1/2})\left[g\left(S_o - n^2 \frac{u(x)\,|u(x)|}{R(x)^{4/3}}\right) + \frac{u(x)\,c(x)}{B(x)}\left(\frac{\partial B}{\partial x}\right)\right] dx.$$

When the integrals of Eqs.(4.44) and (4.45) are evaluated and the averaged Riemann invariants obtained, the time-averaged depth and velocity are finally computed as:

$$(4.46): \quad \overline{U}_{j+1/2}^{n+1/2} = \frac{\overline{W}_1 + \overline{W}_2}{2},$$

$$(4.47): \quad \overline{C}_{j+1/2}^{n+1/2} = \frac{\overline{W}_1 - \overline{W}_2}{4},$$

$$(4.48): \quad \overline{h}_{j+\frac{1}{2}}^{n+\frac{1}{2}} = \frac{(\overline{C}_{j+\frac{1}{2}}^{n+\frac{1}{2}})^2}{g}.$$

Integration of Eqs.(4.44) and (4.45) can be done in several ways. For the case of a rectangular channel it is possible to obtain an analytical solution for the first term only, but for the general case of a natural channel, numerical integration must be used for all terms. Analytical integration of the first term slightly improves steep-front resolution, but only for the hypothetical case of frictionless horizontal channel, while for real (frictional) channels no improvement in the resolution can be observed; therefore numerical integration is applied for all terms of Eqs.(4.44) and (4.45).

For numerical integration of Eqs.(4.44) and (4.45) three methods are used: trapezium-tangent, trapezium-chord, and Simpson rule. The following expressions can be applied to all three of them:

$$(4.49):\quad \overline{W}_1=\frac{1}{2\alpha+\beta}\left[\alpha\left(u_L+2c_L+u_{j+\frac{1}{2}}+2c_{j+\frac{1}{2}}\right)+\beta\left(u_{ML}+2c_{ML}\right)\right]+$$

$$+\frac{\Delta t}{2\alpha+\beta}\left\{\alpha\left[g\left(S_{oL}-n^2\frac{u_L|u_L|}{R_L^{4/3}}\right)-\frac{u_L c_L}{B_L}\left(\frac{\partial B}{\partial x}\right)_L\right]+\right.$$

$$\left.+\frac{\beta}{2}\left[g\left(S_{oL}-n^2\frac{u_{ML}|u_{ML}|}{R_{ML}^{4/3}}\right)-\frac{u_{ML}c_{ML}}{B_{ML}}\left(\frac{\partial B}{\partial x}\right)_L\right]\right\},$$

and:

$$(4.50):\quad \overline{W}_1=\frac{1}{2\alpha+\beta}\left[\alpha\left(u_R-2c_R+u_{j+\frac{1}{2}}-2c_{j+\frac{1}{2}}\right)+\beta\left(u_{MR}-2c_{MR}\right)\right]+$$

$$+\frac{\Delta t}{2\alpha+\beta}\left\{\alpha\left[g\left(S_{oR}-n^2\frac{u_R|u_R|}{R_R^{4/3}}\right)+\frac{u_R c_R}{B_R}\left(\frac{\partial B}{\partial x}\right)_R\right]+\right.$$

$$\left.+\frac{\beta}{2}\left[g\left(S_{oR}-n^2\frac{u_{MR}|u_{MR}|}{R_{MR}^{4/3}}\right)+\frac{u_{MR}c_{MR}}{B_{MR}}\left(\frac{\partial B}{\partial x}\right)_R\right]\right\},$$

where u_{ML} , h_{ML} , u_{MR} , etc. are the values of the flow variables interpolated at points between the feet of the characteristics and the point $X_{j+\frac{1}{2}}$ (Fig.4.5). (As described at the beginning of the section, it is necessary to use the appropriate interpolation zone, which is dictated by the type of flow, to convey appropriate information into the solution (see Fig.4.3).) For α=1 and ß=0 the trapezium-

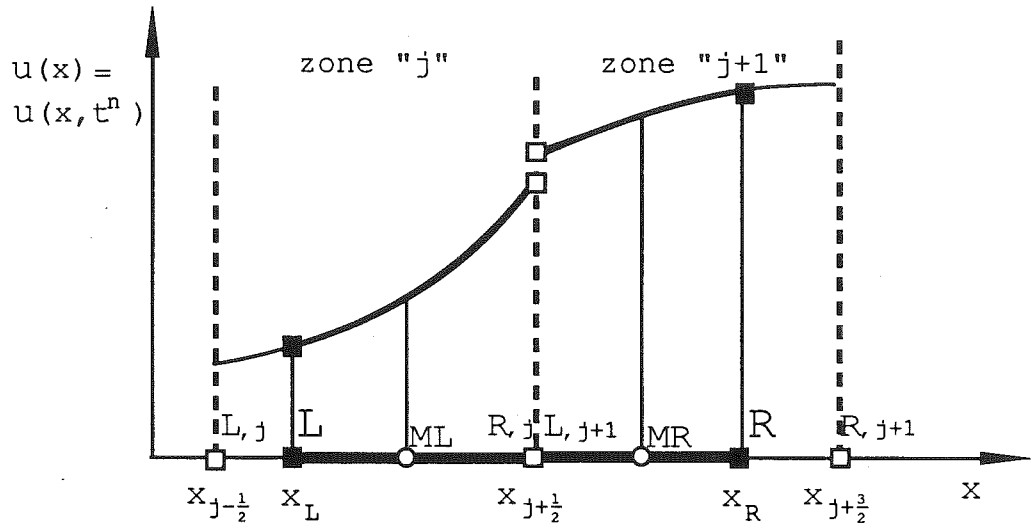

Figure 4.5 Interpolation for the integration of the Riemann invariants

chord rule is recovered from Eqs.(4.49) and (4.50); for α=0 and ß=1 the trapezium-tangent rule results, and for α=1 and ß=4 the Simpson rule is obtained.

All three methods lead to results similar to those of the first approach - where the approximation vector $\overline{U}_{j+\frac{1}{2}}^{n+\frac{1}{2}}$ is simply taken as the mid-time vector $U_{j+\frac{1}{2}}^{n+\frac{1}{2}}$ obtained by the method of characteristics. Since the latter approach gives equally good results, without the complications of integration of the Riemann invariants, it is suggested as a better choice, and used henceforth.

IV.2.2 Discontinuous solution

When the relative difference between the values of velocities and/or depths at the midpoint $X_{j+\frac{1}{2}}$ (in Fig.4.6) for the different interpolation zones "j" and "j+1" exceeds some tolerance (which depends on the particular case), i.e. when:

$$(4.51): \quad \frac{|h_{R,j}-h_{L,j+1}|}{h_{R,j}+h_{L,j+1}} > \varepsilon_h, \quad \text{or} \quad \frac{|u_{R,j}-u_{L,j+1}|}{u_{R,j}+u_{L,j+1}} > \varepsilon_u,$$

it is assumed that a discontinuity exists, and a procedure different from the one described above is applied (since the

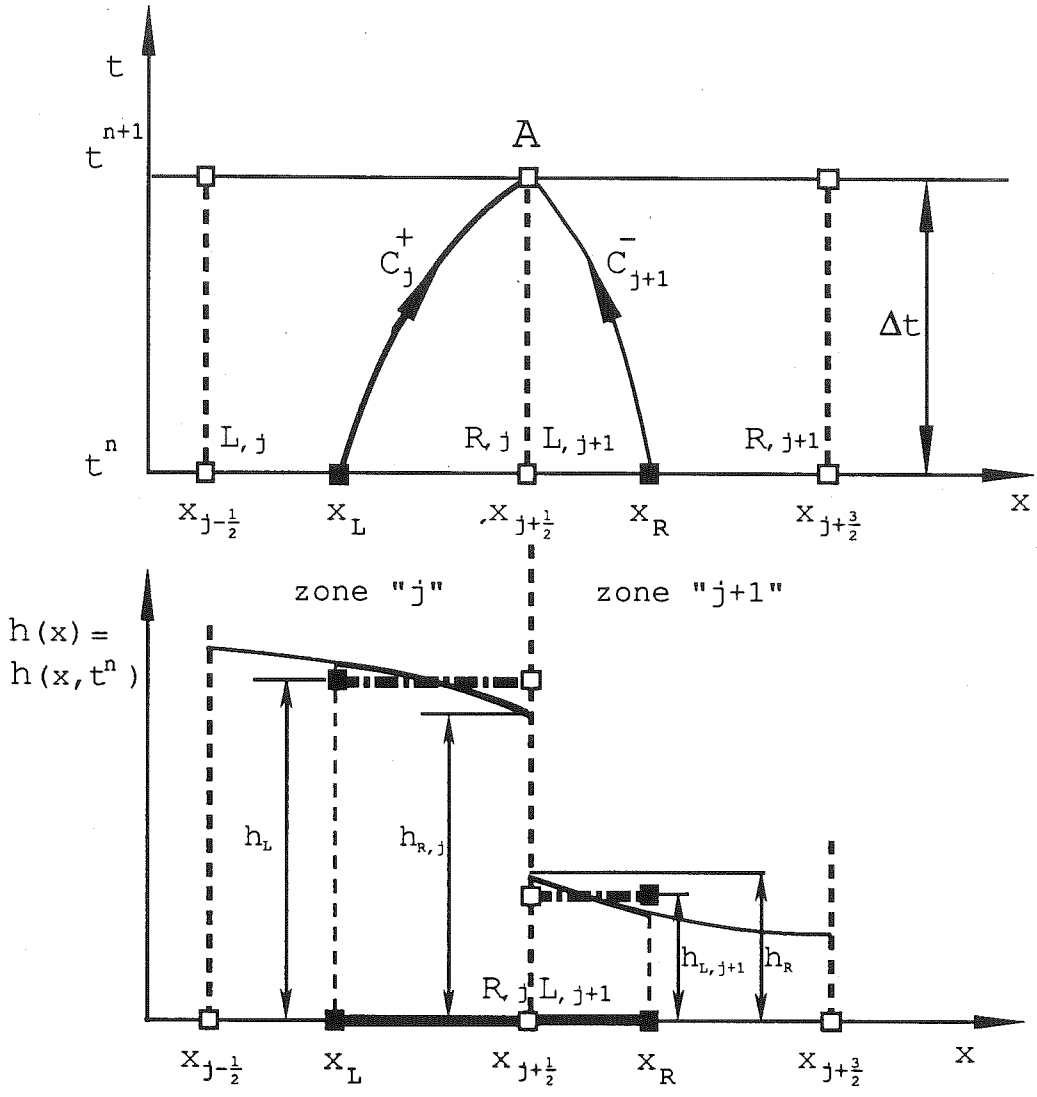

Figure 4.6. Discontinuous depth profile

basic method of characteristics cannot be used for discontinuities).

The problem to be solved is called a generalized Riemann problem. It differs from the "ordinary" Riemann problem (or simply the Riemann problem) in that at the initial time for the former the velocities and depths on both sides of discontinuity are functions of the spatial variable, while they are strictly uniform for the latter. The generalized Riemann problem can be solved using the shock-fitting technique, which leads to tremendous practical difficulties, as described earlier in chapter II.

The approach used in the present work is based on the solution of the "ordinary" Riemann problem, where the depths and velocities on both sides of the discontinuity are approximated as uniform (dashed line in Fig.4.6). The idea from Colella and Woodward (1984), which uses averaging of velocity and depth over the domain of dependence, separately for each side of the discontinuity, is applied to obtain the "average uniform" state on both sides of discontinuities.

IV.2.2.1 Averaging left and right state for Riemann problem

The first goal is to obtain representative values for depths and velocities on both sides of discontinuities to initiate the Riemann problem. It is considered that the best approach is to use the information from the domain of

dependance of the point A, separately for both sides of the discontinuity. Since the method of characteristics cannot be used for discontinuous flow, an approximation must be introduced to obtain the domains of dependence. The values of depth and velocity at point A, used for determining the domain of dependance, are approximated with the values at the boundaries of interpolation zones: $h_{R,j}$, $u_{R,j}$ for the left side of the discontinuity, and $h_{L,j+1}$, $u_{L,j+1}$ for the right side:

(4.52): $$X_L = X_{j+½} - \Delta t\,(u_{R,j}+c_{R,j})\,,$$

(4.53): $$X_R = X_{j+½} - \Delta t\,(u_{L,j+1}-c_{L,j+1})\,.$$

After the left and right domains of dependence are determined, the averaging of depths and velocities is performed by integration of appropriate PPM interpolation polynomials Eqs.(4.23-4.26), which yields:

(4.54): $$h_L = h_{L,j} + \frac{1}{1-\xi_L}\left[(\Delta h_j + h_{6,j})\,\frac{1-\xi_L^2}{2} - h_{6,j}\frac{1-\xi_L^3}{3}\right],$$

and:

$$(4.55): \quad u_L = u_{L,j} + \frac{1}{1-\xi_L}\left[(\Delta u_j + u_{6,j})\frac{1-\xi_L^2}{2} - u_{6,j}\frac{1-\xi_L^3}{3}\right],$$

for the zone "j", left of the discontinuity, and:

$$(4.56): \quad h_R = h_{L,j+1} + (\Delta h_{j+1} + h_{6,j+1})\frac{\xi_R}{2} - h_{6,j+1}\frac{\xi_R^2}{3},$$

and:

$$(4.57): \quad u_R = u_{L,j+1} + (\Delta u_{j+1} + u_{6,j+1})\frac{\xi_R}{2} - u_{6,j+1}\frac{\xi_R^2}{3}.$$

for the zone "j+1", on the right side of the discontinuity. Here ξ_L and ξ_R are dimensionless lengths introduced in Eq.(4.27). If the flow in the zone ahead of the discontinuity is supercritical (Fig.4.7), the foot of the characteristic for that zone will lie outside the zone, and the above-mentioned averaging equations will not be valid. In such a case the characteristic is "moved" back to the point $X_{j+½}$, which, for flow in the positive x direction results in:

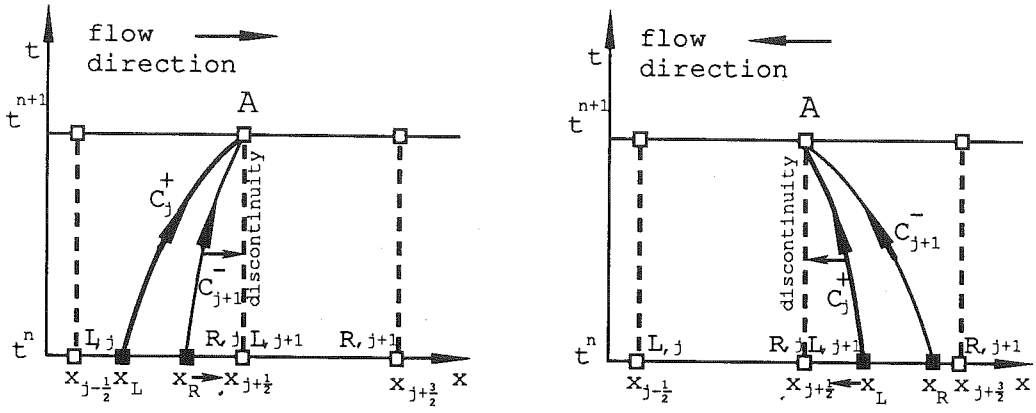

a. characteristics plane

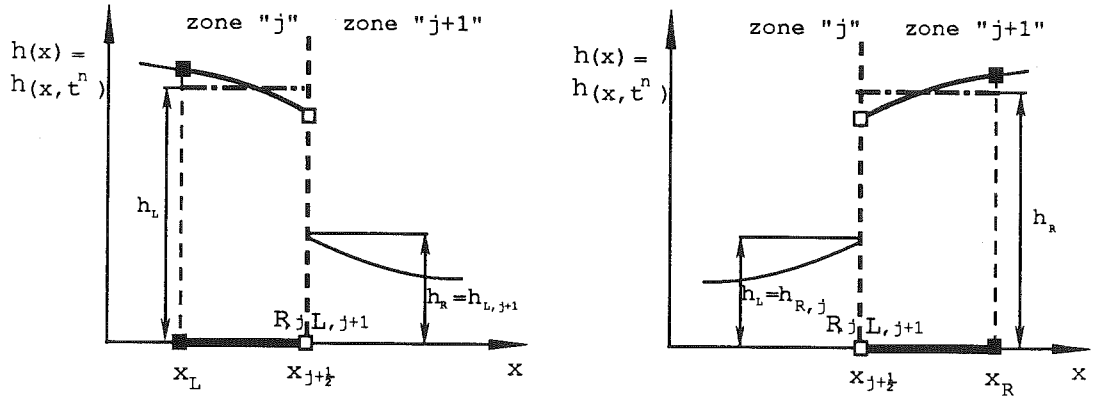

b. depth profile

Figure 4.7 Domain of dependence for supercritical flow

(4.58): $h_R = h_{L,j+1}$ and $u_R = u_{L,j+1}$,

and for flow in the negative direction (reverse flow) in:

(4.59): $h_L = h_{R,j}$ and $u_L = u_{R,j}$.

IV.2.2.2 Riemann solver

The Riemann problem is treated in detail in the literature (Courant and Friedrichs,1948; Stoker,1957); only a basic explanation and the solution procedure are presented here.

A discontinuity in a horizontal frictionless channel is considered. This is a reasonable simplification, since the resistance and gravity forces are small over the short length of horizontal channel containing the discontinuity. At the initial time t^n a discontinuity exists at the point $X_{j+½}$, and in the zones left and right of it the flow is uniform with variables u_L and h_L, and u_R and h_R, respectively (dashed lines in Fig.4.8).

Two general cases are possible. For the first case, where the velocity u_L is greater then u_R (Fig.4.8) a so-called simple surge (Stoker,1957) occurs. The steep front (discontinuity) moves with some speed W from the zone of

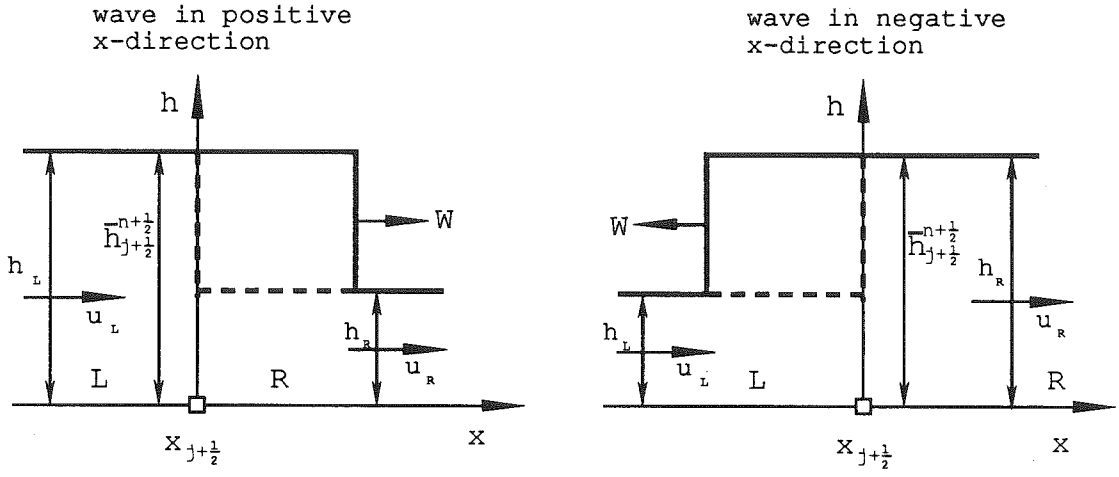

Figure 4.8 Riemann problem

higher depth into the zone of lower depth, changing the uniform flow ahead of the front into a type of uniform flow behind it. This means that between times t^n and t^{n+1}, a constant state occurs at the point $X_{j+½}$, and therefore the desired time averages are:

(4.60): $\overline{h}^{n+½}_{j+½} = h_L$ and $\overline{u}^{n+½}_{j+½} = u_L$,

for the flow in the positive x direction and:

(4.61): $\overline{h}^{n+½}_{j+½} = h_R$ and $\overline{u}^{n+½}_{j+½} = u_R$.

when the flow is in the negative direction.

If at the initial time t^n the velocity u_L is less than u_R , a different type of flow results. The positive steep-front surge advances into a zone of smaller depth, but a negative fan-shaped wave moves into the zone of larger depth (Fig.4.9). This problem is treated in detail by Stoker (1957), as an analytical solution of the dam-break problem in a horizontal frictionless rectangular channel. As for the case of the previously explained simple wave, the surge can move in either direction along the x-axis, depending on the flow conditions. For both cases the physics of the phenomenon, and accordingly the mathematical treatment,

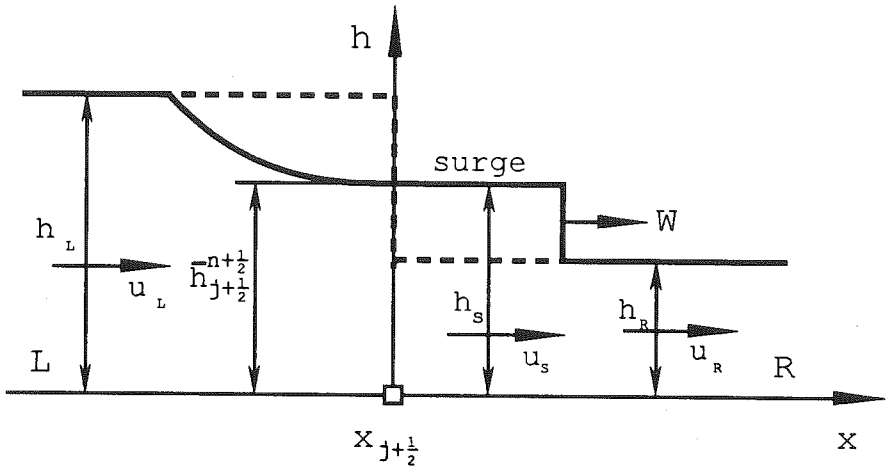

Figure 4.9 Stoker problem

are the same, the only difference being in the form of final expressions. Therefore, only the case of the surge moving in the positive direction is described herein; similar expressions are valid for a surge moving in the reverse direction.

Depending on the ratio of the initial depths upstream and downstream of the "dam-site" (discontinuity), the flow in the surge can be subcritical or supercritical. However, in both cases (sub/supercritical flow) the depth and velocity at the "dam-site" are constant in time at the point $X_{j+½}$ (see Stoker,1957, or Henderson,1966), which, as in the case of the simple surge, means that they are the needed averaged values for the time interval t^n - t^{n+1}.

When the flow in the surge is subcritical, the velocity and depth of the surge prevail at $X_{j+½}$, i.e.:

(4.62): $\overline{h}_{j+½}^{n+½} = h_s$ and $\overline{u}_{j+½}^{n+½} = u_s$.

The surge variables (velocity u_s , depth h_s , and speed W) are computed from the continuity and momentum conservation equations for the moving discontinuity (Eqs.2.6 and 2.7), along with the compatibility condition along the positive characteristic connecting the surge (point S) with the undisturbed zone behind the "fan" (Fig.4.9). For a

frictionless, horizontal rectangular channel these relations can be simplified. The continuity equation becomes:

(4.63): $h_S(u_S-W) = h_R(u_R-W)$;

the momentum equation becomes:

(4.64): $g\frac{h_S^2}{2} + (u_S-W)^2 h_S = g\frac{h_R^2}{2} + (u_R-W)^2 h_R$;

and the compatibility condition (Riemann invariant) becomes:

(4.65): $u_L + 2\sqrt{gh_L} = u + 2\sqrt{gh} = u_S + 2\sqrt{gh_S}$.

Equations (4.62)-(4.65) are manipulated to express the depth h_s implicitly:

(4.66): $2\sqrt{gh_S} - u_L - 2c_L + u_R + \left(1-\frac{h_R}{h_S}\right)\sqrt{\frac{g}{2}\frac{h_S}{h_R}(h_S+h_R)} = 0$,

which is easily solved by the bisection method. Velocity u_s is then computed from the compatibility condition Eq.(4.65).

For the case of supercritical flow in the surge, the flow variables at the dam-section $X_{j+½}$ are obtained using the compatibility condition Eq.(4.65) and the equation of the negative characteristic:

$$(4.67): \quad \frac{dx}{dt} = \frac{X_{j+½} - X_{j+½}}{t} = 0 = u - c = \overline{u}^{n+½}_{j+½} - \overline{c}^{n+½}_{j+½},$$

which yields the desired depth and velocity:

$$(4.68): \quad \overline{u}^{n+½}_{j+½} = \frac{1}{3}(u_L + 2c_L),$$

and:

$$(4.69): \quad \overline{h}^{n+½}_{j+½} = \frac{1}{9g}(u_L + 2c_L)^2.$$

This completes the procedure for obtaining the averaged vector $\overline{U}^{n+½}_{j±½}$.

The entire algorithm for the Godunov method, for one time step and at one point, is summarized in the following:

1. From the previously computed reach averages

$\langle U \rangle_j^n$, the spatial distribution of primary variables is obtained using PPM interpolation (or, for the case of the linear model, using linear interpolation);

2. The predictor values - time averaged vectors $\overline{U}_{j\pm\frac{1}{2}}^{n+\frac{1}{2}}$ - are then computed by the appropriate procedure for the type of flow (continuous vs. discontinuous, subcritical vs. supercritical, etc.);

3. These values are, finally, substituted into the conservation Eq.(4.14) to solve for the grid averaged vector $\langle U \rangle_j^{n+1}$.

IV.3 Boundary conditions

The de St.Venant equations are a system of two hyperbolic partial-differential equations in two variables, and as such need two initial and two boundary conditions for a properly posed problem. The boundary requirements are determined by the type of flow; according to principles based on the method of characteristics, for subcritical flow one boundary condition is needed at each (upstream and downstream) boundary, while for supercritical flow both boundary conditions are at the upstream boundary (otherwise

the flow information could not be conveyed into the flow region).

In the present work, for the upstream boundary condition prescribed discharge is considered, and at the downstream boundary prescribed depth or a rating curve is used. The various special boundary conditions (such as weirs, gates branches, etc.) have not been treated herein, since the objective of the work is not to obtain an industrial code, but to develop and test a scheme which can be later used as the basis of a complex model.

IV.4 Points between the boundaries and the "Godunov points"

One of the main disadvantages of the piecewise parabolic method (PPM) is that one needs to know the values of variables at two points left and right of the point of computation (in the case of a nonuniform grid, three points are needed if the shock-steepening algorithm is used). This means that the points close to the boundary must be treated with a different method. Any method capable of treating discontinuities can be used (Lax-Wendroff, MacCormack, even characteristics with "local" shock-fitting), but the most natural way is to use the linear interpolation variant of the Godunov method. Moreover, the linear variant does not suffer from this anomaly of the PPM variant, which is the

most important advantage of the former.

Again, the best way of handling the points between the boundary and the "Godunov points" should be developed during subsequent industrialization of the method.

CHAPTER V. TEST COMPUTATIONS FOR DE St.VENANT EQUATIONS

V.1 General description and purpose of tests

The primary goal of this chapter is to assess the performance of the modified Godunov method (for both the PPM and linear schemes) in computation of discontinuous open-channel flow, and to compare it with other methods commonly used. A secondary goal is to assess the performance of the two variants of the Godunov method (the PPM and linear method).

To this end, a computer code for the Godunov scheme using PPM interpolation, based on the algorithm developed in the previous chapter, has been written. Another code for the Godunov method with linear interpolation has also been developed. Program listings with annotation and examples of input and output data files are available in Savic and Holly, (1991). As stated before, rectangular but nonprismatic channels are considered, since the objective of the present work is not to prepare an industrial code, but to develop and test the method; for these purposes nonprismaticity is the most important property of channel geometry (Strelkoff,1989). The Godunov scheme is compared

with the analytical solution when available, i.e. for the case of horizontal prismatic frictionless channel. For frictional and sloped channels, the method of characteristics with shock fitting is used as a "true" solution in judging the accuracy of steep-front resolution. Methods commonly used for discontinuous open-channel flow computations - the Preissmann scheme (applied in DAMBRK, CARIMA and most other flood-propagation codes), the Lax-Wendroff scheme, and the MacCormack scheme - are coded and used for comparison. The performances of the MacCormack and the Lax-Wendroff methods differ primarily in that the former is less stable for computing strong shocks, and artificial viscosity must be added to alleviate the problem. This additional damping distorts the results significantly, especially for very strong shocks (Fig.5.1), and therefore no further comparisons with the MacCormack method are presented herein.

First the tests for a frictionless horizontal prismatic channel, for which analytical solutions exist, are performed. Then the tests for a real flow in a sloped, frictional, but still prismatic channel are described. Finally, the most general case of a nonprismatic frictional channel is investigated, and conclusions about the performance of the schemes, in particular the Godunov scheme, are presented.

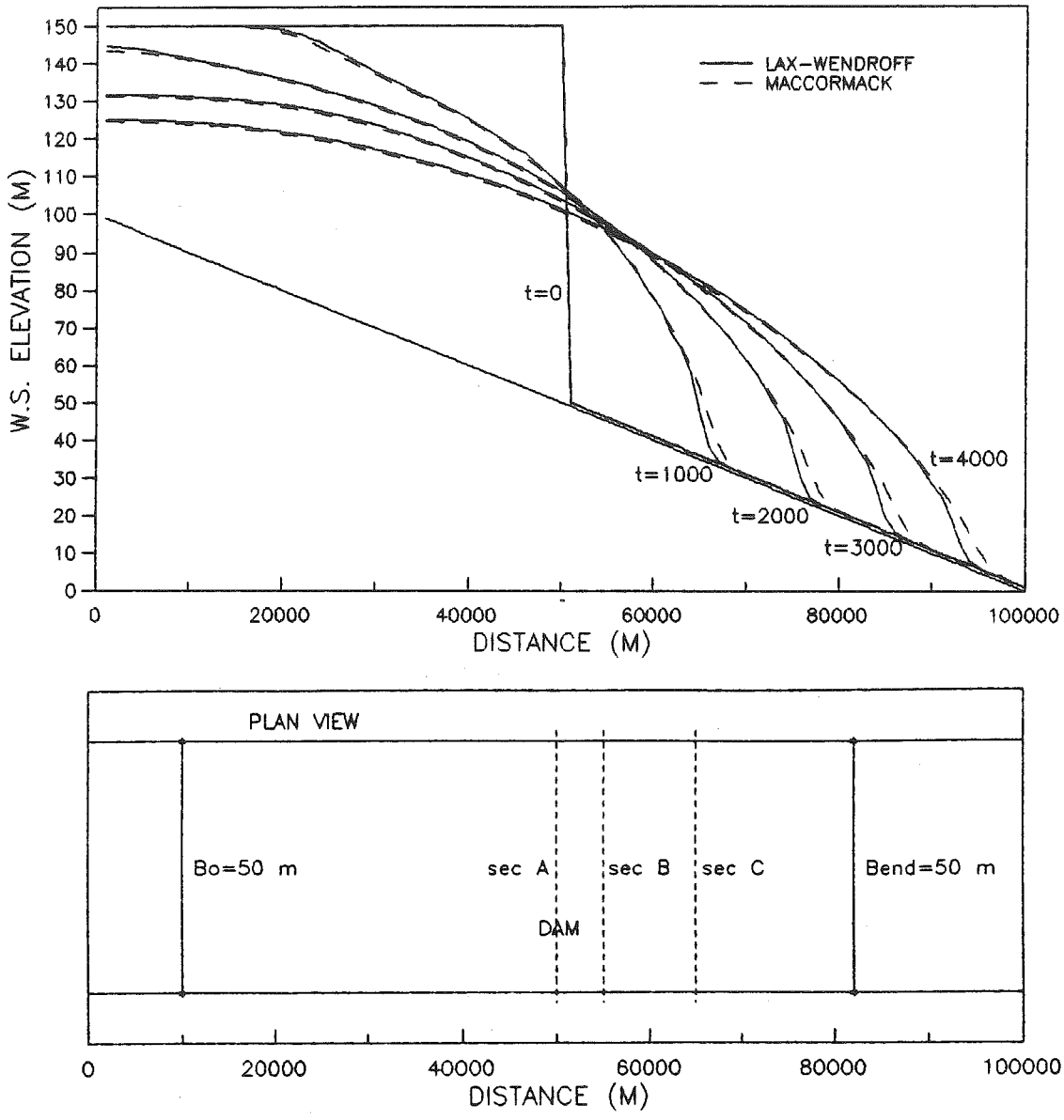

Figure 5.1 Time evolution of water-surface profiles for high-dam dambreak in prismatic rough channel; comparison between the MacCormack and Lax-Wendroff methods

In all of these groups of tests the dam-break computations are considered to be the most important, being both the primary goal of this work and the most representative and severe cases of discontinuous open-channel flow. In addition to dam-break flows, some other examples are given depending on the type of flow under study.

The results of computations are typically presented in three forms. The most common form is water-surface profiles at different times, which offers the most complete view of the unsteady event. In addition, it gives the most useful practical information, since the maximum water levels and the time of their occurrence are the most important parameters required for dam-break flood protection. Two other forms of results presented here are the discharge and depth hydrographs at characteristic sections in a channel. The discharge hydrographs proved to be more sensitive to numerical oscillations (see Figs.5.34, 5.35 and 5.66 and 5.67), and are therefore more frequently presented.

The dam-break computations are conceived to encompass a wide range of cases. To this end, the channel parameters which are considered to be the most important to test the performance of the scheme are varied within some reasonable limits (see Fig.5.2). To permit observation of the influence of inertial effects, the ratio of the initial

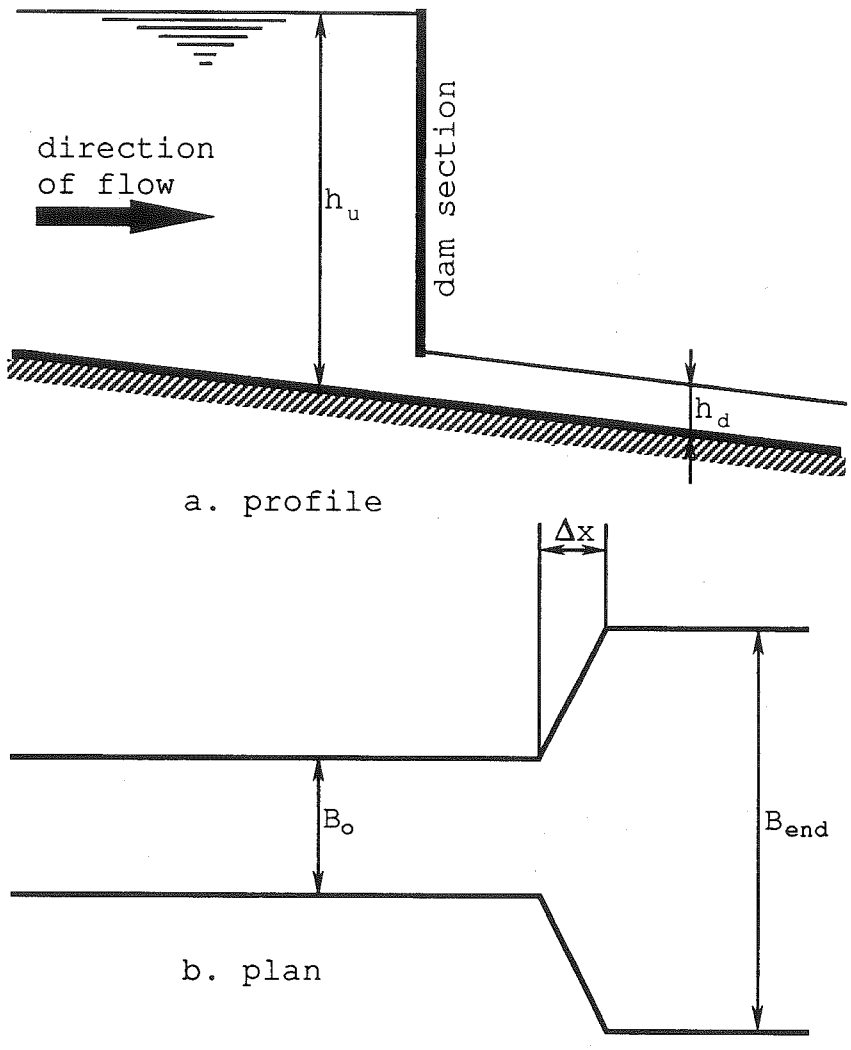

Figure 5.2 Definition sketch for the dam-break test computations

depth behind the dam (upstream depth) to the initial depth below the dam (downstream depth) , h_u/h_d, is varied from 10/1 to 100/1. To estimate the effect of the flow resistance on the performance of the computations, the Manning roughness coefficient is varied from zero (for the frictionless channel) to 0.04 (representative value for natural rivers). To test the influence of nonprismatic channel geometry, the change of width in one spatial step (B_o/B_{end}) is varied from 1/5 to 5/1. Such abrupt changes of channel width are adopted as being typical of the topography of canyon rivers. The initial condition is a uniform flow downstream of the dam, and horizontal water level upstream. The time step for the Godunov method and for the other tested methods is set as large as possible for a stable solution.

V.2 Tests for a frictionless prismatic channel

In this section the frictionless flow in a horizontal and prismatic channel is considered. The goal is to use the available analytical solutions (which can be obtained only for this type of flow) for comparison with the Godunov method. Comparisons of Godunov method with the Preissmann and Lax-Wendroff schemes are also presented.

The analytical solutions for the open channel unsteady flow are described in the literature (see Stoker,1957; Henderson,1966), and only brief descriptions and

explanations for the presented cases are given here. Three general cases are considered in this section:

1. A simple negative wave,
2. A positive wave, and
3. A total instantaneous dambreak.

V.2.1 Simple wave

The first case deals with the so called simple wave, which is a negative elementary wave produced (in this case) by reducing the discharge at the upstream boundary. The objective of this test is to demonstrate the capability of the Godunov method to obtain accurate results for continuous (non-shock) flows. The results of the simple-wave computations are presented in Figs.(5.3)-(5.7).

A frictionless, prismatic and horizontal channel 8 km long and 50 m wide is adopted with a spatial step of 125 m. The initial condition is a constant depth of 5 m and a constant discharge of 250 cms. The discharge at the upstream boundary is linearly decreased from 250 cms to 50 cms in 40 seconds. The downstream boundary condition is a prescribed constant depth of 5 m.

In Figs.(5.3)-(5.7) the evolution of the water-surface profiles in time is presented. In Fig.(5.3) the two Godunov methods differing in interpolation procedure (PPM and linear) are compared. One can observe significantly more

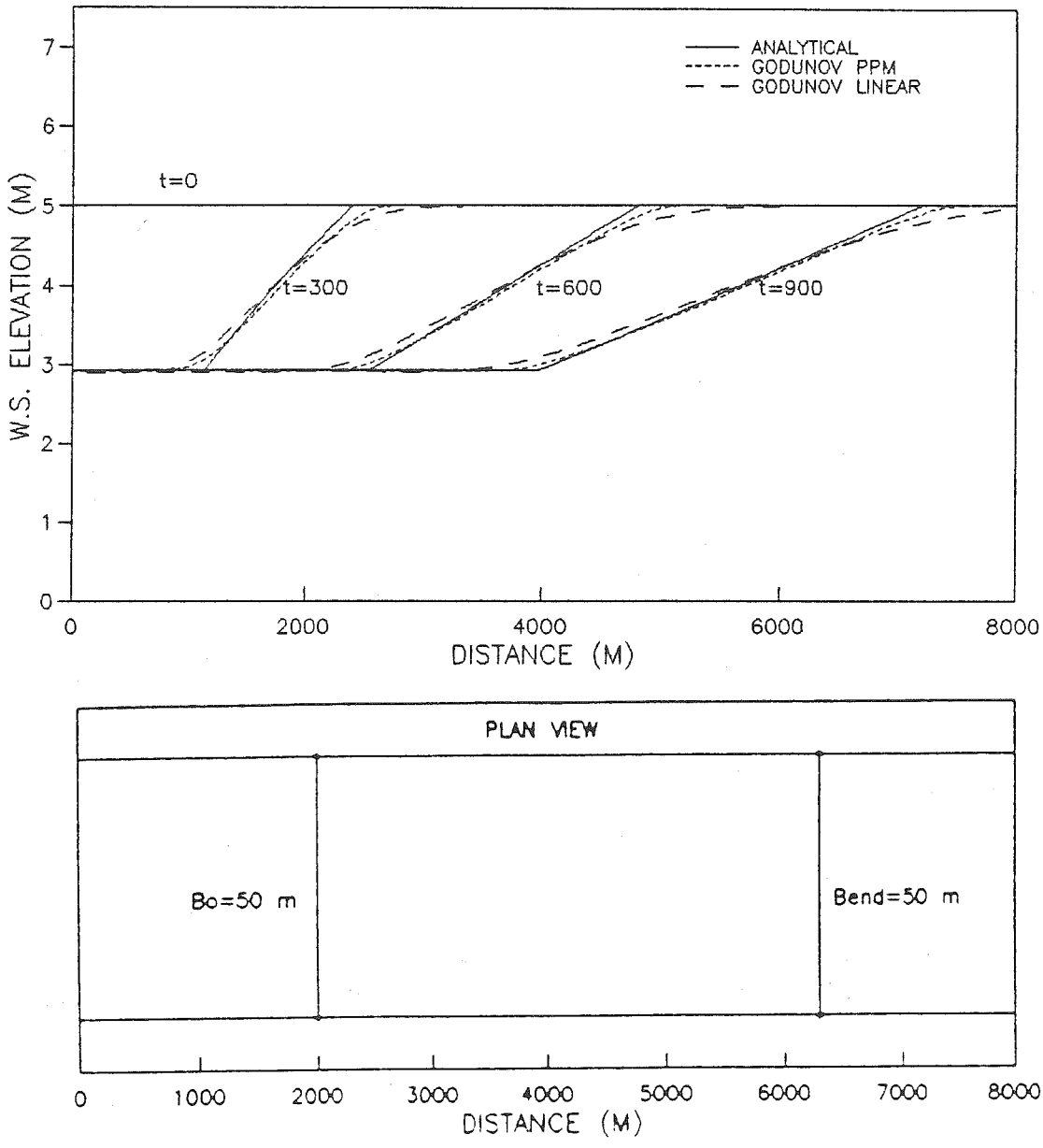

Figure 5.3 Time evolution of water-surface profiles for the simple wave problem; comparison among the analytical solution, PPM Godunov and linear Godunov methods

diffusion in the results of the linear method. Also it is noted that the error is diminishing in time for the PPM method, but increasing for the linear method. The latter is a logical consequence of numerical damping, and the former comes from the fact that for the PPM method the linear method is used for the first two near-boundary points (see section IV.5); consequently the diffusion error introduced from the linear method has large influence for the points close to the boundary, while it fades out for points that are far enough from the boundary. If the near-boundary points are treated with the Lax-Wendroff method, numerical oscillations result, as shown in Fig.(5.4). This can be expected from the results of the Lax-Wendroff method alone (Fig.5.5) showing strong numerical oscillations (which is a characteristic of this second-order scheme, as explained in section II.4).

In Fig.(5.6) the Godunov method is compared with the fixed-grid method of characteristics. Since linear interpolation is used for the fixed-grid method, the presence of numerical diffusion is noticeable. Even though the computation is made with the maximum value of Courant number close to unity (Cr=0.96), it is impossible to maintain a Courant number near unity for all the points of an unsteady flow field; consequently when linear interpolation is used those points having smaller Courant

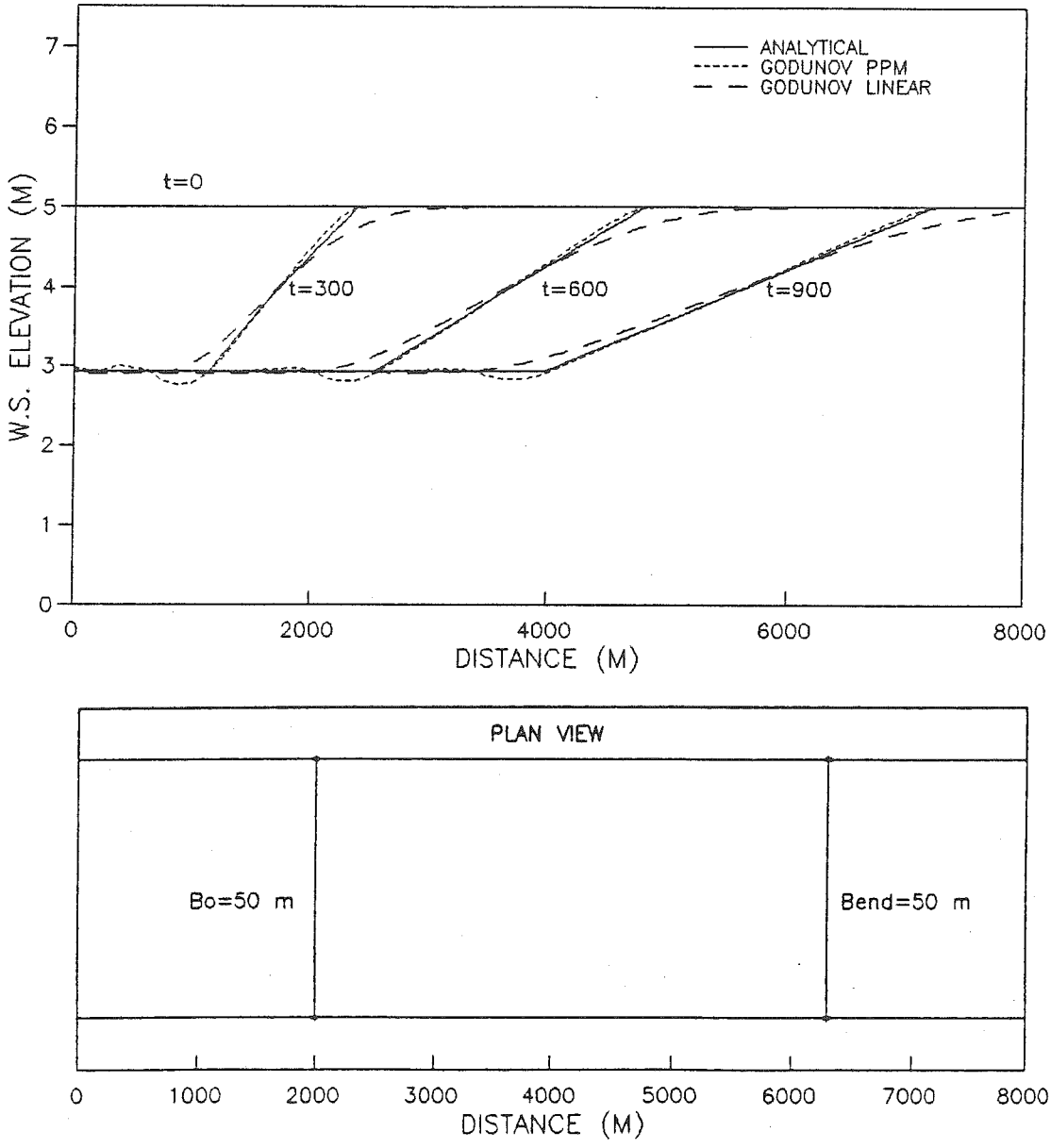

Figure 5.4 Time evolution of water-surface profiles for the simple wave problem; comparison among the analytical solution, PPM Godunov and linear Godunov methods; close-to-the-boundary points for the PPM Godunov method computed using the Lax-Wendroff method

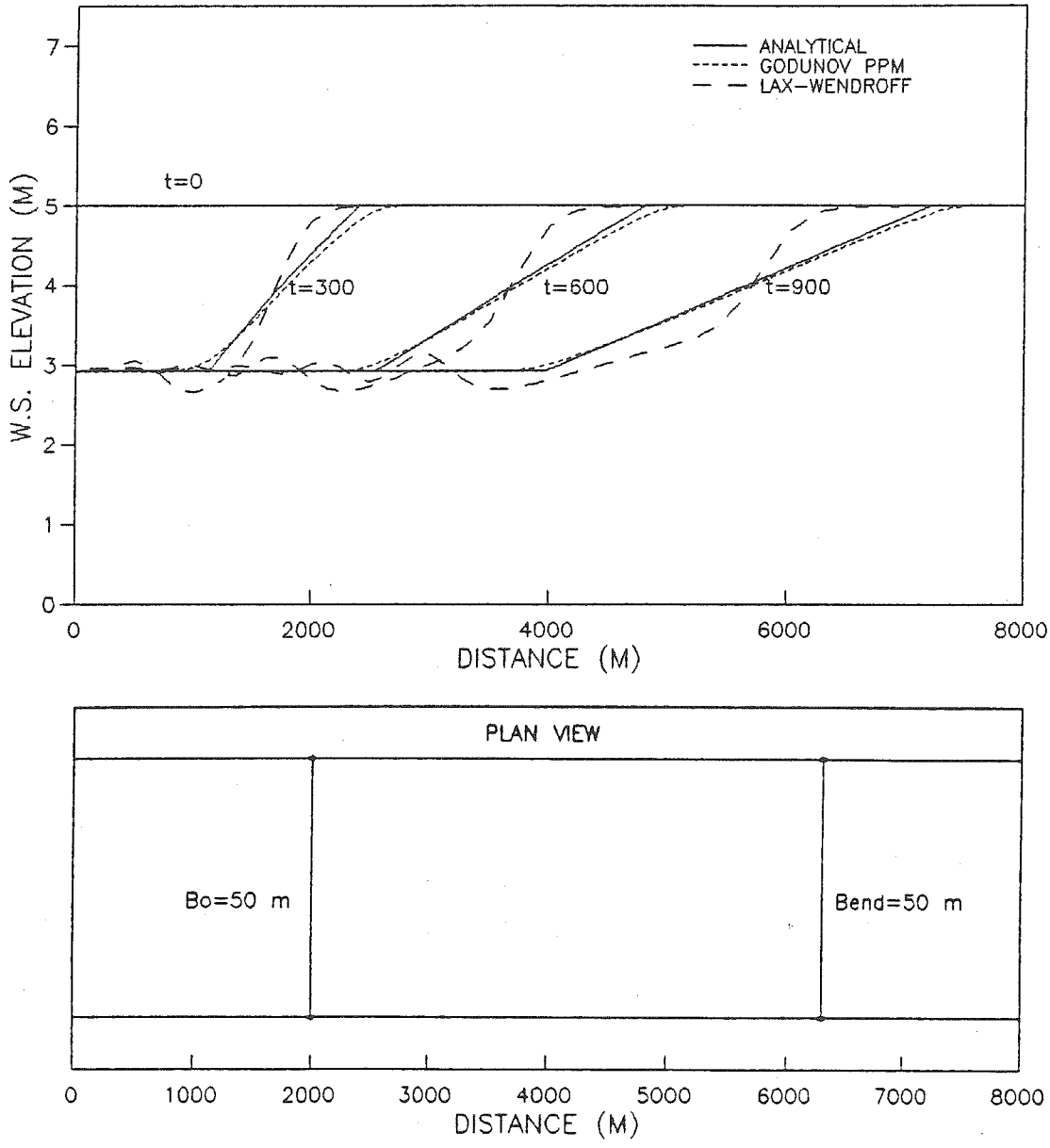

Figure 5.5 Time evolution of water-surface profiles for the simple wave problem; comparison among the analytical solution, PPM Godunov and Lax-Wendroff methods

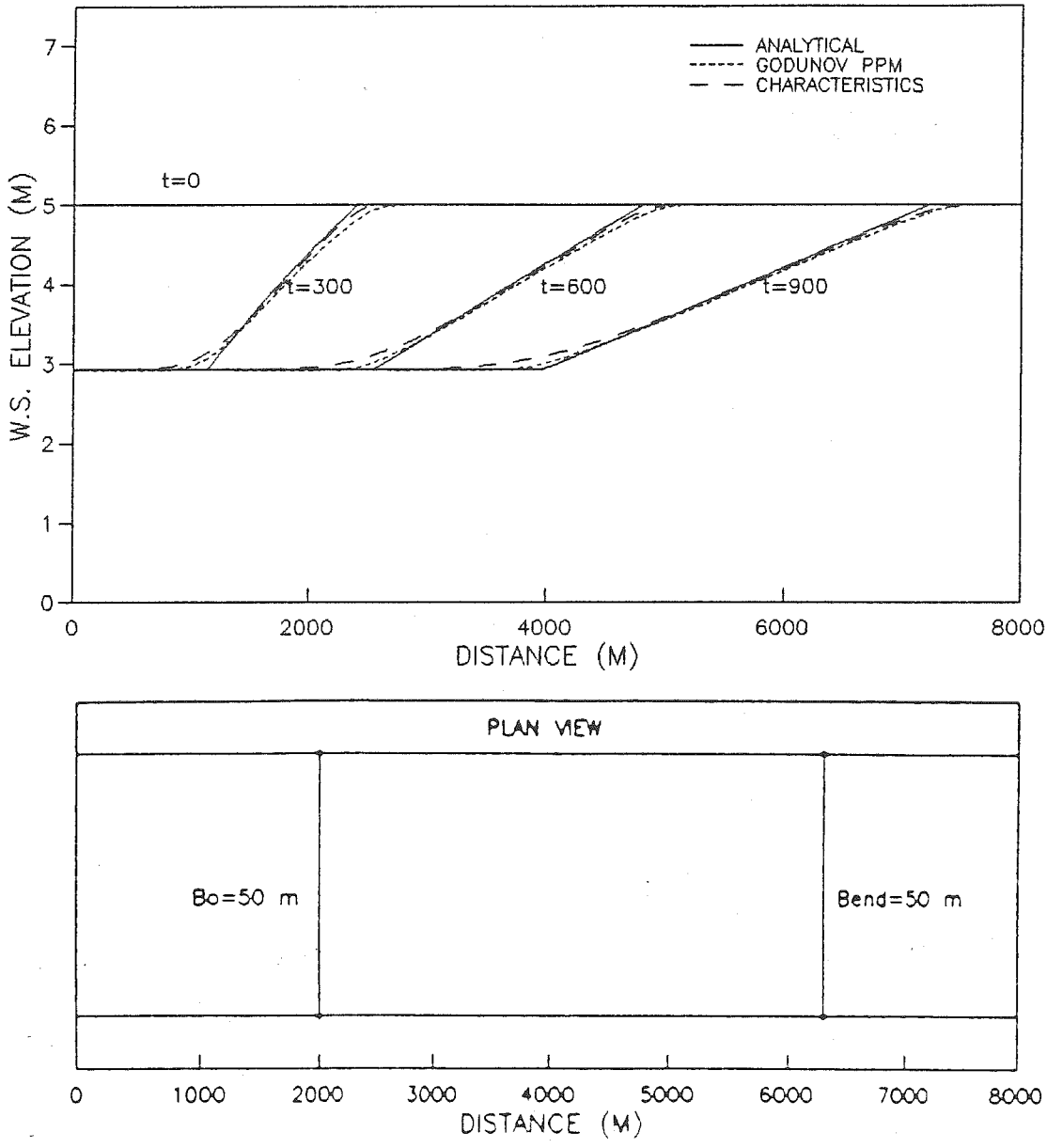

Figure 5.6 Time evolution of water-surface profiles for the simple wave problem; comparison among the analytical solution, PPM Godunov and method of characteristics

numbers suffer from damping of small wavenumber components and numerical diffusion results.

The Preissmann method with a temporal-weighting coefficient of 0.52 and a Courant number of Cr=0.96 gives almost the exact analytical solution, as shown in Fig.(5.7) where it is compared with the analytical solution and the PPM Godunov method.

The relative mass (volume) conservation error for Godunov points (excluding the boundary points and near-boundary points, as defined in section III.6) for both Godunov schemes was of the order of the computer accuracy (close to the 10^{-16}). The overall conservation error (including the boundaries and the near-boundary points) was $2 \cdot 10^{-3}$ for the PPM method and $3 \cdot 10^{-3}$ for the linear method. The Lax-Wendroff method yielded an error of $2 \cdot 10^{-4}$, the fixed-grid method of characteristics $4 \cdot 10^{-3}$, and the Preissmann method $5 \cdot 10^{-7}$.

V.2.2 Positive wave

The second test case presents a positive wave, resulting from increasing the discharge at the upstream boundary, causing a steep-front surge comprising the superposition of elementary waves (as explained in section II.1). A channel with the same characteristics as for the previous case is used, with the same initial conditions;

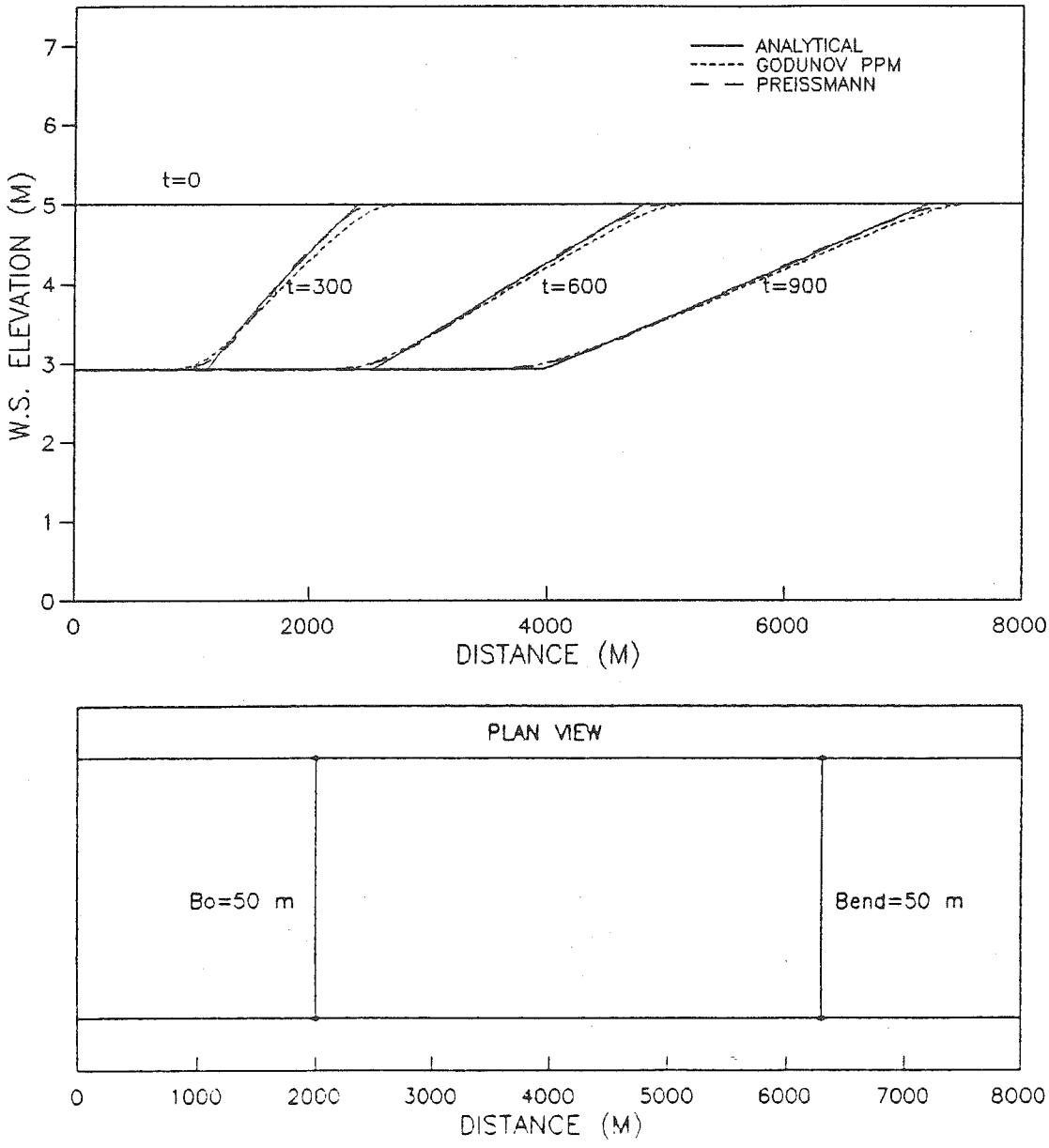

Figure 5.7 Time evolution of water-surface profiles for the simple wave problem; comparison among the analytical solution, PPM Godunov and Preissmann methods

only the upstream boundary condition is changed. Now the discharge is linearly increased from 250 cms/m to 500 cms, again in 40 seconds.

The time evolution of water surface profiles for the PPM and linear Godunov method is presented in Fig.(5.8). The steep-front resolution is much better preserved for the PPM method, remaining confined within one computational reach for the entire time of the computation, while it is gradually smeared by numerical diffusion for the case of the linear method. The agreement of the results of both Godunov methods with the analytical solution is good; the computed values of velocity, depth and wave-speed agree with the analytical solution up to the third significant digit. Again, a small mass conservation error is obtained: $9 \cdot 10^{-4}$ overall, and $5 \cdot 10^{-16}$ for the Godunov points.

No stable solution could be obtained with the Lax-Wendroff method, regardless of grid resolution or the time step (i.e. the Courant number). As anticipated from the results for the simple negative wave (Fig.5.5), without a source of dissipation (channel roughness), large numerical oscillations destroy the Lax-Wendroff solution.

The Preissmann and the PPM Godunov methods are compared in Fig.(5.9). To avoid numerical oscillations the temporal-weighting coefficient for the Preissmann method has to be increased to 0.65, thus resulting in numerical diffusion and

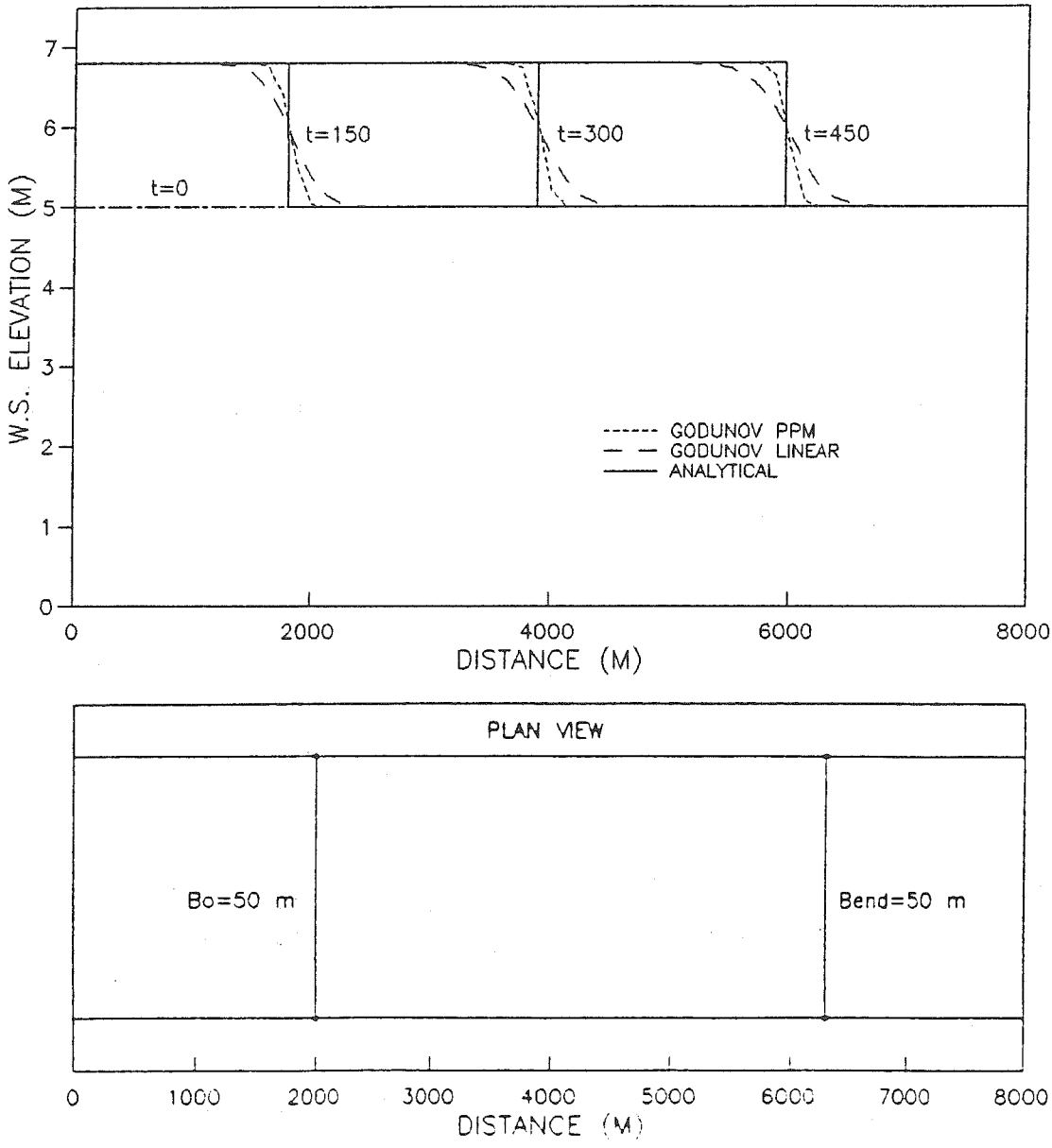

Figure 5.8 Time evolution of water-surface profiles for the positive wave problem; comparison among the analytical solution, PPM Godunov and linear Godunov methods

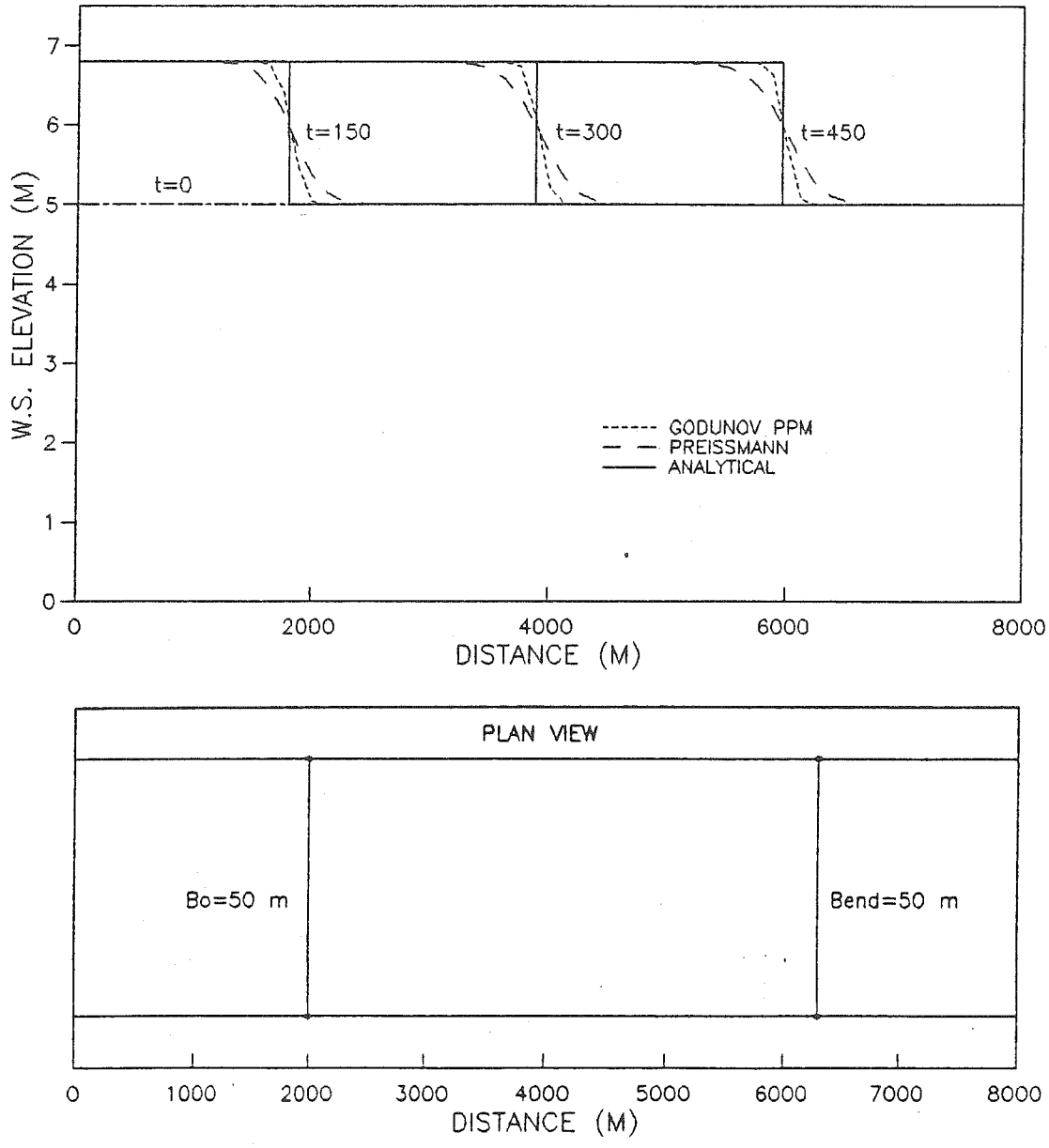

Figure 5.9 Time evolution of water-surface profiles for the positive wave problem; comparison among the analytical solution, PPM Godunov and Preissmann methods

smearing of the wave front. The mass conservation error for the Preissmann method for this case is $2 \cdot 10^{-4}$.

V.2.3 Dambreak for a low dam

The last test case for the frictionless channel concerns the dam-break problem. The physical description and analytical solution for the case of a total and instantaneous dambreak in the wetted downstream channel (the Stoker solution), which is treated here, is already explained in section IV.2.2 on the Riemann solver.

Two values for the upstream-to-downstream depth ratio, h_u/h_d=10/1 and h_u/h_d=100/1 (see Fig.5.2) are considered. (For the sake of simplicity, in the following these are referred as to the cases of a low and a high dam.)

For the case of a low dam a 20 km long and 50 m wide horizontal channel is adopted, with the dam located 10 km from the upstream boundary. A spatial step of 250 m is used. The initial condition is a uniform depth of 1 m downstream of the dam, 10 m upstream of the dam, and a constant discharge of 50 cms. The upstream boundary condition is a prescribed constant discharge of 50 cms, and the downstream boundary condition is a uniform-flow rating curve.

In Figs.(5.10) and (5.11) the results of the PPM and linear Godunov methods are compared with the analytical

Stoker solution. In Fig.(5.10) the time evolution of the water-surface profiles is presented. Both Godunov methods agree well with the analytical solution, though the PPM method performs significantly better than the linear method - both in terms of numerical diffusion, and the resolution and wave-speed of the shock. The wave speed for the Godunov methods is slightly higher than for the analytical solution. This speed error (being around 2 % at the end of the computations) is a consequence of mass conservation; numerical diffusion in the zone of surge close to the steep front results in slightly reduced depths within the surge, and the outcome of mass conservation principle is an extension of the surge length, which increases the speed of the front. The front is practically confined within one spatial step for the PPM method (though small smearing is observed for the adjacent reaches). Smearing of the linear method is much larger and is a result of stronger diffusion, which is the consequence of linear interpolation. For the flow zone outside the steep-front region the maximum relative error in depths does not exceed 3 % for the PPM method, and 9 % for the linear method, while on the average the error is much smaller (around 0.5% for the PPM method, and 1.5% for the linear method). It is worth noting that a mixed flow regime occurs (subcritical flow in the reservoir and downstream of the surge, and supercritical flow within

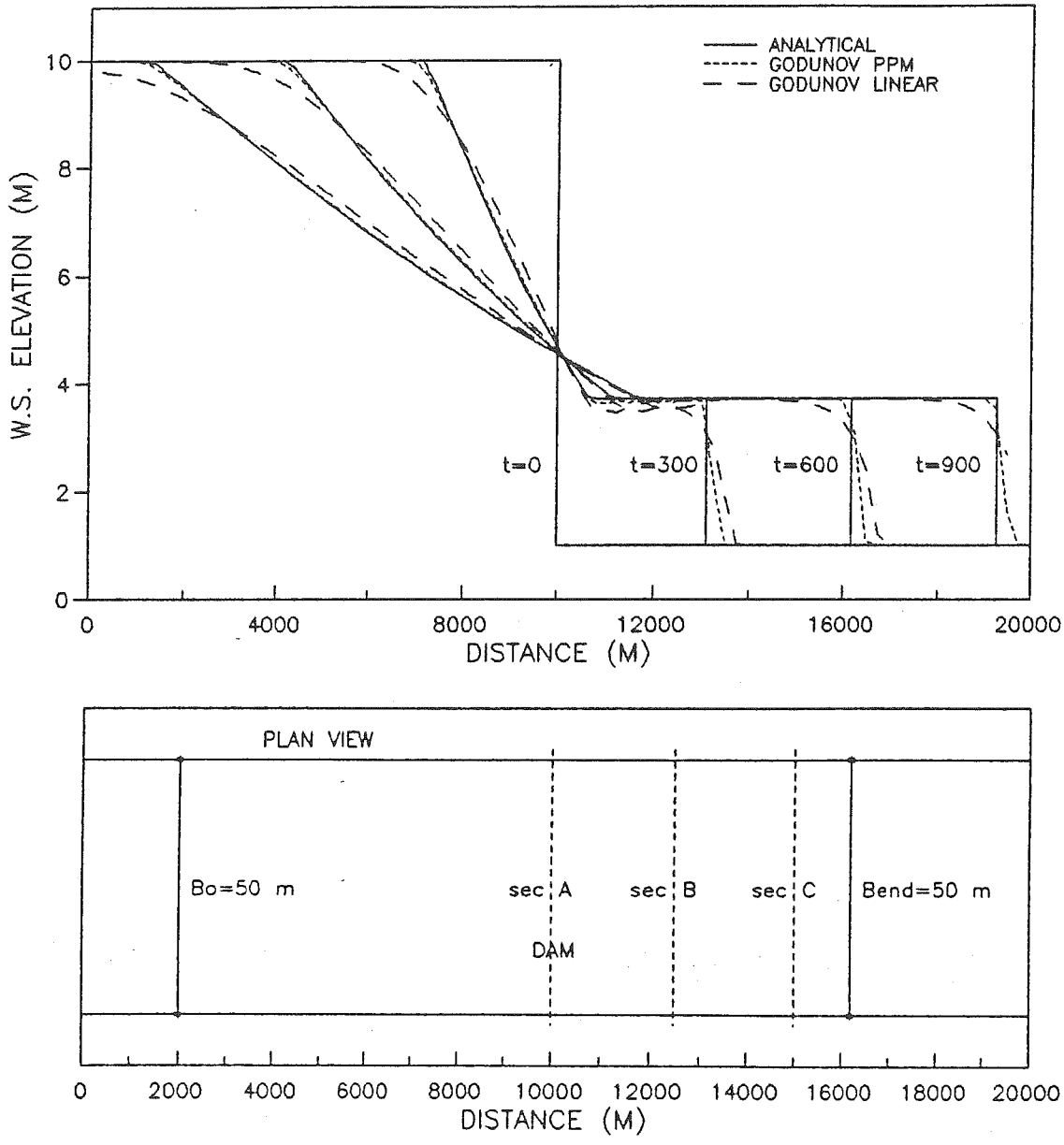

Figure 5.10 Time evolution of water-surface profiles for low-dam dambreak in a frictionless prismatic channel; comparison among the analytical solution, PPM Godunov and linear Godunov methods

the surge, where the Froude number is Fr=1.29), which is a situation difficult to handle efficiently (or to handle at all) for most numerical schemes. No problems of this kind have been observed with the Godunov scheme, which operated with Courant numbers close to unity.

In Fig.(5.11) the discharge hydrographs at sections A (10 km from the upstream end, i.e. the dam section), B (12.5 km from the upstream end) and C (15 km from the upstream end) for the PPM and linear Godunov methods are compared with the analytical solution. The same general behavior observed in the water-surface profile time evolution (Fig.5.10), can be seen here. The PPM method follows closely the analytical solution with small diffusion and some shift, while significantly more diffusion can be observed for the linear method. The relative discharge errors for the points out of the shock zone were less then 0.1 % for the PPM method, and 1.5 % for the linear method. (The original Godunov method, without interpolation, was also tested, but it could not produce reasonable results.)

In Figs.(5.12) and (5.13) a comparison is made between the Godunov PPM and the fixed-grid shock-fitting method of characteristics. The shock itself is better represented for the shock-fitting method (due to the shock-fitting algorithm); on the other hand, the flow in the reservoir is better represented by the Godunov method (see Fig.5.12),

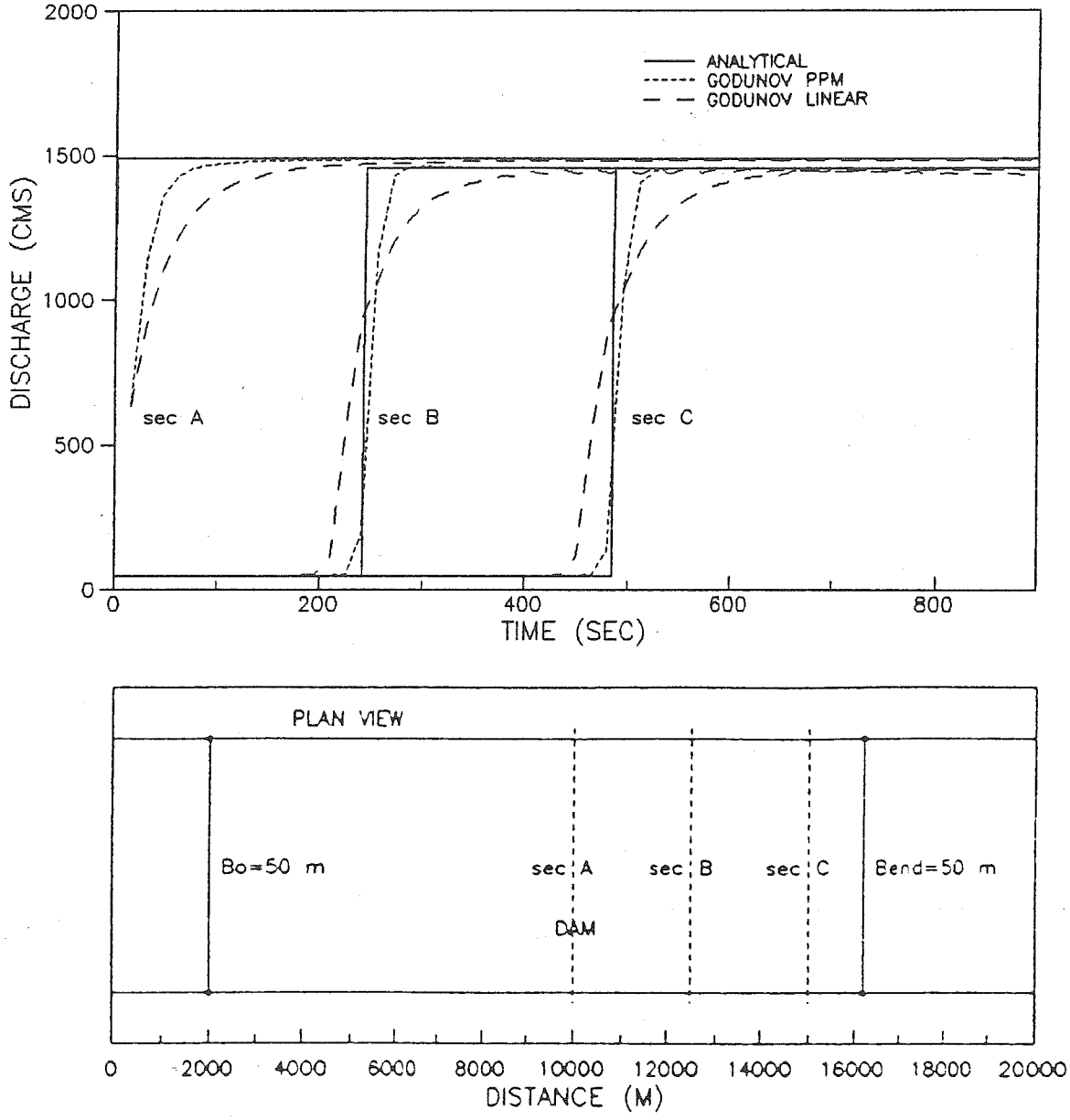

Figure 5.11 Discharge hydrographs for low-dam dambreak in a frictionless prismatic channel; comparison among the analytical solution, PPM Godunov and linear Godunov methods

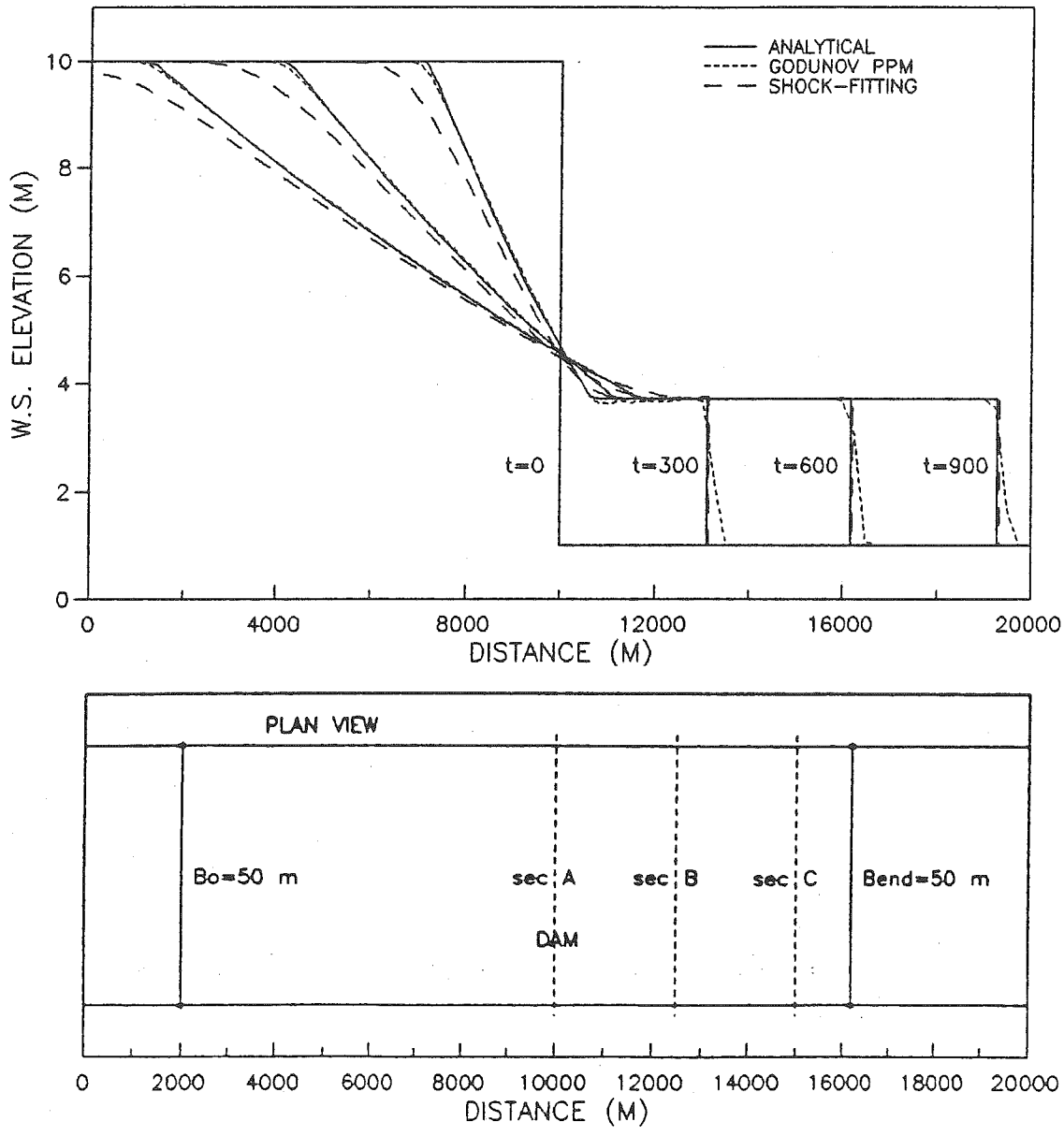

Figure 5.12 Time evolution of water-surface profiles for low-dam dambreak in a frictionless prismatic channel; comparison among the analytical solution, PPM Godunov and shock-fitting methods

because of the large numerical diffusion of the fixed-grid characteristics method based on linear interpolation (as explained earlier). In Fig.(5.13) the discharge hydrographs are compared for the shock-fitting and PPM Godunov methods. As expected, the shock fitting method gives better results for the times during which the steep front passes across the section.

The overall relative mass conservation error for the PPM method was $0.8 \cdot 10^{-4}$ (all points), and $0.7 \cdot 10^{-15}$ (Godunov points only). Similar values are obtained for the linear method, while for the shock-fitting method the error was $0.4 \cdot 10^{-2}$.

No successful computations could be obtained with the Lax-Wendroff and Preissmann methods. For the Lax-Wendroff method the absence of roughness eliminated the potential damping of numerical instability. For the Preissmann method, the mixed flow regime (the Froude number of the surge is 1.29) cannot be accommodated in the double sweep algorithm. (To alleviate the problem, complete matrix inversion can be used for the Preissmann method instead of the double sweep algorithm, but this requires careful treatment of the shock as an internal boundary condition and leads to a tremendous increase in computer time and memory requirements.)

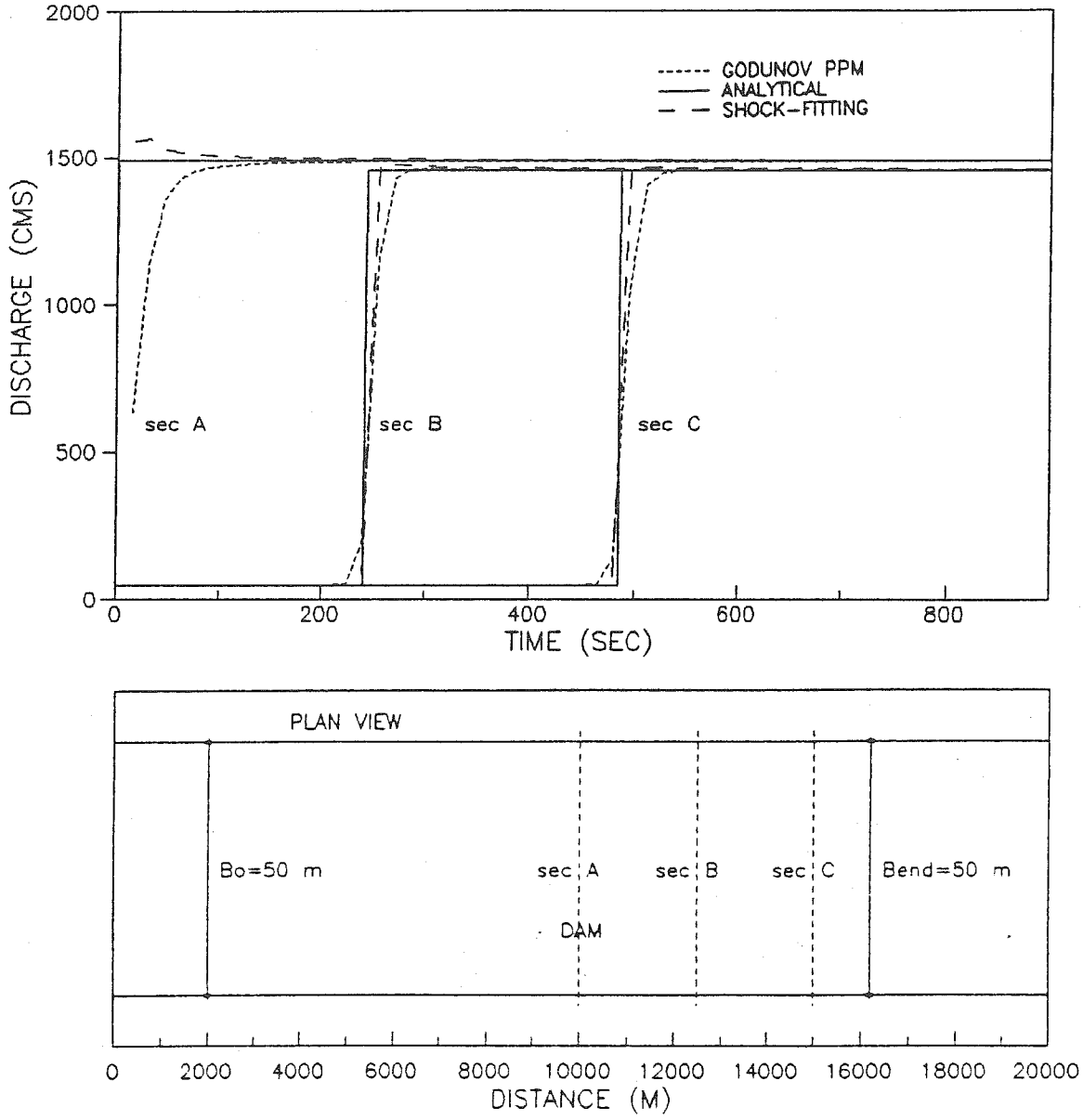

Figure 5.13 Discharge hydrographs for low-dam dambreak in a frictionless prismatic channel; comparison among the analytical solution, PPM Godunov and shock-fitting methods

V.2.4 Dambreak for a high dam

In Figs.(5.14)-(5.17) the case of the high dam (i.e. the case of an upstream-to-downstream depth ratio of h_u/h_d=100/1 (see Fig.5.2) is considered. A channel 100 km long and 50 m wide is adopted, with the dam located 50 km downstream of the upstream boundary. A spatial step of 1000 m is used. The initial condition is a uniform depth of 1 m downstream of the dam, and 100 m upstream of the dam, with a constant discharge of 50 cms. The upstream boundary condition is a prescribed constant discharge of 50 cms, and the downstream boundary condition is a uniform-flow rating curve.

In Figs.(5.14) and (5.15) the results of the PPM and linear Godunov methods are compared with the analytical solution. First, in Fig.(5.14) the time evolution of the water-surface profiles is given. Good agreement with the analytical solution is observed for both of the Godunov methods. Again, the PPM method performs better then the linear method, especially with respect to much smaller numerical diffusion in the reservoir, and better shock resolution. The wave speed error is approximately 1% at the end of the computations, and the maximum error in depths for the region outside of the discontinuity is less then 1.5% for the PPM method and 6 % for the linear method. The shock is confined to one spatial step. The same observation

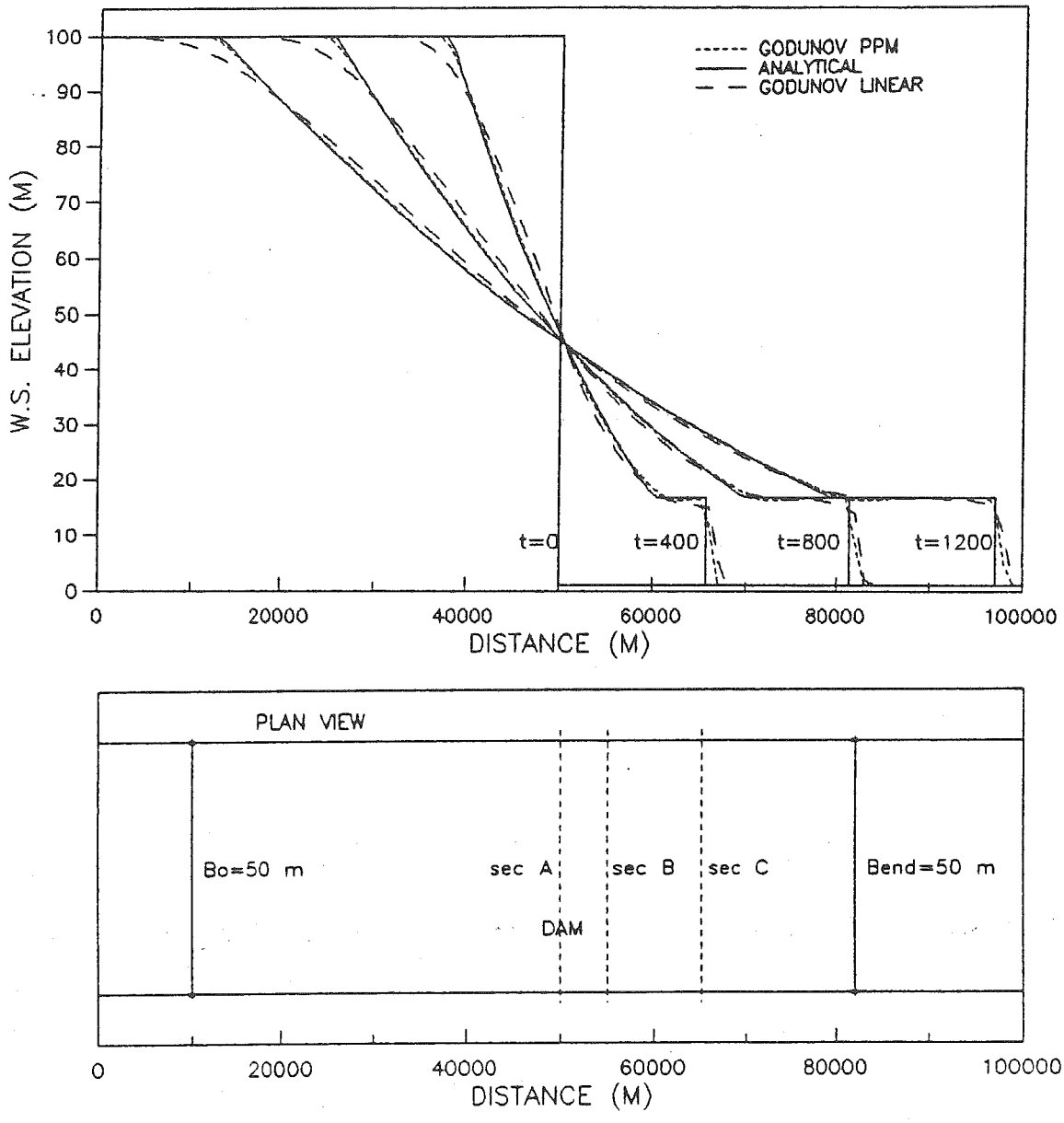

Figure 5.14 Time evolution of water-surface profiles for high-dam dambreak in a frictionless prismatic channel; comparison among the analytical solution, PPM Godunov and linear Godunov methods

stands for the discharge hydrographs (Fig.5.15) which are, for this case, presented at sections A (50 km from the upstream end - the dam section), B (60 km from the upstream end) and C (70 km from the upstream end). The results of the PPM method agree very well with the analytical solution, except for a small phase shift in the vicinity of the shock. The maximum relative error in discharges (for times outside of the shock-passing interval) is 4.2%, while for the most of the computational time the error is less than 0.5%. For the linear Godunov method larger diffusion error (maximum of 5.3 %, and "averaged" less than 2 %), and worse overall agreement with the analytical solution is observed.

In Figs.(5.16) and (5.17) the Godunov PPM and the fixed-grid shock-fitting method of characteristics are compared. Although the shock is preserved exactly for the shock-fitting method, the wave speed is now slightly better determined by the Godunov method (Fig.5.16), i.e. one can observe that the speed for the shock-fitting method is increasing faster relative to the analytical, than is the speed of the Godunov method. The flow in the reservoir is represented significantly better by the Godunov method (for the reasons explained earlier). In Fig.(5.17) the discharge hydrographs are compared for the shock-fitting (characteristics) and PPM Godunov method. Contrary to the case of the low dam, here the Godunov method is superior to

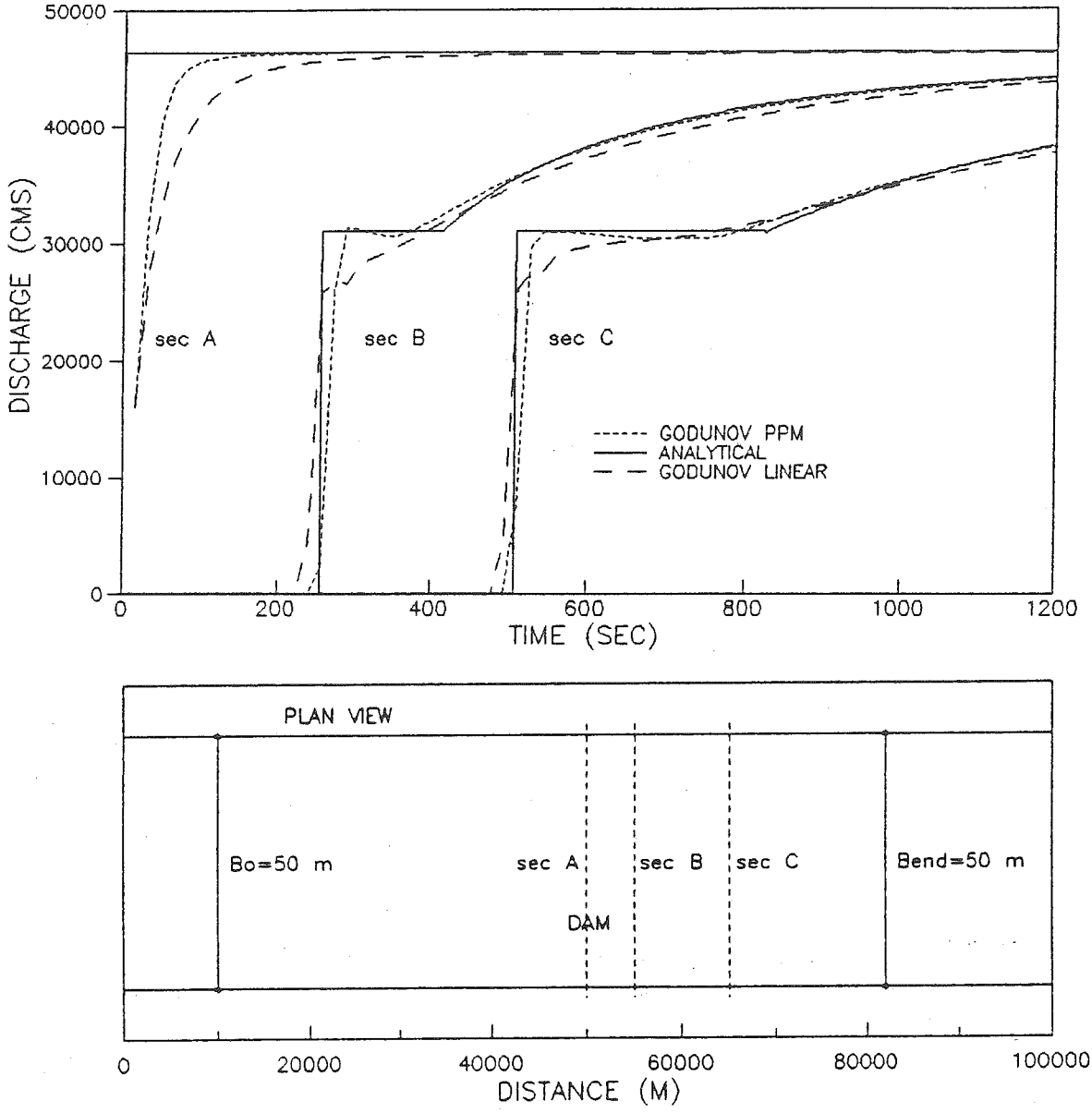

Figure 5.15 Discharge hydrographs for high-dam dambreak in a frictionless prismatic channel; comparison among the analytical solution, PPM Godunov and linear Godunov methods

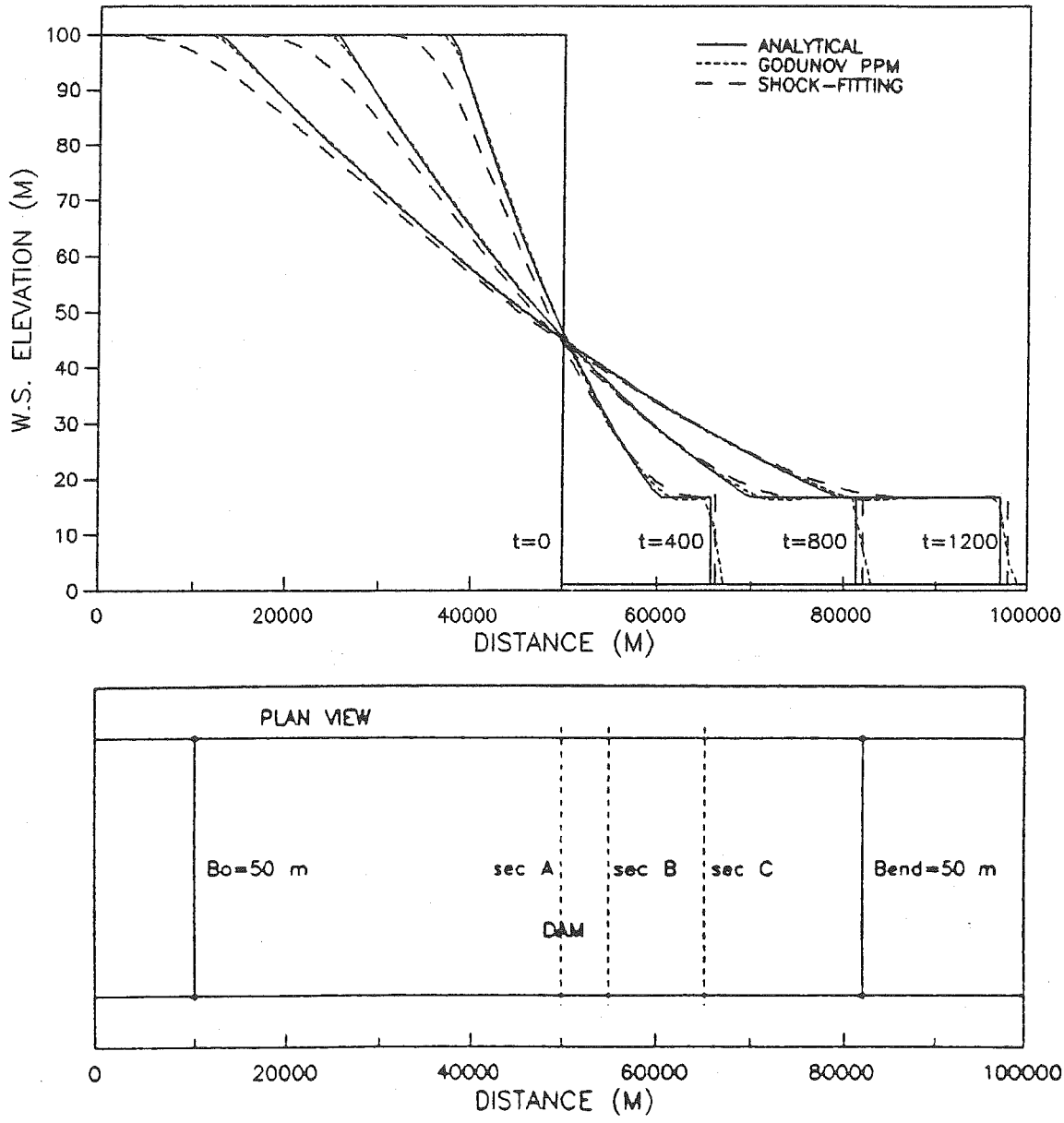

Figure 5.16 Time evolution of water-surface profiles for high-dam dambreak in a frictionless prismatic channel; comparison among the analytical solution, PPM Godunov and shock-fitting methods

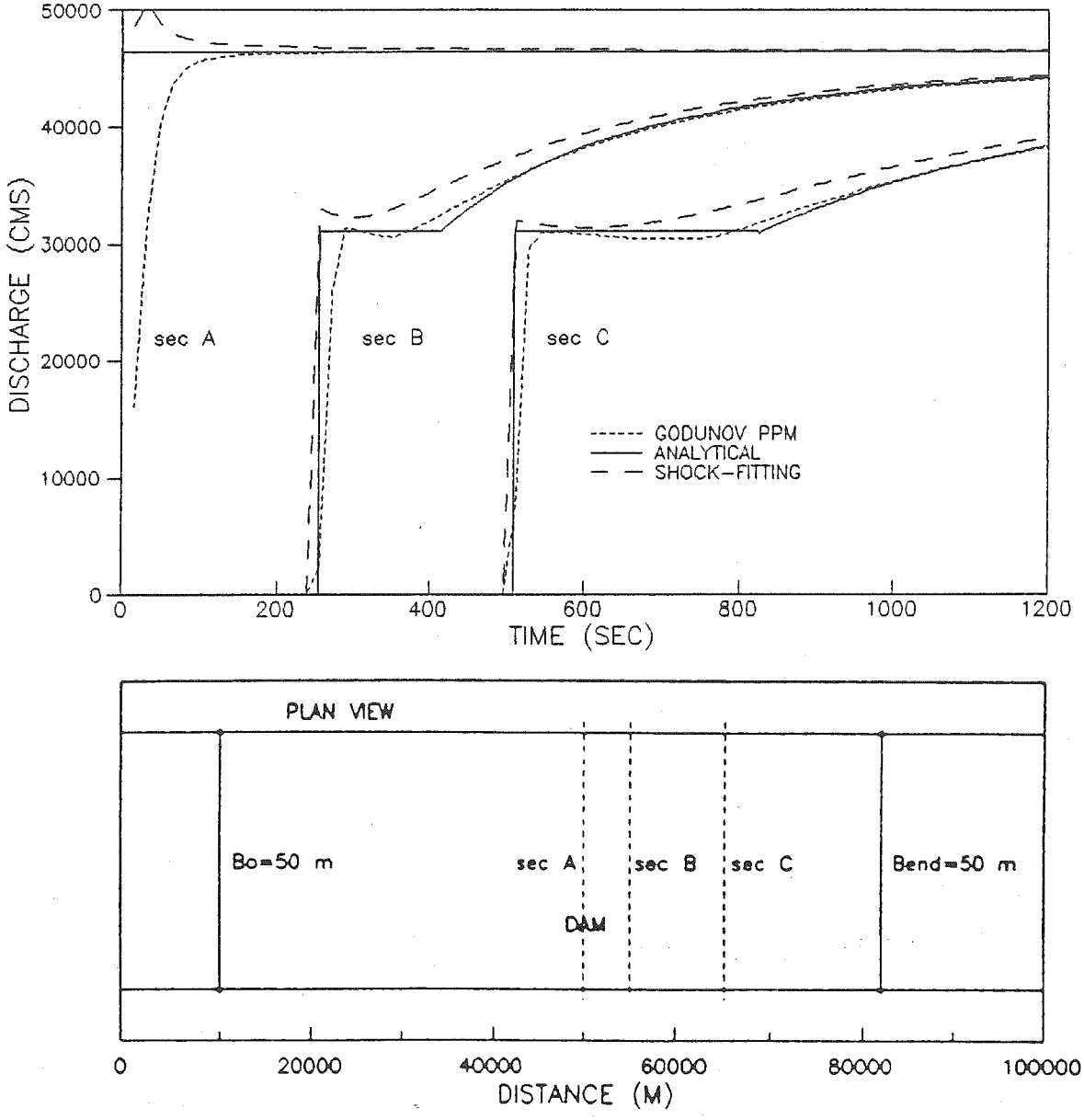

Figure 5.17 Discharge hydrographs for high-dam dambreak in a frictionless prismatic channel; comparison among the analytical solution, PPM Godunov and shock-fitting methods

the shock-fitting method, except for the small length of time of the arrival and passage of the shock. The explanation is that for the method of characteristics (the shock-fitting method) in the case of larger upstream-to-downstream depth ratio, larger differences in Courant numbers at different points of the flow field greatly reduces the accuracy of linear interpolation, thus making numerical diffusion more pronounced.

The overall relative mass conservation error for the PPM method is $0.3 \cdot 10^{-5}$ (all points), $0.3 \cdot 10^{-15}$ (Godunov points only), and $0.1 \cdot 10^{-1}$ for the shock-fitting method of characteristics.

Again, no successful computations were obtained using the Lax-Wendroff and Preissmann methods.

From the above tests one can conclude that for the case of a frictionless horizontal channel the Godunov scheme (in particular the PPM method) applied to steep-front computations outperforms the competitive Lax-Wendroff and Preissmann schemes. It copes naturally with the mixed flow regime. Good mass conservation is achieved and, in particular for the PPM method, good resolution of the front, which is on the average confined to one computational step.

V.3 Tests for a frictional prismatic channel

This section tests the performance of the Godunov

method for the case of a real frictional and sloped channel. The prismatic case is presented separately from a nonprismatic case to isolate the influence of the resistance and gravity effects contained within the source term, and problems in their integration in time and space. This is a step towards treatment of the more realistic case of nonprismatic channels, with their additional source-term contributions, which are then treated in section V.4. The analytical solution for the frictional sloped channel does not exist, because of the nonlinearity in the source term.

Two test situations are presented in this section:

1. A positive surge (induced by upstream boundary operations); and

2. A total and instantaneous dambreak.

The first test case is a kind of introductory illustration of the effect of roughness on the numerical solution and on the flood waves themselves.

V.3.1 Positive surge

A prismatic rectangular channel, 100 km long and 50 m wide with a slope of 0.1 % and Manning roughness coefficient of 0.04, is used with a spatial step of 1000 m. The initial condition is a uniform flow with a depth of 3 m and the corresponding discharge of 228.72 cms. The upstream boundary condition is a prescribed discharge, increasing

linearly from 250 to 1000 cms in 40 seconds. The downstream boundary condition is a uniform-flow rating curve.

In Figs.(5.18)-(5.20) the time evolution of the water-surface profiles is shown for the Godunov (PPM and linear), Lax-Wendroff, and Preissmann methods. High resistance, obtained through the large roughness coefficient, produces enough natural damping to diffuse a steep front. At the same time it dampens artificial oscillations, otherwise present for the Lax-Wendroff method (and Preissmann method with a temporal-weighting coefficient close to 0.5). Consequently, very good agreement among all compared methods, as well as small conservation errors, are achieved.

V.3.2 Dambreak for a low dam with small roughness

Now for the dam-break cases, two ratios of the upstream-to-downstream depth are considered: a low dam with a depth ratio of 10/1, and a high dam with the ratio of 100/1. Two different roughnesses, one a Manning coefficient of 0.015, corresponding to a crude concrete channel, and the other 0.040, corresponding roughly to natural rivers, are used.

First the case of a low dam is considered. A channel 20 km long and 50 m wide, with a slope of 0.1 %, is used with a spatial step of 250 m and a Manning roughness coefficient of 0.015. The initial condition (see Fig.5.2)

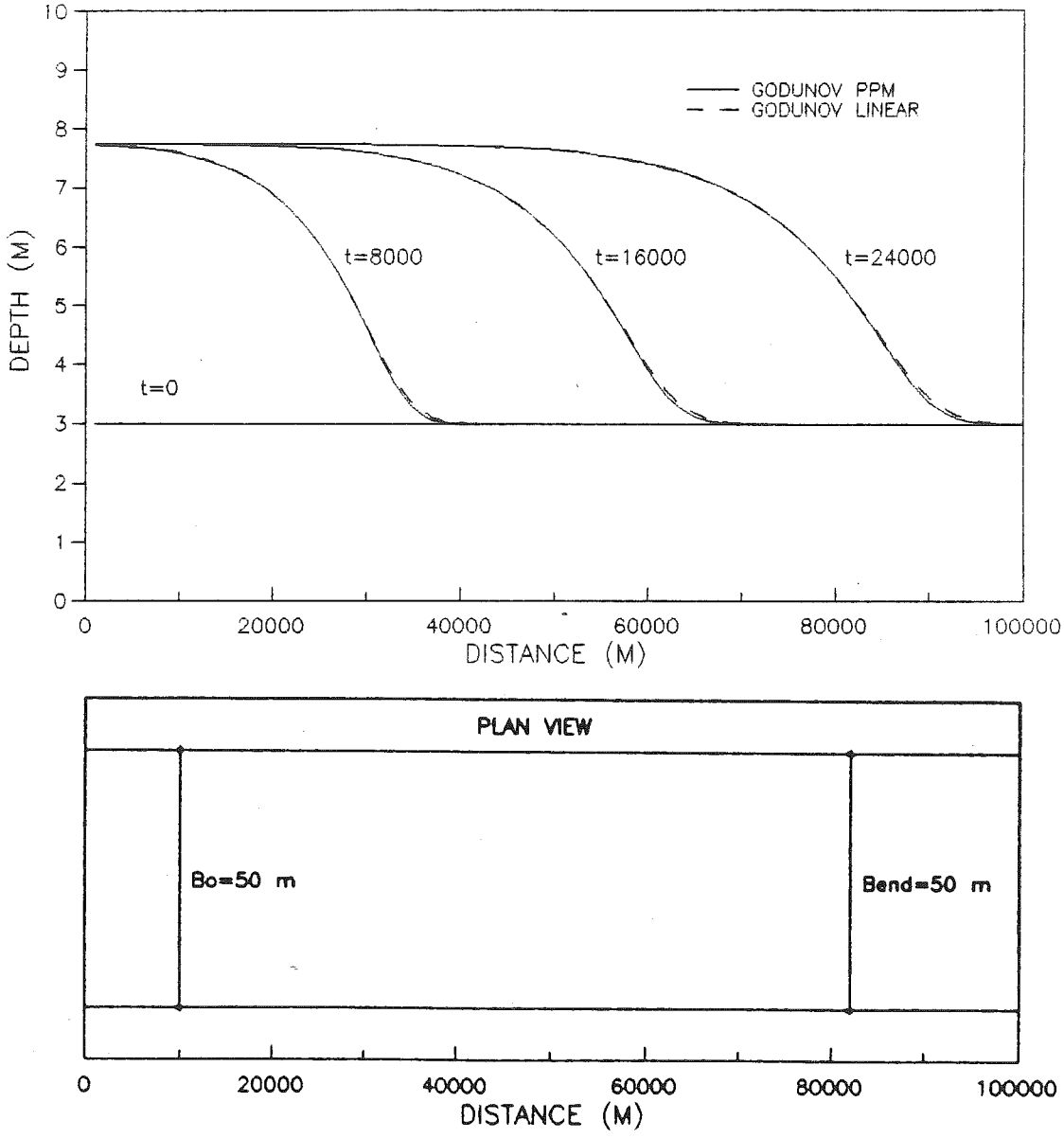

Figure 5.18 Time evolution of water-surface profiles for the positive wave in a frictional channel; comparison between PPM Godunov and linear Godunov methods

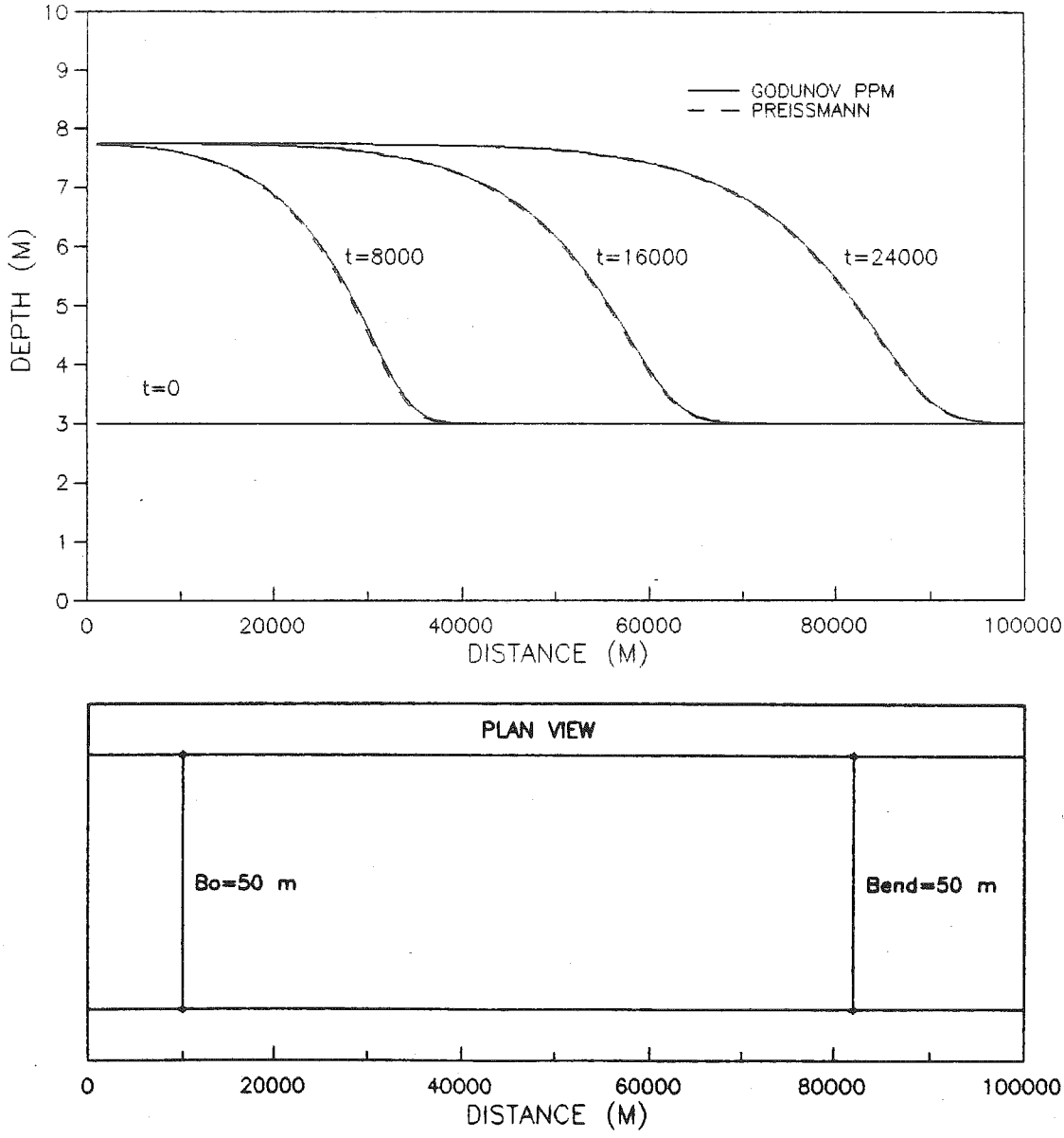

Figure 5.19 Time evolution of water-surface profiles for the positive wave in a frictional channel; comparison between PPM Godunov and Preissmann methods

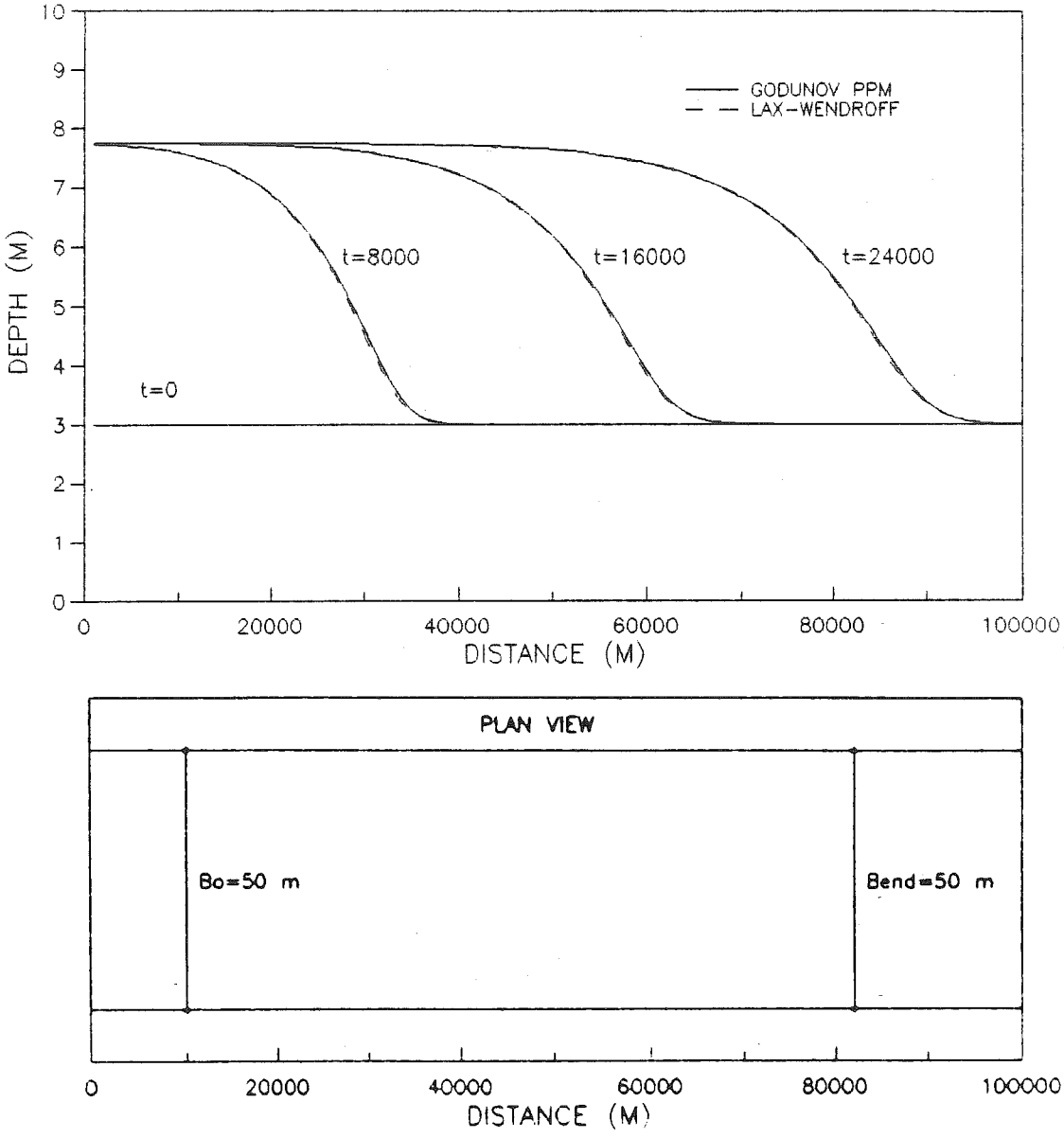

Figure 5.20 Time evolution of water-surface profiles for the positive wave in a frictional channel; comparison between PPM Godunov and Lax-Wendroff methods

is a uniform flow downstream of the dam, with depth of 1 m and a corresponding discharge of 102.89 cms. It is assumed that the water level is initially constant and horizontal in the reservoir upstream; this suppression of upstream backwater effects has no effect on the dam-break computations. (The discharge is initially 102.89 cms in the entire computational region, regardless of whether this presents a true steady state or not). The upstream boundary condition is a constant discharge of 102.89 cms, and the downstream boundary condition is a uniform-flow rating curve.

In Fig.(5.21) the time evolution of water-surface profiles for the Godunov PPM and linear Godunov methods are compared. One can observe better agreement between the two methods then for the case of a frictionless channel (compare Fig.5.10). Still, it is clear that the PPM method gives better resolution in the zone of discontinuity, and produces less numerical diffusion, particularly in the reservoir. It is important to note that the discontinuity is still confined to a zone of approximately one spatial step for the PPM method, and is slightly more smeared for the linear method. For both methods, and in general for all Godunov computations for prismatic and nonprismatic frictional channels, overall mass conservation error is less than 10^{-5}, and around 10^{-16} for the Godunov points only.

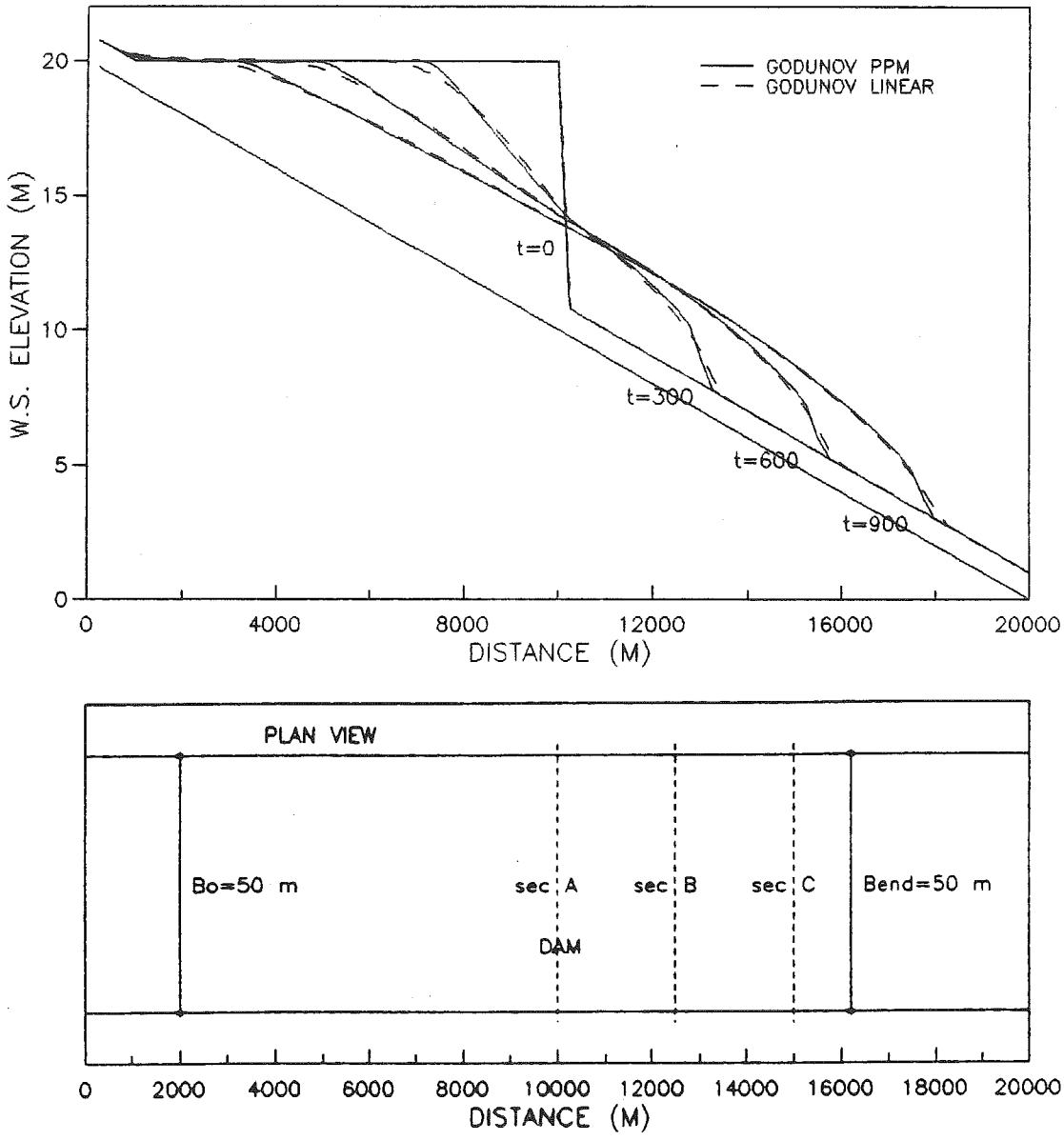

Figure 5.21 Time evolution of water-surface profiles for low-dam dambreak in a prismatic channel of small roughness; comparison between the PPM Godunov and linear Godunov methods

In Figs.(5.22) and (5.23) the Godunov PPM method is compared with the shock-fitting method. From Fig.(5.22) one can observe that the resolution of the front for the shock-fitting method is clearly better (since there can be no smearing for the shock-fitting method). However, as mentioned before, the Godunov method is weaker in that respect (front resolution) only for the smearing within one spatial step; this shortcoming is of little practical importance. Based on the experience from the frictionless cases (where the results for the shock-fitting method suffered from significant numerical diffusion), disagreement between the two methods in the reservoir is attributed to diffusion of the shock-fitting method. Again, the shock-fitting method of has a large mass conservation error of $1 \cdot 10^{-2}$. Comparison of the discharge hydrographs for the Godunov PPM and the shock-fitting methods at the sections A (the dam section, 10 km from the upstream boundary), B (12.5 km form the upstream boundary) and C (15 km from the upstream boundary) are given in Fig.(5.23). Some numerical oscillations are present for the Godunov method, but they are easily removed by reduction of the spatial step. The hydrographs at sections B and C ascend more abruptly for the shock-fitting method than for the Godunov method, reflecting the instantaneous arrival of the perturbation (the shock). It can be observed that the values of the shock-fitting

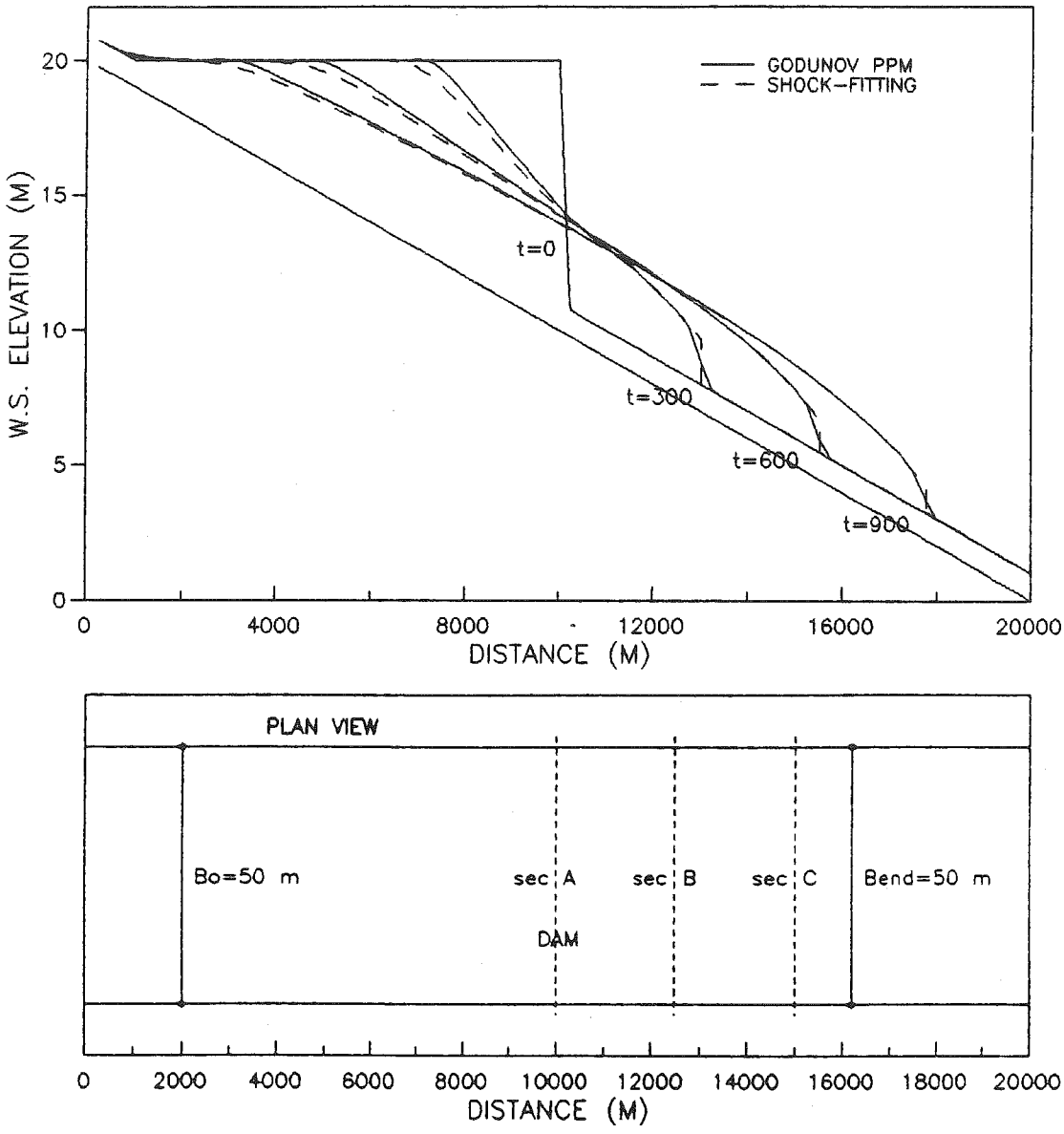

Figure 5.22 Time evolution of water-surface profiles for low-dam dambreak in a prismatic channel of small roughness; comparison between the PPM Godunov and shock-fitting methods

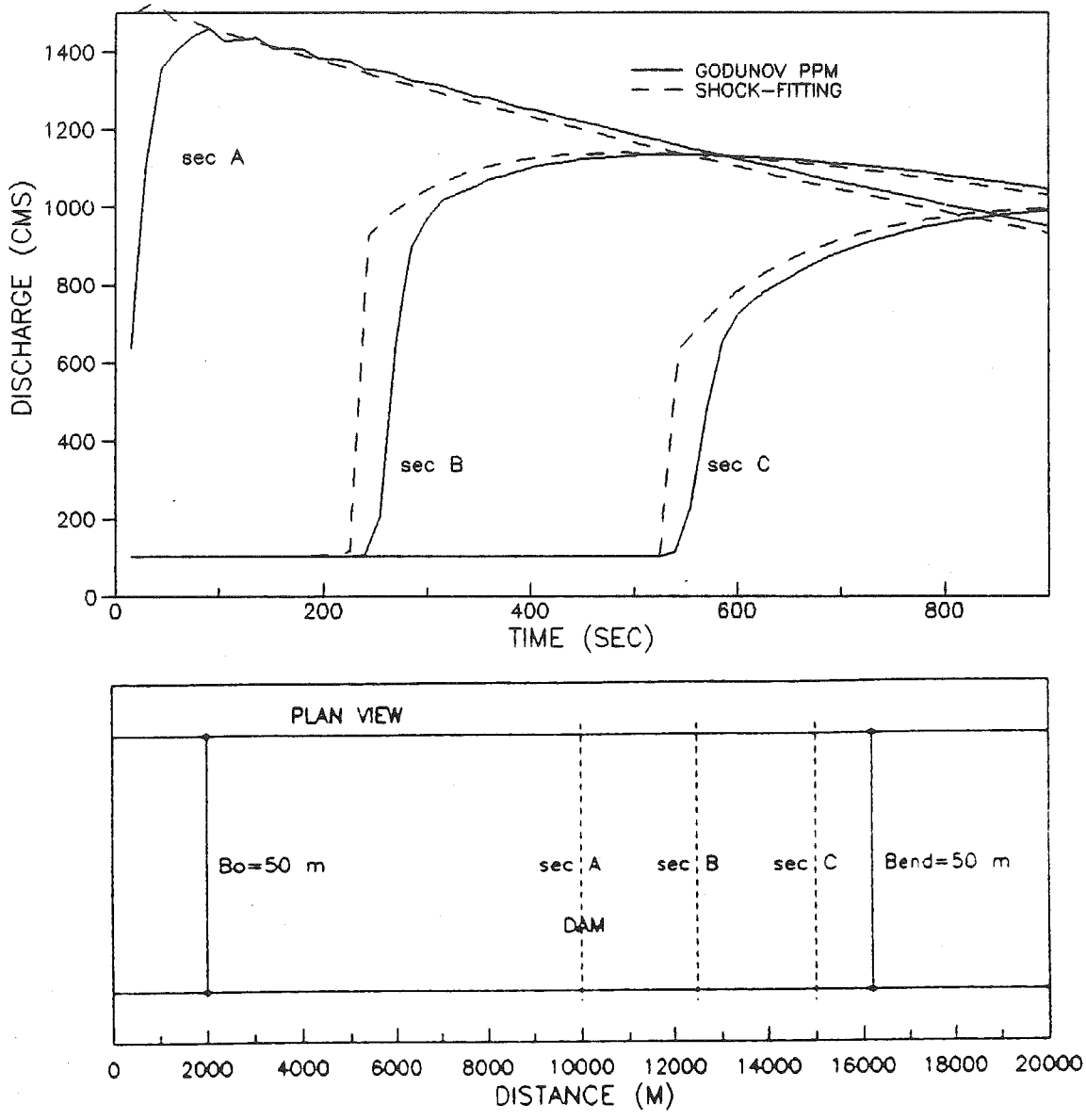

Figure 5.23 Discharge hydrographs for low-dam dambreak in a prismatic channel of small roughness; comparison between the PPM Godunov and shock-fitting methods

discharges at large times are consistently smaller then those of the Godunov method, a consequence of the large conservation error for the former method.

In Figs.(5.24) and (5.25) the Godunov PPM and the Preissmann methods are compared. Successful computation with the Preissmann method was possible only for a large time step (inducing a Courant number of 2.7), which jumps over the mixed flow regime occurring in the first stages of the computation. The result is (as expected by Fennema and Chaudhry, 1986) large numerical diffusion and smearing of the front (Fig.5.24). The mass conservation error for the Preissmann method is $3 \cdot 10^{-6}$.

A successful computation with the Lax-Wendroff method could not be obtained, no matter how small the time step; numerical oscillations were still too strong for the small resistance to diffuse them.

V.3.3 Dambreak for a low dam with large roughness

The same channel is used as for the previous set of computations except that now the Manning roughness is 0.040, producing a scenario of realistic dambreak in a natural river. The discharge for the initial and upstream boundary conditions is reduced to 38.51 cms, to keep the same normal depth of 1 m in a uniform flow downstream of the dam.

Due to the influence of the high resistance, the shock

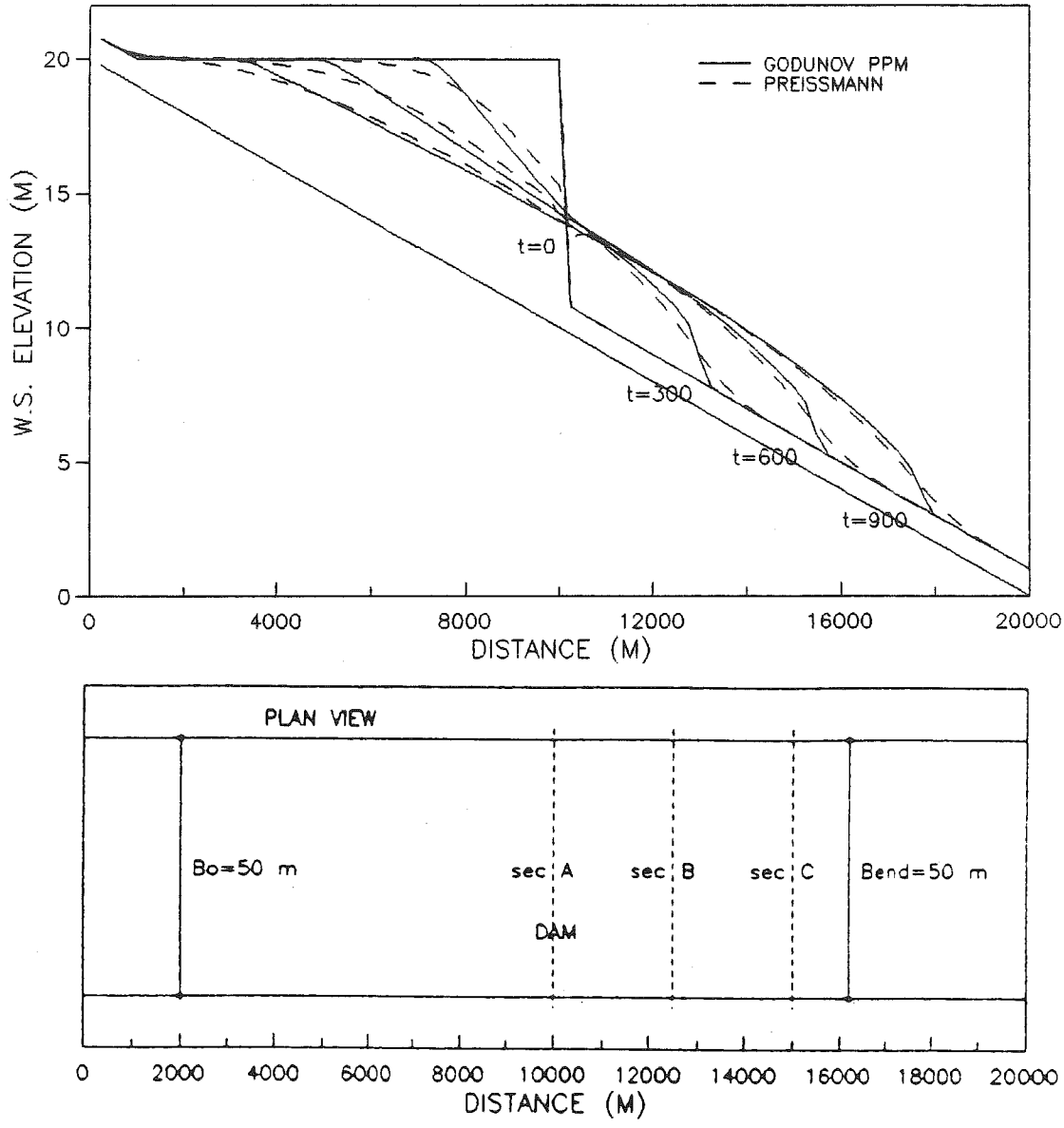

Figure 5.24 Time evolution of water-surface profiles for low-dam dambreak in a prismatic channel of small roughness; comparison between the PPM Godunov and Preissmann methods

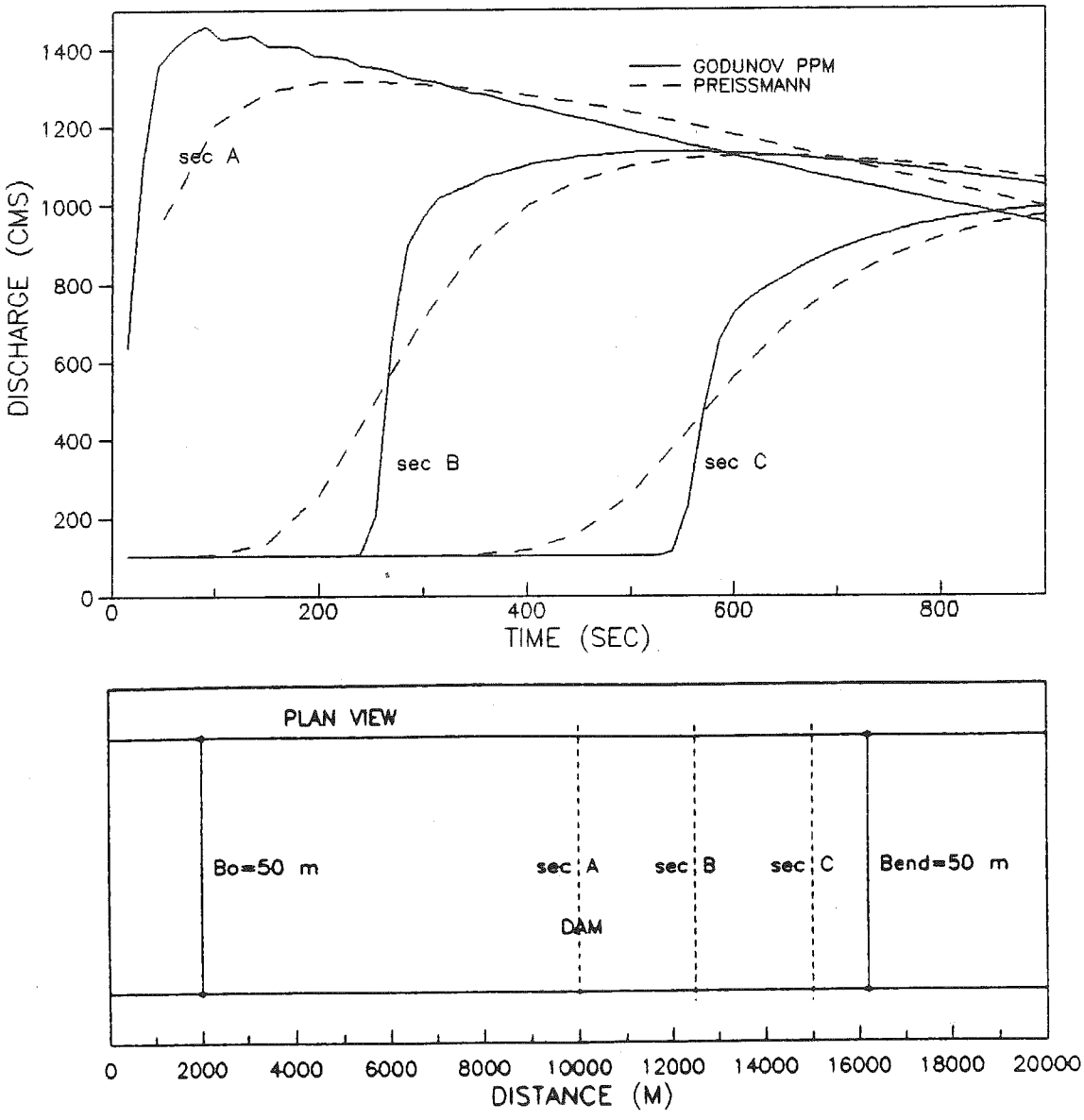

Figure 5.25 Discharge hydrographs for low-dam dambreak in a prismatic channel of small roughness; comparison between the PPM Godunov and Preissmann methods

is very soon diffused, mixed regime does not occur, and the computations for all methods are more stable. In general, the results of all methods agree well with one another, although the shock-fitting method has a significant conservation error ($1 \cdot 10^{-2}$) and diffusion in the reservoir zone Fig.(5.28).

The two Godunov methods agree here almost perfectly in water-surface profiles (Fig.5.26), except for some small differences in the shock zone and in the upstream portions of the reservoir. The discharge hydrographs on Fig.(5.27) also agree well, except for the peak discharge at the dam section - a quantity of little practical significance.

The results of water-surface elevation profiles computed by the PPM Godunov and the shock-fitting methods are presented in Fig.(5.28). One can observe very good agreement in the shape of the surge, which confirms that the resolution of the Godunov method is excellent.

The computation for the Preissmann method is now possible with a Courant number of unity, though still requiring a large value of the temporal-weighting coefficient, 1.0. Consequently, the smearing (Figs.5.29 and 5.30) is now much smaller then in the case of smaller roughness. The results of the Lax-Wendroff and PPM Godunov method are compared in Figs.(5.31) and (5.32). Very small differences can be observed for the water-surface elevations

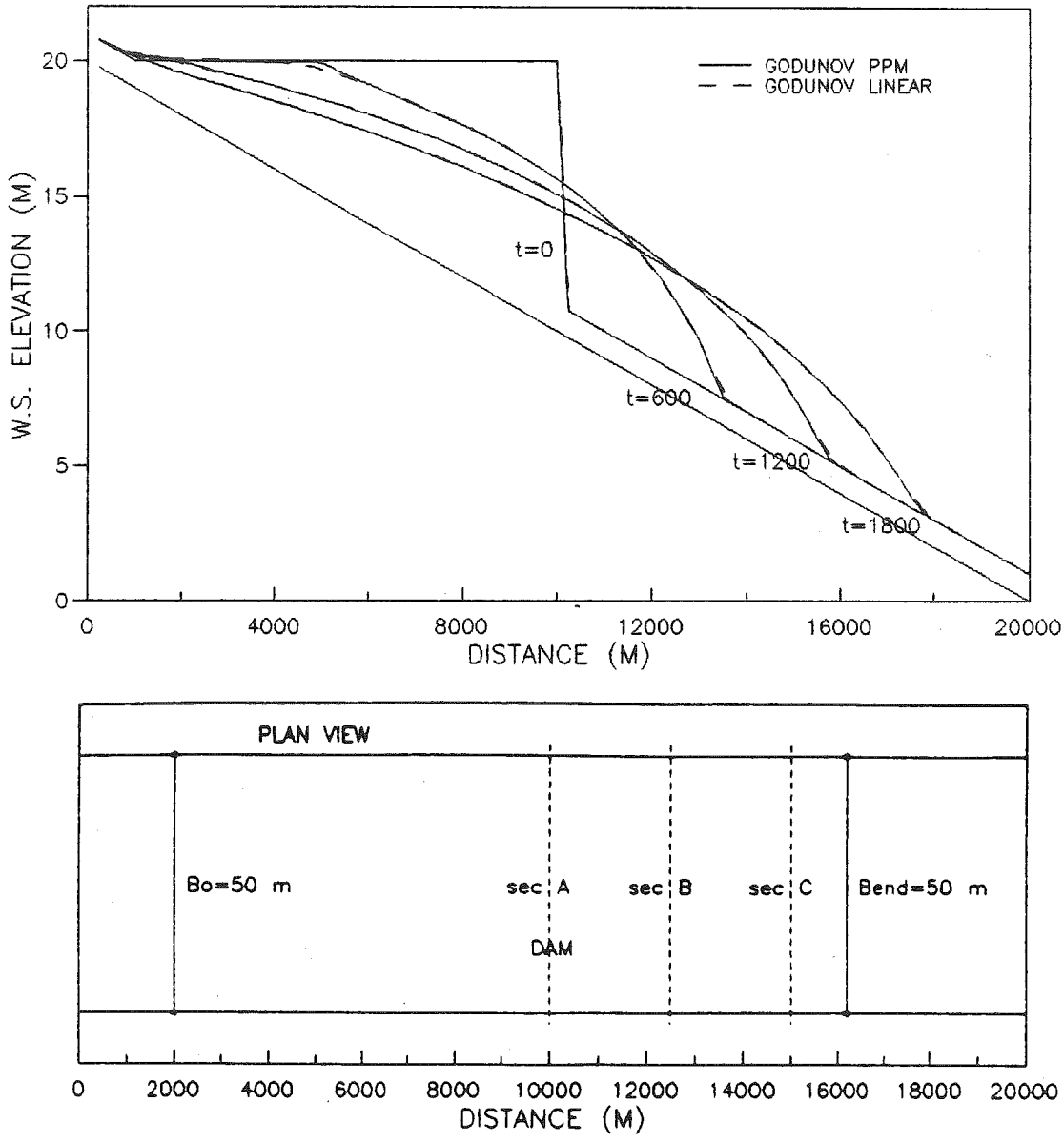

Figure 5.26 Time evolution of water-surface profiles for low-dam dambreak in a prismatic channel of large roughness; comparison between the PPM Godunov and linear Godunov methods

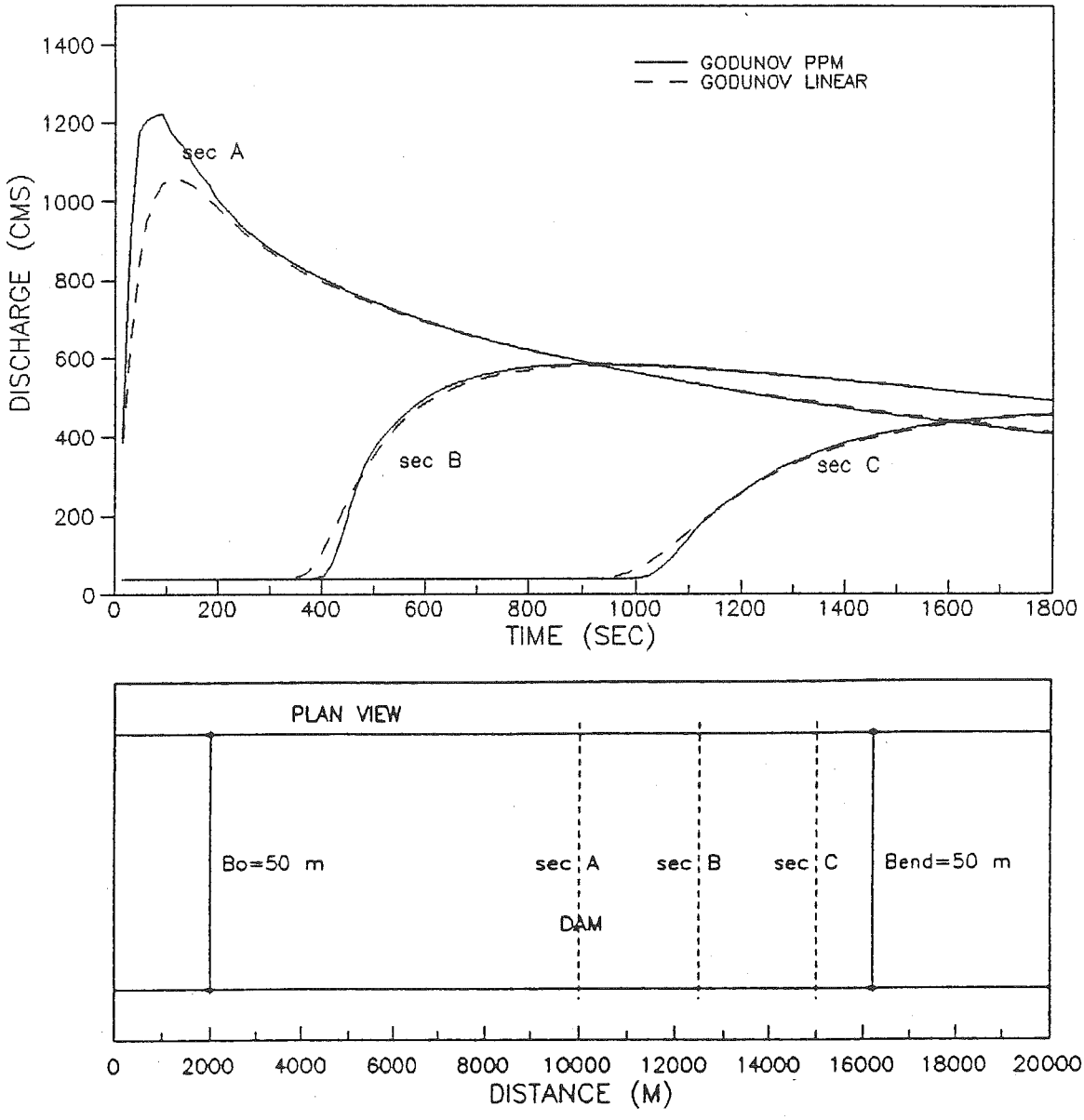

Figure 5.27 Discharge hydrographs for low-dam dambreak in a prismatic channel of large roughness; comparison between the PPM Godunov and linear Godunov methods

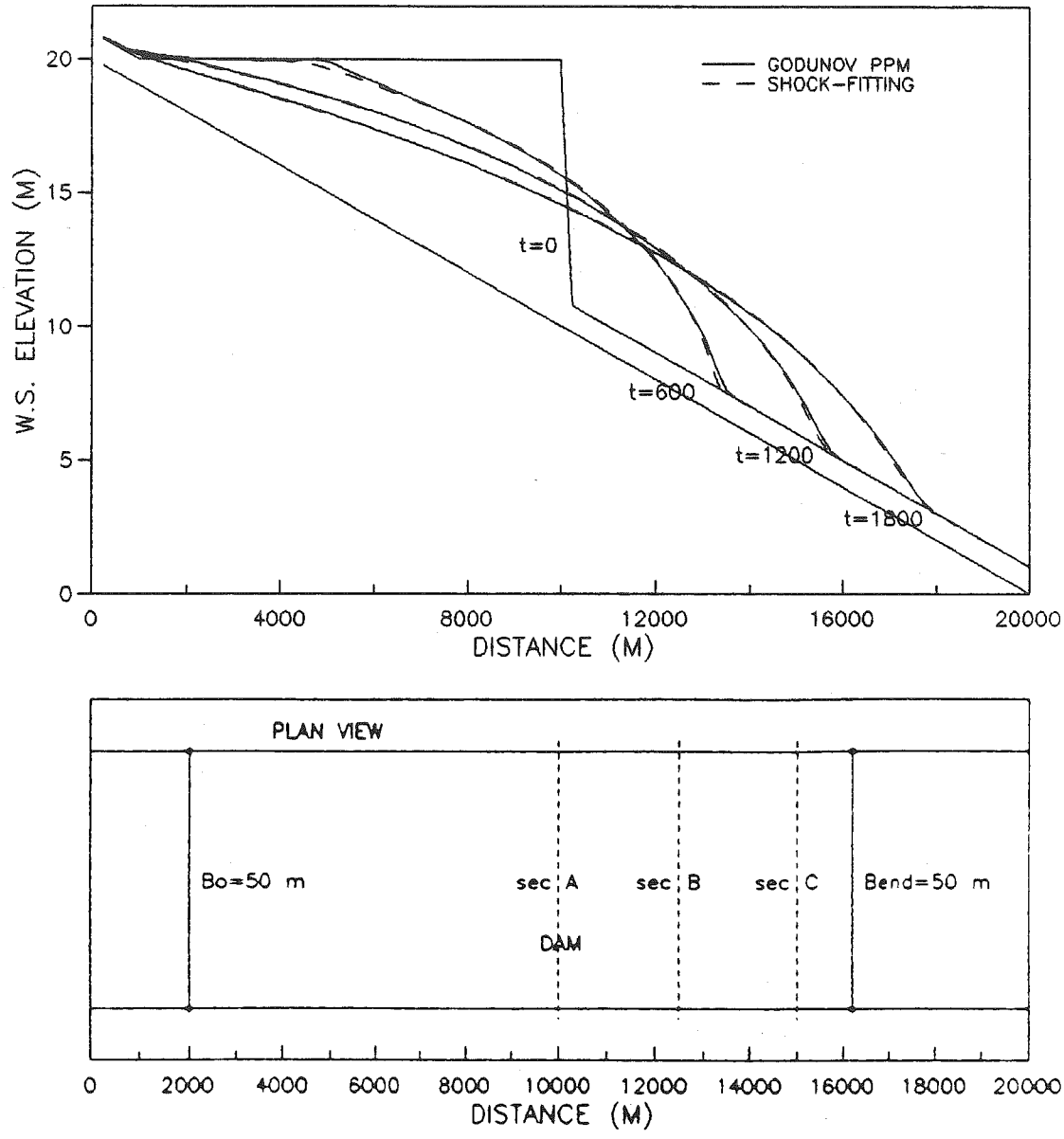

Figure 5.28 Time evolution of water-surface profiles for low-dam dambreak in a prismatic channel of large roughness; comparison between the PPM Godunov and shock-fitting methods

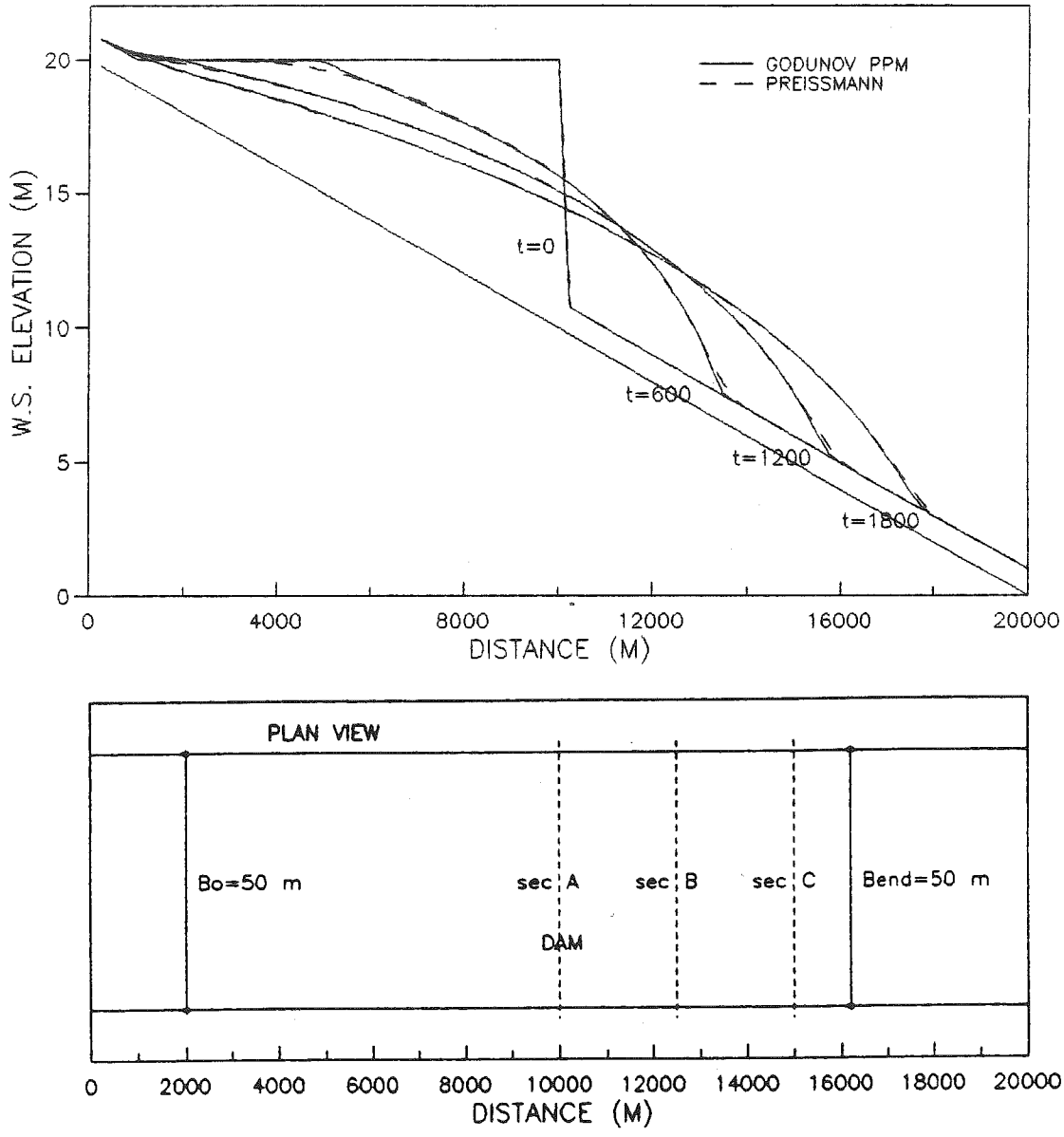

Figure 5.29 Time evolution of water-surface profiles for low-dam dambreak in a prismatic channel of large roughness; comparison between the PPM Godunov and Preissmann methods

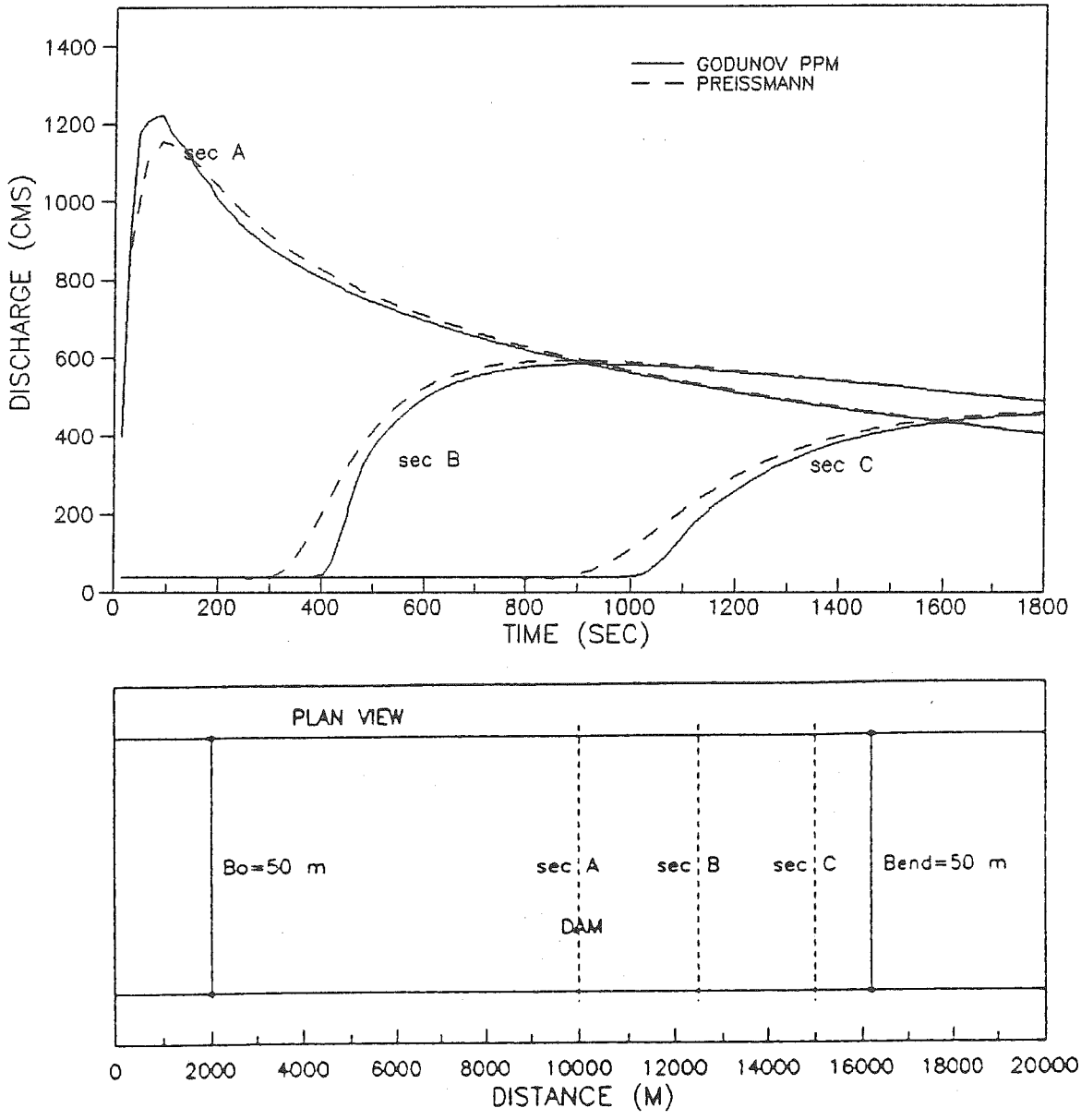

Figure 5.30 Discharge hydrographs for low-dam dambreak in a prismatic channel of large roughness; comparison between the PPM Godunov and Preissmann methods

(5.31), while the hydrographs (Fig.5.32) for the Lax-Wendroff method still suffer from numerical oscillations.

V.3.4 Dambreak for high dam with small roughness

The case of a high dam (upstream-to-downstream depth ratio of 100/1) is considered next. Mixed regime is inevitable for such a large ratio of upstream to downstream depths, so that under no circumstances could successful computations be obtained with the Preissmann method in a double sweep context.

First, the case of smaller roughness (Manning coefficient of 0.015) is considered. A channel 100 km long, 50 m wide, with a slope of 0.1% and a spatial step of 1000 m is used. The initial and boundary conditions are the same as for the case of a low dam, except for the reservoir elevation, which is in compliance with the 100 m high dam.

In Figs.(5.33)-(5.35) the Godunov PPM and linear methods are compared. As in the case of the low dam better agreement is achieved than for the frictionless channel (consequence of the influence of roughness). The PPM method sill performs better with respect to the diffusion in the reservoir and smearing of the shock front. The front resolution for the PPM method is again confined to a zone of approximately one spatial step. In Fig.(5.34) the discharge hydrographs are presented for the sections A (dam section 50

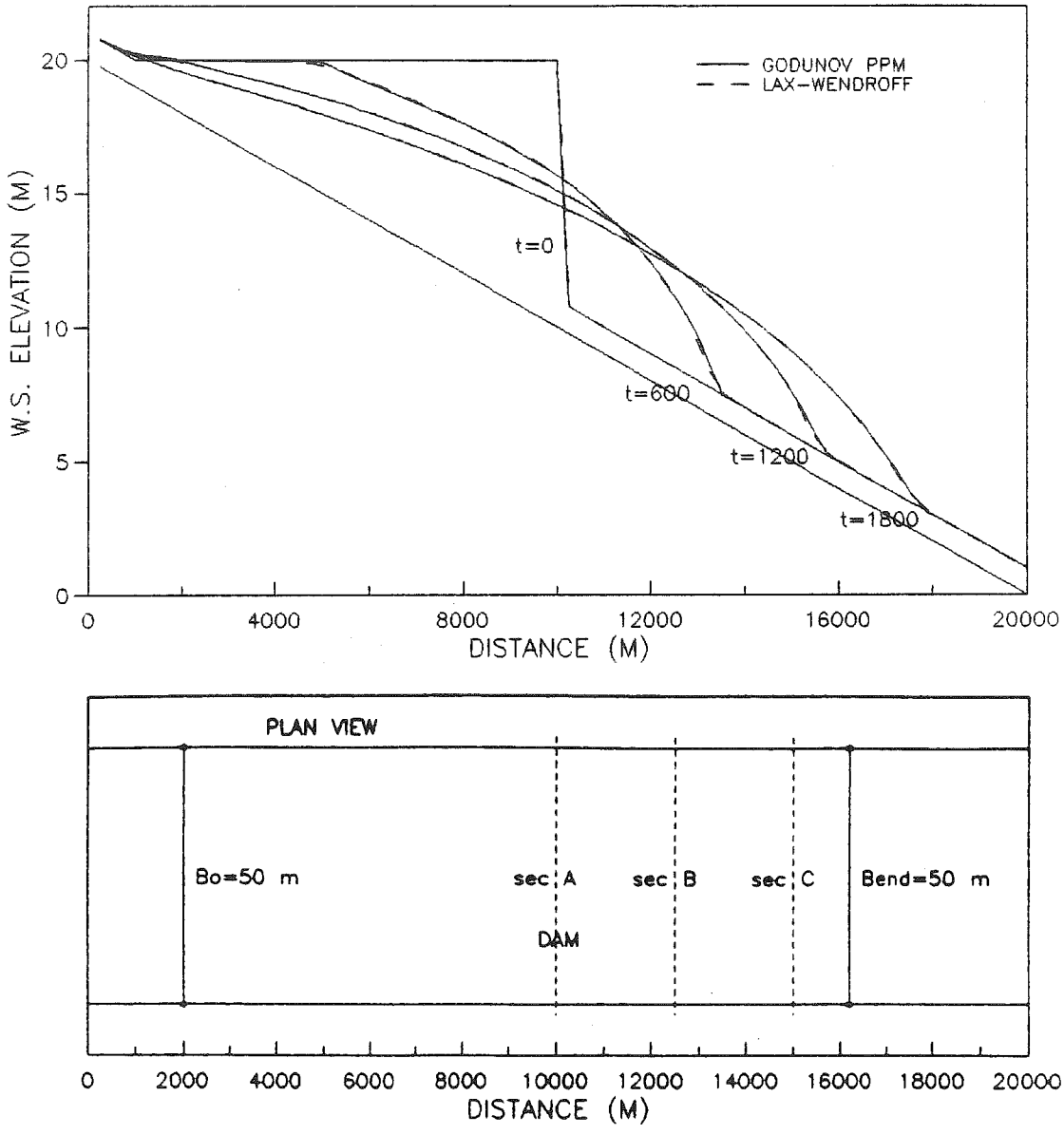

Figure 5.31 Time evolution of water-surface profiles for low-dam dambreak in a prismatic channel of large roughness; comparison between the PPM Godunov and Lax-Wendroff methods

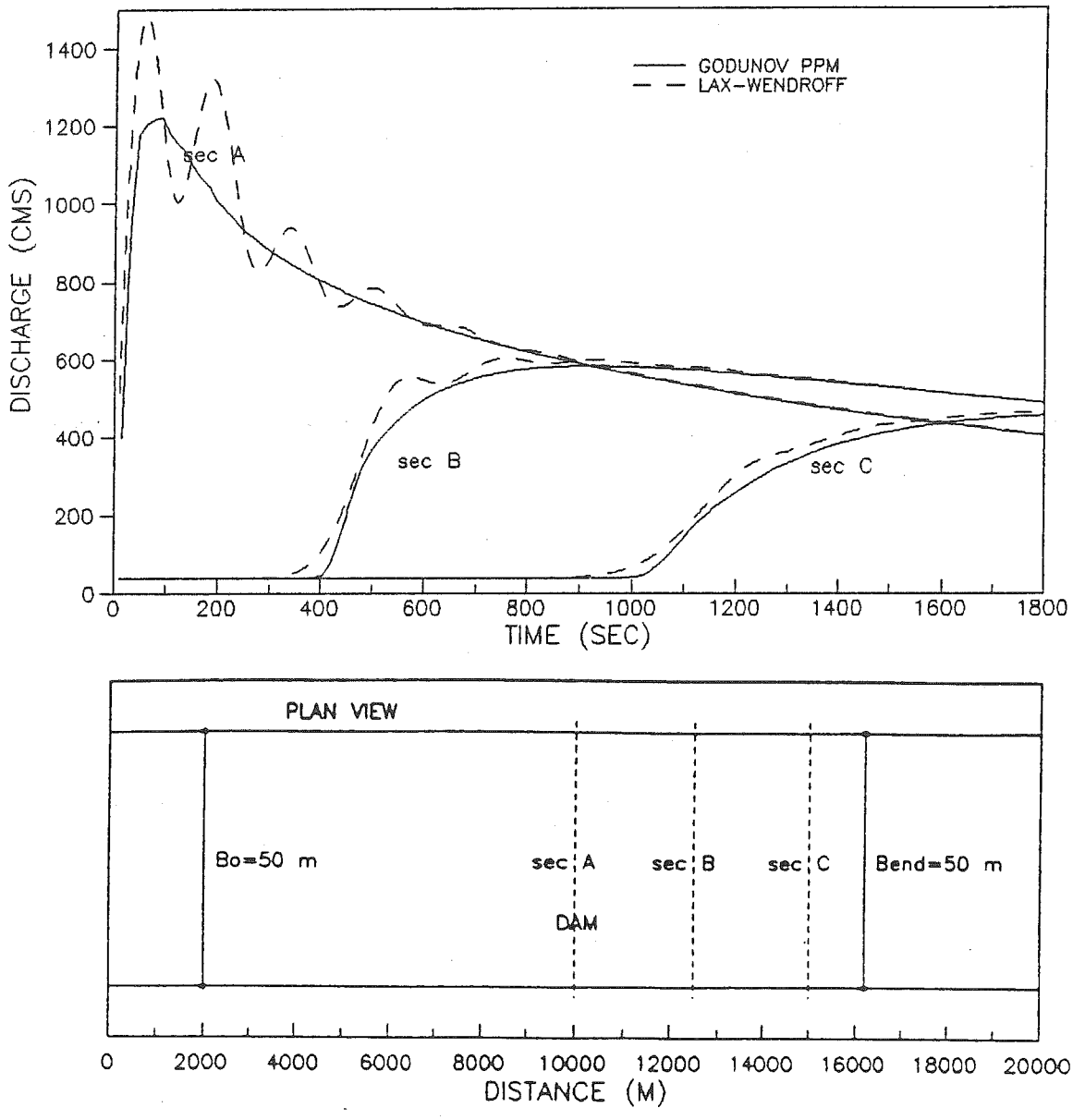

Figure 5.32 Discharge hydrographs for low-dam dambreak in a prismatic channel of large roughness; comparison between the PPM Godunov and Lax-Wendroff methods

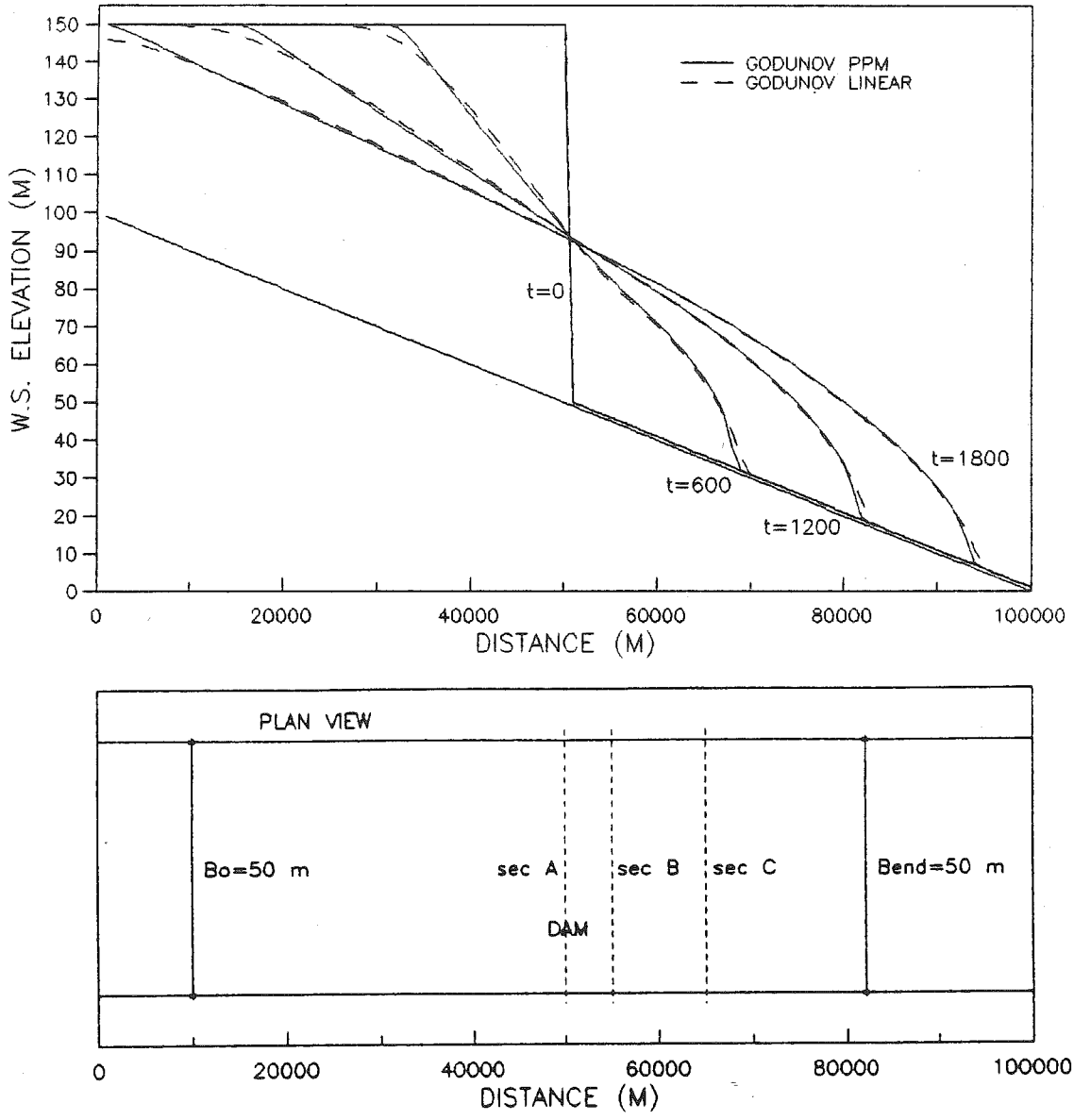

Figure 5.33 Time evolution of water-surface profiles for high-dam dambreak in a prismatic channel of small roughness; comparison between the PPM Godunov and linear Godunov methods

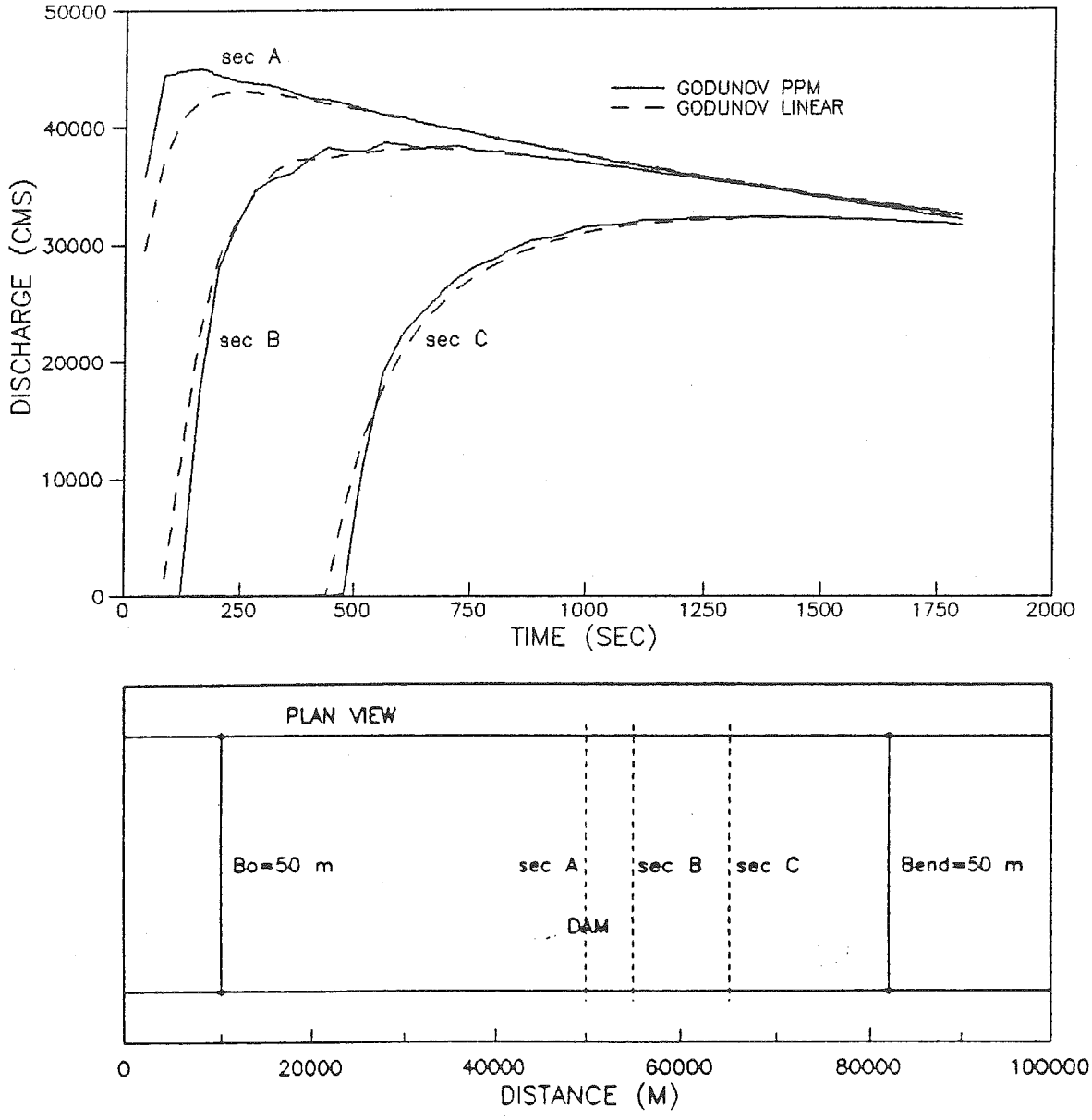

Figure 5.34 Discharge hydrographs for high-dam dambreak in a prismatic channel of small roughness; comparison between the PPM Godunov and linear Godunov methods

km from the upstream end), B (60 km from the upstream end), and C (70 km from the upstream end). The PPM method shows some oscillations, which can be eliminated at the expense of smaller time or\and spatial steps, and the linear method is more diffusive, as one can expect from the previous considerations. In Fig.(5.35) the depth hydrographs at the same sections (A, B, and C) are presented. They do not contribute much to the analysis of the results, since they cannot offer any more information (there is even no oscillations as in the case of the discharge hydrographs for the PPM method).

As in the previous case of a low dam, mass conservation is poor for the shock-fitting method (Fig.5.36), and smearing in the reservoir zone is observed. The conservation error ($1.5 \cdot 10^{-2}$) is still small enough to allow for a fairly reliable comparison between the two methods and judgment on the influence of the shock-fitting algorithm on the quality of the resolution. Since in the shock-fitting results the shock almost completely dies out some 40 km downstream of the dam, and the resemblance with the Godunov method is still very good, it seems that the Godunov method representation, with the shock zone of one spatial step, would be quite satisfactory in all possible practical applications.

For the reasons mentioned earlier, the Lax-Wendroff

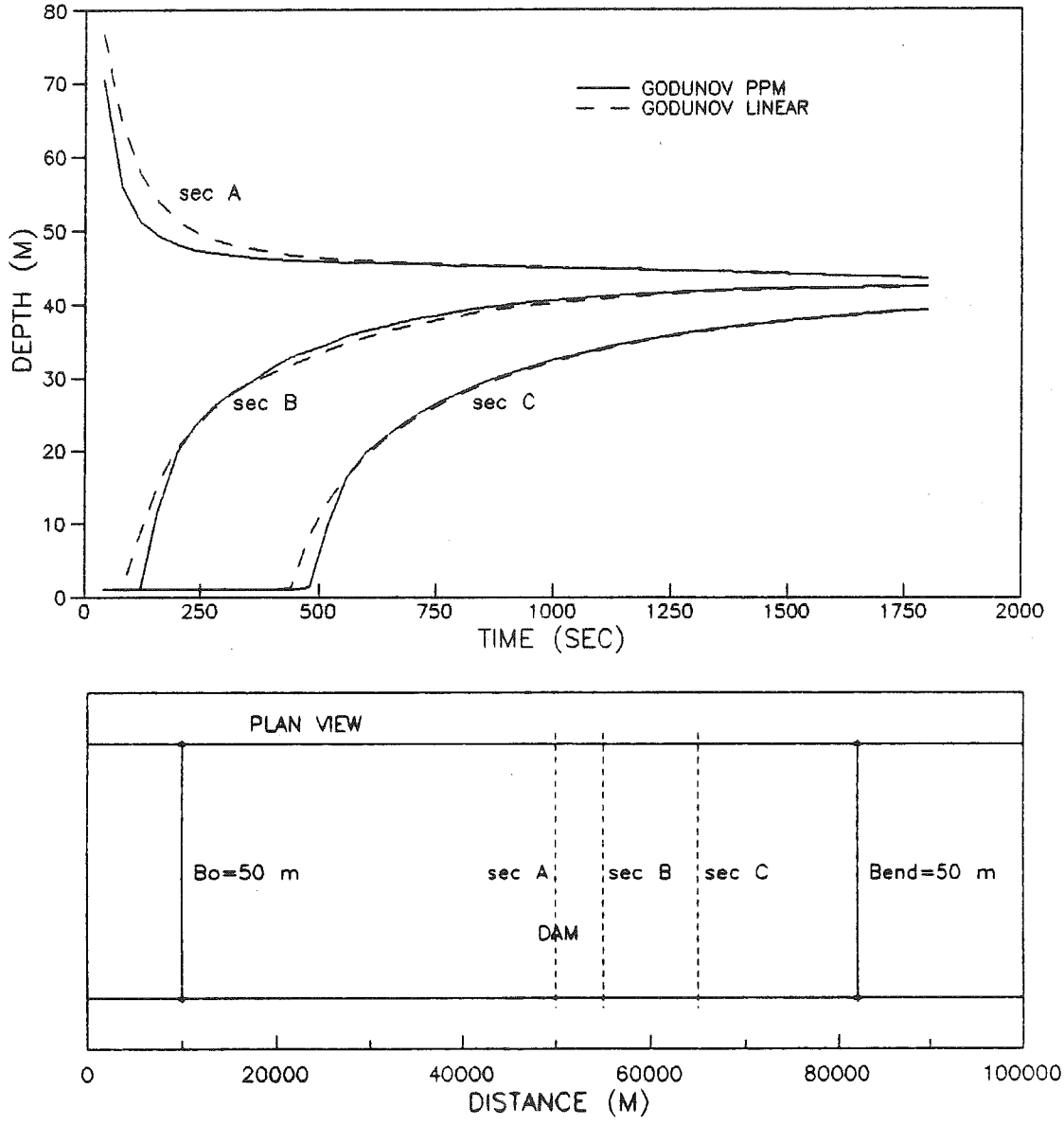

Figure 5.35 Depth hydrographs for high-dam dambreak in a prismatic channel of small roughness; comparison between the PPM Godunov and linear Godunov methods

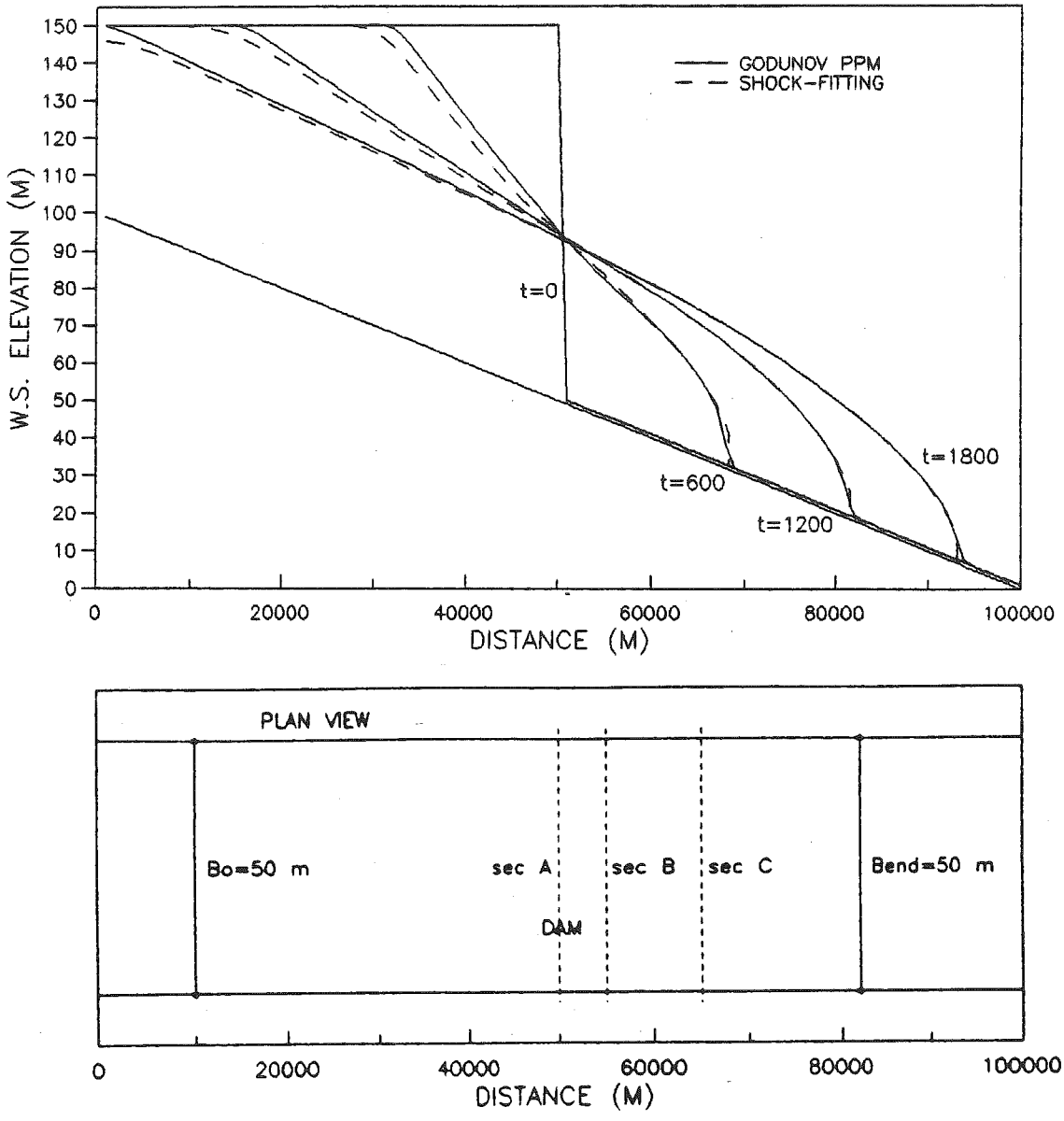

Figure 5.36 Time evolution of water-surface profiles for high-dam dambreak in a prismatic channel of small roughness; comparison between the PPM Godunov and shock-fitting methods

method could not give a stable solution; it becomes unstable within a few time steps at the beginning of the computations.

V.3.5 Dambreak for high dam with large roughness

The case of a large resistance is the last case treated in this section. The same channel is used as before; only the roughness is increased to 0.040, and consequently the initial and boundary condition discharges are reduced to maintain the same normal depth of 1 m for the reach downstream of the dam.

In Figs.(5.37) and (5.38) the two Godunov methods are compared. The same trend is observed as for the case of a low dam, namely, the agreement increases with the roughness coefficient, and the only perceptible discrepancy is at the ends of the disturbed region (i.e. at the front of the surge and at the back of the reservoir, see Fig.5.37).
The discharge hydrographs also agree well, the only difference being in the peak of the dam-section hydrograph (Fig.5.38).

Figures (5.39) and (5.40) compare the PPM Godunov method with the shock-fitting method. The linear interpolation used for the shock-fitting method, in this case with strongly curved water-surface profiles (see Fig.5.39), leads to a large mass conservation error (over

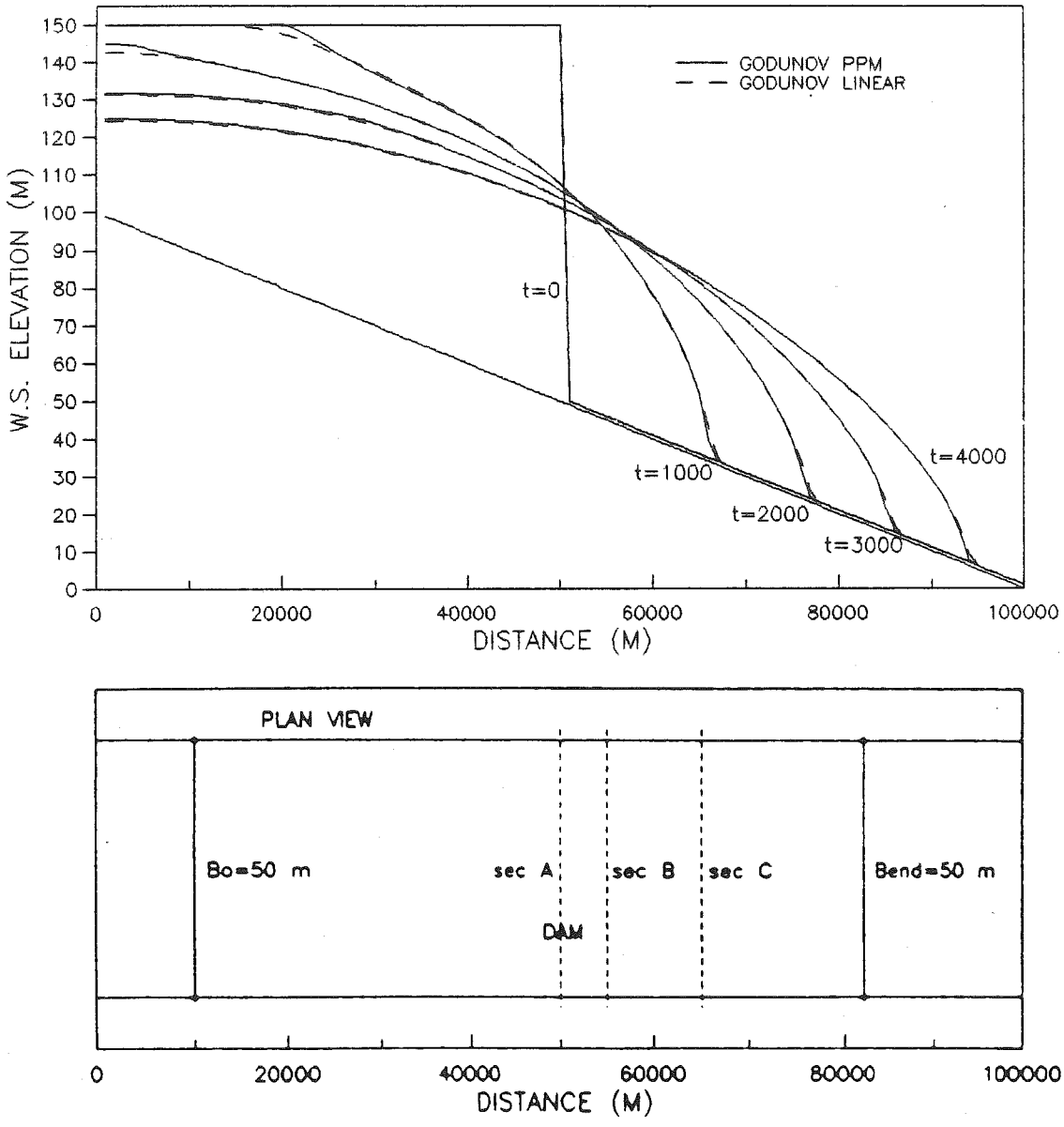

Figure 5.37 Time evolution of water-surface profiles for high-dam dambreak in a prismatic channel of large roughness; comparison between the PPM Godunov and linear Godunov methods

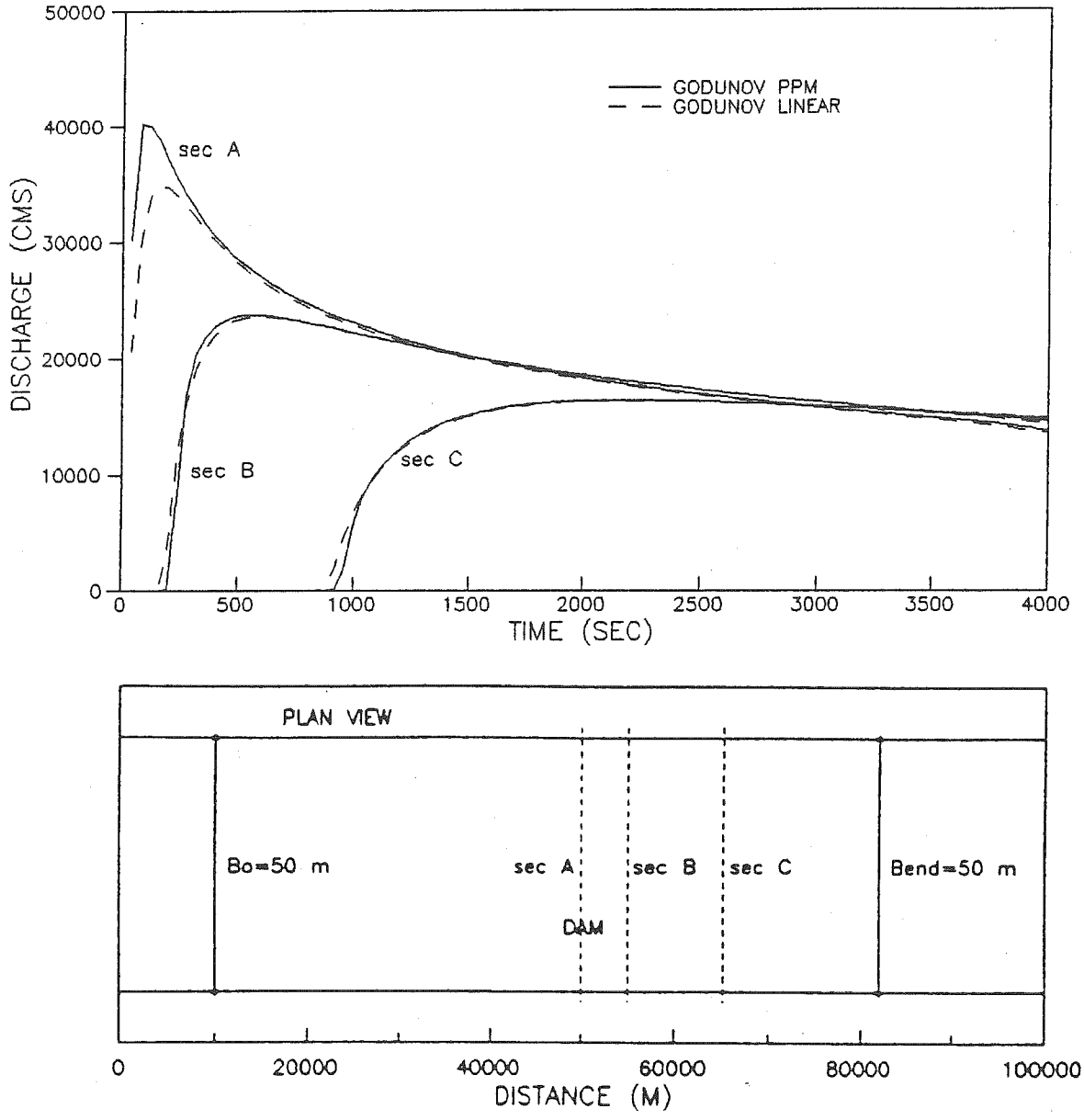

Figure 5.38 Discharge hydrographs for high-dam dambreak in a prismatic channel of large roughness; comparison between the PPM Godunov and linear Godunov methods

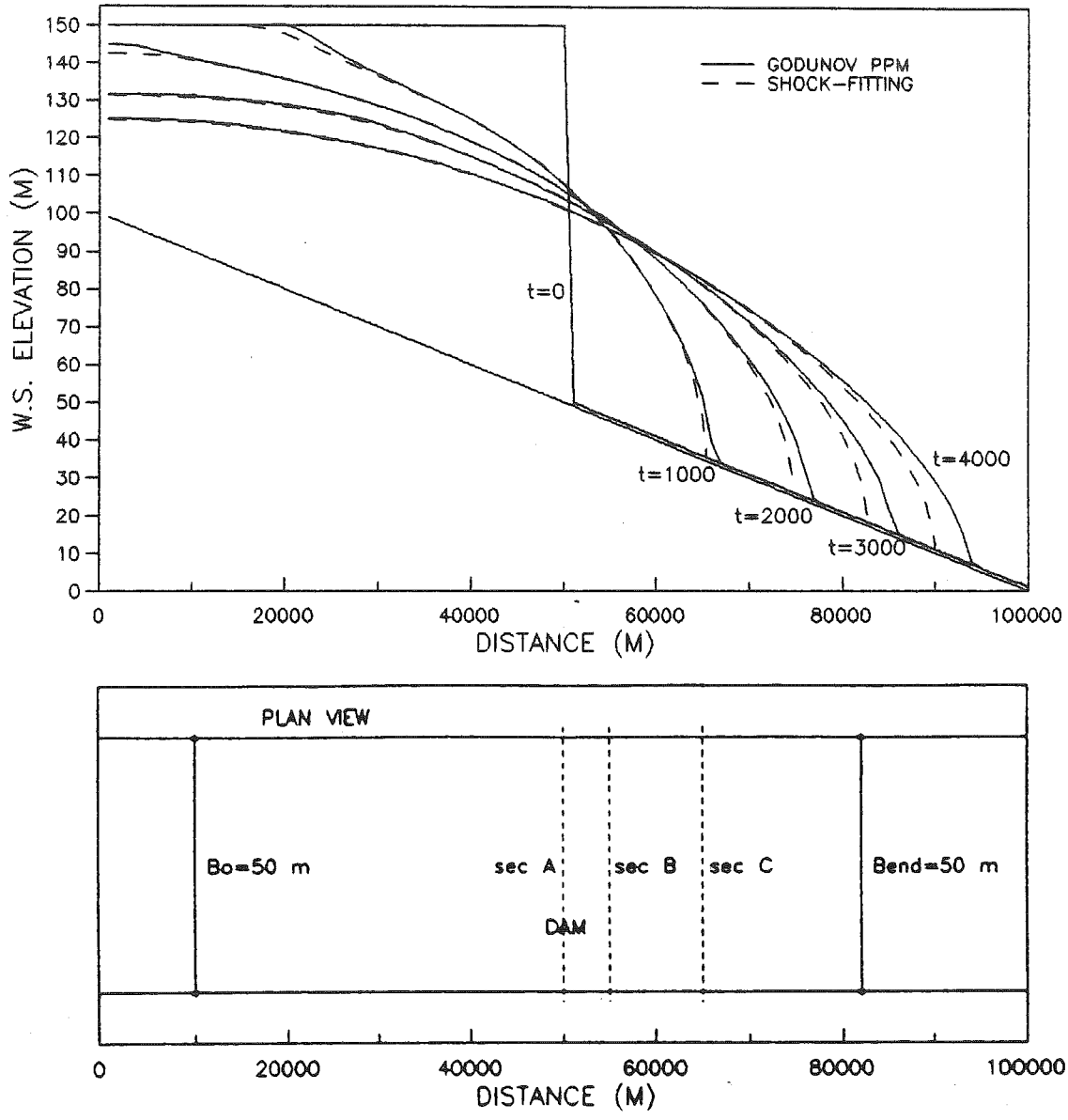

Figure 5.39 Time evolution of water-surface profiles for high-dam dambreak in a prismatic channel of large roughness; comparison between the PPM Godunov and shock-fitting methods

4%), and consequently to a speed error (as explained earlier in section V.1 on the frictionless dambreak). Apparently, some type of parabolic interpolation is required if a more reliable shock-fitting method is needed. Nevertheless, there is no reason to suspect that the shape of the front is distorted, therefore the shock-fitting result can still serve its purpose of providing an estimate for the shock smearing of the Godunov method. Comparison of water-surface elevations between the Godunov PPM and shock-fitting methods (Fig.5.39) shows that the shape of the surge of the Godunov method is in good agreement with that of the shock-fitting method. The discharge hydrographs (Fig.5.40) also agree well, except for the one at section C, where the erroneous speed affects arrival of the perturbation.

The results of the computations for the Lax-Wendroff method are compared with the PPM Godunov method in Figs.(5.41) and (5.42). It is important to note that a stable computation for the Lax-Wendroff method has been possible only with a Courant number five times less (i.e. time step five times smaller) than that used for the Godunov method (the Courant number for the Godunov method is close to 0.9). From the time evolution of the water-surface elevations one can observe very good agreement in all zones of the flow field, with slightly better resolution and less diffusion in the Godunov method. However, the unavoidable

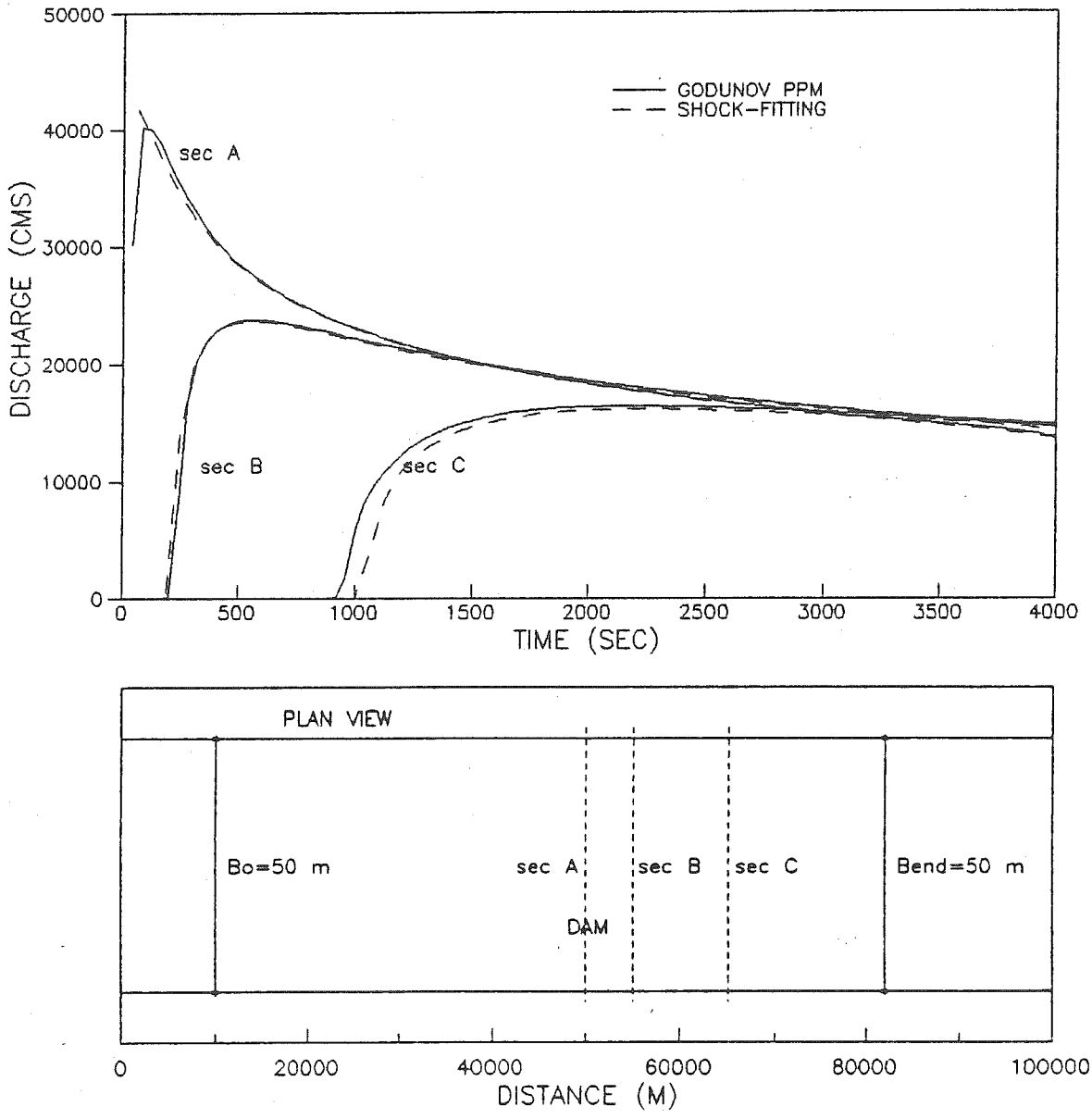

Figure 5.40 Discharge hydrographs for high-dam dambreak in a prismatic channel of large roughness; comparison between the PPM Godunov and shock-fitting methods

numerical oscillations of the Lax-Wendroff method are present in the discharge hydrographs (Fig.5.42). They gradually die out, without much affecting the water-surface elevation profiles (Fig.5.41), which are the results of primary practical importance.

In summary, the Godunov method (particularly the Godunov PPM method) shows the best performance among all the compared methods. It works with mixed flow regimes at large time steps (still limited by the Courant-Friedrichs-Levy law); the resolution of the front is on the average confined to one spatial step for the PPM; and to two or three spatial steps for the linear method. The conservation properties of the scheme are excellent.

V.4 Tests for a frictional non-prismatic channel

Finally, the case of a non-prismatic sloped and frictional channel is considered. This is the most delicate problem to deal with for the one-dimensional open-channel flow equations (Strelkoff, 1989), and the capability successfully to compute dam-break flow in channels with sudden changes of cross-sectional geometry (sudden expansions and sudden constrictions) is indispensable for any future practical application.

Three flow situations are tested in this section:

1. Steady flow for a channel with sudden

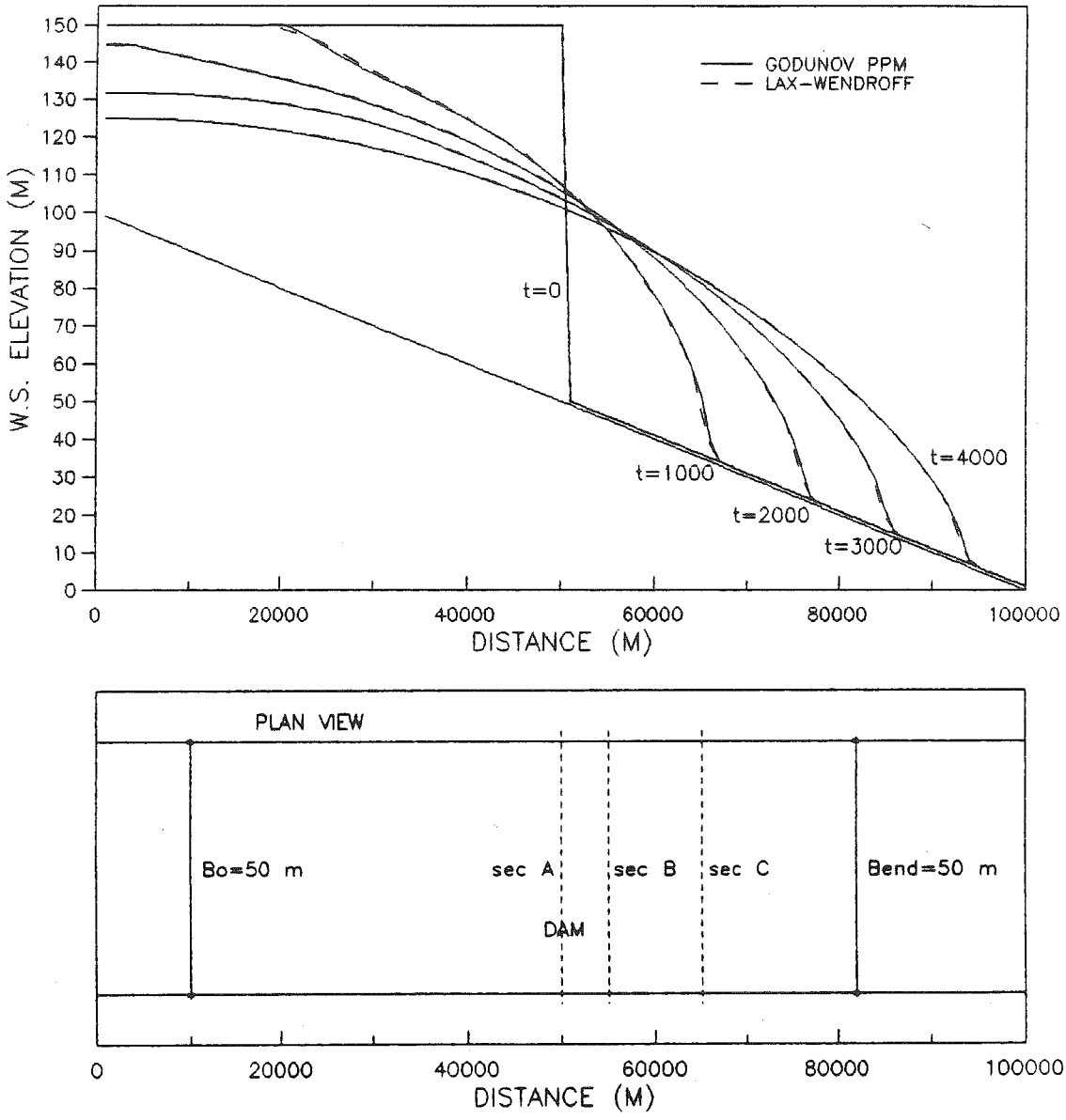

Figure 5.41 Time evolution of water-surface profiles for high-dam dambreak in a prismatic channel of large roughness; comparison between the PPM Godunov and Lax-Wendroff methods

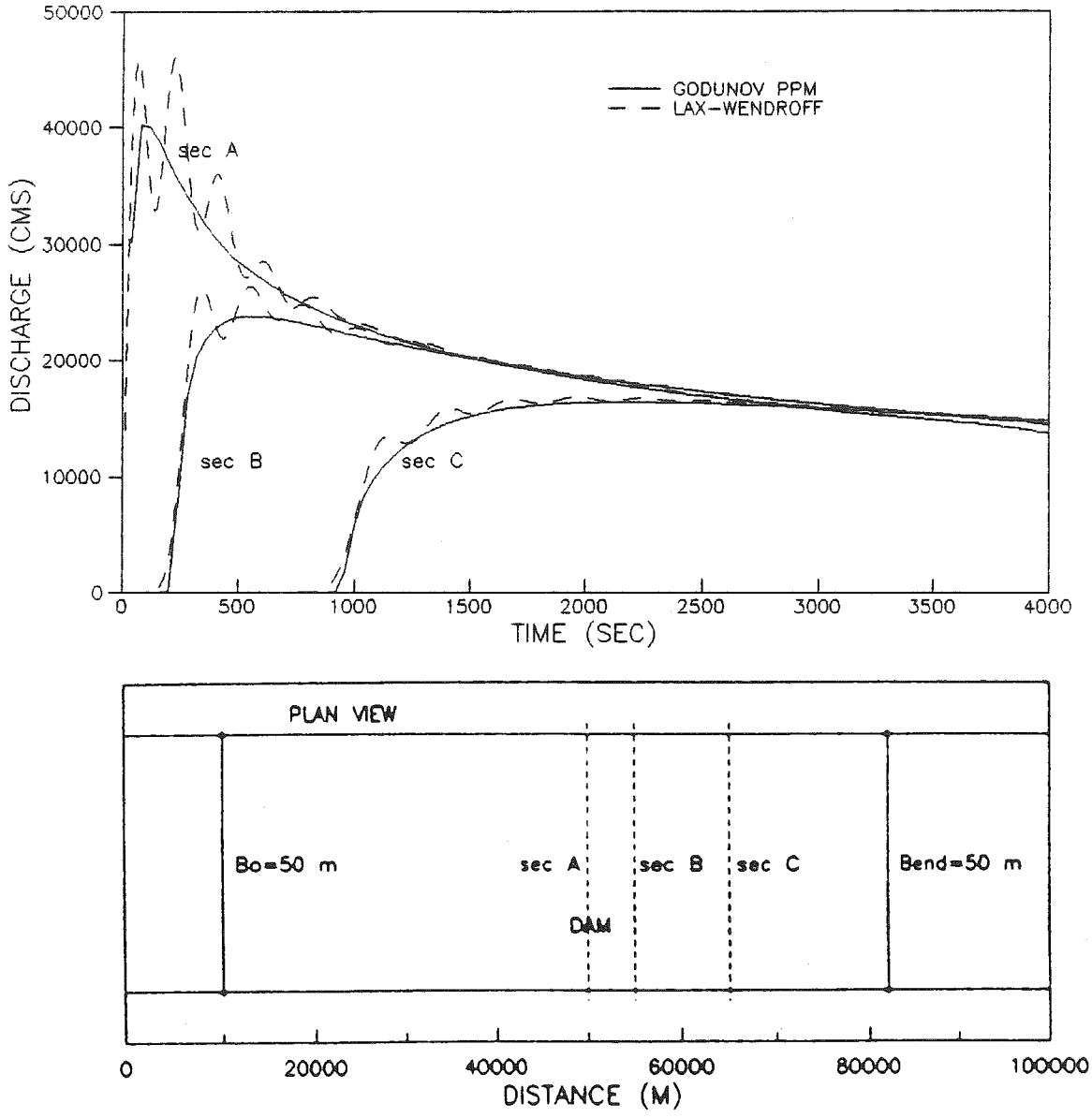

Figure 5.42 Discharge hydrographs for high-dam dambreak in a prismatic channel of large roughness; comparison between the PPM Godunov and Lax-Wendroff methods

expansion;

2. Flood propagation in a highly non-prismatic channel with randomly distributed widths;

3. Instantaneous and total dam-break flows for the sudden expansion and sudden constriction cases.

V.4.1 Steady flow

The first test case deals with steady flow in a channel for the case of sudden expansion in the cross-sectional width in one spatial step. This example is chosen to demonstrate and explain some ambiguities resulting from using the staggered grid in the Godunov predictor-corrector algorithm (see chapter IV for an explanation of the algorithm).

A rectangular channel 20 km long, with a slope of 0.1 % and a Manning roughness coefficient of 0.040 is used. The width of the channel is 10 m for the first 10 km (measured from the upstream boundary), then within a single spatial step of 1000 m, it changes to 30 m, remaining constant to the downstream end of the channel. The unsteady initial condition is a constant depth of 2 m and constant discharge of 36.06 cms for the entire channel. The upstream boundary condition is a prescribed constant discharge of 36.06 cms, and the downstream boundary condition is a uniform-flow rating curve. After approximately 20,000 seconds a steady

state is established.

A comparison between the Godunov PPM and the Preissmann method (with the a temporal-weighting coefficient of 0.52) is presented in Figs.(5.43)-(5.46). In all figures for the Godunov method the values at the mid-points (the predictor-step flux values) are plotted in addition to the grid-averaged values. In Figs.(5.43) and (5.45) the depths at the initial condition, and after the steady state is established (around 20,000 seconds), are presented. In Figs.(5.44) and (5.46) the discharge hydrographs at sections 10 and 16 km from the upstream end are presented. In Figs.(5.43) and (5.44) a spatial step of 1000 m was used, while in Figs. (5.45) and (5.46) it is reduced to 500 m.

The most intriguing behavior is observed in the hydrograph of Fig.(5.44) for the expansion section A (10 km from the upstream end). Here the grid-averaged discharge for the Godunov method apparently does not converge to the steady state discharge. However, the corresponding mid-point discharge agrees well with that of the Preissmann method, and converges to the appropriate steady-flow value. Moreover, this discrepancy is reduce by decreasing the spatial step (compare Figs.5.44 and 5.46).

Explanation of this behavior is found in the fact that the values obtained in the conservative Godunov step by integral Eqs.(4.15) and (4.16) are averages of reach

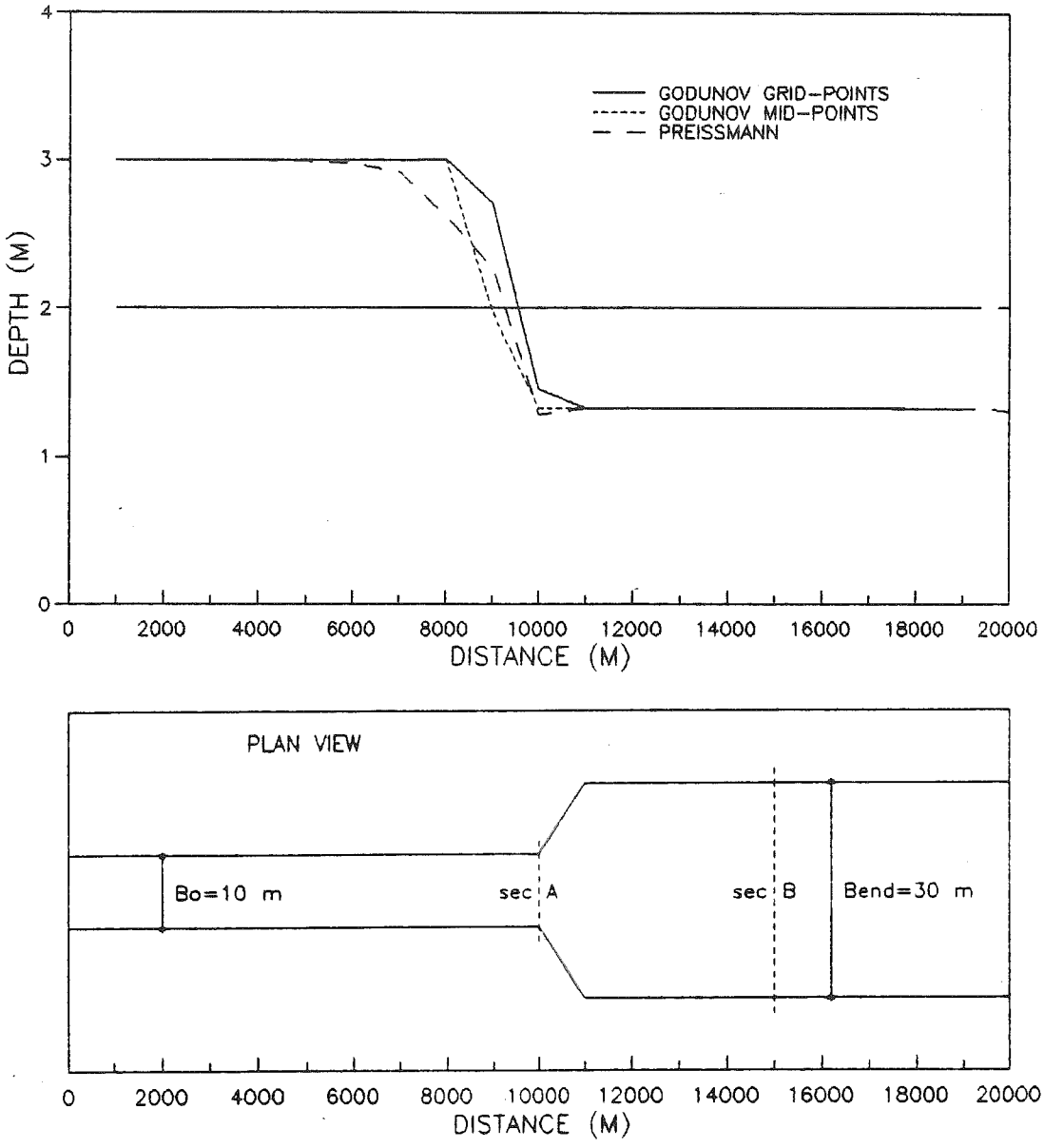

Figure 5.43 Water-surface profiles for the steady-flow in a frictional channel with sudden expansion; comparison between the PPM Godunov and Preissmann methods

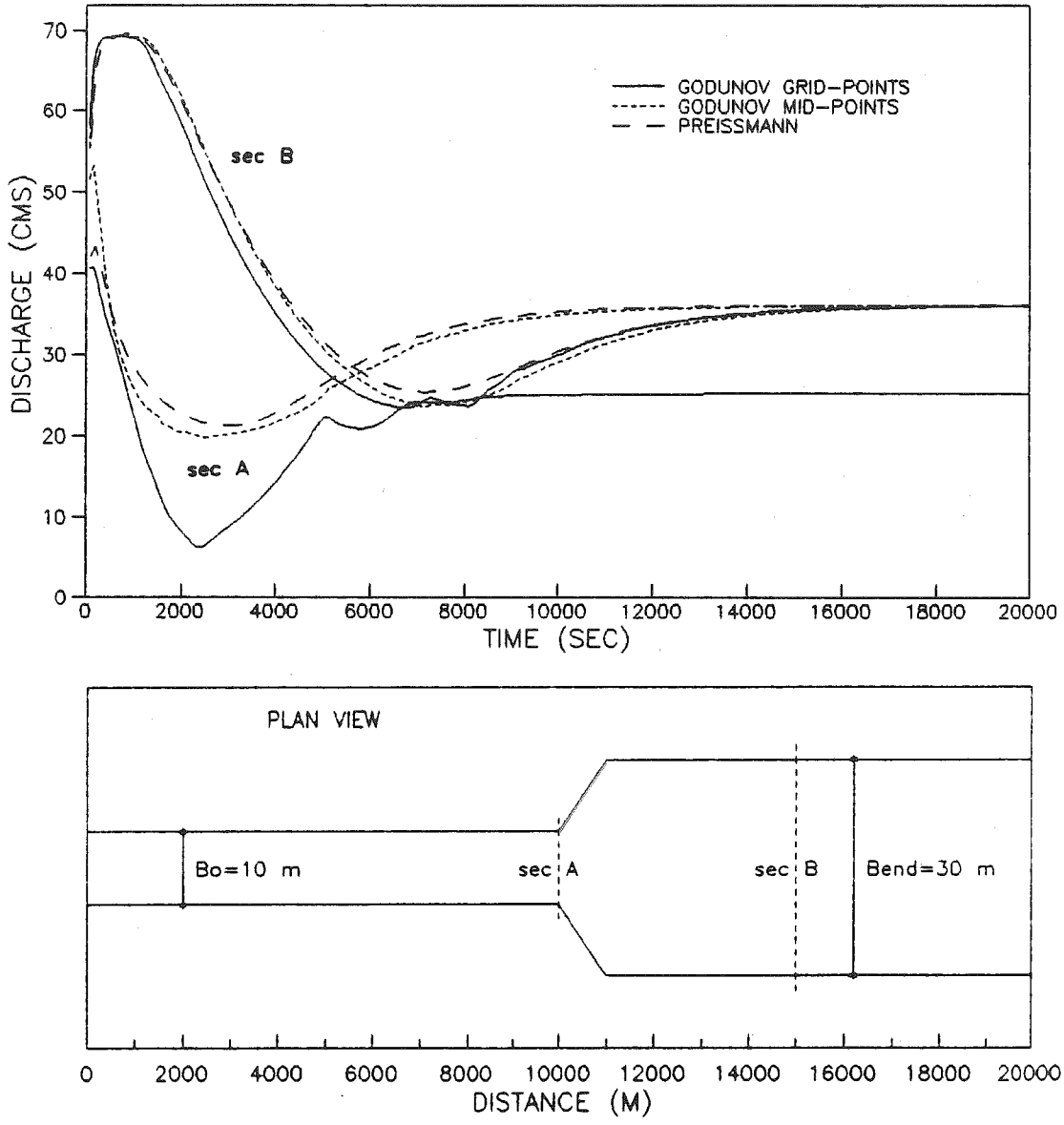

Figure 5.44 Discharge hydrographs for the steady-flow in a frictional channel with sudden expansion; comparison between the PPM Godunov and Preissmann methods

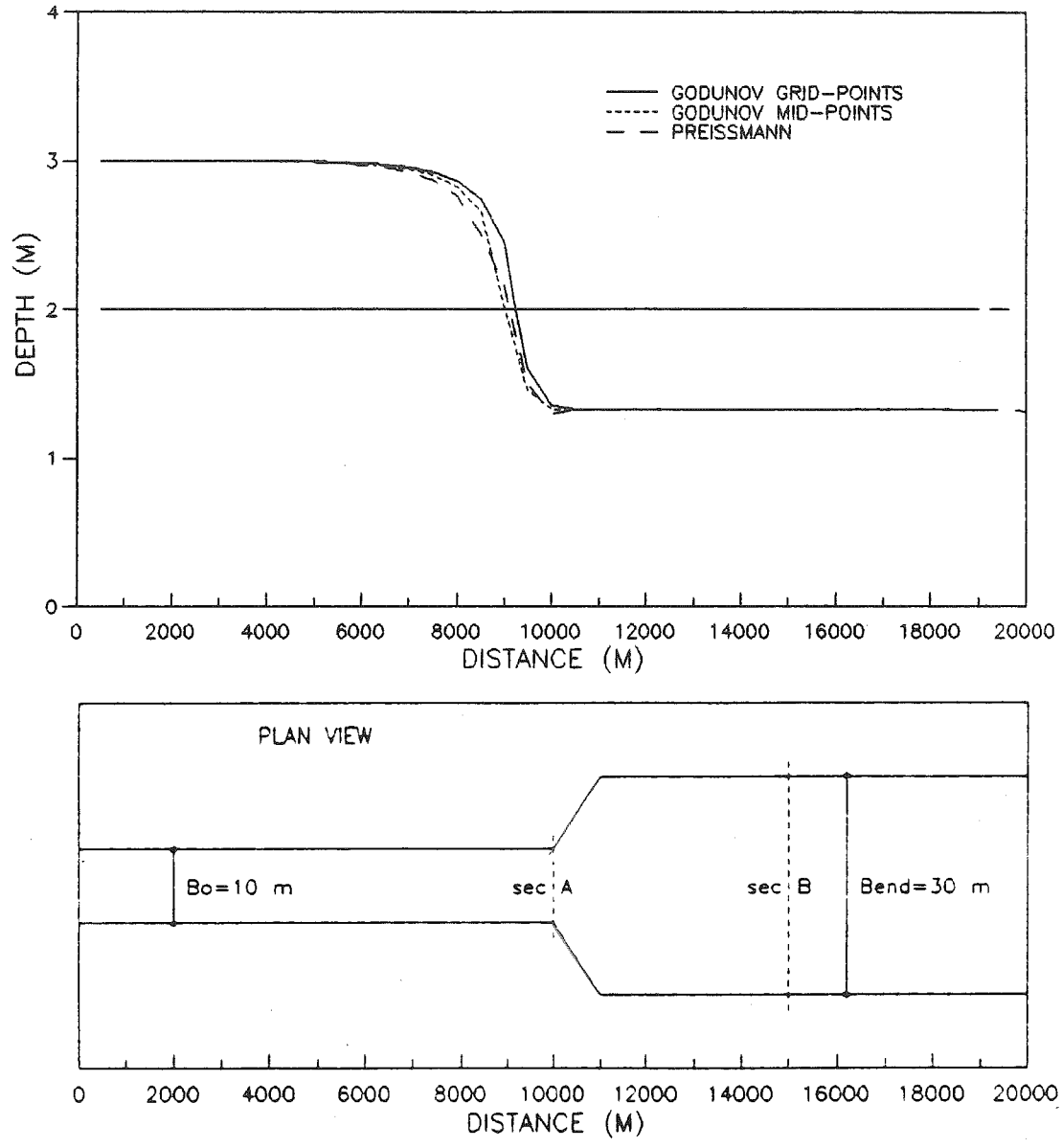

Figure 5.45 Water-surface profiles for the steady-flow in a frictional channel with sudden expansion; comparison between the PPM Godunov and Preissmann methods, refined (halved) spatial step

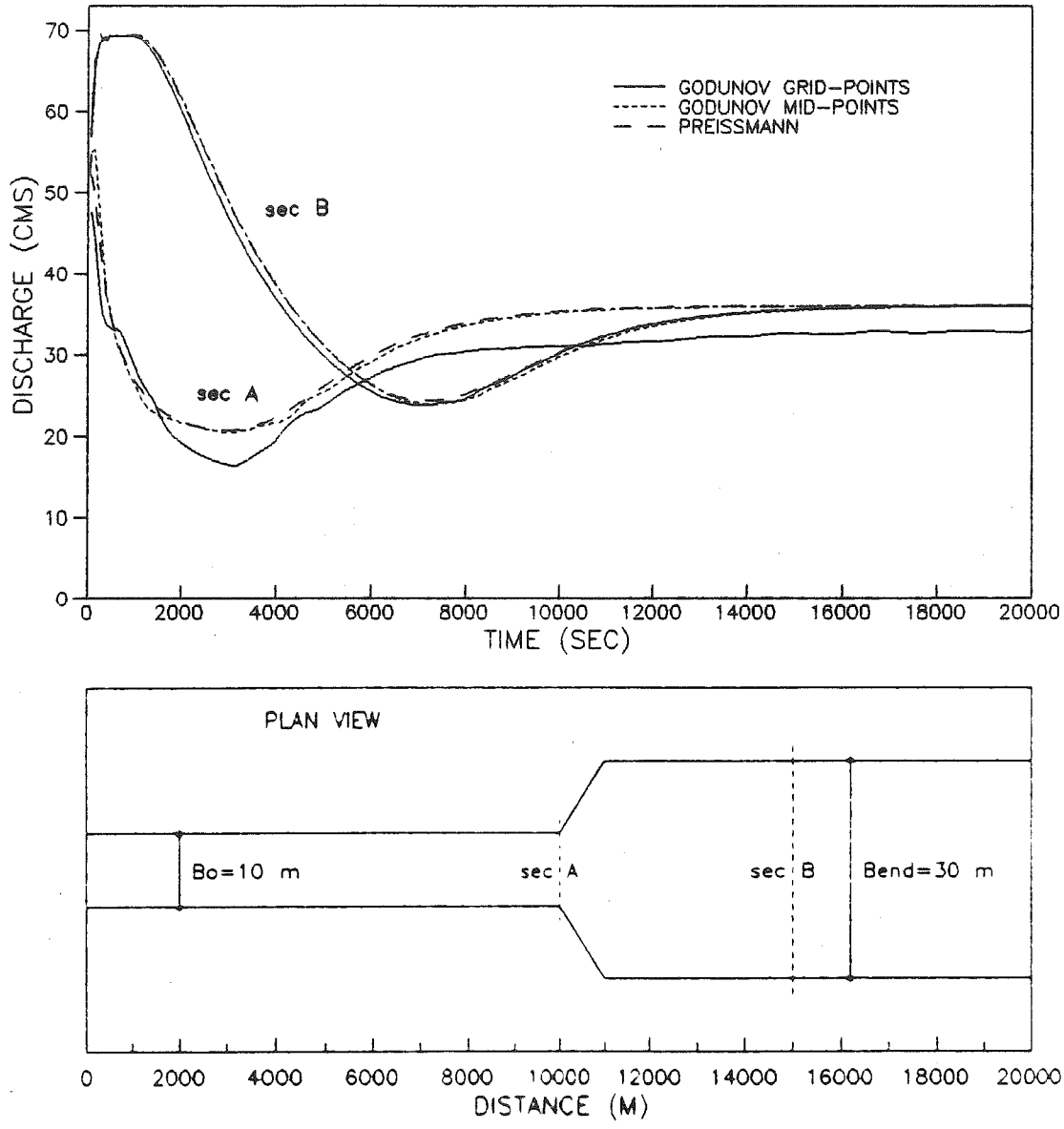

Figure 5.46 Discharge hydrographs for the steady-flow in a frictional channel with sudden expansion; comparison between the PPM Godunov and Preissmann methods, refined (halved) spatial step

quantities: the grid-averaged area is the mass per unit mass and unit length, and the grid-averaged discharge is the momentum per unit mass and unit length. Only when the reach shrinks to a point do the averaged values become the "true" area and discharge, as confirmed by comparison between Figs.(5.44) and (5.46). This corroborates the convergence property of the scheme, defined through the Lax theorem (see Cunge et. al., 1980). For a finite length of reach neither the averaged area nor the averaged discharge represent anything relating to the discrete cross section (and both discharge and area are section quantities). They are what has been stated before: average measures of the mass and momentum in the reach per unit mass and unit length. As such, these grid-averages perform their function of perfectly preserving mass and momentum in the reach, but (particularly for strongly nonprismatic channels) they are not appropriate representations of the cross-sectional quantities. Since the cross-sectional discharges and areas, where geometry is prescribed, are needed for practical application, one must obtain them at the midpoints where the time averaged fluxes are computed (flux is by definition linked with section properties). The same observations can be made for the linear Godunov method.

The steady flow profile presented in Fig.(5.45) can be corroborated by any procedure for backwater computation,

though for such a simple case one can use elementary open-channel flow analysis. It is clear (see Henderson, 1966) that in the narrow reach of the channel, upstream of the transition, an M2 backwater curve occurs, converging to a normal depth of 3.00 m further upstream, while in the wider reach of the channel a normal depth of 1.33 m occurs for the entire region.

V.4.2 Flood propagation in a channel with randomly distributed widths

In the second test the intention is to present some difficulties with both the Godunov and Preissmann methods in treating highly nonprismatic channels, and to propose a way of coping with these problems. To this end flood propagation in a channel with randomly distributed widths is chosen. The channel is 20 km long, with a bottom slope of 0.1 %, Manning roughness coefficient of 0.040, and the width normally distributed with a mean of 400 m and a standard deviation of 200 m. It is considered that such a channel may be considered a fairly good approximation of an extremely nonprismatic natural river. The spatial step is 1000 m. The upstream boundary condition is an imposed hydrograph of triangular shape, with a base discharge of 500 cms and a peak discharge of 9000 cms. The downstream boundary condition is a uniform-flow rating curve. The

initial condition is a constant depth of 2 m and discharge of 500 cms.

In Fig.(5.47) and (5.48) the two Godunov methods (PPM and linear) are compared. Both water-surface profiles (Fig.5.47) and discharge hydrographs (Fig.5.48) agree well with each other. Some oscillations can be seen on the ascending limb of the PPM hydrograph for section B (which is not unusual for higher-order methods); this can be eliminated by decreasing the time step, or refining the computational grid (see Fig.5.52).

In Figs.(5.49) and (5.50) the PPM Godunov method is compared with the Preissmann method. In general, unsatisfactory agreement is achieved for the water-surface profiles; for some reaches the differences in water-surface elevations (Fig.5.49) exceeds 10 %, and considerable phase shift occurs also. Discharge hydrographs agree much better (Fig.5.50), but still with a noticeable phase shift. The agreement in both water-surface profiles and hydrographs improves significantly with grid refining of a factor of two (linearly interpolating additional section between the original sections, retaining the same gradient in width change). This does not mean that for a nonprismatic channel one always has to interpolate profiles to get acceptable results, but for abrupt changes of a cross-section this device certainly helps.

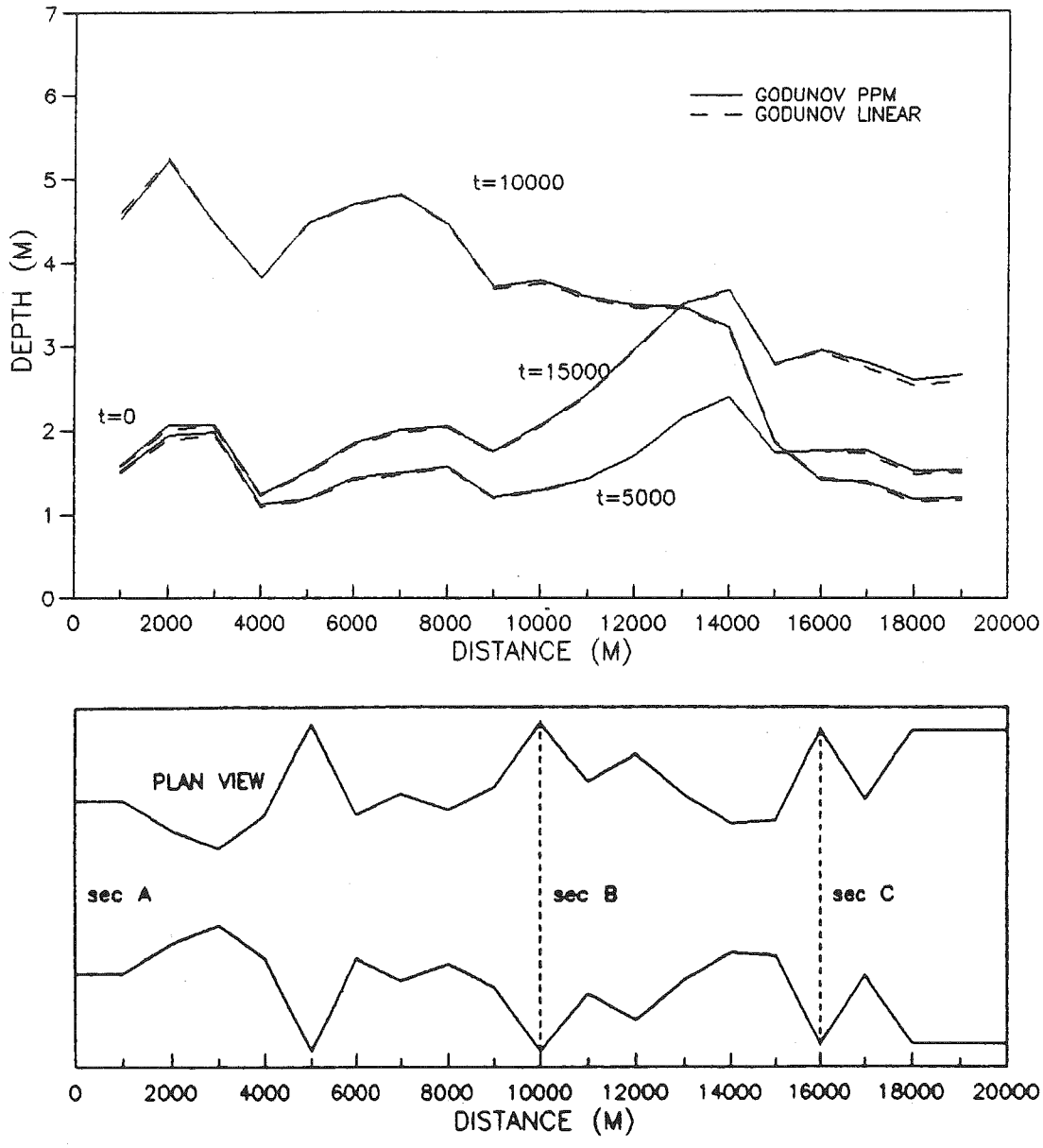

Figure 5.47 Time evolution of water-surface profiles for flood propagation in a frictional channel with normally distributed widths; comparison between the PPM Godunov and linear Godunov methods

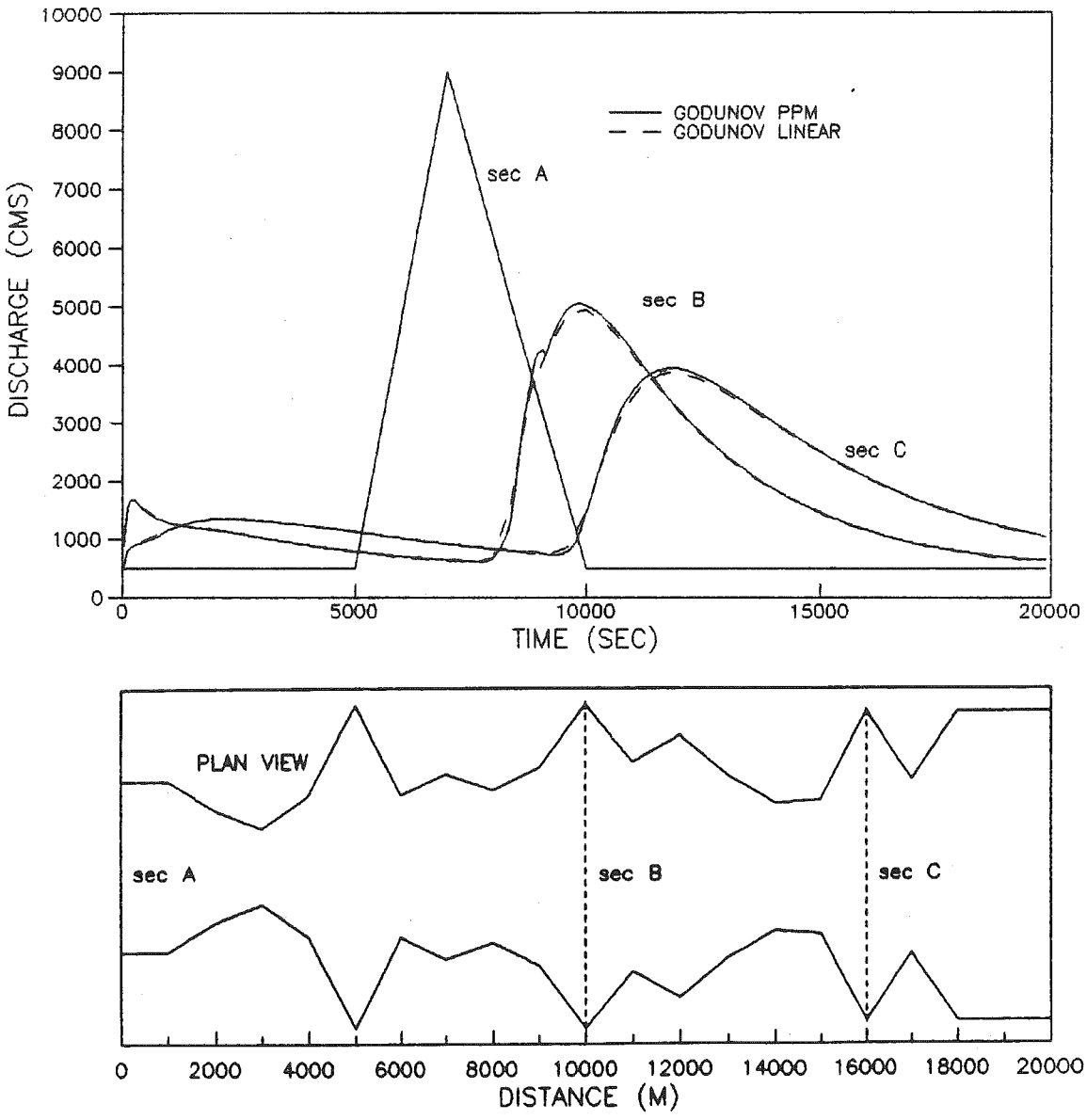

Figure 5.48 Discharge hydrographs for flood propagation in a frictional channel with normally distributed widths; comparison between the PPM Godunov and linear Godunov methods

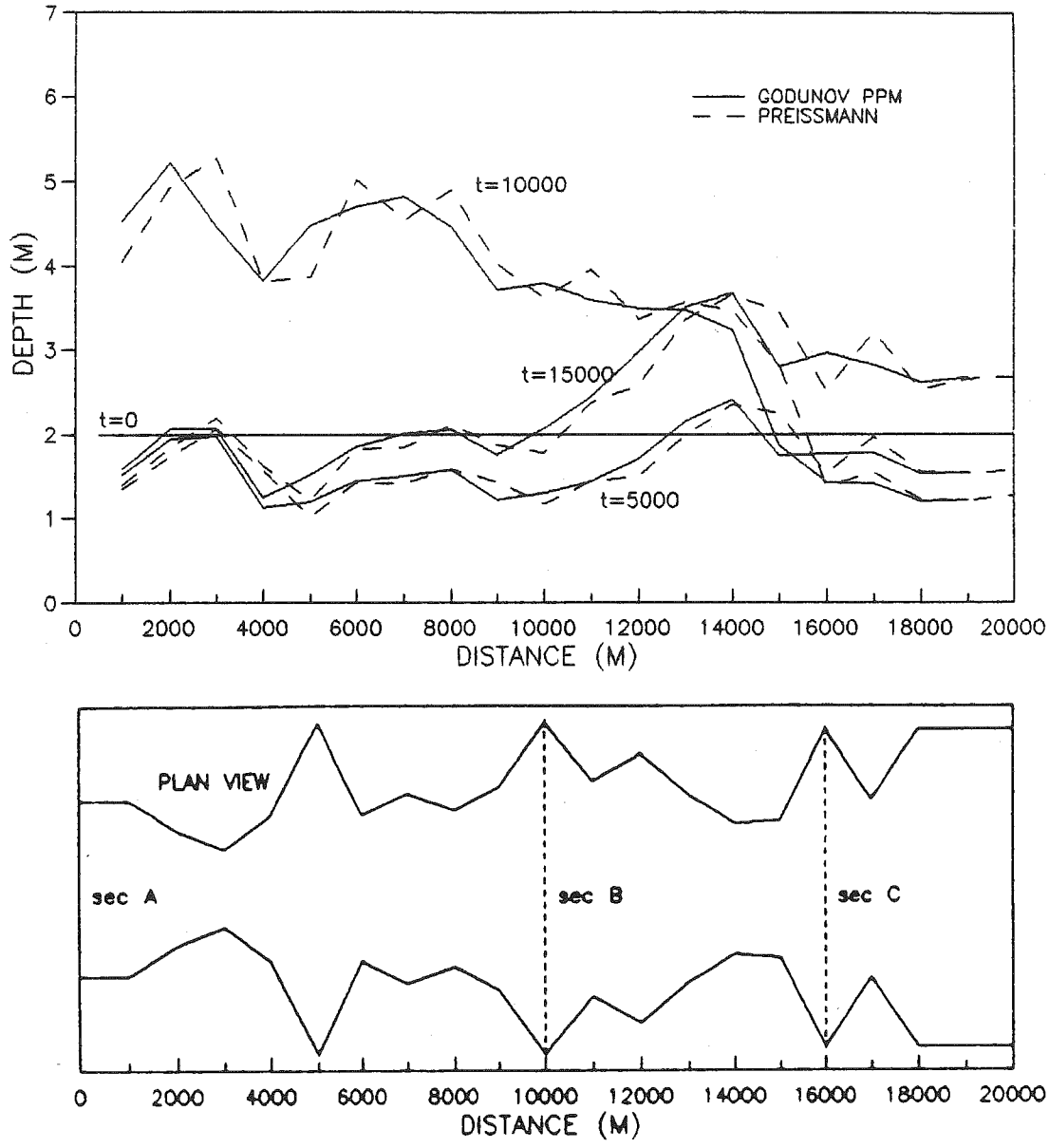

Figure 5.49 Time evolution of water-surface profiles for flood propagation in a frictional channel with normally distributed widths; comparison between the PPM Godunov and Preissmann methods

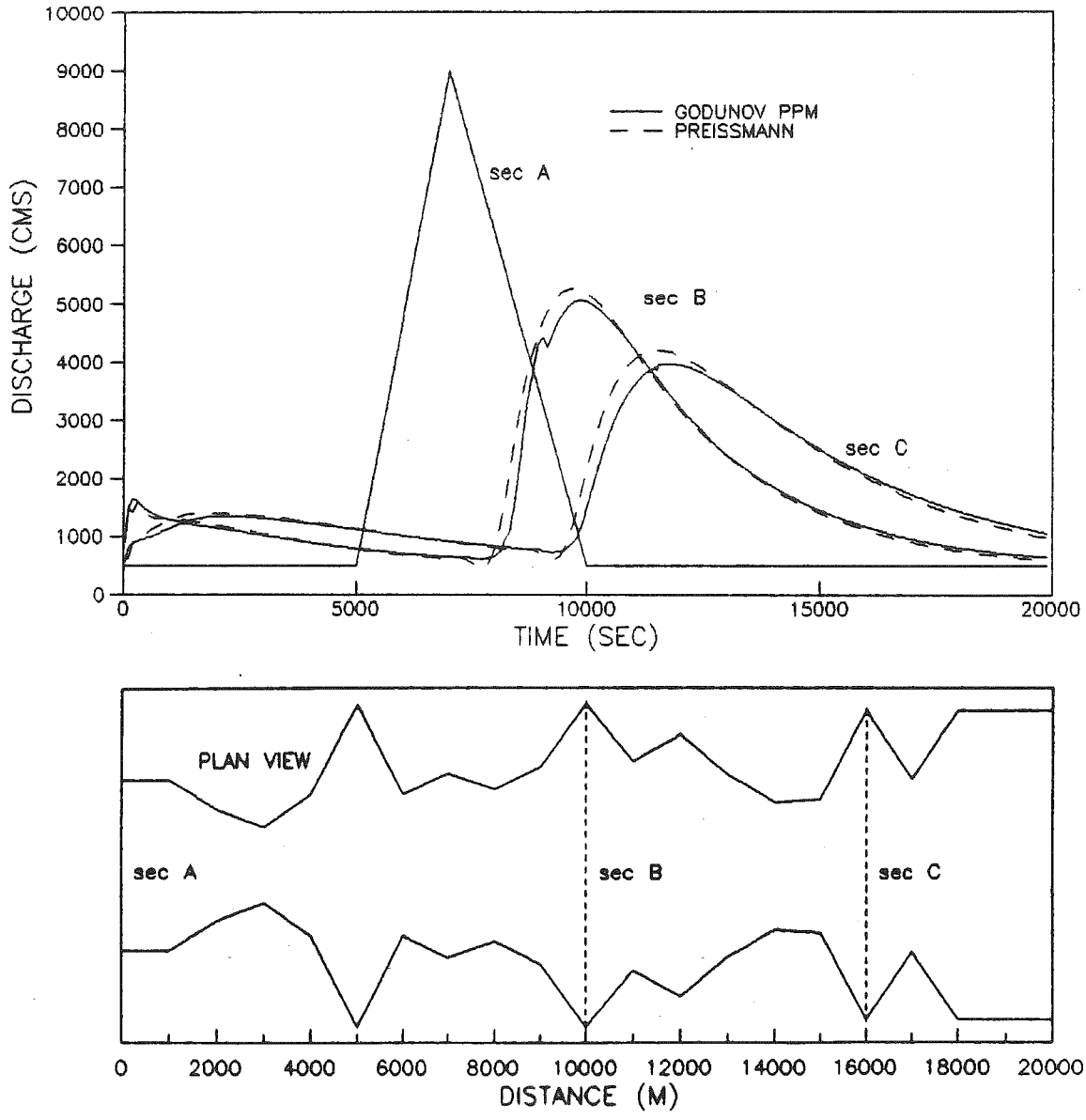

Figure 5.50 Discharge hydrographs for flood propagation in a frictional channel with normally distributed widths; comparison between the PPM Godunov and Preissmann methods

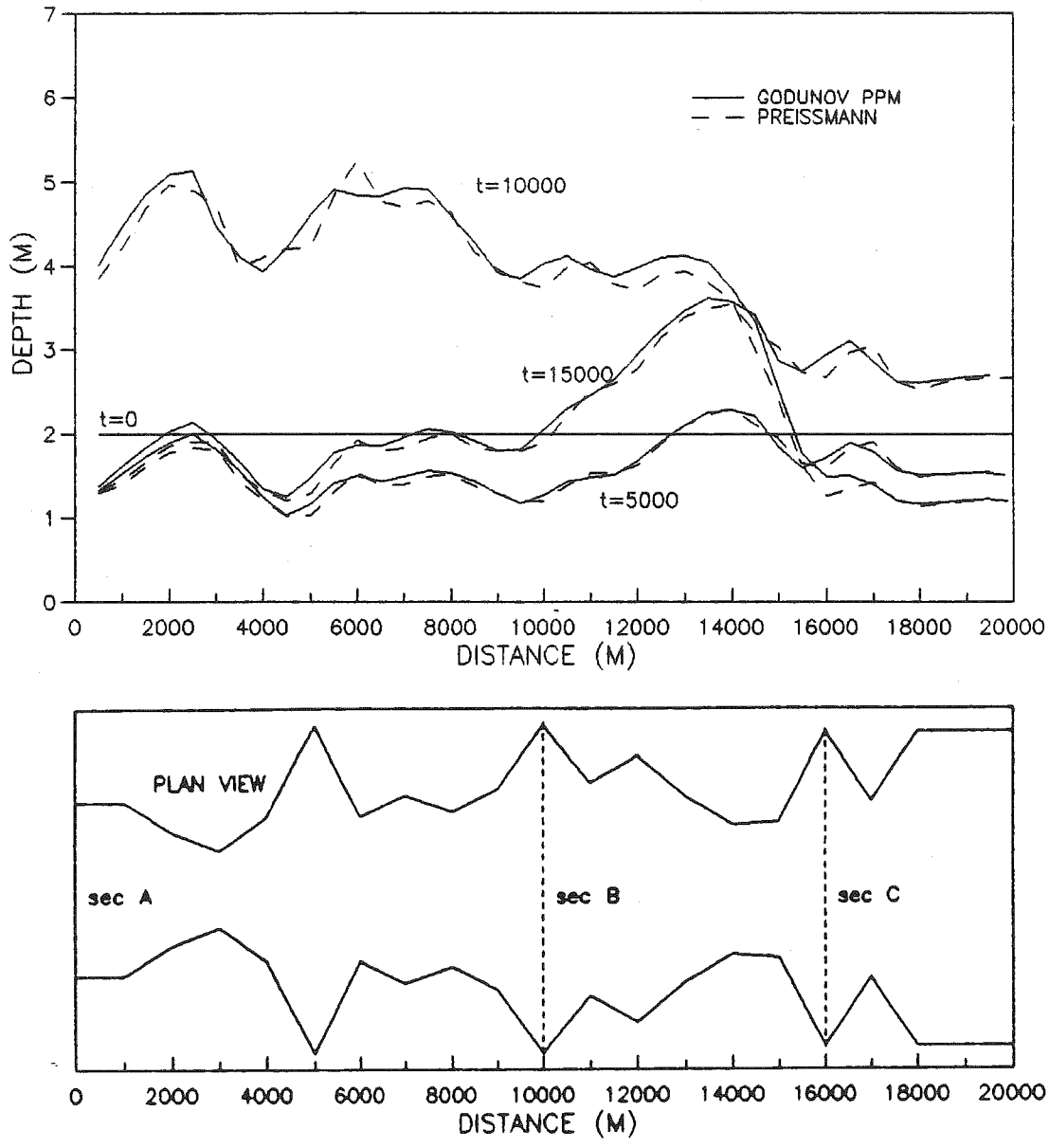

Figure 5.51 Time evolution of water-surface profiles for flood propagation in a frictional channel with normally distributed widths; comparison between the PPM Godunov and Preissmann methods, refined spatial grid

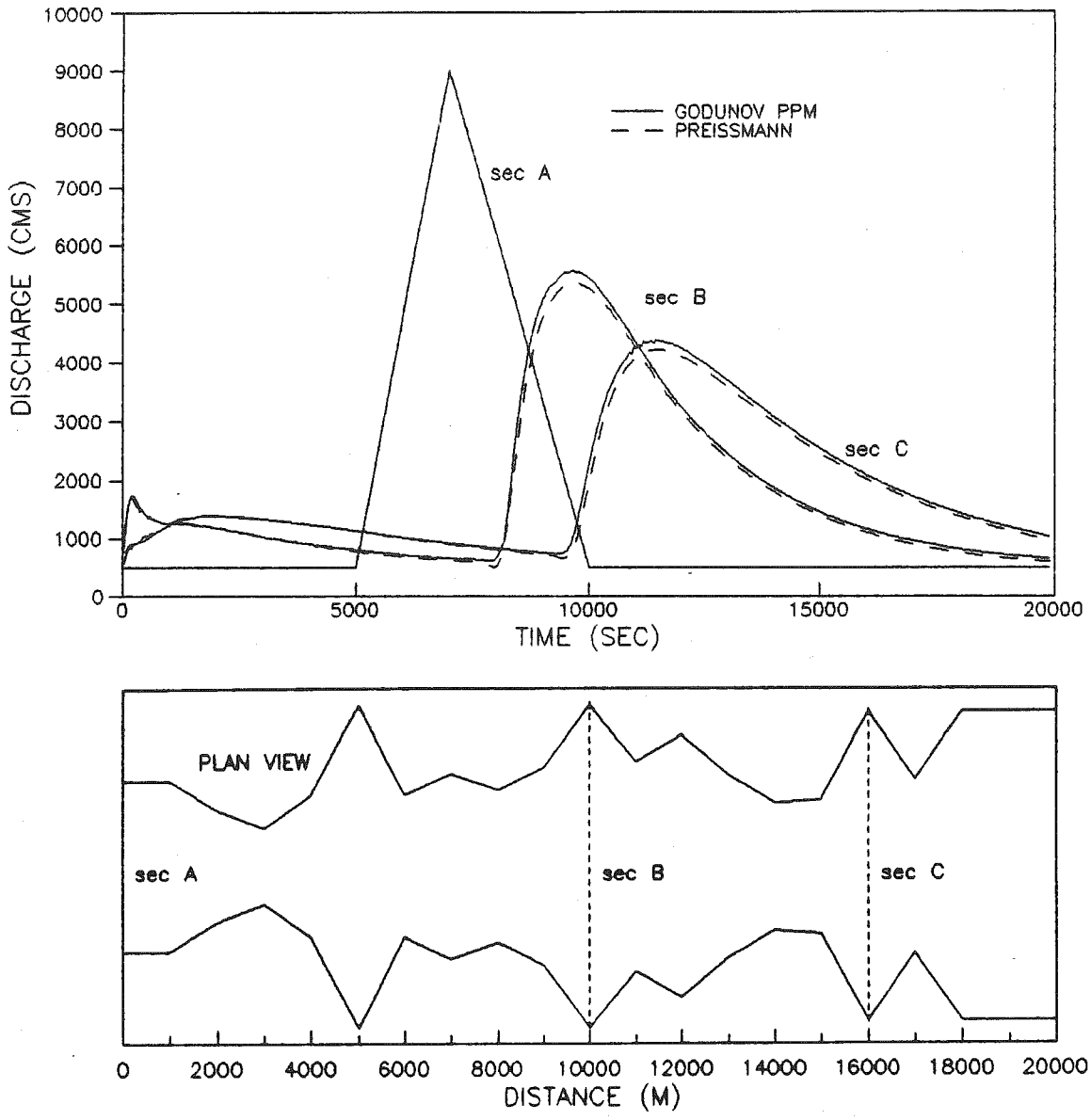

Figure 5.52 Discharge hydrographs for flood propagation in a frictional channel with normally distributed widths; comparison between the PPM Godunov and Preissmann methods

Now the instantaneous dam-break problem is considered. The same cases are treated as in the previous section on prismatic channels, but now the width of the channel varies. The most characteristic cases, sudden expansion and sudden contraction, where the width changes within one spatial step, are chosen. Again, two different upstream-to-downstream depth ratios are considered (Fig.5.2): a low dam (with a depth ratio of 10/1), and a high dam (with a depth ratio of 100/1); also two different roughnesses, Manning coefficients of 0.015 and 0.040, are tested to appreciate the influence of the frictional resistance.

First the case of the low dam is considered. The same channel is used as for the prismatic tests, 20 km long and with a slope of 0.1 %, and a spatial step of 250 m. The constant width of the reach before the width transition, located 12.5 km from the upstream end, is 50 m, then it changes within one spatial step to 250 m for the expansion case, and to 10 m for the constriction case, remaining the same for the rest of the downstream channel length. The dam is located 10 km downstream of the upstream end. The initial and boundary conditions are the same as for the prismatic case: constant depth downstream of the dam, constant level in the reservoir, and constant discharge for the initial condition; constant inflow for the upstream boundary condition, and a uniform-flow rating curve for the

downstream boundary condition.

V.4.3 Dambreak for a low dam with sudden expansion and small roughness

First the case of a sudden expansion, with a small roughness coefficient (0.015) is presented. In Figs.(5.53)-(5.55) the Godunov and shock-fitting methods are compared. From time evolution of water-surface profiles (Fig.5.53) one can observe that after the wave has reached the wider part of the channel, the depth decreases, and accordingly the wave speed also decreases (compared with the case of a prismatic channel in Fig.5.21). The change in water-surface elevation at the transition reach seems to be too sharp for the Godunov method. As in the random-width channel test this can be smoothed by refining the grid, which however requires a smaller time step to meet the stability requirement. Besides some small smearing in water-surface profiles in the reservoir region (Fig.5.53), and some small diffusion in hydrographs (Fig.5.54), the two Godunov methods agree well.

Successful computations have not been possible with either the Preissmann or the Lax-Wendroff methods, for the reasons explained in the previous sections. On the other hand the shock-fitting method of characteristics suffered

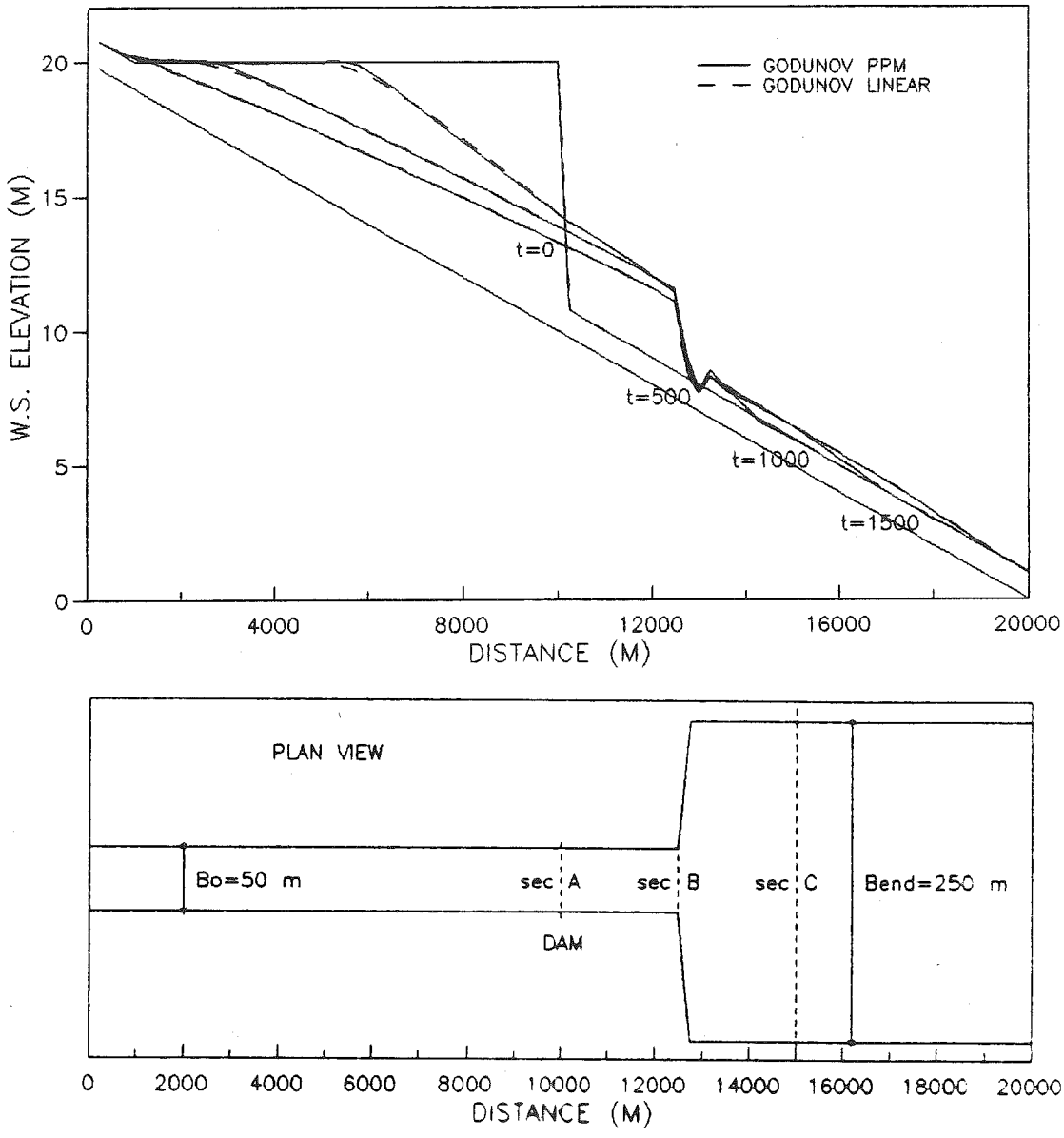

Figure 5.53 Time evolution of water-surface profiles for low-dam dambreak in a channel of small roughness with sudden expansion; comparison between the PPM Godunov and linear Godunov methods

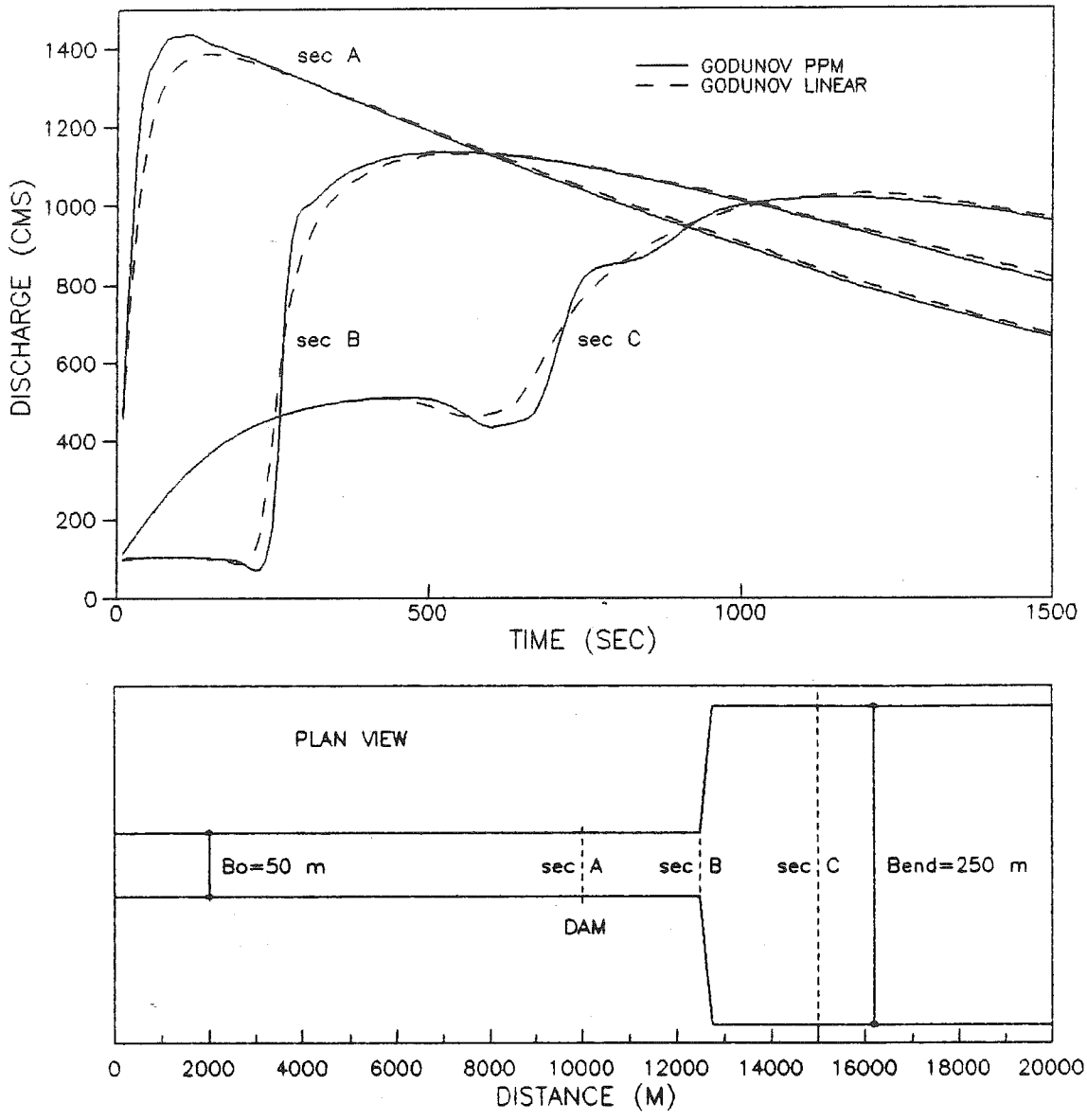

Figure 5.54 Discharge hydrographs for low-dam dambreak in a channel of small roughness with sudden expansion; comparison between the PPM Godunov and linear Godunov methods

from a large mass conservation error (above 10 %). Comparing the Godunov and the shock-fitting methods (Fig.5.55) one observes the same differences noted for the prismatic cases: diffusion (smearing) in the reservoir for the shock-fitting method, and fast diffusion of the steep front produced by frictional effects. The overall mass conservation error for all nonprismatic Godunov computations is between $2 \cdot 10^{-5}$ and $4 \cdot 10^{-4}$, while the error for the Godunov points is again much smaller (between $8 \cdot 10^{-17}$ and $5 \cdot 10^{-16}$).

For all subsequent cases the mass-conservation errors of the shock-fitting method were unacceptably large (25% and more); consequently the results of the shock-fitting method are not used for comparisons in further discussion.

V.4.4 Dambreak for a low dam with sudden expansion and large roughness

In Figs.(5.56)-(5.60) the case of the low dam with higher roughness (Manning coefficient of 0.040) is presented. Again, the depth decreases in the wider part of the channel (Fig.5.56), but it is considerably higher compared with the previous case, due to the effect of stronger resistance. In Figs.(5.56) and (5.57) the PPM and linear Godunov methods are compared. Very good agreement is achieved, both in water-surface profiles (Fig.5.56) and

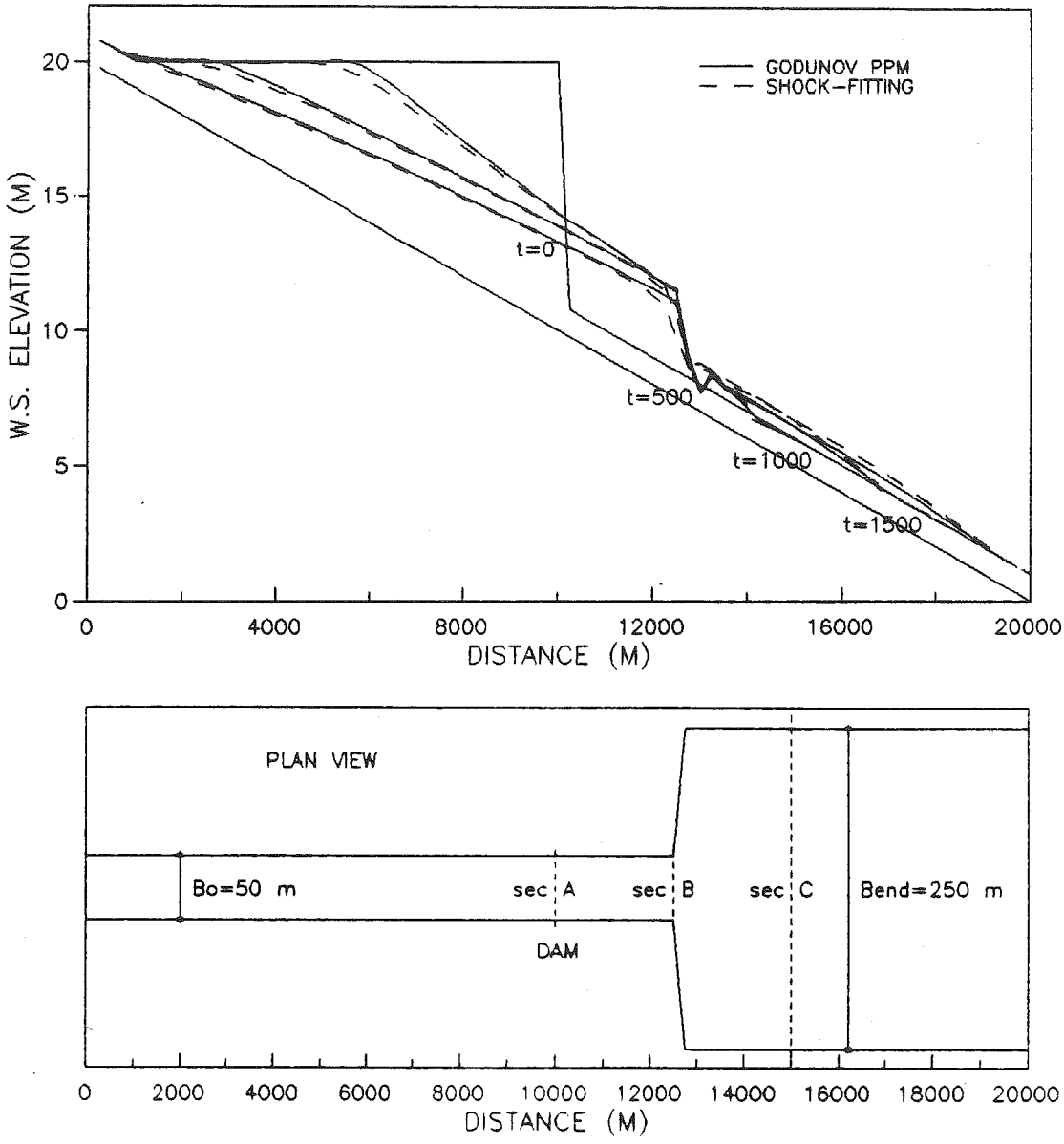

Figure 5.55 Time evolution of water-surface profiles for low-dam dambreak in a channel of small roughness with sudden expansion; comparison between the PPM Godunov and shock-fitting methods

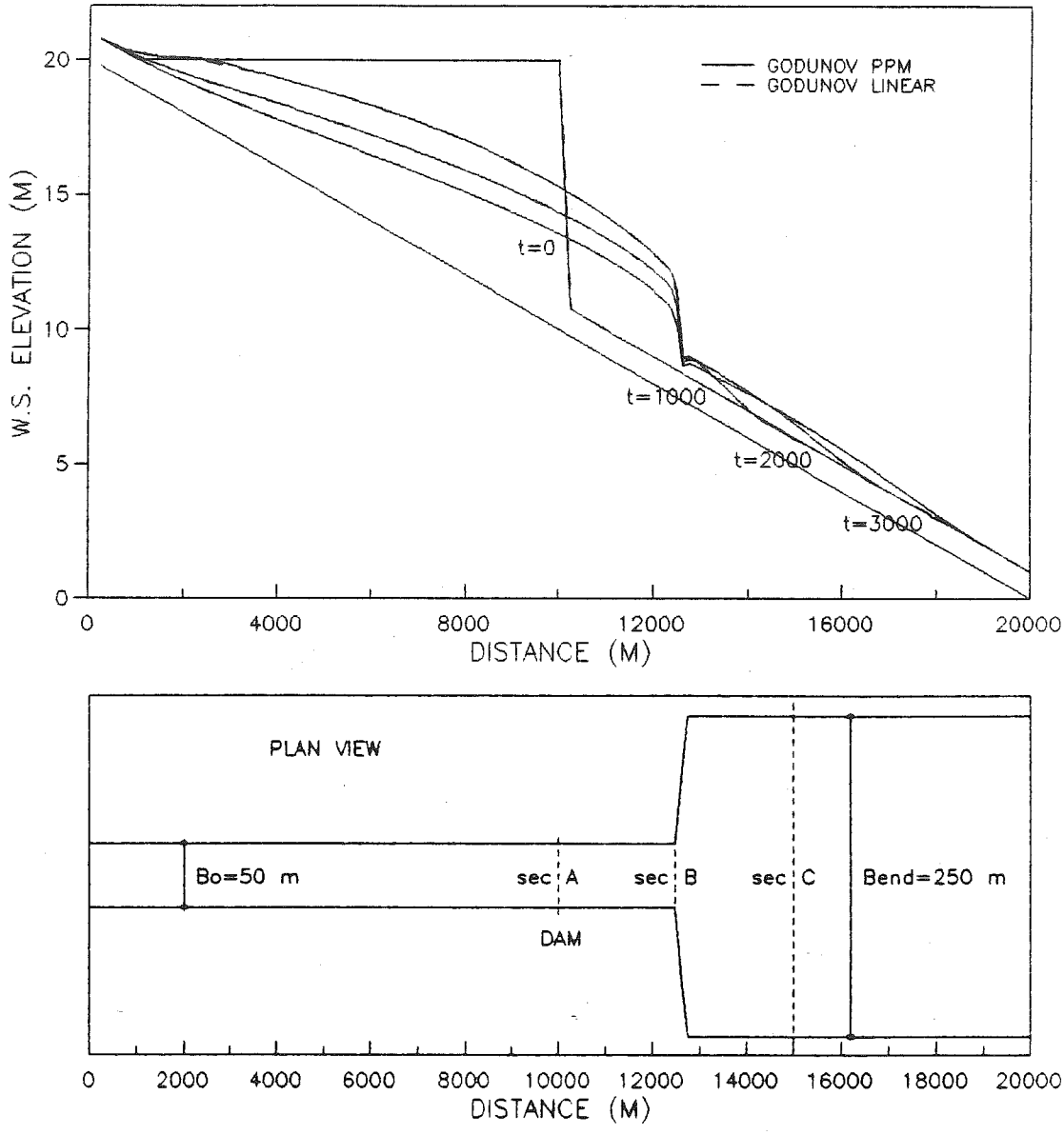

Figure 5.56 Time evolution of water-surface profiles for low-dam dambreak in a channel of large roughness with sudden expansion; comparison between the PPM Godunov and linear Godunov methods

discharge hydrographs (Fig.5.57). This corroborates the observation made for the frictional prismatic channels, that for the larger roughness coefficient natural dissipation due to the resistance effects tends to decrease the difference between the two Godunov methods.

In Figs.(5.58)-(5.60) the PPM Godunov method is compared with the Preissmann and the Lax-Wendroff methods, which were able to produce a stable solution for this high roughness case; large frictional resistance suppressed occurrence of supercritical flow and mixed regime, enabling successful performance of the Preissmann method, and at the same time dampened numerical oscillations for the Lax-Wendroff method.

In general good agreement between the compared methods is attained. To obtain a successful computation with the Preissmann method large time steps and a temporal-weighting coefficient of 1.0 must be used, so some diffusion of the profiles occurs in the reservoir, the transition, and the surge front itself (Fig.5.58). The water-surface elevations for the Lax-Wendroff method agree even better with the Godunov method (Fig.5.59) than do the Preissmann predictions. The only difference can be observed in the zone immediately upstream of the transition. On the other hand a three-times smaller time step was needed for the Lax-Wendroff method compared to the Godunov method to obtain the

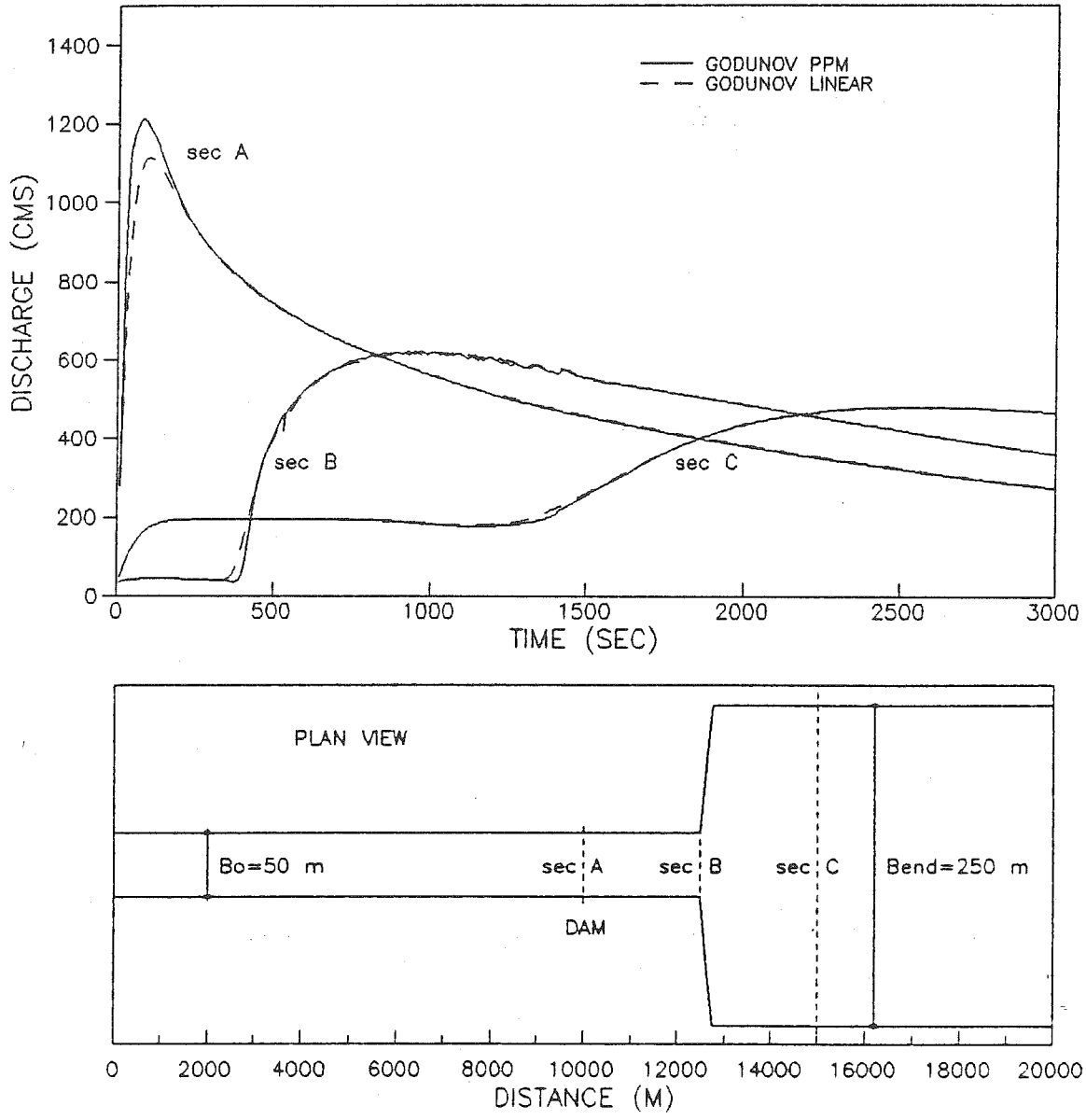

Figure 5.57 Discharge hydrographs for low-dam dambreak in a channel of large roughness with sudden expansion; comparison between the PPM Godunov and linear Godunov methods

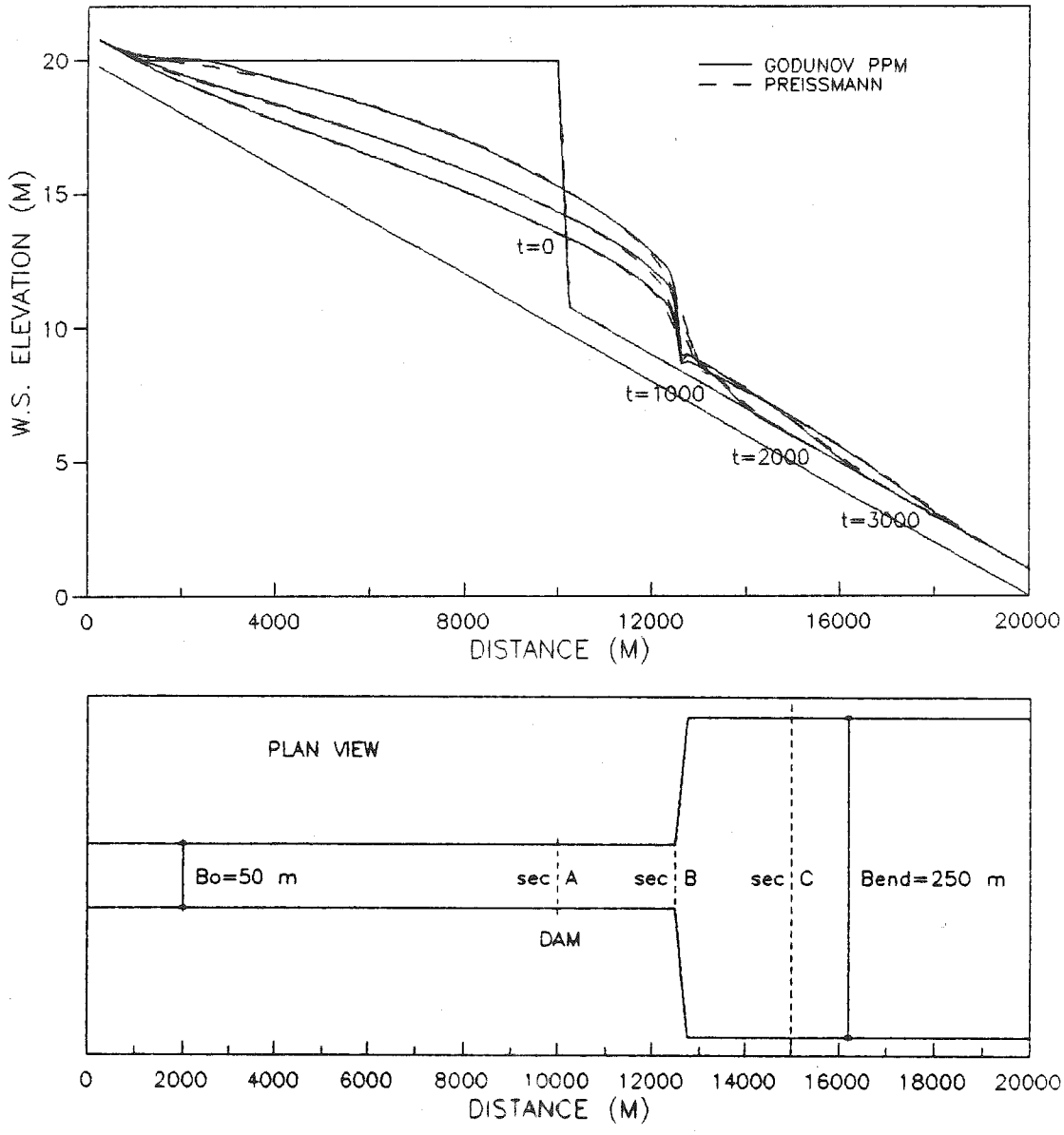

Figure 5.58 Time evolution of water-surface profiles for low-dam dambreak in a channel of large roughness with sudden expansion; comparison between the PPM Godunov and Preissmann methods

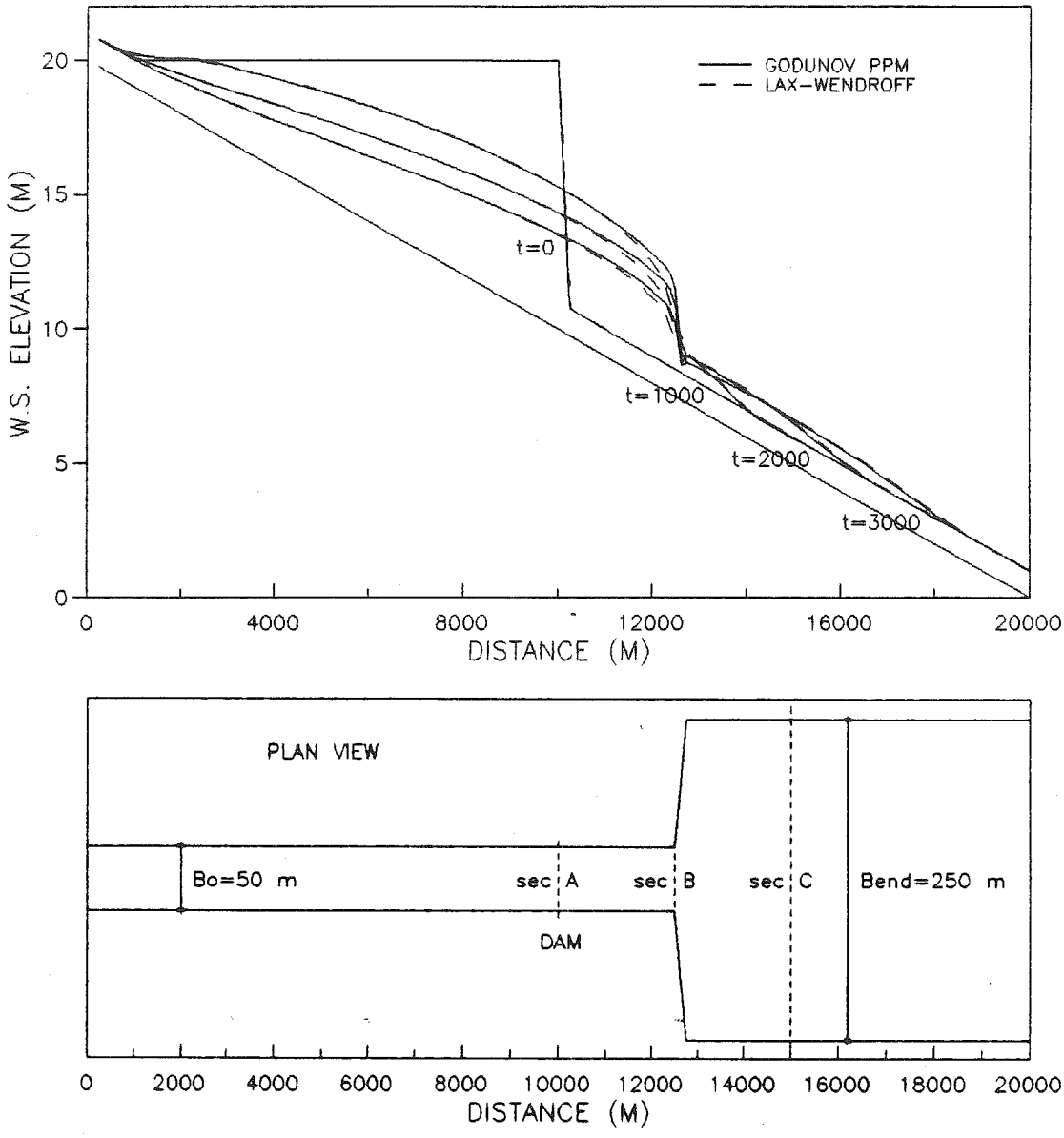

Figure 5.59 Time evolution of water-surface profiles for low-dam dambreak in a channel of large roughness with sudden expansion; comparison between the PPM Godunov and Lax-Wendroff methods

solution. Spurious oscillations still persist in the discharge hydrographs for the Lax-Wendroff method (Fig.5.60), though they do not greatly affect the practical utility of the results (i.e. water surface-elevation and wave speed). The mass-conservation errors are $2 \cdot 10^{-7}$ for the Preissmann method, and $7 \cdot 10^{-5}$ for the Lax-Wendroff method.

V.4.5 Dambreak for a low dam with sudden constriction and small roughness

Now we consider the case of a sudden constriction for the low dam (10/1 depth ratio). First the channel with small roughness (Manning coefficient of 0.015) is considered. The only methods that could produce a result were the two Godunov methods (PPM and linear); as in earlier cases, mixed flow regime disabled the Preissmann method, and large numerical oscillations plagued the Lax-Wendroff method. The results are presented in Figs.(5.61) and (5.62). The physical phenomenon is correctly represented; after the surge reaches the constriction (see Fig.5.61), whose conveyance is insufficient to pass the oncoming flow, water accumulates upstream of the constriction in order to increase the energy (pressure gradient) required to pass the flow. This produces a wave moving upstream. The effect of superposition of elementary positive waves (explained in

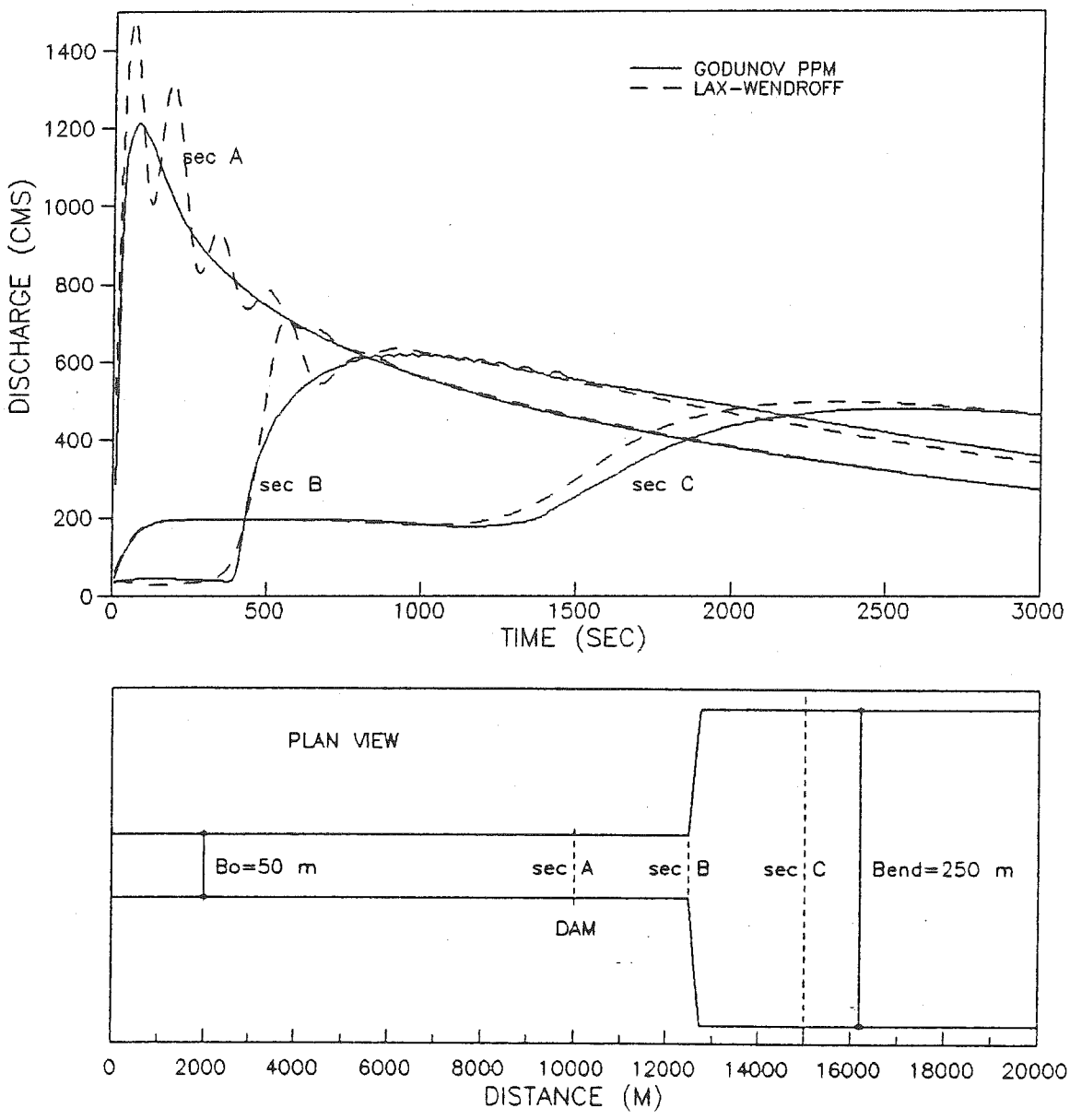

Figure 5.60 Discharge hydrographs for low-dam dambreak in a channel of large roughness with sudden expansion; comparison between the PPM Godunov and Lax-Wendroff methods

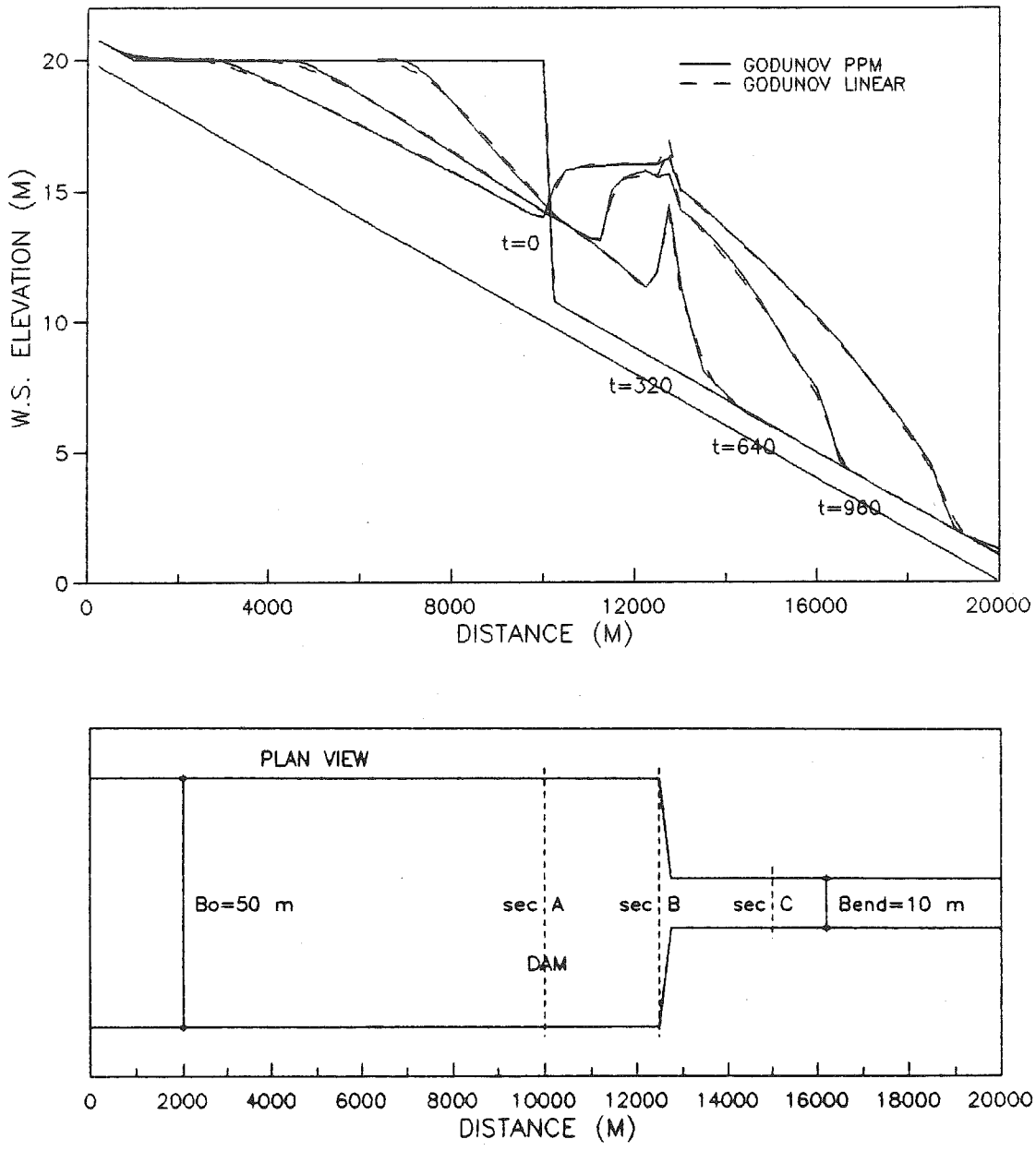

Figure 5.61 Time evolution of water-surface profiles for low-dam dambreak in a channel of small roughness with sudden constriction; comparison between the PPM Godunov and linear Godunov methods

chapter 2) produces a steep front moving back towards the reservoir, and flooding the initially spared (unflooded) region on its way back. This is a very common practical situation for dam-break flood predictions in canyons, where accumulation of water upstream of the constriction produces much larger depths, both upstream and downstream of the constriction, than those which would result if there were no constriction. Nevertheless, the constriction has also a positive effect on the region far downstream, by reducing the discharge as observed in Fig.(5.62) (the same principle as in flood control with spillways of narrow width).

From Fig.(5.61) one can observe good agreement between the Godunov PPM and linear methods for water-surface profiles with the usual increased diffusion for the linear method. Spurious oscillations occur for the PPM method in discharge hydrographs (Fig.5.62) at the constriction section, but as shown before they can be reduced on the expense of using smaller spatial steps (refining the grid).

V.4.6 Dambreak for a low dam with sudden constriction and large roughness

In Fig.(5.63)-(5.67) the case of a sudden constriction for the low dam and a larger roughness coefficient of 0.040 is presented. In Fig.(5.63) evolution of water-surface profiles for the Godunov PPM and linear methods is compared.

The same physical description of the low-roughness case is valid. The only difference is produced by the effect of higher resistance on smoothing the steep fronts of both surges: the one passing from the constriction towards the downstream boundary and the other moving back to the reservoir. Also, the spurious oscillations in the constriction-section hydrograph are now smoothed (Fig.5.64).

The Preissmann method could not yield a stable solution here, and the Lax-Wendroff method needs three times smaller time step to produce an acceptable stable solution, but still with noticeable oscillations in water-surface profiles (Fig.5.65), and particularly in hydrographs (5.66). If one excludes those numerical oscillations the results of the Godunov and Lax-Wendroff schemes agree very well, except for the insignificant smearing of the wave front for the Lax-Wendroff method (Fig.5.65), and some shift in discharge and depth hydrographs (Figs.5.66 and 5.67).

V.4.7 Dambreak for a high dam with sudden expansion and small roughness

Now the case of a high dam (upstream-to-downstream depth ratio of 100/1) is considered. The same channel is used as for the prismatic tests: 100 km long, with a slope of 0.1 %, and a spatial step of 1000 m. The constant width of the reach upstream of the transition, located 55 km from

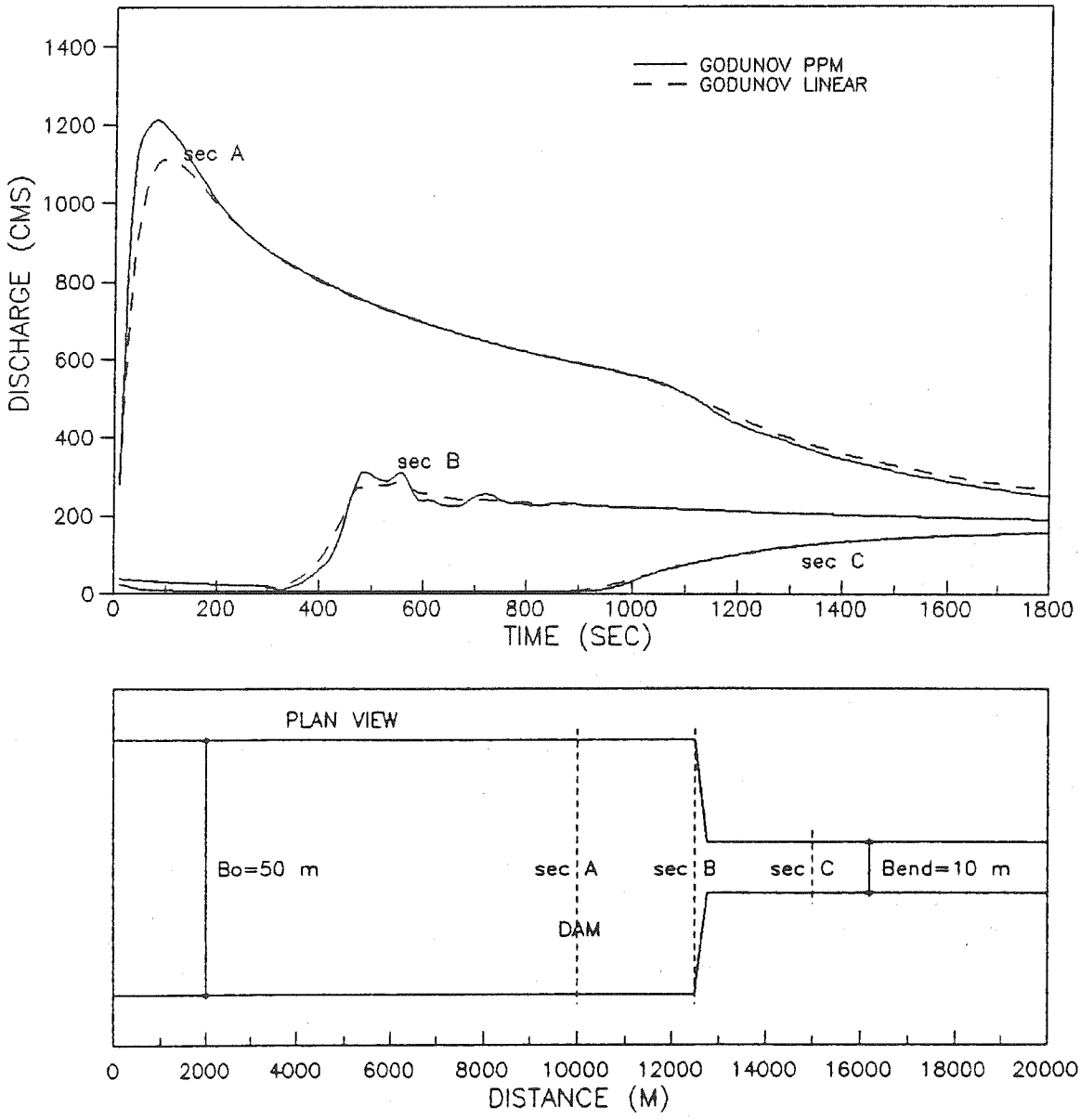

Figure 5.64 Discharge hydrographs for low-dam dambreak in a channel of large roughness with sudden constriction; comparison between the PPM Godunov and linear Godunov methods

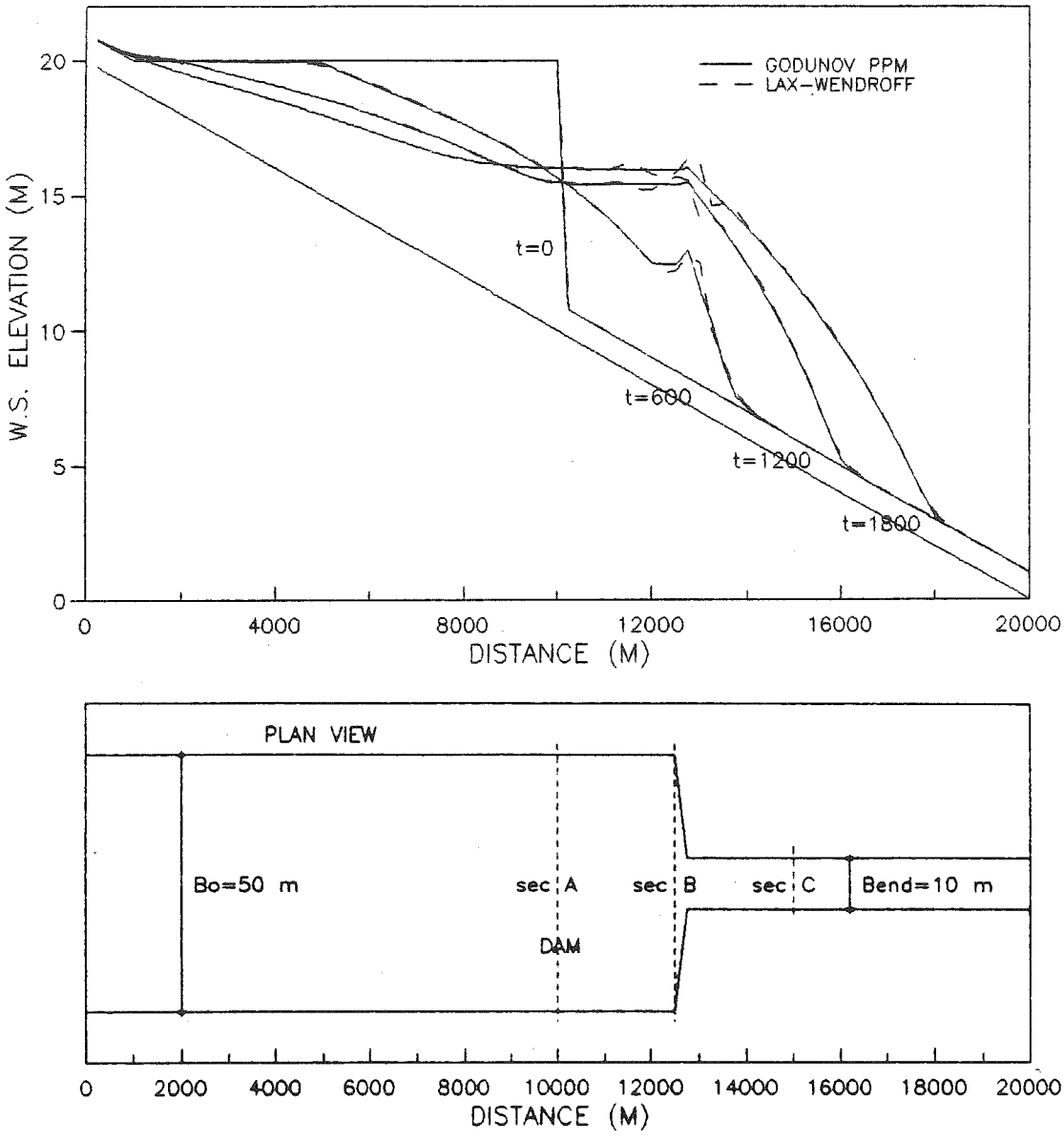

Figure 5.65 Time evolution of water-surface profiles for low-dam dambreak in a channel of large roughness with sudden constriction; comparison between the PPM Godunov and Lax-Wendroff methods

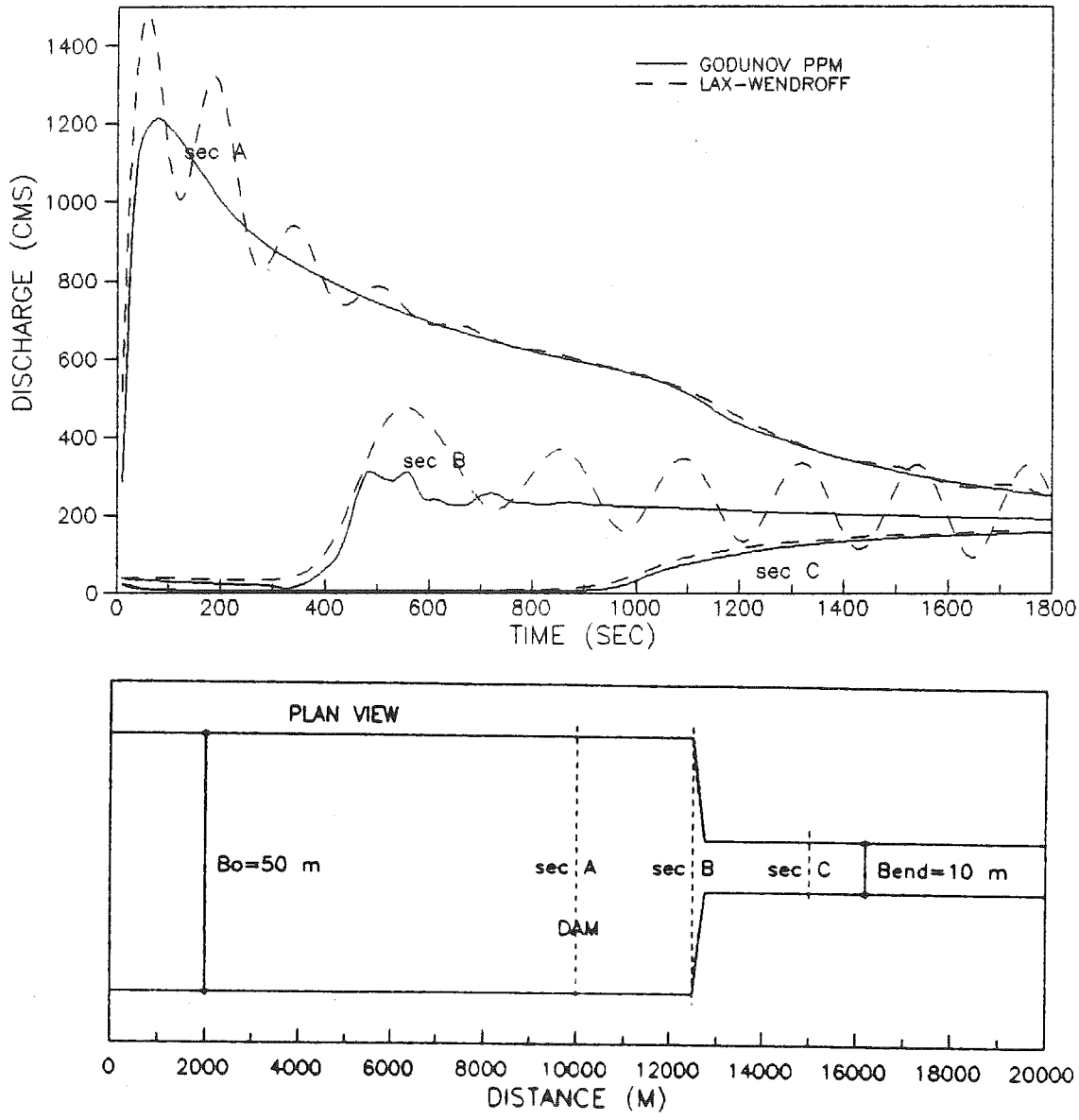

Figure 5.66 Discharge hydrographs for low-dam dambreak in a channel of large roughness with sudden constriction; comparison between the PPM Godunov and Lax-Wendroff methods

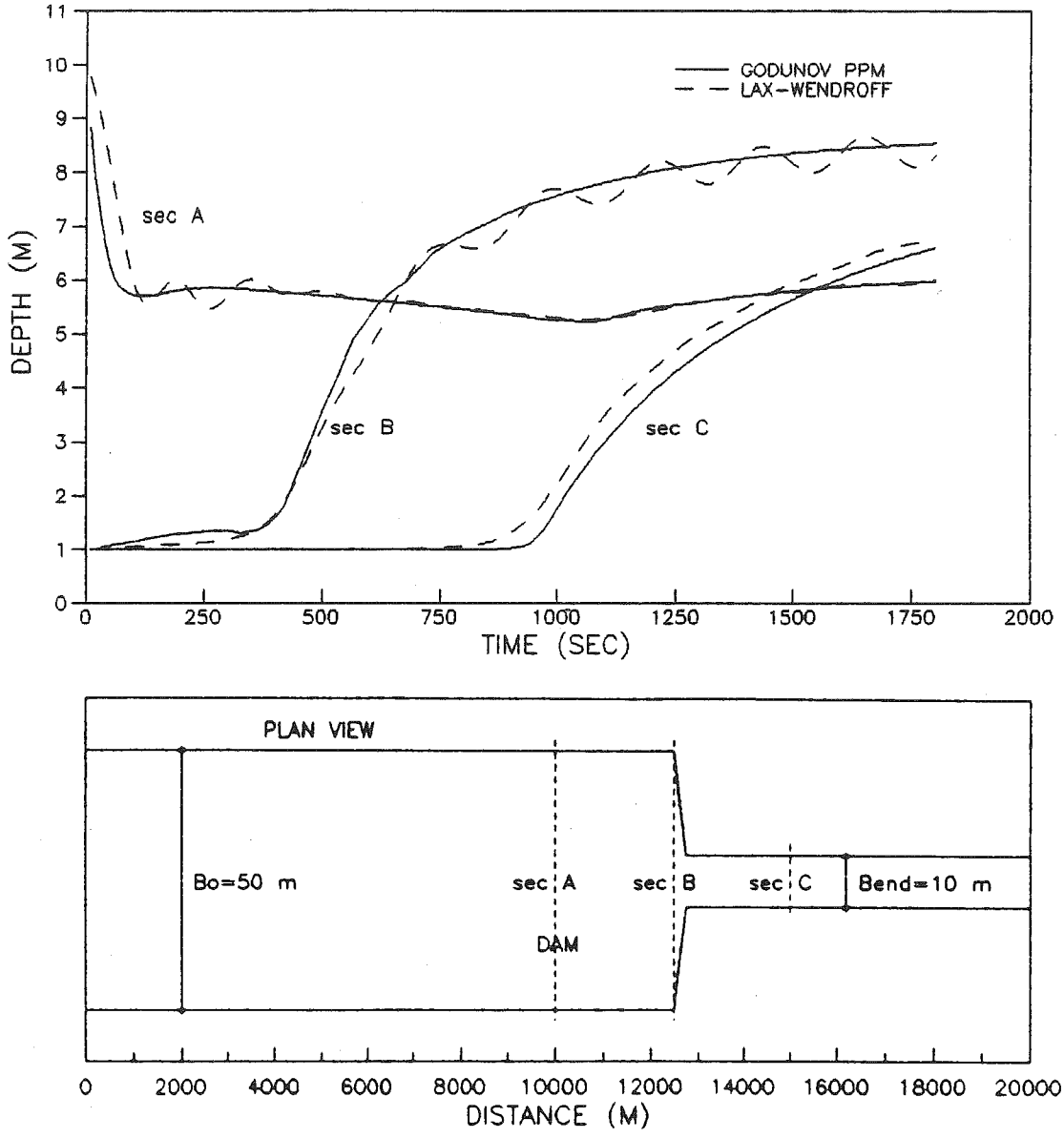

Figure 5.67 Depth hydrographs for low-dam dambreak in a channel of large roughness with sudden constriction; comparison between the PPM Godunov and Lax-Wendroff methods

the upstream end, is 50 m; then it changes within one spatial step to 250 m for the expansion case, and to 10 m for the constriction case, remaining the same for the rest of the channel. The dam section is 50 km downstream of the upstream boundary. The initial condition is a constant depth downstream of the dam, constant level in the reservoir, and constant discharge. A constant inflow is prescribed for the upstream boundary condition, and a uniform-flow rating curve is used for the downstream boundary condition.

The case of a sudden expansion with a small roughness coefficient is presented in Figs.(5.68) and (5.69). Only the Godunov methods were capable of yielding results for such a severe case. The temporal evolution of water surface-profiles for the two Godunov methods is shown in Fig.(5.68). The depths drop through the expansion section which consequently reduces the speed of the surge. Except for some diffusion in the reservoir for the linear method, good agreement between the two methods is observed. The discharge hydrographs also agree well, with some oscillations for the PPM method, and very small diffusion for the linear method.

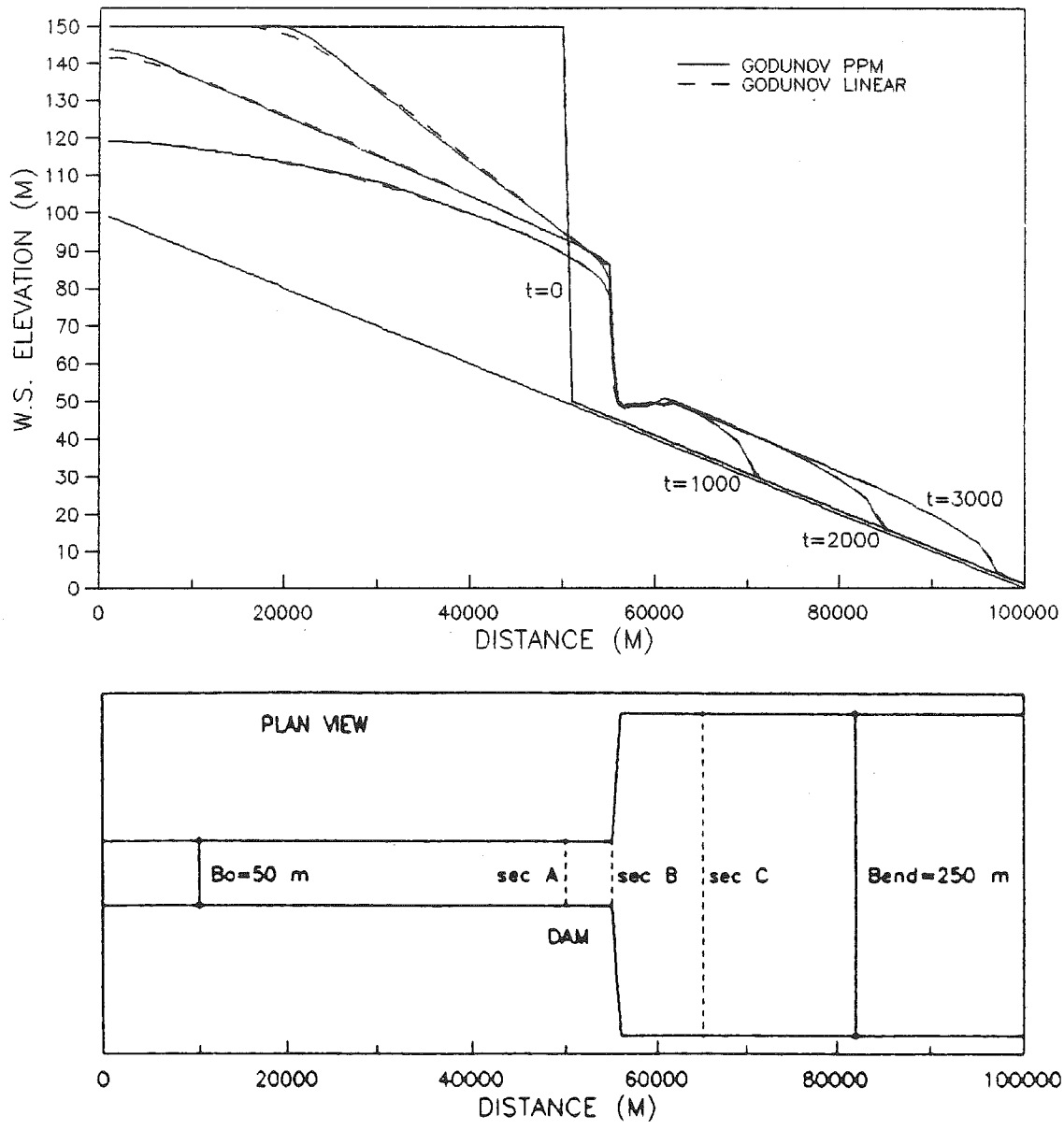

Figure 5.68 Time evolution of water-surface profiles for high-dam dambreak in a channel of small roughness with sudden expansion; comparison between the PPM Godunov and linear Godunov methods

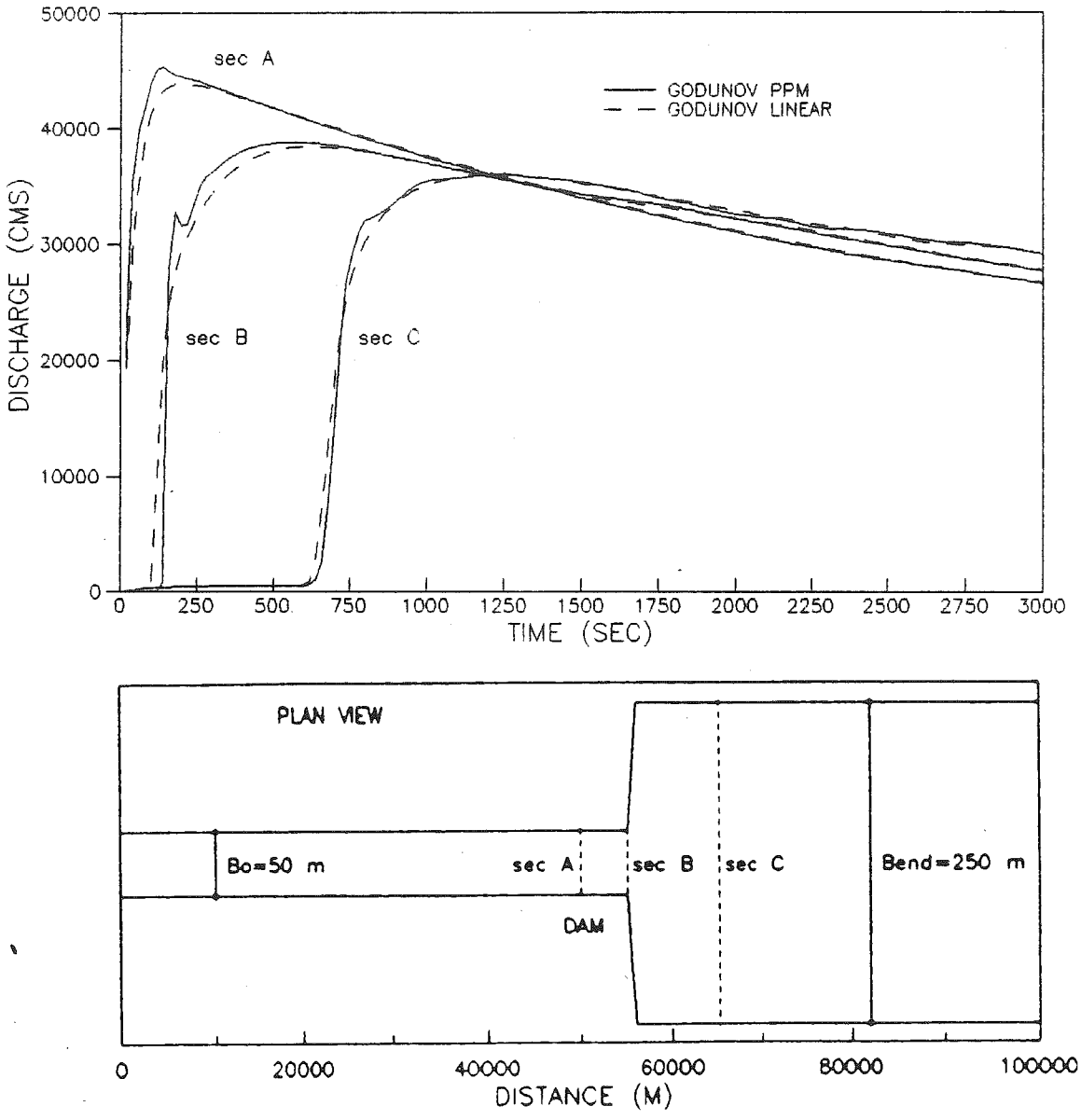

Figure 5.69 Discharge hydrographs for high-dam dambreak in a channel of small roughness with sudden expansion; comparison between the PPM Godunov and linear Godunov methods

V.4.8 Dambreak for a high dam with sudden expansion and large roughness

The case of a sudden expansion for the channel with higher resistance (Manning coefficient of 0.040) is considered next. In Fig.(5.70) the results of the Godunov PPM method computations with and without an interpolated profile, analogous to the one introduced for the steady-flow test within the width transition, are presented. In both cases the same gradient of channel widening is preserved. This comparison is shown to confirm the results of the steady-flow case (see Fig.5.43-5.46 and accompanying discussion), namely that refining the grid for the Godunov method smooths artificial fronts and peaks. The PPM and linear Godunov methods produce solutions which are graphically indistinguishable!

In Figs.(5.71) and (5.72) the Godunov PPM and the Lax-Wendroff methods are compared. To obtain a successful solution for the Lax-Wendroff method one must use ten times smaller time steps then for the Godunov method. The water-surface profiles for the two methods agree very well, the only perceptible difference being in the reservoir for the first stages of computation. Again, the discharge

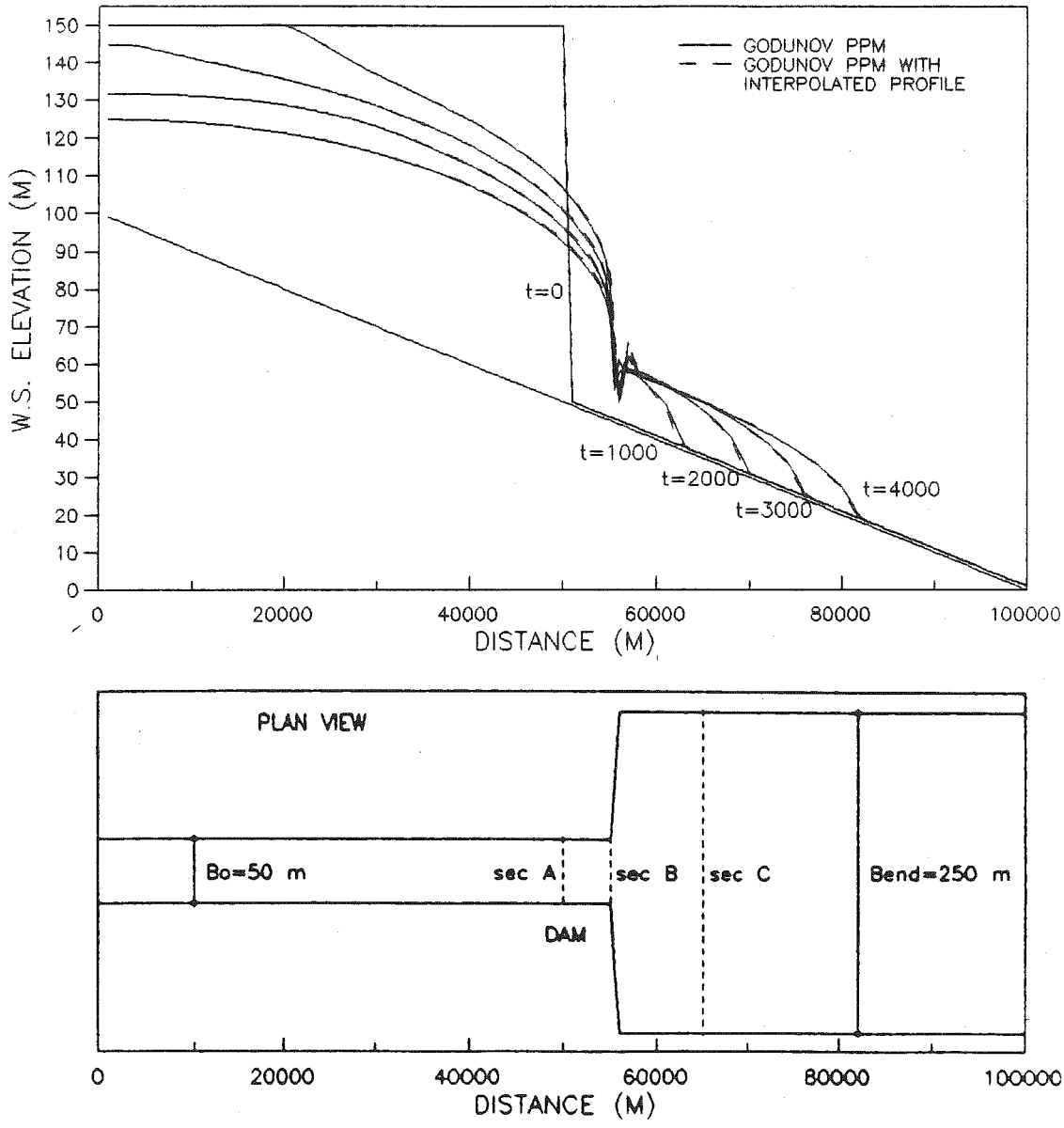

Figure 5.70 Time evolution of water-surface profiles for high-dam dambreak in a channel of large roughness with sudden expansion; comparison between the PPM Godunov with and without interpolated profile

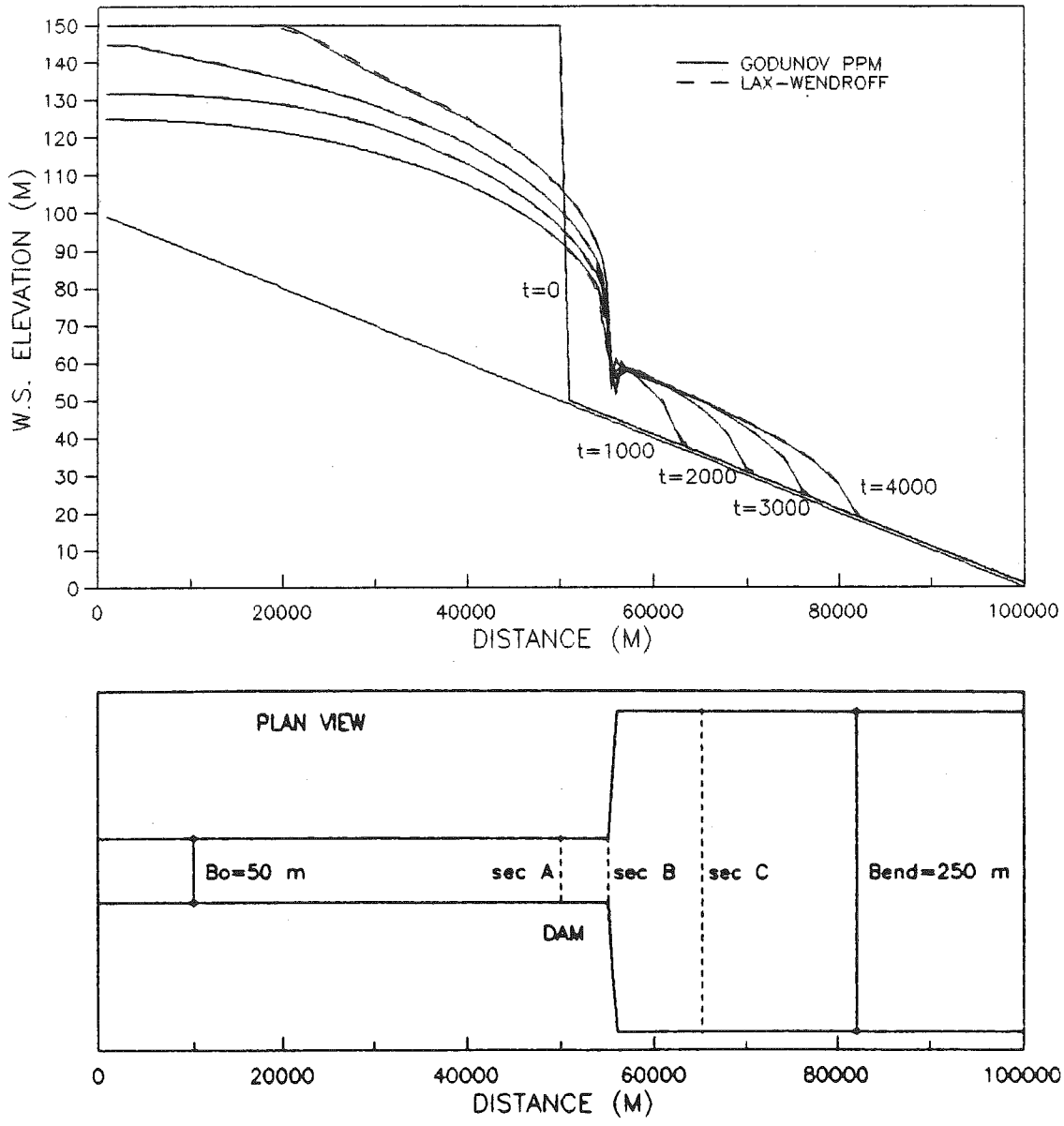

Figure 5.71 Time evolution of water-surface profiles for high-dam dambreak in a channel of large roughness with sudden expansion; comparison between the PPM Godunov and Lax-Wendroff methods

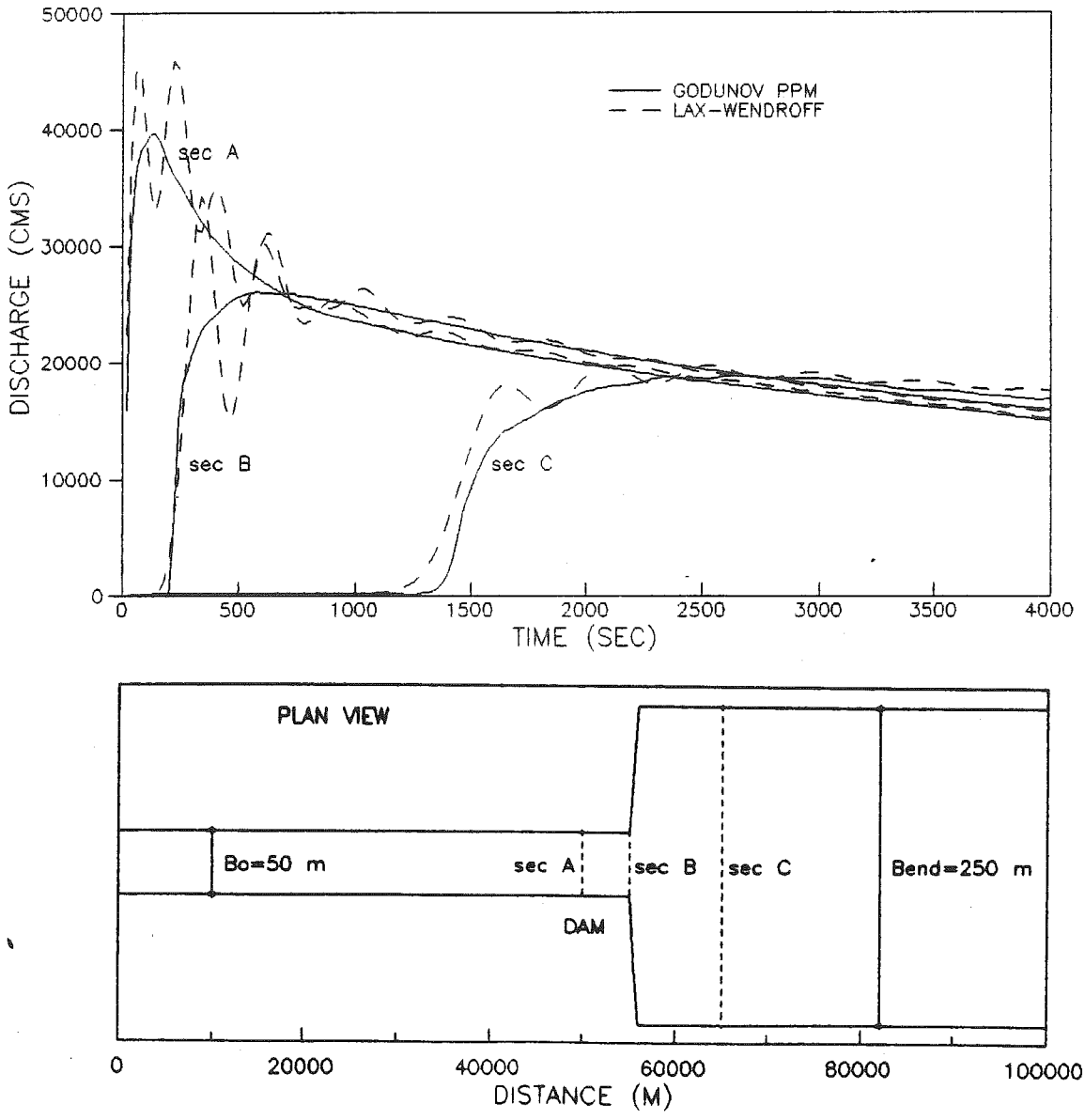

Figure 5.72 Discharge hydrographs for high-dam dambreak in a channel of large roughness with sudden expansion; comparison between the PPM Godunov and Lax-Wendroff methods

hydrographs for the Lax-Wendroff method suffer from strong oscillations, and some shift can also be observed. The mass conservation error for the Lax-Wendroff method is $3 \cdot 10^{-5}$.

V.4.9 Dambreak for a high dam with sudden constriction and small roughness

Finally the case of a sudden constriction for the high dam is presented. Again, in the case of small roughness (Manning coefficient of 0.015) only the Godunov methods produce stable results. The comparison between the Godunov PPM and linear methods is shown in Fig.(5.73) and (5.74). The physical phenomenon is qualitatively the same as in the case of a low dam, but now the changes in variables are much stronger, which results in very strong shocks; some oscillations can be observed in water-surface profiles for the PPM method (Fig.5.73). One can also notice that the linear method smears somewhat the front of the surge moving in a positive direction, and also produces some diffusion in the reservoir. The front of the PPM method is still confined to one spatial step. The spurious oscillations in discharge hydrographs for the PPM method (Fig.5.74), can be expected from the water-surface profiles. They are particularly strong for the constriction section, and though gradually die out, should be reduced by refining the spatial

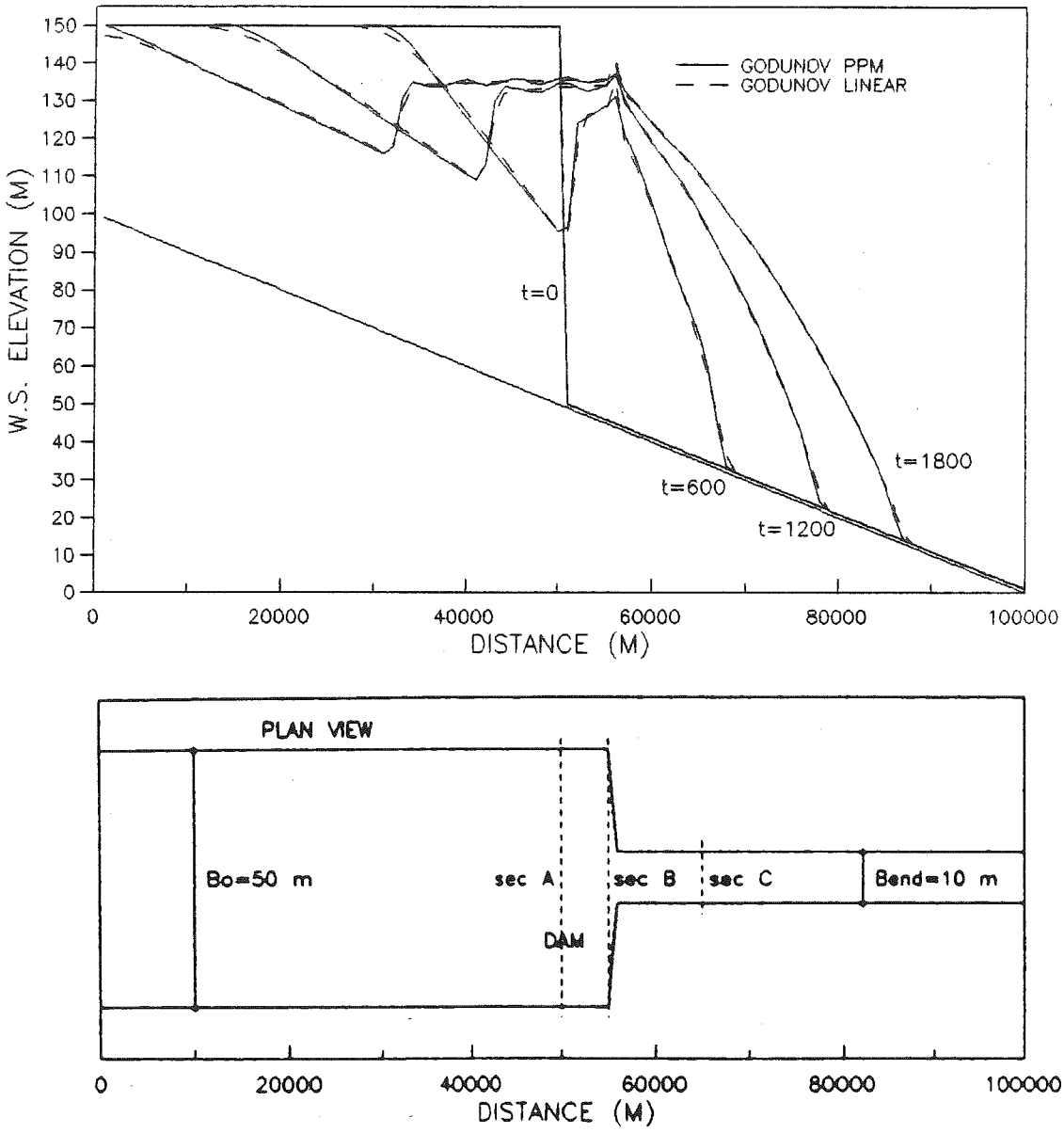

Figure 5.73 Time evolution of water-surface profiles for high-dam dambreak in a channel of small roughness with sudden constriction; comparison between the PPM Godunov and linear Godunov methods

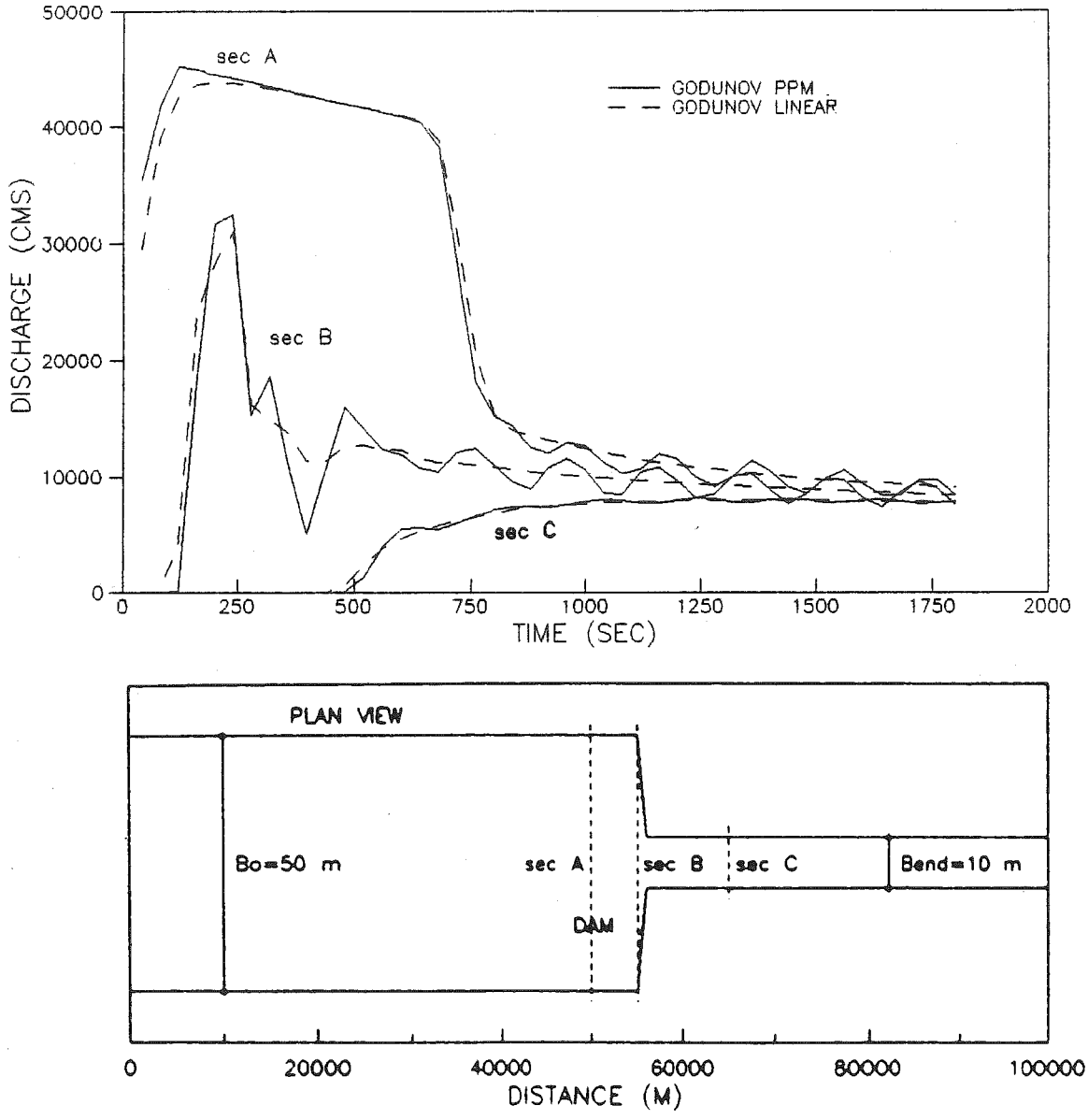

Figure 5.74 Discharge hydrographs for high-dam dambreak in a channel of small roughness with sudden constriction; comparison between the PPM Godunov and linear Godunov methods

grid.

Again the Lax-Wendroff method becomes unstable in a few time steps; no stable computations are possible.

V.4.10 Dambreak for a high dam with sudden constriction and large roughness

The last test case deals with the sudden constriction for a high dam and a channel of large roughness. The effect of roughness smooths out the steep fronts of both surges, and in addition reduces spurious oscillations. In Fig.(5.75) the temporal evolution of water-surface profiles for the PPM and linear Godunov methods is presented. The two methods agree well except for some smearing of the linear method in the zones of fronts and the reservoir. Oscillations in the PPM method are greatly reduced compared to the case of smaller roughness (Fig.5.76).

The water-surface profiles for the Lax-Wendroff and Godunov methods are compared in Fig.(5.77). The "successful" computation for the Lax-Wendroff method is obtained for a time step ten times smaller than that of the Godunov method. Apparently, artificial damping (viscosity) has to be added in the Lax-Wendroff method in order to obtain reasonable results, but this also produces diffusion and smearing of the front (see Fig.5.1).

The computations for nonprismatic channels have again

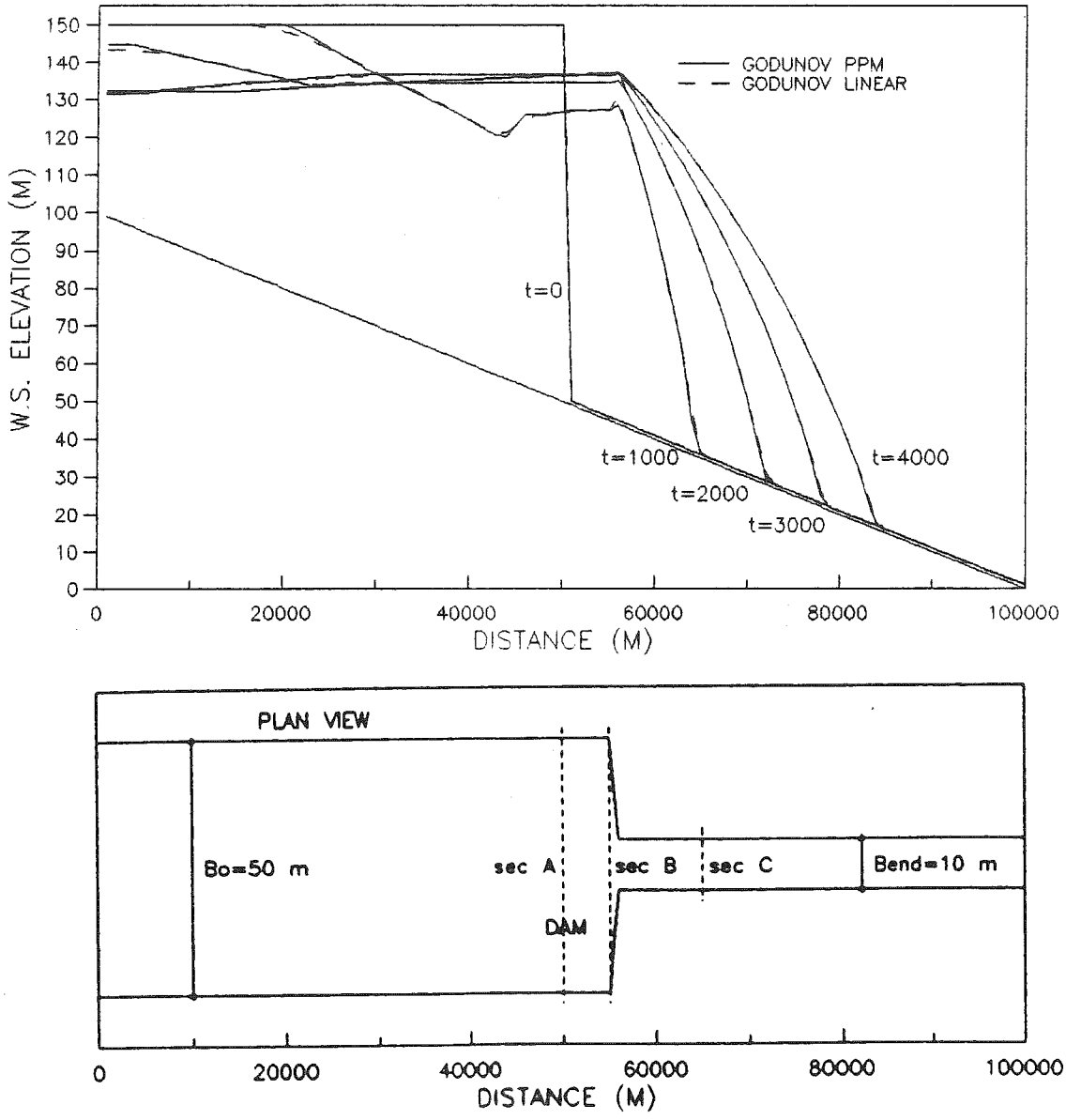

Figure 5.75 Time evolution of water-surface profiles for high-dam dambreak in a channel of large roughness with sudden constriction; comparison between the PPM Godunov and linear Godunov methods

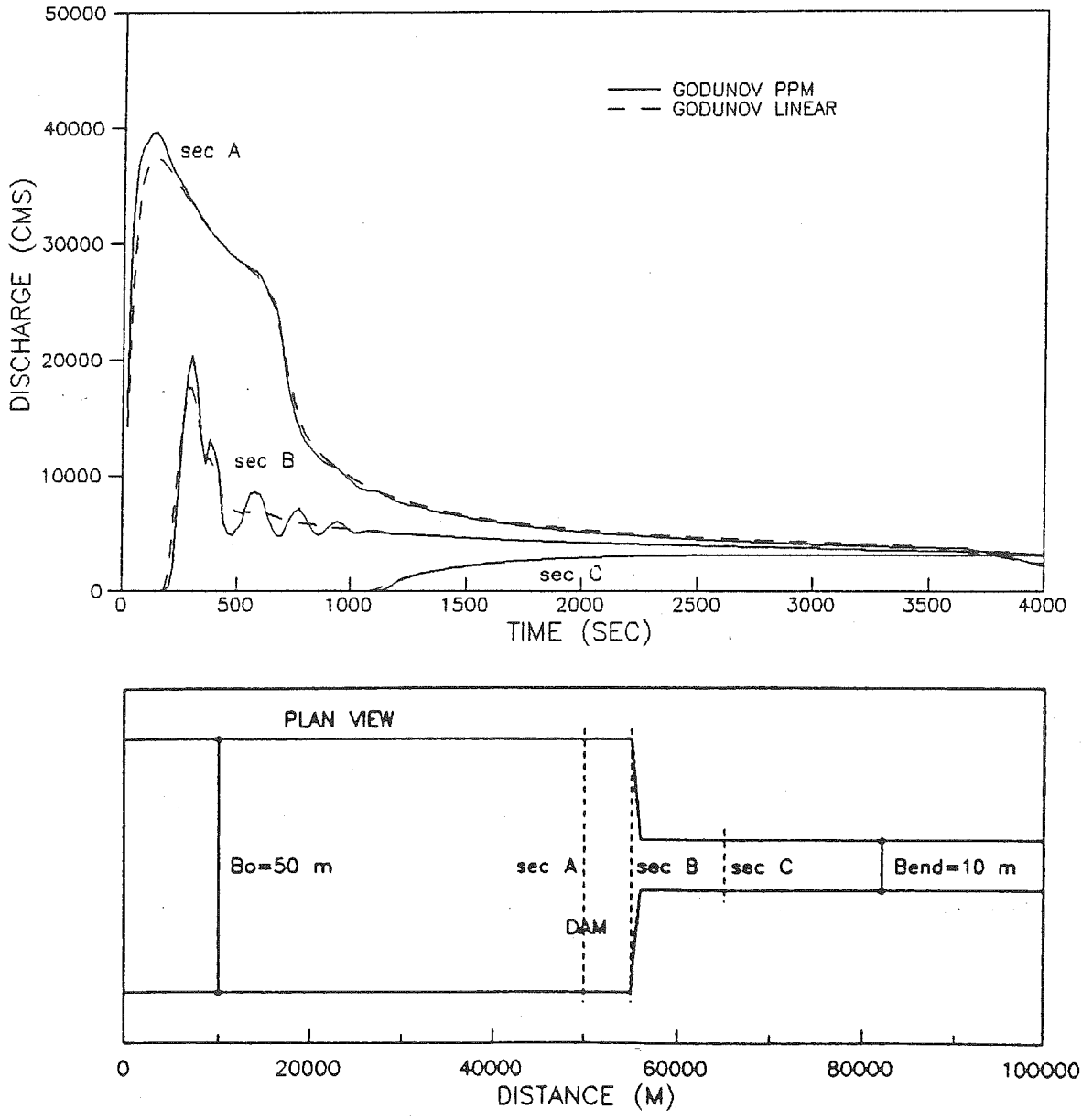

Figure 5.76 Discharge hydrographs for high-dam dambreak in a channel of large roughness with sudden constriction; comparison between the PPM Godunov and linear Godunov methods

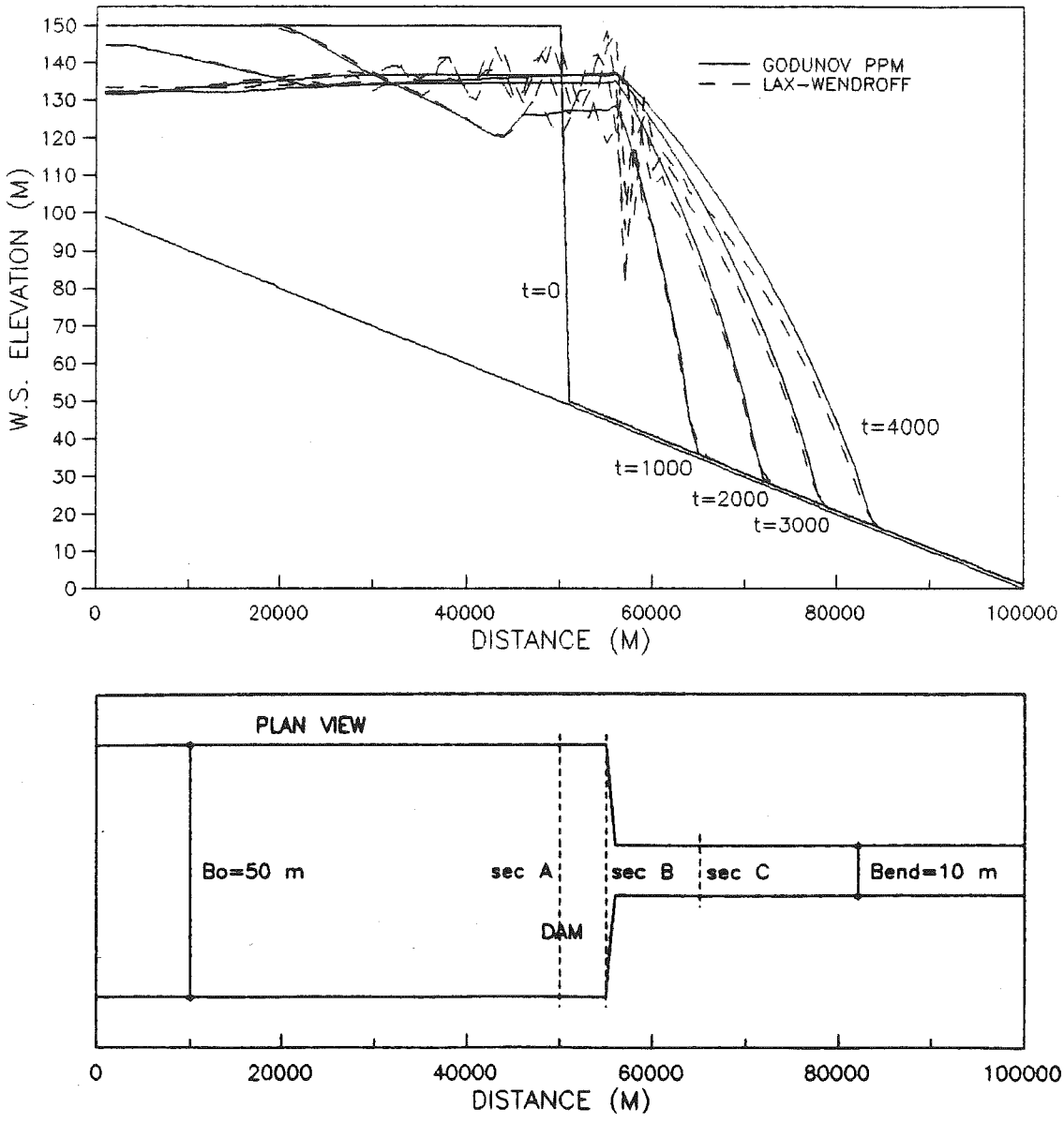

Figure 5.77 Time evolution of water-surface profiles for high-dam dambreak in a channel of large roughness with sudden constriction; comparison between the PPM Godunov and Lax-Wendroff methods

shown the advantages of the Godunov method over conventional methods (the Preissmann and the Lax-Wendroff methods) in coping with mixed-flow regimes and with very strong shocks. However, they have also shown that refining the computational grid is often required for abrupt expansions, to avoid artificial oscillations; this involves reducing the time step to satisfy the stability condition, and therefore increasing significantly the computational time.

V.4.11 Dambreak for a high dam with sudden change in bed elevation

The sudden change in bed elevation (bottom slope) has also been tested, but is not presented here systematically. This situation does not pose computational challenges like those of severe nonprismaticity.

One illustration of the computation for a channel with variable bottom slope is presented in Fig.(5.78)-(5.80). The same type of channel, and the same type of boundary and initial conditions, are used as for the prismatic channel computations for a high dam, with the same upstream-to-downstream depth ratio of 100/1, width of 50 m, and a Manning roughness coefficient of 0.04. A higher downstream depth of 3 m is now chosen to avoid using a very dense spatial grid, since a larger number of spatial steps is required to obtain a stable solution for a shallow depth of

1 m in the transition. A dam height of 300 m is chosen to retain the same upstream-to-downstream depth ratio of 100/1. The bottom slope in the reservoir is the same as before, i.e. 0.1 %; then follows a horizontal reach between the dam section and section 61 (located 10 km downstream of the dam), then a sudden drop in the bottom elevation, with a slope of 4.0 %, occurs between sections 61 and 62 (1 km apart), and the rest of the channel is almost horizontal with a slope of 0.03 %.

A comparison between the PPM and linear Godunov methods in shown in Figs.(5.77) and (5.78), while the Lax-Wendroff method is compared with the PPM Godunov in Fig.(5.80). The results in general agree well, though noticeable oscillations are present for the Lax-Wendroff method, in particular for the first stage of the flood (see Fig.5.80). The solution reflects the physical phenomenon: after the surge has passed the steep transition and reached the mild-slope zone, the backwater effect produces a wave in the upstream direction (similarly to the effect of a sudden constriction).

Again, the time step required for a successful run with the Lax-Wendroff method is ten times smaller than the appropriate time step for the Godunov method.

In all examined cases the shock-modifying procedure for the PPM interpolation, which is explained in Appendix A,

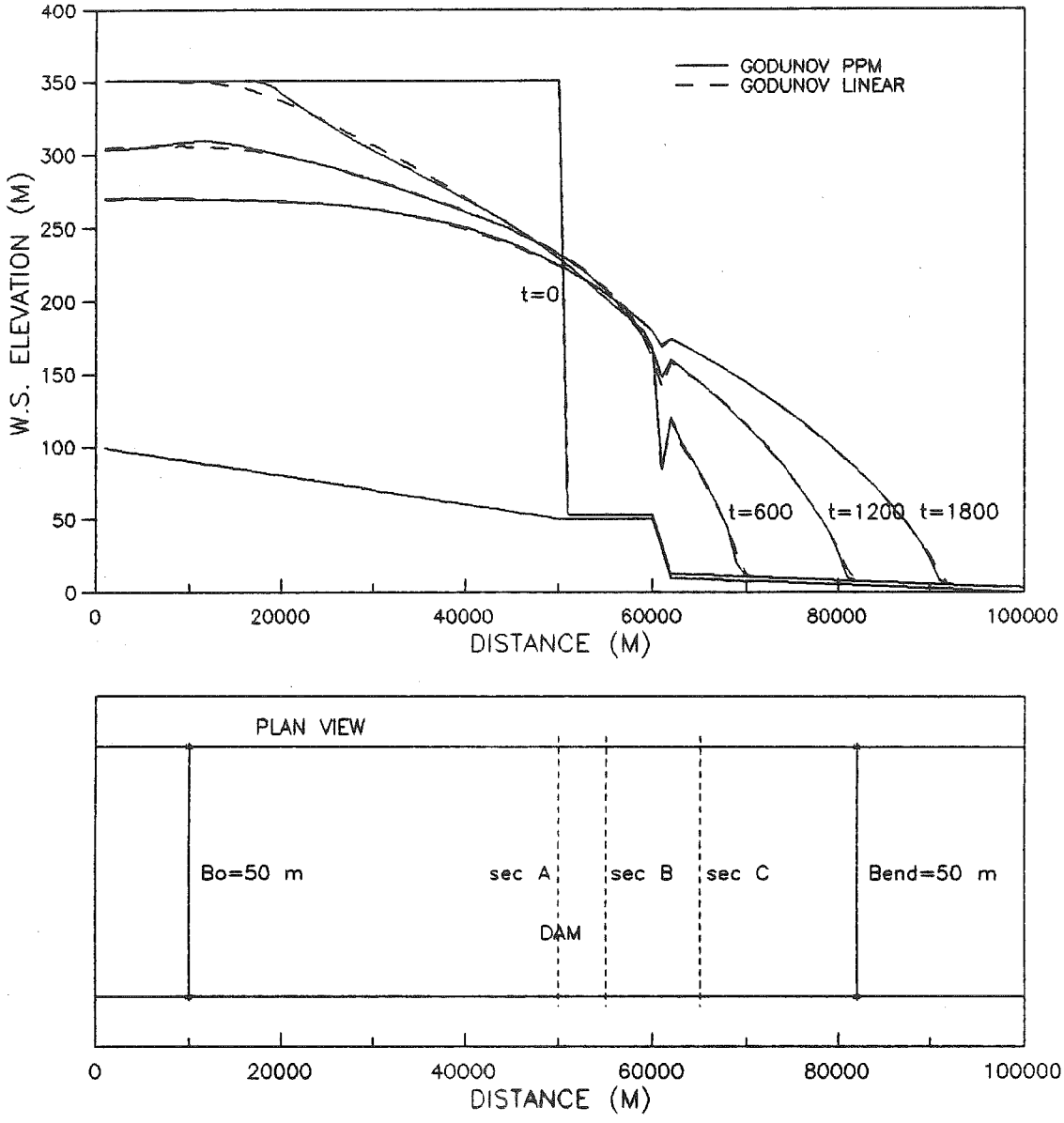

Figure 5.78 Time evolution of water-surface profiles for high-dam dambreak in a prismatic channel of large roughness with variable bottom slope; comparison between the PPM Godunov and linear Godunov methods

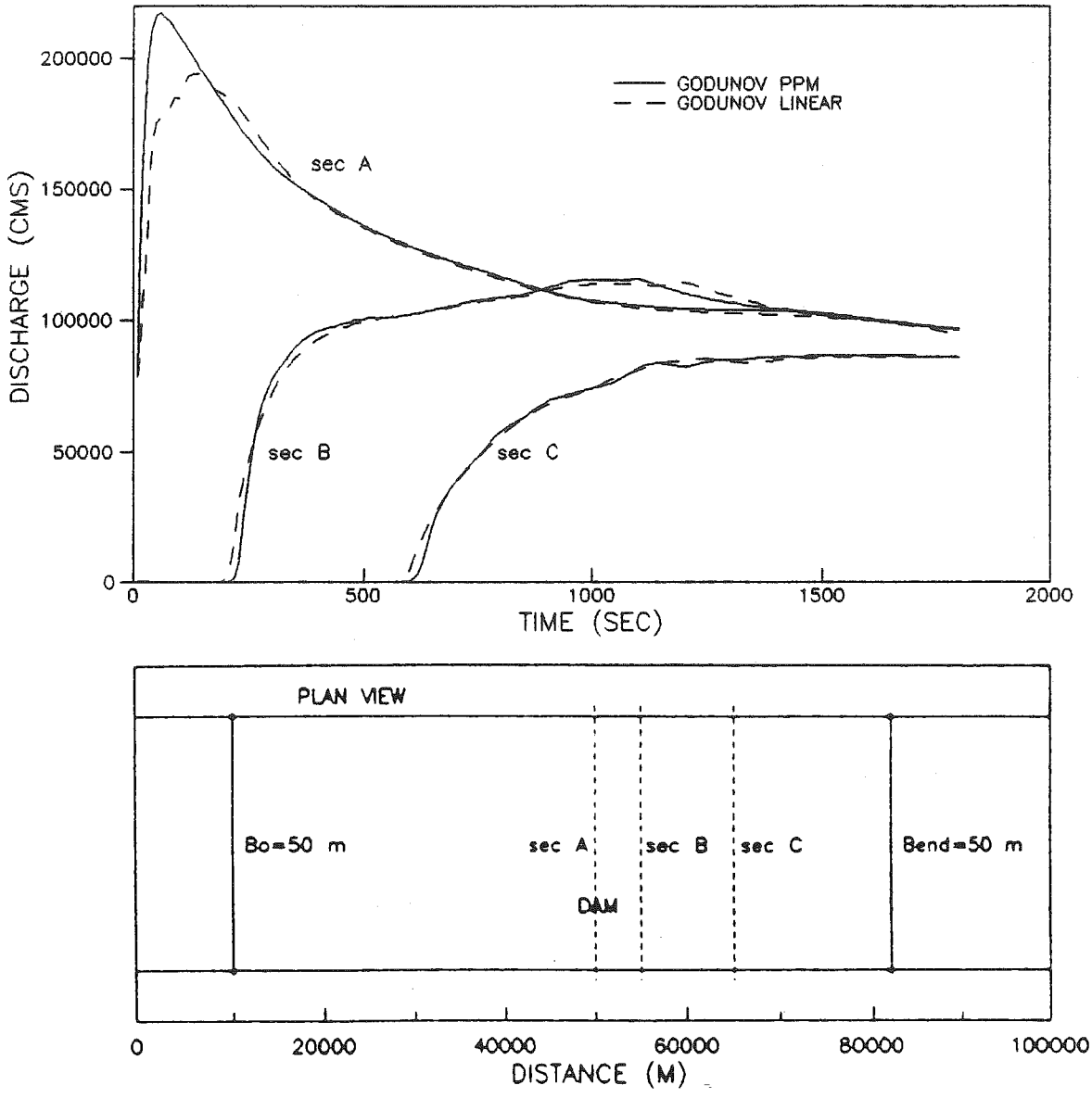

Figure 5.79 Discharge hydrographs for high-dam dambreak in a prismatic channel of large roughness with variable bottom slope; comparison between the PPM Godunov and linear Godunov methods

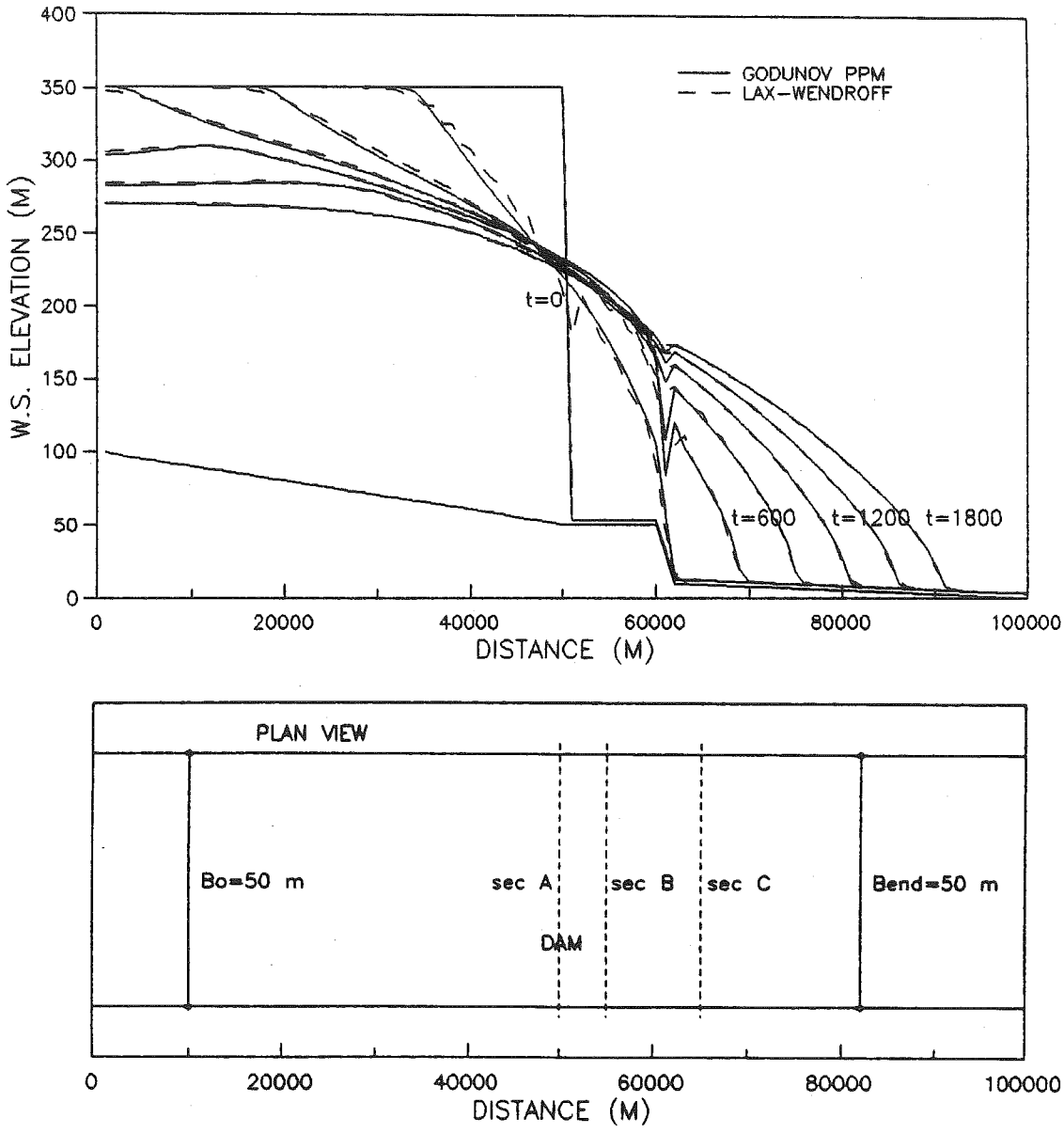

Figure 5.80 Time evolution of water-surface profiles for high-dam dambreak in a prismatic channel of large roughness with variable bottom slope; comparison between the PPM Godunov and Lax-Wendroff methods

does not contribute much to the quality of the results. The resolution of the front can be only marginally improved, and determination of the necessary coefficients is a cumbersome task (in particular for nonprismatic channels), involving many trials and experience, which seriously jeopardizes the robustness and practical utility of the scheme. Consequently, use of the shock-modifying procedure is not recommended.

V.5 General remarks

This chapter closes with some general comments in an attempt to summarize the presented tests and present a clear picture of the advantages and disadvantages of the examined methods, in particular the Godunov methods.

In general, the Godunov method (actually both the PPM and the linear methods) show significantly better performance, compared to the Preissmann, Lax-Wendroff and MacCormack methods, for the computation of instantaneous dambreaks. The Godunov method can successfully compute mixed-flow regimes for both frictionless and frictional channels, whereas the Preissmann method fails whenever a mixed regime occurs, and the Lax-Wendroff method requires much smaller time steps for those few cases it can deal with. The shock-fitting method of characteristics is primarily used for the steep front resolution comparison,

since the complications in detecting and tracking reflected discontinuities makes the method almost hopelessly complicated for any practical application. In addition, very large mass-conservation errors result for the shock-fitting method, attributable to the linear interpolation, rendering it inferior to the Godunov methods, for which the conservation error is negligible.

Comparisons with the shock-fitting method show that the resolution of the front for the Godunov PPM method, for all the examined cases, stays within one spatial step, i.e. there is practically no smearing of the front. The linear Godunov method produces more smearing, due to numerical diffusion (which comes from the linear interpolation), confining the wave front to, on the average, three spatial steps. Nevertheless, it is observed that for the case of higher roughness, appropriate for natural rivers, the steep front is gradually smoothed out by resistance effects, which somewhat weakens the advantages of the PPM method's sharp front resolution. On the other hand the linear method is less susceptible to numerical oscillations. A more thorough evaluation of the two Godunov methods is presented in chapter VII.

The average relative computational times for the schemes (with the same time and spatial steps), related to the linear Godunov method, are:

Godunov PPM 1.03

Godunov linear 1.00

Preissmann (3 iterations) 1.82

Lax-Wendroff 0.47

Shock-fitting characteristics ... 0.72.

Although the Lax-Wendroff method has the lowest computational time per time step, one has to keep in mind that for most of the computations presented, it required much smaller time steps than the Godunov method to obtain a stable solution. The implicit Preissmann scheme cannot use its potential of a (theoretically) unlimited time step, since the resulting smearing compromises the solution (see Figs.5.24, and also Fennema and Chaudhry, 1986). In this light, if the shock-fitting method is disregarded due to its complexity, the Godunov method has a computational time advantage over the other methods considered.

The main problem observed here for the Godunov method, is the need to interpolate additional cross-sections between sections where severe expansion occurs.

CHAPTER VI. TOWARDS GENERALIZATION TO TWO DIMENSIONS

In this chapter some ideas and guidance for applying the modified Godunov scheme to the two-dimensional open channel flow equations are presented. There is a definite need for a two-dimensional approach to the dam-break problem. The sudden expansion of a narrow canyon into a wide valley, and the case of a partial (but instantaneous) dam breach, are not properly represented by a one-dimensional model. Immediately below a channel expansion the flow is not always confined by the valley boundaries (walls), but rather can remain jetlike before filling the entire cross-section further downstream. In addition to this inadequacy in a one-dimensional physical description of the phenomenon, difficulties also occur in application of numerical methods to the one-dimensional equations for severely abrupt expansions, as shown in chapter V.

Despite these weaknesses of one-dimensional methods, two-dimensional methods, though investigated and developed for hypothetical cases (see for example Katopodes and Strelkoff, 1978; Fennema and Chaudhry, 1990), are still not widely used for practical dam-break problems. The reasons include requirements for large computer storage and much

more computer time than needed for one-dimensional methods; more complicated algorithms; and delicate treatment of boundary conditions. It is perhaps not possible to avoid these sorts of problems with the Godunov algorithm; but it may be possible to obtain a two-dimensional method which may retain the advantages of the one-dimensional implementation: capability to work with mixed flow regimes, and to deal with very strong shocks and preserve good resolution of the front. The goal is also to avoid the difficulties of the one-dimensional method produced by the nonprismatic term for the case of a severe expansion.

The purpose of the this chapter is not to provide a complete algorithm for the two-dimensional dam-break method, but rather to outline a procedure for potential application of the Godunov PPM (and linear) methods to the two-dimensional open-channel flow equations. First the two-dimensional flow equations are revisited. Then the Godunov conservation step is presented as two-dimensional extension of the one-dimensional method, developed in detail in chapter IV. Finally, some ideas for the flux-approximation procedure are presented.

VI.1 Proposed numerical implementation

The numerical implementation of the Godunov method to the two-dimensional flow equations should not be considered as a direct generalization of the one-dimensional algorithm. The ideas remain the same, but the implementation becomes more delicate, particularly for the computation of the time-averaged fluxes in the predictor step, since now the method of characteristics becomes the so-called method of bicharacteristics, where the trajectories are conoides instead of the simple lines of the one-dimensional approach.

The two-dimensional open-channel flow equations are presented in chapter II, and are rewritten here for convenience.

The continuity equation is:

$$(2.8): \quad \frac{\partial h}{\partial t} + \frac{\partial}{\partial x}(uh) + \frac{\partial}{\partial y}(vh) = 0,$$

the momentum equation in the x-direction is:

$$(2.9): \quad \frac{\partial (uh)}{\partial t} + \frac{\partial}{\partial x}(u^2 h) + \frac{\partial}{\partial y}(vuh) + \frac{\partial}{\partial x}\left(\frac{h^2}{2}\right) = gh(S_{ox} - S_{fx}),$$

and the momentum equation in the y-direction is:

$$(2.10): \quad \frac{\partial (vh)}{\partial t} + \frac{\partial}{\partial x}(uvh) + \frac{\partial}{\partial y}(v^2 h) + \frac{\partial}{\partial y}\left(\frac{h^2}{2}\right) = gh(S_{oy} - S_{fy}),$$

where the friction slopes S_{fx} and S_{fy} are expressed as:

$$(2.10a): \quad S_{fx} = n^2 \frac{u\sqrt{u^2+v^2}}{h^{4/3}}, \text{ and } S_{fy} = n^2 \frac{v\sqrt{u^2+v^2}}{h^{4/3}}.$$

The matrix form of the Eqs.(2.8)-(2.10) is:

$$(2.11): \quad \frac{\partial U}{\partial t} + \frac{\partial}{\partial x}[F(u)] + \frac{\partial}{\partial y}[G(U)] = H(U, x, y, t),$$

In the conservative step Eq.(2.11) is integrated between the times t^n and t^{n+1}, and spatial positions $X_{j+½}$ and $X_{j-½}$, and $Y_{i+½}$ and $Y_{i-½}$ (see Fig.6.1), which yields:

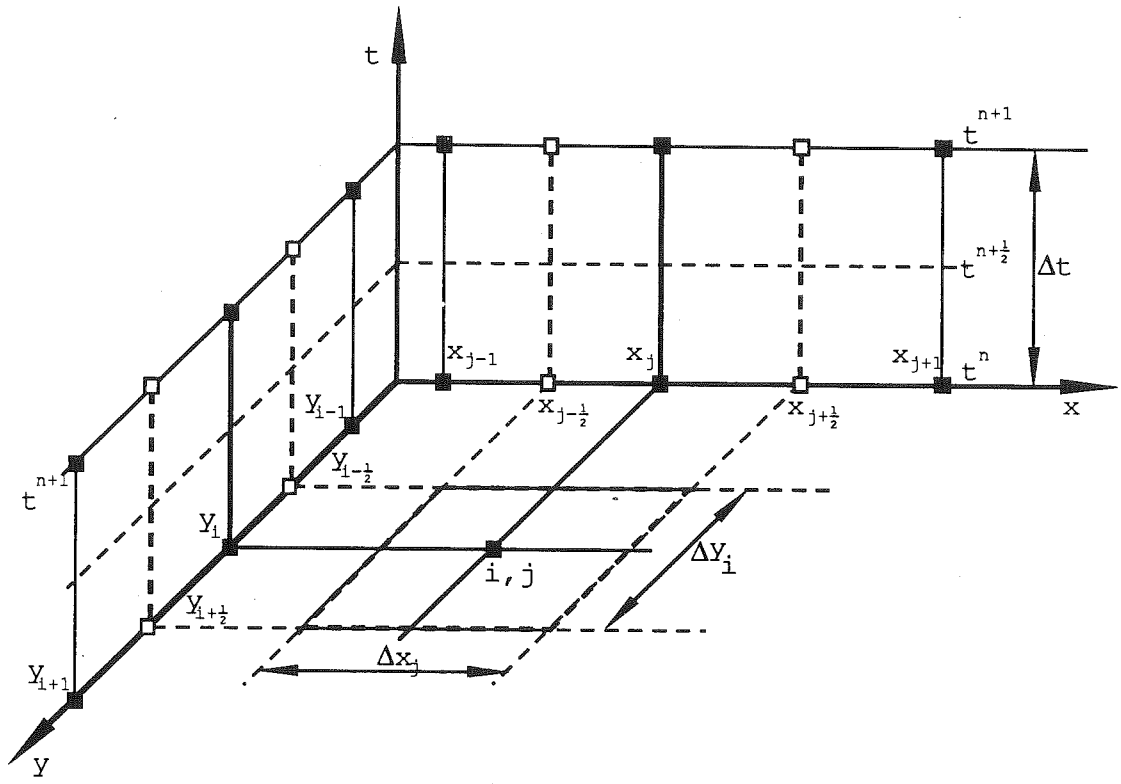

Figure 6.1 Definition sketch for the two-dimensional Godunov method

$$(6.1): \quad \langle U\rangle_{j,i}^{n+1} = \langle U\rangle_{j,i}^{n} -$$

$$- \frac{1}{\Delta x_j \Delta y_i} \int_{t^n}^{t^{n+1}} \int_{y_{i-\frac{1}{2}}}^{y_{i+\frac{1}{2}}} \{F[U(x_{j+\frac{1}{2}}, y, t)] - F[U(x_{j-\frac{1}{2}}, y, t)]\} dy\, dt -$$

$$- \frac{1}{\Delta x_j \Delta y_i} \int_{t^n}^{t^{n+1}} \int_{x_{j-\frac{1}{2}}}^{x_{j+\frac{1}{2}}} \{G[U(x, y_{i+\frac{1}{2}}, t)] - G[U(x, y_{i-\frac{1}{2}}, t)]\} dx\, dt +$$

$$+ \frac{1}{\Delta x_j \Delta y_i} \int_{t^n}^{t^{n+1}} \int_{x_{j-\frac{1}{2}}}^{x_{j+\frac{1}{2}}} \int_{y_{i-\frac{1}{2}}}^{y_{i+\frac{1}{2}}} H(x, y, t)\, dy\, dx\, dt,$$

where the spatial average $\langle U\rangle_{j,i}^{n}$ is defined as:

$$(6.2): \quad \langle U\rangle_{j,i}^{n} = \frac{1}{\Delta x_j \Delta y_i} \int_{x_{j-\frac{1}{2}}}^{x_{j+\frac{1}{2}}} \int_{y_{i-\frac{1}{2}}}^{y_{i+\frac{1}{2}}} U(x, y, t^n)\, dy\, dx.$$

As in the case of one-dimensional equations, the following notation is introduced:

$$(6.3): \quad \langle U\rangle_{j,i}^{n+1} = \langle U\rangle_{j,i}^{n} - \frac{\Delta t}{\Delta x_j} (\overline{F}_{j+\frac{1}{2},i}^{n+\frac{1}{2}} - \overline{F}_{j-\frac{1}{2},i}^{n+\frac{1}{2}}) -$$

$$- \frac{\Delta t}{\Delta y_i} (\overline{G}_{j,i+\frac{1}{2}}^{n+\frac{1}{2}} - \overline{G}_{j,i-\frac{1}{2}}^{n+\frac{1}{2}}) + \Delta t \overline{H}_{j,i}^{n+\frac{1}{2}}$$

where the time-averaged fluxes $\overline{F}_{j\pm\frac{1}{2},i}^{n+\frac{1}{2}}$, $\overline{G}_{j,i\pm\frac{1}{2}}^{n+\frac{1}{2}}$ and the source

term $\overline{H}^{n+1/2}_{j,i}$ are defined as:

$$(6.4): \quad \overline{F}^{n+1/2}_{j+1/2,i} = \frac{1}{\Delta t \Delta y_i} \int_{t^n}^{t^{n+1}} \int_{y_{i-1/2}}^{y_{i+1/2}} F[U(x_{j+1/2}, y, t)\, dy dt,$$

$$(6.5): \quad \overline{G}^{n+1/2}_{j,i+1/2} = \frac{1}{\Delta t \Delta x_j} \int_{t^n}^{t^{n+1}} \int_{x_{j-1/2}}^{x_{j+1/2}} G[U(x, y_{i+1/2}, t)\, dx dt,$$

$$(6.6): \quad \overline{H}^{n+1/2}_{j,i} = \frac{1}{\Delta t \Delta x_j \Delta y_i} \int_{t^n}^{t^{n+1}} \int_{x_{j-1/2}}^{x_{j+1/2}} \int_{y_{i-1/2}}^{y_{i+1/2}} H(x, y, t)\, dy dx dt,$$

and similarly for the rest of the flux terms.

Approximation of the time-averaged fluxes and the source term, which comprises the predictor step, is the most delicate portion of the method. The proposition, based on experience from the one-dimensional case (see chapter IV), is first to obtain the time-averaged approximation of the dependent variable vector U, and then to compute the time-averaged flux as:

(6.7): $\overline{F}^{n+\frac{1}{2}}_{j+\frac{1}{2},i} = F(\overline{U}^{n+\frac{1}{2}}_{j+\frac{1}{2},i})$,

rather than averaging the fluxes themselves. With such an approximation the conservative (Godunov) step Eq.(6.3) can be rewritten in scalar form as:

$$(6.8): \quad \langle h\rangle^{n+1}_{j,i} = \langle h\rangle^{n}_{j,i} - \frac{\Delta t}{\Delta x_j}\left[(\overline{uh})^{n+\frac{1}{2}}_{j+\frac{1}{2},i} - (\overline{uh})^{n+\frac{1}{2}}_{j-\frac{1}{2},i}\right] - \left[(\overline{vh})^{n+\frac{1}{2}}_{j,i+\frac{1}{2}} - (\overline{vh})^{n+\frac{1}{2}}_{j,i-\frac{1}{2}}\right]$$

for the continuity equation;

$$(6.9): \quad \langle uh\rangle^{n+1}_{j,i} = \langle uh\rangle^{n}_{j,i} - \frac{\Delta t}{\Delta x_j}\left[(\overline{u^2h+g\frac{h^2}{2}})^{n+\frac{1}{2}}_{j+\frac{1}{2},i} - (\overline{u^2h+g\frac{h^2}{2}})^{n+\frac{1}{2}}_{j-\frac{1}{2},i}\right] - \left[(\overline{uvh})^{n+\frac{1}{2}}_{j,i+\frac{1}{2}} - (\overline{uvh})^{n+\frac{1}{2}}_{j,i-\frac{1}{2}}\right]' + g\Delta t\,\overline{h}^{n+\frac{1}{2}}_{j,i}\left(\frac{Z_{j-\frac{1}{2},i}-Z_{j+\frac{1}{2},i}}{\Delta x_j} - n^2\frac{\overline{u}^{n+\frac{1}{2}}_{j,i}\sqrt{(\overline{u}^{n+\frac{1}{2}}_{j,i})^2+(\overline{v}^{n+\frac{1}{2}}_{j,i})^2}}{(\overline{h}^{n+\frac{1}{2}}_{j,i})^{4/3}}\right),$$

for the X-momentum equation; and

$$(6.10): \quad \langle vh \rangle_{j,i}^{n+1} = \langle vh \rangle_{j,i}^{n} - \frac{\Delta t}{\Delta x_j}\left[(\overline{uvh})_{j+\frac{1}{2},i}^{n+\frac{1}{2}} - (\overline{uvh})_{j-\frac{1}{2},i}^{n+\frac{1}{2}} \right] -$$

$$- \left[(\overline{v^2 h + g\frac{h^2}{2}})_{j,i+\frac{1}{2}}^{n+\frac{1}{2}} - (\overline{v^2 h + g\frac{h^2}{2}})_{j,i-\frac{1}{2}}^{n+\frac{1}{2}} \right] +$$

$$+ g \Delta t \; \overline{h}_{j,i}^{n+\frac{1}{2}} \left(\frac{Z_{j,i-\frac{1}{2}} - Z_{j,i+\frac{1}{2}}}{\Delta y_i} - n^2 \frac{\overline{v}_{j,i}^{n+\frac{1}{2}} \sqrt{(\overline{u}_{j,i}^{n+\frac{1}{2}})^2 + (\overline{v}_{j,i}^{n+\frac{1}{2}})^2}}{(\overline{h}_{j,i}^{n+\frac{1}{2}})^{4/3}} \right)$$

for the Y-momentum equation, where:

$$(6.11): \quad \begin{cases} \overline{h}_{j,i}^{n+\frac{1}{2}} = \frac{1}{4} (\overline{h}_{j+\frac{1}{2},i}^{n+\frac{1}{2}} + \overline{h}_{j-\frac{1}{2},i}^{n+\frac{1}{2}} + \overline{h}_{j,i+\frac{1}{2}}^{n+\frac{1}{2}} + \overline{h}_{j,i-\frac{1}{2}}^{n+\frac{1}{2}}) \\ \overline{u}_{j,i}^{n+\frac{1}{2}} = \frac{1}{4} (\overline{u}_{j+\frac{1}{2},i}^{n+\frac{1}{2}} + \overline{u}_{j-\frac{1}{2},i}^{n+\frac{1}{2}} + \overline{u}_{j,i+\frac{1}{2}}^{n+\frac{1}{2}} + \overline{u}_{j,i-\frac{1}{2}}^{n+\frac{1}{2}}) \\ \overline{v}_{j,i}^{n+\frac{1}{2}} = \frac{1}{4} (\overline{v}_{j+\frac{1}{2},i}^{n+\frac{1}{2}} + \overline{v}_{j-\frac{1}{2},i}^{n+\frac{1}{2}} + \overline{v}_{j,i+\frac{1}{2}}^{n+\frac{1}{2}} + \overline{v}_{j,i-\frac{1}{2}}^{n+\frac{1}{2}}) \end{cases}$$

The spatially averaged velocities $\langle u \rangle_{j,i}^{n+1}$ and $\langle v \rangle_{j,i}^{n+1}$ are then computed from:

$$(6.12): \quad \langle u \rangle_{j,i}^{n+1} = \frac{\langle uh \rangle_{j,i}^{n+1}}{\langle h \rangle_{j,i}^{n+1}},$$

$$(6.13): \quad \langle v \rangle_{j,i}^{n+1} = \frac{\langle vh \rangle_{j,i}^{n+1}}{\langle h \rangle_{j,i}^{n+1}}.$$

Now the problem of approximation of the time-averaged vectors $\bar{U}^{n+\frac{1}{2}}_{j\pm\frac{1}{2},i}$ and $\bar{U}^{n+\frac{1}{2}}_{j,i\pm\frac{1}{2}}$ must be dealt with. A suggestion based on the one-dimensional case is to adopt the values of $U^{n+\frac{1}{2}}_{j\pm\frac{1}{2},i}$ and $U^{n+\frac{1}{2}}_{j,i\pm\frac{1}{2}}$, computed at the mid-time $t^{n+\frac{1}{2}}$ by the method of characteristics, for the time-averaged vectors $\bar{U}^{n+\frac{1}{2}}_{j\pm\frac{1}{2},i}$ and $\bar{U}^{n+\frac{1}{2}}_{j,i\pm\frac{1}{2}}$. The algorithm for computing the mid-time vectors $U^{n+\frac{1}{2}}_{j\pm\frac{1}{2},i}$ and $U^{n+\frac{1}{2}}_{j,i\pm\frac{1}{2}}$ should be able to deal with continuous and discontinuous problems, though it is suggested, based on experience with the one-dimensional method, that for initial investigations only continuous cases should be considered.

For obtaining the mid-time vectors $U^{n+\frac{1}{2}}_{j\pm\frac{1}{2},i}$ and $U^{n+\frac{1}{2}}_{j,i\pm\frac{1}{2}}$, two characteristics approaches for two dimension can be used. One approach is to use the so-called bicharacteristics method (see Courant and Hilbert, 1937), applied to dam-break flows by Katopodes and Strelkoff, 1978. The other approach, which is suggested for initial research, is to us the split-operator algorithm applied by Benque et al.,(1982) to tidal flows. In addition to offering significant computational simplifications compared to the bicharacteristics approach, the latter approach can be relatively easily adjusted to deal with the dry-bed problem, which is an essential

capability for practical application of any two-dimensional methods (as explained in chapter II).

Some preliminary explanations of the split-operator method are now presented; for the details needed for future investigations, one should refer to Benque et al.,(1982).

The method originally consisted of three steps: advection, diffusion and propagation. Although momentum diffusion is important for accurate modeling of momentum-transfer processes, it may be omitted for the initial investigation for the sake of simplicity; therefore only two steps will be considered, namely: the advection step, where inertial terms of the momentum equations are treated, and the propagation step, where the continuity equation and the remaining terms of the momentum equations are dealt with.

In the advection step the inertial terms (defined in chapter II as the terms describing the advective transfer and accumulation of momentum) of Eqs.(2.9) and (2.10) are treated separately as:

$$(6.14): \qquad \frac{\partial(uh)}{\partial t} + \frac{\partial}{\partial x}(u^2h) + \frac{\partial}{\partial y}(vuh) = 0,$$

$$(6.15): \qquad \frac{\partial(vh)}{\partial t} + \frac{\partial}{\partial x}(uvh) + \frac{\partial}{\partial y}(v^2h) = 0.$$

After extracting the continuity Eq.(2.8), one can cast Eqs.(6.14) and (6.15) into the characteristic form:

(6.16): $$\frac{\partial u}{\partial t} + u\frac{\partial u}{\partial x} + v\frac{\partial u}{\partial y} = 0$$

(6.17): $$\frac{\partial v}{\partial t} + u\frac{\partial v}{\partial x} + v\frac{\partial v}{\partial y} = 0,$$

which can be rewritten as total derivatives in the velocity components u and v:

(6.18): $$\frac{Du}{Dt} = 0,$$

(6.19): $$\frac{Dv}{Dt} = 0,$$

along the path:

(6.20): $$u = \frac{dx}{dt} \text{ and } v = \frac{dy}{dt}.$$

Equations (6.18), (6.19) and (6.20) state that along the path AB (see Fig.6.2) there is no change in either of the velocity components (u and v) between the two time levels t^n and t^{n+1}. The task is to obtain the foot of the trajectory (Eq.6.20), point B, at which $u_B = u_A$, and $v_B = v_A$. This is accomplished through an iteration procedure, and involves interpolation of velocity values from the previous time step t_n. The velocities obtained during the advection step are denoted as u_a^{n+1} and v_a^{n+1}.

In the propagation step the flow Eqs.(2.8), (2.9) and (2.10) are solved without the advective inertial terms, since advection has been accounted for in the previous advection step. Accordingly, the "propagation" momentum equations are:

$$(6.21): \quad \frac{\partial(uh)}{\partial t} + \frac{\partial}{\partial x}\left(\frac{h^2}{2}\right) = gh\left(S_{ox} - n^2 \frac{u\sqrt{u^2+v^2}}{h^{4/3}}\right),,$$

in the x-direction and:

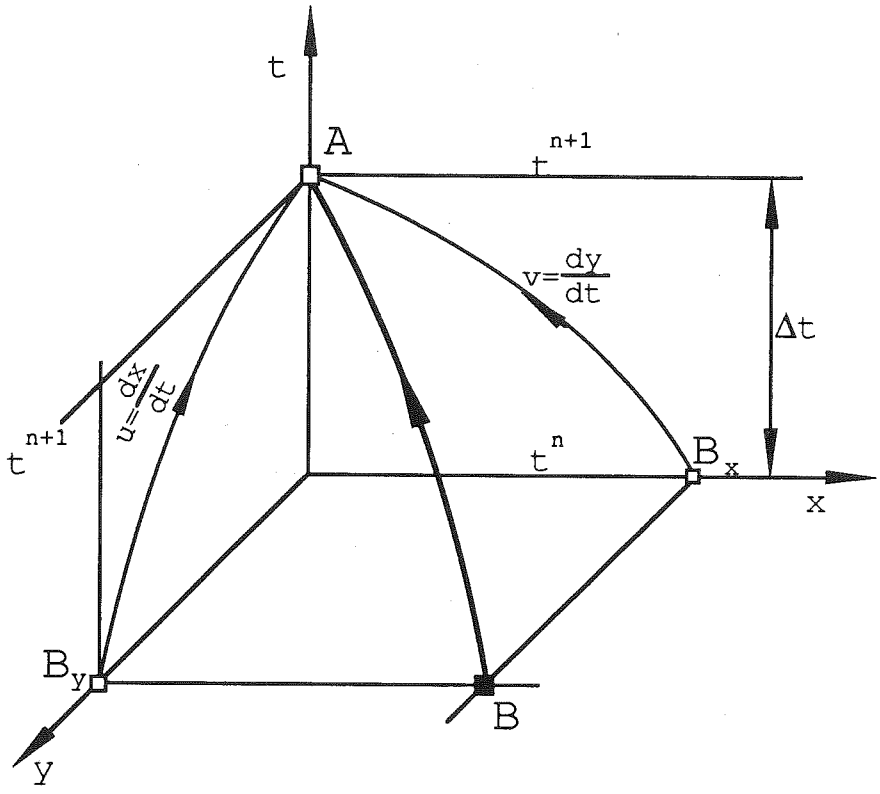

Figure 6.2 Definition sketch for the advection step in the flux computation

$$(6.22): \quad \frac{\partial (vh)}{\partial t} + \frac{\partial}{\partial y}\left(\frac{h^2}{2}\right) = gh\left(S_{oy} - n^2 \frac{v\sqrt{u^2+v^2}}{h^{4/3}}\right),,$$

in the y-direction, while the continuity equation remains as before (Eq.2.8). Equations (6.21), (6.22) and (2.8) are then approximated as:

$$(6.23): \quad \frac{h^{n+1} - h^n}{\Delta t} + \alpha\left[\frac{\partial}{\partial x}(uh)^{n+1} + \frac{\partial}{\partial y}(vh)^{n+1}\right] + \\ + (1-\alpha)\left[\frac{\partial}{\partial x}(uh)^n + \frac{\partial}{\partial y}(vh)^n\right] = 0$$

for continuity;

$$(6.24): \quad \frac{(uh)^{n+1} - (uh)_a^n}{\Delta t} + g\left[\alpha \frac{\partial}{\partial x}\left(\frac{h^2}{2}\right)^{n+1} + (1-\alpha)\frac{\partial}{\partial x}\left(\frac{h^2}{2}\right)^n\right] + \\ + g\left[\alpha n^2 \left(\frac{(uh)\sqrt{(uh)^2+(vh)^2}}{h^{7/3}}\right)^{n+1} + \right. \\ \left. + (1-\alpha) n^2 \left(\frac{(uh)\sqrt{(uh)^2+(vh)^2}}{h^{7/3}}\right)_a^{n+1}\right] = \\ = g S_{ox}\left[\alpha h^{n+1} + (1-\alpha) h^n\right]$$

for the x-momentum; and

$$(6.25): \quad \frac{(vh)^{n+1}-(vh)_a^n}{\Delta t} + g\left[\alpha \frac{\partial}{\partial y}\left(\frac{h^2}{2}\right)^{n+1} + (1-\alpha)\frac{\partial}{\partial y}\left(\frac{h^2}{2}\right)^{n}\right] +$$

$$+g\left[\alpha n^2\left(\frac{(vh)\sqrt{(uh)^2+(vh)^2}}{h^{7/3}}\right)^{n+1} +\right.$$

$$\left. + (1-\alpha) n^2\left(\frac{(vh)\sqrt{(uh)^2+(vh)^2}}{h^{7/3}}\right)_a^{n+1}\right] =$$

$$= g S_{oy}\left[\alpha h^{n+1} + (1-\alpha) h^n\right]$$

for the y-momentum, where the subscript "a" designates the value obtained in the advection step, and α is a time-weighting coefficient less then unity (superscripts "n" and "n+1" denote consecutive time levels). For convenience the unit discharges (uh) and (vh) are treated as dependent variables in the propagation step, instead of the velocities u and v (see Benque et al., 1982).

The terms of Eqs.(6.24) and (6.25) which involve unit discharges at time t^{n+1}, are then linearized around the values known from the advection step, using a Taylor series expansion:

$$(6.26): \quad \frac{(uh)^{n+1} - (uh)_a^{n+1}}{\Delta t} + g\left[\alpha \frac{\partial}{\partial x}\left(\frac{h^2}{2}\right)^{n+1} + (1-\alpha)\frac{\partial}{\partial x}\left(\frac{h^2}{2}\right)^{n}\right] +$$

$$+gn^2\left[\left(\frac{(uh)\sqrt{(uh)^2+(vh)^2}}{h^{7/3}}\right)_a^{n+1} +\right.$$

$$+\alpha\frac{\partial}{\partial h}\left(\frac{(uh)\sqrt{(uh)^2+(vh)^2}}{h^{7/3}}\right)_a^{n+1}\Delta h +$$

$$\left.+\alpha\frac{\partial}{\partial (uh)}\left(\frac{(uh)\sqrt{(uh)^2+(vh)^2}}{h^{7/3}}\right)_a^{n+1}[(uh)^{n+1} - (uh)_a^{n+1}]\right] =$$

$$= gS_{ox}[\alpha h^{n+1} + (1-\alpha)h^n],$$

for the x-momentum equation; and

$$(6.27): \quad \frac{(vh)^{n+1} - (vh)_a^{n+1}}{\Delta t} + g\left[\alpha \frac{\partial}{\partial y}\left(\frac{h^2}{2}\right)^{n+1} + (1-\alpha)\frac{\partial}{\partial y}\left(\frac{h^2}{2}\right)^{n}\right] +$$

$$+gn^2\left[\left(\frac{(uh)\sqrt{(vh)^2+(vh)^2}}{h^{7/3}}\right)_a^{n+1} +\right.$$

$$+\alpha\frac{\partial}{\partial h}\left(\frac{(vh)\sqrt{(uh)^2+(vh)^2}}{h^{7/3}}\right)_a^{n+1}\Delta h +$$

$$\left.+\alpha\frac{\partial}{\partial (vh)}\left(\frac{(vh)\sqrt{(uh)^2+(vh)^2}}{h^{7/3}}\right)_a^{n+1}[(vh)^{n+1} - (vh)_a^{n+1}]\right] =$$

$$= gS_{oy}[\alpha h^{n+1} + (1-\alpha)h^n],$$

for the y-momentum equation. Expressions for the unknown unit discharges $(uh)^{n+1}$ and $(vh)^{n+1}$ are then obtained from Eqs.(6.26) and (6.27) and substituted into the continuity Eq.(6.23), which is linearized and solved for the remaining unknown h^{n+1} . Finally, the unit discharges are computed from Eqs.(6.26) and (6.27).

Whichever algorithm is used in a predictor step (Benque's operator-splitting, or Katopodes-Strelkoff's bicharacteristics), one has to recover the continuous functions U(x,y,t) from the spatial averages $\langle U \rangle_{j,i}$ obtained as the result of the conservative step (Eq.6.3). To this end the linear or the PPM (piecewise parabolic) interpolation procedure may be used. The PPM procedure is more elaborate to develop and implement, and in addition requires an auxiliary method at the points where there is not enough information to apply the PPM interpolation (so called close-to-the-boundary points, explained in section IV.4). On the other hand the PPM method proved to give somewhat better performance than the linear one for the one-dimensional case; and it is strongly recommended by both Benque et al., and Katopodes and Strelkoff, to use parabolic interpolation in order to avoid the numerical diffusion which would result from linear interpolation. The final decision on the type of interpolation should be made in the

course of development of the method for the two-dimensional case. Again, for the beginning of the investigation, it is suggested to adopt the simpler linear method.

For the discontinuous case one first needs to detect the discontinuity, which should be obtained by a procedure similar to those used for the one-dimensional flow equations and described in section IV.3.2. It must be anticipated that discontinuities can appear in both spatial directions, since lateral surges can result from abrupt changes in geometry. For the computation of the discontinuities themselves the Riemann solver used for the one-dimensional method must be extended to the momentum equation in the Y-direction (the direction, normal to the main flow). The domains of dependence, needed to provide the initial stages for the Riemann problem (see chapter IV), are to be computed using the split-operator method (explained above) for each side of the discontinuity.

It is re-emphasized that the material presented in this chapter is guidance towards development of a two-dimensional method - not the complete algorithm; considerable research may be required to obtain a final algorithm capable of producing reliable results. Particular attention must be paid to the part of the algorithm which approximates the time-averaged fluxes, and to the development of the boundary conditions. Some completely new ideas may be required (e.g.

the fluxes for the discontinuous solution), but first the old ones should be thoroughly investigated.

CHAPTER VII. SUMMARY AND CONCLUSIONS

The primary goal of the present work was to analyze and assess the possibility of application of the modified Godunov method to discontinuous one-dimensional open-channel flow problems, and thus provide a basis for potential industrial applications. The secondary goal was to lay the foundations for further generalization of the Godunov method for two-dimensional open-channel flow problems.

The need for this work, explained in detail in chapter II, comes from the lack of reliable numerical tools for computation of open-channel flows with strong shocks, in particular those associated with instantaneous dambreaks. Presently available and commonly used numerical methods for dam-break computations are reviewed and evaluated in chapter II, as are potentially new methods, all of them coming from gas dynamics. The Godunov method, modified first by Van Leer, and then refined by Colella and Woodward through their piecewise parabolic interpolation method (PPM), is chosen for further investigation because of its good performance, especially in mass-conservation and steep-front resolution.

In chapter III, the modified Godunov scheme is applied to the one-dimensional scalar equations (linear advection

and Burgers' equations) as test, or model equations, to get an insight into and experience with the behavior of the method, before generalization to the full open-channel flow equations. Tests of the explicit variant of the modified Godunov method for the scalar equations show good agreement with the analytical solution and the Holly-Preissmann method. Particularly good performance is observed for problems involving discontinuities. On the other hand, the implicit variant of the method suffers from excessive numerical diffusion and oscillations, and is accordingly abandoned. (In addition, since the time step must be limited for discontinuous flow computations in order to preserve the resolution and avoid smearing, the implicit scheme is deprived of its main advantage - a large time step.)

In chapters IV and V the de St. Venant one-dimensional equations are treated. New algorithms for two variants of the Godunov method are developed and presented in chapter IV (a detailed derivation is given for Colella and Woodward's PPM method, and the method based on linear interpolation is outlined).

In chapter V the tests intended to show the behavior of the Godunov methods (PPM and linear) and compare them with other commonly used methods for discontinuous open-channel flow computations are presented.

The tests have shown the superiority of the Godunov methods for computation of discontinuous open-channel flows (in particular dam-break flows) over the other compared methods. The Godunov methods are able to produce stable solutions for a much wider range of problems (i.e. wider ratio of upstream-to-downstream depths, channel roughness, etc.). An especially important feature is the capability of the Godunov methods to work successfully with so-called mixed flow regimes, where within the same reach both supercritical and subcritical flow occur. The "conventional" type of Preissmann method (i.e. the one using the double sweep algorithm) cannot deal with mixed flow regimes; a complete matrix inversion must be performed, thus significantly increasing the computational time. For very strong shocks (resulting from a large ratio of upstream-to-downstream depths, see Fig.5.2) the Lax-Wendroff and MacCormack methods require time steps several times smaller than those of the Godunov methods to achieve a stable solution. Even for such small time steps large spurious oscillations occur for the Lax-Wendroff and MacCormack methods, so that introduction of artificial viscosity (damping) is necessary to reduce them, and sometimes even to obtain a stable solution; however, for the discontinuous flows this diffusion produces an undesirable smearing of the front. Both Godunov methods (PPM and linear) produce a

stable solution for very strong socks without artificial damping and with large time steps, limited only by the Courant condition (i.e. the Courant number should be less than unity).

The Godunov methods are the only methods among those analyzed herein able to produce a stable solution for cases of frictionless dambreaks with mixed flow regimes. The results of these computations, in particular the results of the PPM Godunov method, agree very well with the analytical (Stoker's) solution. The front is confined within one computational step, insignificant smearing occurs for the rest of the flow, and the celerity (speed) error is small. Somewhat larger diffusion occurs for the linear method for frictionless flows, with more smearing of the front. However, when the realistic case of a frictional channel (in particular with higher roughness) is considered, the two Godunov methods produce more or less the same results, with slightly more smearing for the linear method, but with some spurious oscillations in discharges for the PPM method. Very good mass conservation is achieved with the Godunov methods, though for the test cases presented herein, only the shock-fitting method of characteristics suffered from a large mass-conservation error.

Concerning computational time, the Lax-Wendroff and MacCormack methods are the most efficient per time step, but

since they require much smaller time steps than the Godunov methods to produce a stable solution, the Godunov methods are still more economical. The computational time per time step for the Preissmann method is approximately two times larger than that of the Godunov methods. Since front resolution requires that the time step be kept small enough to maintain a Courant number close to unity, the Preissmann method cannot use its potentially large time step, and is therefore inferior to the Godunov methods with respect to computational time, as well. The computational times for the PPM and linear Godunov methods are almost the same, so neither of the two variants has an advantage in that respect. One could argue that the computational time is not an important issue in this era of powerful supercomputers; but in the engineering PC and work-station environment, CPU considerations are still relevant.

The disadvantages of the PPM Godunov method are an algorithm more complicated than for other explicit methods, requirements for using a staggered grid, and the problems involved with the boundaries. In particular, the points close to the boundaries must be computed by some other method (presumably the linear Godunov method) since there are not enough neighboring points to provide information for the PPM interpolation. The linear Godunov method does not suffer from this problem (i.e. it does not require an

auxiliary method for the close-to-the-boundary points), and is preferred over the PPM method in that one respect.

The only problem for both Godunov methods (PPM and linear) is observed for the case of an abrupt expansion of the channel width, where artificially steep water-surface profiles are produced upstream of the expansion reach (see Figs.5.43-5.46). To avoid this spurious steepening, one has to refine the spatial grid within the transitional reach, i.e. to introduce additional interpolated sections between the actual sections of an abrupt expansion. This reduction of spatial step also requires a reduction of the time step (to meet the stability requirements), and consequently increases the overall computational time.

An introduction to generalization of the Godunov method to two-dimensional open-channel flow problems is presented in chapter VI, providing a basis for further research in that direction.

For application of the Godunov methods (PPM and linear) to practical one-dimensional dam-break problems, one needs to introduce changes necessary to treat arbitrary cross-sectional geometry. Generalized internal and external boundary conditions (such as weirs, inundations, tributaries, localized energy loss, etc.) also must be provided.

Since neither of the two Godunov methods examined here

has a clear advantage over the other, both algorithms should be used as possible candidates for practical application in the initial stage of developing an industrial code (for example a single channel with particular boundary conditions).

More research should also be conducted to identify and investigate new ideas for improving the performance of the Godunov methods for the case of an abrupt expansion.

Finally, the need for a quantitative assessment and comparison of methods, acknowledged in section I.4, must be reiterated. Benchmarks (conventions) for defining the length of the steep front (and accordingly its wavespeed), and for measuring the agreement in flow variables (depths, discharges, wave-speeds, etc.) between two methods (or between a tested method and the analytical solution), based on a statistical approach, should be established and applied in comparative studies. However, the experience of this study suggests that it is not obvious that statistical measures such as root-mean square differences, algebraic differences, etc. would strengthen the qualitative comparisons used herein.

REFERENCES

Abbot,M.B.(1979), Computational Hydraulics; Elements of the Theory of Free Surface Flows, Pitman Publishing Limited, London.

Aknabi,A.A. and Katopodes,N.(1988),"Modes for Flood Propagation on Initially Dry Land", Journal of Hydraulic Engineering, Vol.114, No.7, July, pp 951-706.

Anderson,D.A., Tannehill,J.C. and Pletcher,R.H.(1984), Computational Fluid Mechanics and Heat Transfer, Hemisphere Publishing Corporation, New York.

Basco,D.R.(1989),"Limitations of de Saint Venant Equations in dam-break analysis", Journal of Hydraulic Engineering, Vol.115, No.7, July, pp 689-965.

Bell,J.B. Dawson,C.N. and Shubin,G.R.(1988),"An Unsplit, Higher Order Godunov Method for Scalar Conservation Laws in Multiple Dimensions" Journal of Computational Physics, Vol.74, pp 1-24.

Benque,J.P., Cunge,J.A., Feuillet,J., Hauguel,a. and Holly,F.M.Jr.(1982), "New Method for Tidal Current Computation", Journal of the Waterway, Port, Coastal and Ocean Division, Vol. 108, No. WW3, August, pp 396-417.

Burgers,J.M.(1948),"A mathematical model illustrating the theory of turbulence", Advances in Applied Mechanics, vol.1, pp 171-199.

Carnahan,B.,Luter,H.A. and Wilkes,J.O.(1969), Applied Numerical Methods, John Wiley & Sons.

Colella,P.,Concus P. and Sethian,J.(1983),"Some Numerical Methods for Discontinuous flows in Porous Media", The Mathematics of Reservoir simulation, edited by Ewing,R., SIAM, Philadelphia.

Colella,P. and Woodward,P.R.(1984),"The Piecewise Parabolic Method (PPM) for Gas-Dynamical Simulations", Journal of Computational Physics, Vol.54, pp 174-201.

Courant,R. and Friedrichs,K.O.(1948), Supersonic Flow and Shock Waves, Interscience Publishers, New York.

Courant,R. and Hilbert,D.(1937), Methods of Mathematical Physics, Volume II, John Wiley & Sons, New York.

Cunge,J.A.(1975),"Rapidly Varying Flow in Power and Pumping Canals", Chapter 14 of Unsteady Flow in Open Channels, Water Resources Publications, Fort Collins, Colorado.

Cunge,J.A.(1988),"Notes on possible application of Godunov-type algorithm to open channel flow and advection problems", IIHR unpublished report.

Cunge,J.A.,Holly,F.M,Jr,Verwey,A.(1980), Practical Aspects of Computational River Hydraulics, IIHR 1986 reprent.

Dressler,R.F.(1952),"Hydraulic resistance effect upon the dam-break functions", Journal of Research, National Bureau of Standards, Report 5768, pp 217-225.

Fennema,R.J. and Chaudhry,M.H.(1986),"Explicit numerical schemes for unsteady free-surface flows with shocks", Water Resources Research, Vol. 22, No. 13, pp 1923-1930, December.

Fennema,R.J. and Chaudhry,M.H.(1990),"Explicit methods for 2-D transient free-surface flows", Journal of Hydraulic Engineering, Vol.116, No.8, August, pp 1013-1034.

Fischer,H.B.,List,E.J.,Koh,R.C.Y.,Imberger,J.,Brooks,N.H.(1979), Mixing in Inland and Costal Waters, Academic Press, San Diego.

Fread,D.(1977),"The development and testing of a dam-break flood forecasting model", Proceedings of Dam-Break Flood Routing Model Workshop held in Bethesda, Maryland, October 18-20, U.S. Department of Commerce, National Technical Information Service PB-275 437.

Fryxell,B.A.,Woodward,P.R.,Colella,P and Winkler K.-H.(1986),"An Implicit-Explicit Hybrid Method for Lagrangian Hydrodynamics", Journal of Computational Physics No.63, pp 283-310.

Glaister,P.(1988a),"An Approximate Linearised Riemann Solver for the Euler Equations for Real Gases", Journal of Computational Physics No.74, pp 382-408.

Glaister,P.(1988b),"Approximate Riemann solutions of the shallow water equations", Journal of Hydraulic Research, Vol.26, No.3, pp 293-306.

Godunov,S.K.(1959),"A difference method for the numerical calculation of discontinuous solutions of hydrodynamic equations", Matematiceskij Sbornik 47, No.3,pp 271-306 (in Russian).

Hajdin,G.(1977), Fluid Mechanics, Gradjevinska Knjiga, Beograd (in Serbian).

Hendreson,F.M.(1966), Open Channel Flow, Macmillan Publishing, New York.

Hildebrand,F.B.(1956), Introduction to Numerical Analysis, Dover Publications, New York.

Holly,F.M.Jr. and Preissmann,A.(1977),"Accurate Calculation of Transport in Two Dimensions" Journal of the Hydraulic division, Vol.103, No. HY11, November, pp 1259-1277.

Houghton,D.D. and Kasahara,A.(1968),"Nonlinear shallow fluid flow over an isolated ridge", Communications on Pure and Applied Mathematics, Vol.21, No.1.

Katopodes,N.,Strelkoff,M.(1978),"Computing Two-Dimensional Dam-Break Flood Waves", Journal of the Hydraulic Division, Vol.104, No. HY9, September, pp 1269-1288.

Lax,P.D.(1954),"Weak solutions of non-linear hyperbolic equations and their numerical applications", Communications of Pure and Applied Mathematics, No 7,pp.159-193.

Lax,P.D. and Wendroff,B.(1960),"Systems of conservation laws", Communications on Pure and Applied Mathematics, Vol.13, pp 217-237.

Liggett,J.A.(1975),"Basic equations of unsteady flow", Chapter 2 of Unsteady Flow in Open Channels, Water Resources Publications, Fort Collins, Colorado.

Liggett,J.A. and Cunge,J.A.(1975),"Numerical methods of solution of the unsteady flow equations", Chapter 4 of Unsteady Flow in Open Channels, Water Resources Publications, Fort Collins, Colorado.

MacCormack,R.W.(1969),"The effect of viscosity in hyprvelocity impact cratering", AIAA Paper 69-354.

Miller,W.A. and Cunge,J.A. "Simplified Equations of Unsteady Flow", Chapter 5 of Unsteady Flow in Open Channels, Water Resources Publications, Fort Collins, Colorado.

Patankar,S.V.(1980), Numerical Heat Transfer and Fluid Flow, Hemisphere, Washington, D.C.

Peterka,A.J.(1964), Hydraulic Design of Stilling Basins and Energy Dissipators, U.S.Bureau of Reclamation

Radojkovic,M.(1980), Mathematical Model of Flow of Water in Open Channels, Phd thesis, University of Beograd, Beograd, in Serbian.

Richtmyer,R.D.(1962),"A Survey of Difference Methods for Non-Steady Fluid Dynamics", NCAR Technical Notes 63-2, National Centre for Atmospheric Research, Boulder, Colorado.

Richtmayer,R.D. and Morton,K.W.(1967), Difference Methods for Initial-Value Problem, Interscience Publishers, New York.

Roe,P.L.(1980),"The use of the Riemann problem in finite difference schemes", Proceedings of Seventh International Conference on Numerical Methods in Fluid Dynamics, Stanford, Lecture Notes in Physics No.141, pp 354-359.

Roe,P.L.(1981),"Approximate Riemann Solvers, Parameter Vectors, and Difference Schemes", Journal of Computational Physics, Vol.43, pp 357-372.

Savic,Lj.(1988), Some possibilities to improve the efficiency of numerical models for dambreak computations, Ms. thesis, University of Beograd, Beograd, in Serbian.

Savic,Lj. and Holly,F.M.Jr.(1991),"Computation of Open-channel Discontinuous Flows using the Modified Godunov Method", Limited Distribution Report No. 181, IIHR, The University of Iowa, February.

Schlichting,H.(1979), Boundary Layer Theory, McGraw-Hill, New York.

Stoker,J.J.(1957), Water Waves, Interscience, New York.

Strang,G.(1986), Introducition to Applied Mathematics, Wellesley-Cambridge Press.

Strelkoff,T.(1969),"One-Dimensional Equations of Open-Channel Flow", Journal of the Hydraulic Division, Vol.95, No. HY3, May, pp 861-876.

Strelkoff,T.(1989),"Dam-break flood waves", Megatrends in Hydraulic Engineering, Fort Collins, Colorado.

Strelkoff,T., Schamber,D. and Katopodes,N. (1977),"Comparative analysis of routing techniques for the flood wave from a ruptured dam", Proceedings of Dam-Break Flood Routing Model Workshop held in Bethesda, Maryland, October 18-20, U.S. Department of Commerce, National Technical Information Service PB-275 437.

Terzidis,G. and Strelkoff,T.(1970),"Computation of open channel surges and shocks", Journal of the Hydraulic Division, Vol.96, No. HY12, December, pp 2581-2610.

Thompson,J.F.,Warsi,Z.U.A. and Mastin,C.W.(1985), Numerical Grid Generation, North-Holland.

Toda,K. and Holly,F.M.Jr.(1988),"Hybrid Computation of Nonlinear Advection-Diffusion", Journal of Hydroscience and Hydraulic Engineering, Vol.6, No.1, July, pp 1-11.

Van-Leer,B.(1979),"Towards the Ultimate Conservative Difference Scheme. V. A Second Order Sequel to Godunov's Method", Journal of Computational Physics, Vol.32, pp 101-136.

Vasiliev,O.F.(1970),"Numerical Solution of the Non-Linear problems of Unsteady Flows in Open Channels", Proceedings of the 2-nd International Conference on Numerical Methods in Fluid Dynamics, Berceley 1970, pp 410-421.

Vila,J.P.(1986),"Simplified Godunov Schemes for 2x2 Systems of Conservation Laws", SIAM Journal of Numerical Analysis, Vol.23, No.6, December, pp 1173-1192.

Vila,J.P.(1987),"Schemas numeriques en hydraulique des ecoulemets avec discontinuites", IAHR XXnd Congress, Lausanne.

Warming,R.F. and Hyett,B.J.(1974),"The Modified Equation Approach to the Stability and Accuracy Analysis of Finite-Difference Methods", Journal of Computational Physics, Vol.14, pp 159-179.

White,F.M.(1974), Viscous Fluid Flow, McGraw-Hill, New York.

Whitham,G.B.(1955),"The effects of hydraulic resistance in the dam-break problem", Proceedings, Royal Society of London, Series A., Vol.227, pp 399-407.

Woodward,P.(1986),"Piecewise-Parabolic Methods for Astrophysical Fluid Dynamics", Astrophysical Radiation Hydrodynamics, edited by K.-H.A.Winkler, D.Radial Publishing Company, pp 245-326.

Woodward,P. and Colella,P.(1984),"Review Article: The Numerical Simulation of Two-Dimensional Fluid Flow with Strong Shocks", Journal of Computational Physics, Vol.14, pp 159-179.

Wurbs,R.A.(1987),"Dam-Breach Flood Wave Models", Journal of Hydraulic Engineering, Vol.113, No.1, January, pp 29-46.

Wylie,C.R.(1960), Advanced Engineering Mathematics, McGraw-Hill, New York.

APPENDIX A. PPM INTERPOLATION PROCEDURE

For the flux integration at the midpoints $X_{j+½}$ one needs a piecewise representation of the function $\psi[\rho(x, t^n)] \equiv \psi(x)$ on the interval $X_{j-½} < X < X_{j+½}$. The only information about the function $\psi(x)$ is its averaged value $\langle\psi\rangle_j^n \equiv \psi(\langle\rho\rangle_j^n)$ on the given interval (Fig.A.1). The procedure is based on the piecewise parabolic interpolation (PPM) developed by Woodward and Colella (1984). The aim is to obtain a representation of the function that will:

1. Satisfy the averaged values $\langle\psi\rangle_j^n$ over the interval,
2. Give a good representation of discontinuities,
3. Produce a monotonic function if the original function is monotonic (avoid all artificial overshoots and undershoots).

For approximation of the function $\psi(x)$ a second-order polynomial is used:

$$\text{(A.1):}\quad \psi[\rho(x, t^n)] \equiv \psi(x) \doteq ax^2 + bx + c$$

Coefficients a, b and c of the polynomial are

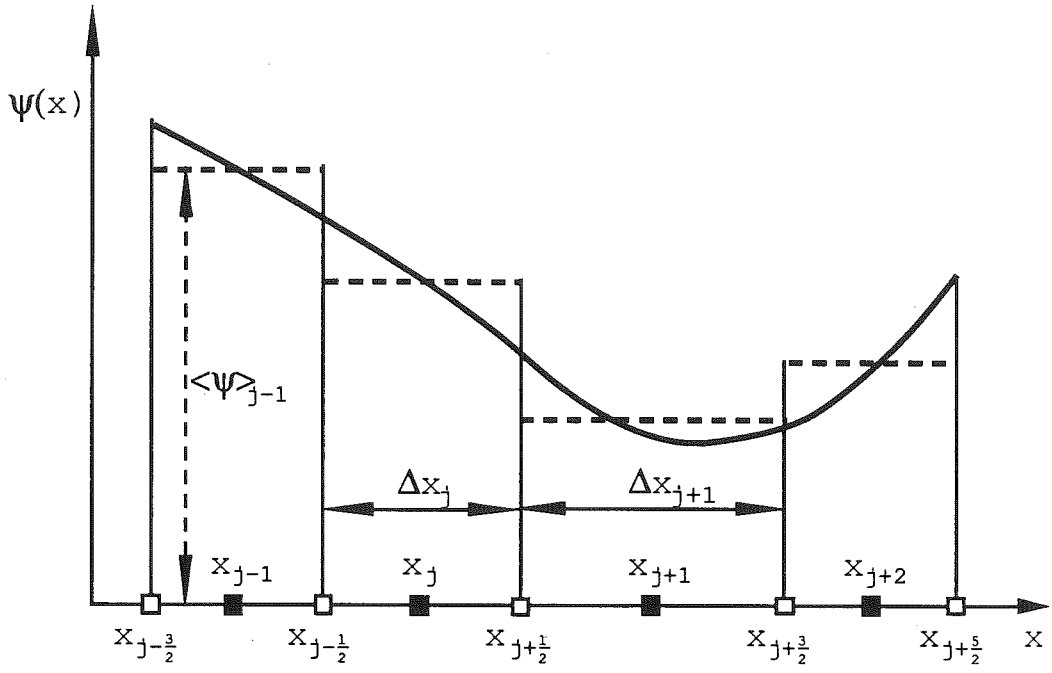

Figure A.1 Reconstructing a function from its averages

determined from the integral condition:

(A.2):

$$\psi(\langle\rho\rangle_j^n) \equiv \langle\psi\rangle_j^n \equiv \psi_j = \frac{1}{\Delta x_j}\int_{x_{j-\frac{1}{2}}}^{x_{j+\frac{1}{2}}} \psi(x)\,dx \doteq \frac{1}{\Delta x_j}\int_{x_{j-\frac{1}{2}}}^{x_{j+\frac{1}{2}}} (ax^2+bx+c)\,dx,$$

and from supposedly known values of $\psi(x)$ at both ends of the interval:

(A.3): $\psi[\rho(x_{j+\frac{1}{2}}, t^n)] \equiv \psi(x_{j+\frac{1}{2}}) \equiv \psi_{j+\frac{1}{2}} \equiv \psi_{R,j}$

(A.4): $\psi[\rho(x_{j-\frac{1}{2}}, t^n)] \equiv \psi(x_{j-\frac{1}{2}}) \equiv \psi_{j-\frac{1}{2}} \equiv \psi_{L,j}$

From the above conditions one obtains the desired polynomial representation:

(A.5): $$\psi(x) \doteq \psi_{L,j} + \frac{x-x_{j-\frac{1}{2}}}{\Delta x_j}\left[\Delta\psi_j + \psi_{6,j}\left(1-\frac{x-x_{j-\frac{1}{2}}}{\Delta x_j}\right)\right],$$

where:

(A.6): $\Delta\psi_j = \psi_{R,j} - \psi_{L,j}$, and,

$$(A.7): \quad \psi_{6,j} = 6\left[\psi_j - \frac{(\psi_{R,j} + \psi_{L,j})}{2}\right].$$

The next step is to obtain the end values $\psi_{L,j}$, and $\psi_{R,j}$. This is also accomplished using the averaged grid values $\langle\Psi\rangle_j^n$. The integral function A(x) is introduced, such that:

$$(A.8): \quad A(x) = \int_0^x \psi(x')\,dx'.$$

Keeping in mind that the reach-average is:

$$(A.9): \quad \langle\psi\rangle_j = \frac{1}{\Delta x_j}\int_{x_{j-½}}^{x_{j+½}} \psi(x')\,dx',$$

one can obtain exact values of the integral function A(x) at the midpoints Xj-½, Xj+½,... as:

(A.10): $A(x_{j+1/2}) = \int_0^{x_{j+1/2}} \psi(x')\,dx' = \sum_{i \le j} \langle\psi\rangle_i^n \Delta x_i$ see Fig.(A.1).

The point $X_{j+1/2}$, where $\psi_{j+1/2}=\psi_R$, is now considered. The integral function A(x) on the interval $X_{j-3/2} < X < X_{j+5/2}$, is approximated by a quartic interpolation polynomial passing through points j-3/2, j-1/2, j+1/2, j+3/2 and j+5/2:

(A.11): $A(x) \doteq a(x-x_{j+1/2})^4 + b(x-x_{j+1/2})^3 + c(x-x_{j+1/2})^2 + d(x-x_{j+1/2}) + e.$

Since A(x) is an integral of the function $\psi(x)$, the first derivative with respect to X, taken at the point $X_{j+1/2}$, of the polynomial Eq.(A.11), is the desired value $\psi(x_{j+1/2})$:

(A.12): $\left.\frac{dA}{dx}\right|_{x=x_{j+1/2}} = d = \psi^n(x_{j+1/2}) = \psi^n_{j+1/2} = \psi^n_R.$

Evaluation of all of the coefficients of the polynomial (A.11) is not necessary. It is enough to obtain the coefficient "d" ,i.e. the value of $\psi^n(x_{j+1/2})$. The resulting expression for $\psi^n(x_{j+1/2})$ is:

$$\psi^n_{R,j} = \psi^n(x_{j+\frac{1}{2}}) =$$

$$= \psi^n_j + \frac{\Delta x_j}{\Delta x_j + \Delta x_{j+1}} (\psi^n_{j+1} - \psi^n_j) + \frac{1}{\Delta x_{j-1} + \Delta x_j + \Delta x_{j+1} \Delta x_{j+2}}$$

(A.13): $$\left\{ \frac{2\,\Delta x_{j+1} \Delta x_j}{\Delta x_j + \Delta x_{j+1}} \left[\frac{\Delta x_{j-1} + \Delta x_j}{2\,\Delta x_j + \Delta x_{j-1}} - \frac{\Delta x_{j+2} + \Delta x_{j+1}}{2\,\Delta x_{j+1} + \Delta x_j} \right] (\psi^n_{j+1} - \psi^n_j) - \right.$$

$$\left. - \Delta x_j \frac{\Delta x_{j-1} + \Delta x_j}{2\,\Delta x_j + \Delta x_{j+1}} \delta\psi^n_{j+1} + \Delta x_{j+1} \frac{\Delta x_{j+1} + \Delta x_{j+2}}{\Delta x_j + 2\Delta x_{j+1}} \delta\psi^n_j \right\}$$

where the "flux gradient" $\delta\psi_j$ is defined as:

(A.14): $$\delta\psi^n_j = \frac{\Delta x_j}{\Delta x_{j-1} + \Delta x_j + \Delta x_{j+1}}$$

$$\left[\frac{2\Delta x_{j-1} + \Delta x_j}{\Delta x_{j+1} + \Delta x_j} (\psi^n_{j+1} - \psi^n_j) + \frac{\Delta x_j + 2\Delta x_{j+1}}{\Delta x_{j-1} + \Delta x_j} (\psi^n_j - \psi^n_{j-1}) \right].$$

For the case of a uniform grid the above expressions simplify to:

(A.13'): $$\psi^n_{j+\frac{1}{2}} = \psi^n_{R,j} = \frac{7}{12} (\psi^n_j + \psi^n_{j+1}) - \frac{1}{12} (\psi^n_{j-1} + \psi^n_{j+2}),$$

and:

(A.14'): $$\delta\psi^n_j = \frac{\psi^n_{j+1} - \psi^n_{j-1}}{2}.$$

In order to avoid artificial oscillations (especially in the vicinity of discontinuities), and to obtain a sharp representation of discontinuities, three procedures are incorporated into the interpolation algorithm.

First, to obtain monotonicity, values at the midpoints $\psi^n_{j+½}$ are not allowed to overshoot adjacent averaged-point values $\langle\psi\rangle^n_j$ and $\langle\psi\rangle^n_{j+1}$. This is provided by using a modified expression for $\delta\psi^n_j \equiv \delta\psi_j$, as follows:

$$(A.15): \qquad \delta_m\psi_j = \begin{cases} \min(|\delta\psi_j|, 2|\psi_{j+1}-\psi_j|, 2|\psi_j-\psi_{j-1}|) * \operatorname{sgn}\delta\psi_j, & \\ \qquad\qquad if\,(\psi_{j+1}-\psi_j)(\psi_j-\psi_{j-1}) > 0 & \\ 0 \qquad\qquad if\,(\psi_{j+1}-\psi_j)(\psi_j-\psi_{j-1}) \le 0 & \end{cases},$$

where the factor 2, multiplying the absolute values of $|\psi_{j+1}-\psi_j|$ and $|\psi_j-\psi_{j-1}|$, is adopted to ensure that the modification is made only when ψ_j (the value of ψ at the point X_j) is very close to either ψ_{j-1} or ψ_{j+1}.

In the vicinity of discontinuities the algorithm is modified to allow for the narrower profile of the discontinuity; procedures for both detecting and computing are needed.

A discontinuity is considered to be present in the zone

if:

1.The third derivative of the solution (Eqs.A.18 and A.19) is "sufficiently large";

2.The second derivative changes sign within the zone (the first condition in Eq.A.19);

3.The third and the first derivatives have opposite signs (Eq.A.19); and finally

4.The change within the reach is "significant" (second condition in Eq.19).

The values of ψ at the point of discontinuity (if any) are modified using the following procedure:

$$(A.16):\quad \psi^{d}_{L,j} = \psi_{L,j}(1-\eta_j) + \left[\psi_{j-1} + \frac{1}{2}\delta_m\psi_{j-1}\right]\eta_j,$$

$$(A.17):\quad \psi^{d}_{R,j} = \psi_{R,j}(1-\eta_j) + \left[\psi_{j+1} - \frac{1}{2}\delta_m\psi_{j+1}\right]\eta_j,$$

where $\psi^{d}_{L,j}$ and $\psi^{d}_{R,j}$ are the values modified due to the discontinuity, $\psi_{L,j}$ and $\psi_{R,j}$ are the values computed by Eq.(A.14), $\delta_m\psi_{j\pm1}$ is the difference operator obtained from Eq.(A.15), and η_j is a weighing factor depending on the intensity of the shock:

(A.18): $\eta_j = \mathrm{MAX}(0, , \min[\eta^1(\tilde{\eta}_j - \eta^2), 1])$.

If η_j is equal to zero, no modification is made. If η_j is equal to unity, the value of $\psi_{L,j}$ depends on the values left of the point X_j only, and $\psi^d_{R,j}$ depends on the values right of the point X_j only. Auxiliary variable $\tilde{\eta}_j$ is defined as:

$$(A.19): \quad \tilde{\eta}_j = -\left(\frac{\delta^2\psi_{j+1} - \delta^2\psi_{j-1}}{x_{j+1} - x_{j-1}}\right)\left[\frac{(x_j - x_{j-1})^3 + (x_{j+1} - x_j)^3}{\psi_{j+1} - \psi_{j-1}}\right],$$

$$\text{if} \quad \begin{cases} (-\delta^2\psi_{j+1})(\delta^2\psi_{j-1}) > 0 \quad \text{with,} \\ [|\psi_{j+1} - \psi_{j-1}| - \epsilon \min(|\psi_{j+1}|, |\psi_{j-1}|)] > 0 \end{cases},$$

otherwise $\tilde{\eta}_j = 0$;

and here:

$$(A.20): \quad \delta^2\psi_j = \frac{1}{\Delta x_{j-1} + \Delta x_j + \Delta x_{j+1}}\left[\frac{\psi_{j+1} - \psi_j}{\Delta x_{j+1} + \Delta x_j} - \frac{\psi_j - \psi_{j-1}}{\Delta x_j + \Delta x_{j-1}}\right].$$

Parameters η^1 and η^2 as well as ϵ are "empirical"

constants evaluating the conditions for the shock, and have to be determined for each case.

One more "device" is added to ensure monotonicity of the functions (especially in the neighborhood of discontinuities). If undershoots or overshoots due to the relative position of ψ_L^n, ψ_j^n and ψ_R^n occur, the following procedure is used to smooth them and render the function monotonic in the reach, Fig.(A.2):

1. If ψ_j^n is a local extremum i.e, if:

$$(A.21): \quad (\psi_{R,j}^n - \Psi_j^n)\cdot(\psi_j^n - \psi_1^n) \le 0, \quad \textit{then } \psi_{R,j}^n = \psi_{1,j}^n = \psi_j^n$$

2. If ψ_j^n is between $\psi_{1,j}^n$ and $\psi_{R,j}^n$, but so close to one of them that the interpolation parabola goes beyond the range of $\psi_{1,j}$ and $\psi_{R,j}$ (Fig.A2), then one of the limits (ψ_1^n, or ψ_R^n) is raised or lowered, so that the extremum can be transferred onto the opposite limit. This is mathematically expressed as:

$$(A.22): \quad \textit{If} \quad (\psi_{R,j}-\psi_{1,j})\left(\psi_j^n - \frac{\psi_{1,j}+\psi_{R,j}}{2}\right) > \frac{(\psi_{R,j}-\psi_{1,j})^2}{6}$$

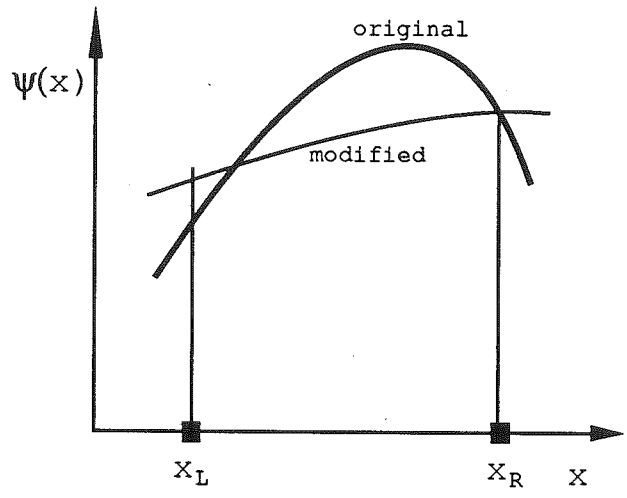

Figure A.2 Modifications due to overshooting

then:

$$\psi_{1,j} = 3\psi_j^n - 2\psi_{R,j} \quad , \text{ and:}$$

(A.23): *If* $$(\psi_{R,j}-\psi_{1,j})\left(\psi_j^n - \frac{\psi_{1,j}+\psi_{R,j}}{2}\right) < -\frac{(\psi_{R,j}-\psi_{1,j})^2}{6}$$

then:

$$\psi_{R,j} = 3\psi_j^n - 2\psi_{1,j}.$$

APPENDIX B. IMPLICIT SCHEME FOR LINEAR ADVECTION

The explicit Godunov scheme becomes unstable for values of the Courant number greater than unity (as is the case with most explicit schemes). To be able to compute for values of Courant number greater than unity, Fryxell et al. (1986) developed an implicit scheme.

In the implicit scheme an entirely different procedure for the approximation of the fluxes is applied, the only similarity with the explicit method being its reliance on the method of characteristics. However, here the characteristic is used to convey information from the grid-point section X_j at some (in general unknown) time to the midpoint section $X_{j+½}$ at time t^{n+1} (see Fig.B.1). Consequently, interpolation in time (not in space, as for the explicit scheme) is used for expressing the fluxes $\psi_{j\pm½}(t)$. To improve the performance of the solution (achieve unconditional stability and lessen numerical diffusion) an intermediate time level "n+½" is introduced, and accordingly another characteristic AB (Fig.B.1) issued from the midpoint level.

The procedure comprises the following steps:

1. Based on the integral conservation Eq. (3.5), the unknown concentrations $\langle\rho\rangle_j^{n+½}$ and $\langle\rho\rangle_j^{n+1}$, are

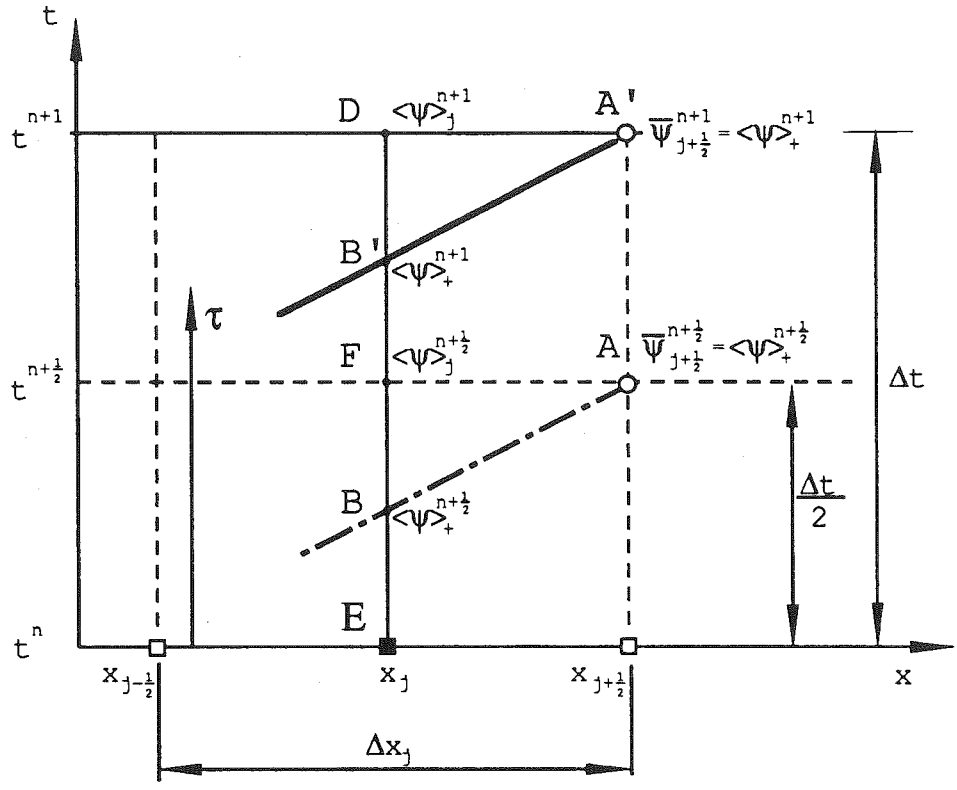

Figure B.1 Implicit Godunov scheme

expressed as functions of the fluxes $\overline{\Psi}_{j+\frac{1}{2}}^{n+\frac{1}{2}}$ and $\overline{\Psi}_{j+\frac{1}{2}}^{n+1}$;

2. To obtain expressions for fluxes $\overline{\Psi}_{j+\frac{1}{2}}^{n+\frac{1}{2}}$ and $\overline{\Psi}_{j+\frac{1}{2}}^{n+1}$ through the method of characteristics one first locates the feet of characteristics B and B'; and

3. Expresses the flux values ψ_B and $\psi_{B'}$ through the reach-averaged values of $\langle\psi\rangle_j^n, \langle\psi\rangle_j^{n+\frac{1}{2}}$ and $\langle\psi\rangle_j^{n+1}$ using parabolic interpolation between the points E, F and D Fig.(B.1); (Observe that $\langle\psi\rangle_j^{n+\frac{1}{2}}$ and $\langle\psi\rangle_j^{n+1}$ are the unknown values, and can be expressed as functions of the concentrations $\langle\rho\rangle_j^n, \langle\rho\rangle_j^{n+\frac{1}{2}}$ and $\langle\rho\rangle_j^{n+1}$. Note also that here $\overline{\psi}$ denotes an approximated, not time-averaged, value of the fluxes.)

4. The resulting system of algebraic equations (linear for the case $\psi=u\rho$) is finally solved for the unknown variables $\langle\rho\rangle_j^{n+\frac{1}{2}}$ and $\langle\rho\rangle_j^{n+1}$.

In the first step the conservation Eq. (3.5) is formally manipulated. The limits of the time integration are changed, so that the upper limit becomes a variable "t":

$$\text{(B.1):} \qquad \langle\rho\rangle_j^{n+1}(t) = \langle\rho\rangle_j^n - \frac{1}{\Delta x_j}\int_0^t [\psi_{j+\frac{1}{2}}(\tau) - \psi_{j-\frac{1}{2}}(\tau)]\, d\tau .$$

To get continuous values of the integrand $\Psi_{j+\frac{1}{2}}(\tau)$ linear interpolation between fluxes $\overline{\Psi}^{n+\frac{1}{2}}_{j+\frac{1}{2}}$ and $\overline{\Psi}^{n+1}_{j+\frac{1}{2}}$ is used, which results in:

(B.2): $$\Psi_{j+\frac{1}{2}}(\tau) = (2\overline{\Psi}^{n+\frac{1}{2}}_{j+\frac{1}{2}} - \overline{\Psi}^{n+\frac{1}{2}}_{j-\frac{1}{2}}) + \frac{2\tau}{\Delta t}(\overline{\Psi}^{n+1}_{j+\frac{1}{2}} - \overline{\Psi}^{n+\frac{1}{2}}_{j-\frac{1}{2}}).$$

The interpolation formula Eq.(B.2) is then substituted into Eq.(b.1), which is then integrated for the values of the upper limit $t=\Delta t$, and $t=\frac{1}{2}\Delta t$, respectively to yield:

(B.3): $$\langle\rho\rangle^{n+1}_j = \langle\rho\rangle^n_j - \frac{1}{\Delta x_j}[\Psi^{n+\frac{1}{2}}_{j+\frac{1}{2}} - \overline{\Psi}^{n+\frac{1}{2}}_{j-\frac{1}{2}}],$$ for $t=\Delta t$ and:

(B.4): $$\langle\rho\rangle^{n+\frac{1}{2}}_j = \langle\rho\rangle^n_j - \frac{1}{\Delta x_j}\left[\frac{3}{4}(\Psi^{n+\frac{1}{2}}_{j+\frac{1}{2}} - \overline{\Psi}^{n+\frac{1}{2}}_{j-\frac{1}{2}}) - \frac{1}{4}(\overline{\Psi}^{n+1}_{j+\frac{1}{2}} - \overline{\Psi}^{n+1}_{j+\frac{1}{2}})\right],$$

for $t=\frac{1}{2}\Delta t$

The next stage is to express the flux functions $\overline{\Psi}^{n+\frac{1}{2}}_{j+\frac{1}{2}}$ and $\overline{\Psi}^{n+1}_{j+\frac{1}{2}}$ in terms of the grid-averaged functions

($\langle\psi\rangle_j^n$, $\langle\psi\rangle_j^{n+½}$ and $\langle\psi\rangle_j^{n+1}$) at the point X_j along the line ED Fig.(B.1). The method of characteristics is used to transfer information from the line ED to line AA'. The "feet" of the characteristics B and B' must be first obtained. The path integration is approximated as:

(B.5): $$x_{j+½}-x_j = \langle u^*\rangle_+^{n+1}(\Delta t-\tau_{B'}),$$

which gives the desired "time-foot" $\tau B'$:

(B.6): $$\tau_{B'} = \Delta t - \frac{x_{j+½}-x_j}{\langle u^*\rangle_+^{n+1}} = \Delta t\left(1-\frac{1}{2\sigma_s}\right),$$

where:

(B.7): $$\langle u^*\rangle_+^{n+1} \doteq \frac{1}{3}\left(u_j^{n+½}+u_j^{n+1}+u_{j+½}^{n+½}\right),$$

and σs is a "superior" Courant number:

(B.8): $$\sigma_s = \Delta\frac{t}{x_{j+½}-x_j}\langle u^*\rangle_+^{n+1}.$$

Similarly for the point B one has:

$$(B.6'): \qquad \tau_{B'} = \frac{\Delta t}{2}\left(1-\frac{1}{\sigma_i}\right),$$

$$(B.7'): \qquad \langle u^* \rangle_+^{n+1/2} \doteq \frac{1}{3}\left(u_j^n + u_j^{n+1/2} + u_{j+1/2}^{n+1/2}\right),$$

$$(B.8'): \qquad \sigma_i = \Delta \frac{t}{x_{j+1/2} - x_j} \langle u^* \rangle_+^{n+1/2}.$$

Once the feet of the characteristics are determined, the values of $\langle \psi \rangle_+^{n+1}$ and $\langle \psi \rangle_+^{n+1/2}$ at the times $\tau_{B'}$ and τ_B are expressed in terms of the grid-averaged functions $\langle \psi \rangle_j^n$, $\langle \psi \rangle_j^{n+1/2}$ and $\langle \psi \rangle_j^{n+1}$, using a parabolic interpolation polynomial through the points E,B and D Fig.(B.1):

$$(B.9): \qquad \langle \psi \rangle_j(\tau) = \frac{2\left(\langle \psi \rangle_D - 2\langle \psi \rangle_F + \langle \psi \rangle_E\right)}{\Delta t^2}\tau^2 +$$

$$+ \frac{4\langle \psi \rangle_F - \langle \psi \rangle_D - 3\langle \psi \rangle_E}{\Delta t}\tau + \langle \psi \rangle_E.$$

The desired relations for the flux functions $\overline{\Psi}_{j+1/2}^{n+1/2}$ and $\overline{\Psi}_{j+1/2}^{n+1}$ are obtained by substituting expressions Eqs.(B.6) and (B.6') for $\tau_{B'}$ and τ_B into interpolation formula Eq(B.9):

$$(B.10):\quad \overline{\Psi}_{j+1/2}^{n+1}=\langle\psi\rangle_{+}^{n+1}=\frac{1-\sigma_s}{2\sigma_s^2}\langle\psi\rangle_j^n+\frac{2\sigma_s-1}{\sigma_s^2}\langle\psi\rangle_j^{n+1/2}+\frac{2\sigma_s^2-3\sigma_s+1}{2\sigma_s^2}\langle\psi\rangle_j^{n+1},$$

$$(B.11):\quad \overline{\Psi}_{j+1/2}^{n+1/2}=\langle\psi\rangle_{+}^{n+1/2}=\frac{1+\sigma_i}{2\sigma_i^2}\langle\psi\rangle_j^n+\frac{\sigma_i^2-1}{\sigma_i^2}\langle\psi\rangle_j^{n+1/2}+\frac{1-\sigma_i}{2\sigma_i^2}\langle\psi\rangle_j^{n+1}.$$

It remains to substitute expressions for fluxes Eqs.(B.10) and (B.11) into the relations for the concentrations Eqs.(B.3) and (B.4). In the case of uniform flow, the substitution $\psi=u\rho$ results in a system of two linear equations in two unknowns $\langle\rho\rangle_j^{n+1/2}$, and $\langle\rho\rangle_j^{n+1}$ (since the values from the previous spatial step "j-1" are known), which is solved for each spatial step:

$$(B.12):\quad \langle\rho\rangle_j^{n+1}-\langle\rho\rangle_j^{n}+\frac{\Delta t}{\Delta x_j}\left[u_j^{n}\left(\frac{1+\sigma_i}{2\sigma_i^2}\right)_j\langle\rho\rangle_j^{n}-u_{j-1}^{n}\left(\frac{1+\sigma_i}{2\sigma_i^2}\right)_{j-1}\langle\rho\rangle_{j-1}^{n}\right]+$$

$$+\frac{\Delta t}{\Delta x_j}\left[u_j^{n+1/2}\left(\frac{\sigma_i^2-1}{\sigma_i^2}\right)_j\langle\rho\rangle_j^{n+1/2}-u_{j-1}^{n+1/2}\left(\frac{\sigma_i^2-1}{\sigma_i^2}\right)_{j-1}\langle\rho\rangle_{j-1}^{n+1/2}\right]+$$

$$+\frac{\Delta t}{\Delta x_j}\left[u_j^{n+1}\left(\frac{1-\sigma_i}{2\sigma_i^2}\right)_j\langle\rho\rangle_j^{n+1}-u_{j-1}^{n+1}\left(\frac{1-\sigma_i}{2\sigma_i^2}\right)_{j-1}\langle\rho\rangle_{j-1}^{n+1}\right]=0,$$

$$(B.13):\quad \langle\rho\rangle_j^{n+1/2}+\frac{3}{4}\frac{\Delta t}{\Delta x_j}\left\{\left[u_j^{n+1/2}\left(\frac{\sigma_i^2-1}{\sigma_i^2}\right)_j\langle\rho\rangle_j^{n+1/2}-u_{j-1}^{n+1/2}\left(\frac{\sigma_i^2-1}{\sigma_i^2}\right)_{j-1}\langle\rho\rangle_{j-1}^{n+1/2}\right]+\right.$$

$$\left.+\left[u_j^{n+1}\left(\frac{1-\sigma_i}{2\sigma_i^2}\right)_j\langle\rho\rangle_j^{n+1}-u_{j-1}^{n+1}\left(\frac{1-\sigma_i}{2\sigma_i^2}\right)_{j-1}\langle\rho\rangle_{j-1}^{n+1}\right]\right\}-$$

$$-\frac{1}{4}\frac{\Delta t}{\Delta x_j}\left\{\left[u_j^{n+1/2}\left(\frac{2\sigma_s-1}{\sigma_s^2}\right)_j\langle\rho\rangle_j^{n+1/2}-u_{j-1}^{n+1/2}\left(\frac{2\sigma_s-1}{\sigma_s^2}\right)_{j-1}\langle\rho\rangle_{j-1}^{n+1/2}\right]+\right.$$

$$\left.+\left[u_j^{n+1}\left(\frac{2\sigma_s^2-3\sigma_s+1}{2\sigma_s^2}\right)_j\langle\rho\rangle_j^{n+1}-u_{j-1}^{n+1}\left(\frac{2\sigma_s^2-3\sigma_s+1}{2\sigma_s^2}\right)_{j-1}\langle\rho\rangle_{j-1}^{n+1}\right]\right\}=$$

$$=\left\{1+\frac{\Delta t}{\Delta x_j}u_j^{n}\left[-\frac{3}{4}\left(\frac{1+\sigma_i}{2\sigma_i^2}\right)_j+\frac{1}{4}\left(\frac{1-\sigma_s}{2\sigma_s^2}\right)_j\right]\right\}\langle\rho\rangle_j^{n}+$$

$$+\frac{\Delta t}{\Delta x_j}u_{j-1}^{n}\left[\frac{3}{4}\left(\frac{1+\sigma_i}{2\sigma_i^2}\right)_{j-1}-\frac{1}{4}\left(\frac{1-\sigma_s}{2\sigma_s^2}\right)_{j-1}\right]\langle\rho\rangle_{j-1}^{n}.$$

Stability analysis for the implicit scheme, performed by Fryxell et al (1986), shows that the implicit method is unconditionally stable for Courant numbers greater than unity, while it is unstable for values of the Courant number less than one (in which case the explicit scheme must be used).

APPENDIX C. NEWTON-RAPHSON PROCEDURE FOR THE METHOD OF CHARACTERISTICS

The Newton-Raphson method is used to compute the velocity u_A and depth h_A from the nonlinear compatibility equations:

$$(C.1): \quad u_A+2c_A = u_L+2c_L+g\frac{\Delta t}{2}\left[\left(S_{oL}-n^2\frac{u_L|u_L|}{R_L^{4/3}}\right)+\left(S_{oL}-n^2\frac{u_A|u_A|}{R_A^{4/3}}\right)\right]-$$

$$-\frac{\Delta t}{2}\left[\frac{u_Lc_L}{B_L}\left(\frac{\partial B}{\partial x}\right)_L+\frac{u_Ac_A}{B_A}\left(\frac{\partial B}{\partial x}\right)_L\right],$$

and:

$$(C.2): \quad u_A-2c_A = u_R-2c_R+g\frac{\Delta t}{2}\left[\left(S_{oR}-n^2\frac{u_R|u_R|}{R_R^{4/3}}\right)+\left(S_{oR}-n^2\frac{u_A|u_A|}{R_A^{4/3}}\right)\right]+$$

$$+\frac{\Delta t}{2}\left[\frac{u_Rc_R}{B_R}\left(\frac{\partial B}{\partial x}\right)_R+\frac{u_Ac_A}{B_A}\left(\frac{\partial B}{\partial x}\right)_R\right]..$$

The Newton-Raphson method (see Carnahan et al.,1969, or Hildebrand,1956) is based on the Taylor-series expansion of a function at the m+1-st iteration around its previous ,i.e. m-th, iteration. To this end the system of compatibility Eqs. (C.1 and C.2) is rewritten as:

$$(C.3): \quad F_1(u_A, h_A) = u_A + 2c_A - u_L - 2c_L - g\frac{\Delta t}{2}\left[\left(S_{oL} - n^2\frac{u_L|u_L|}{R_L^{4/3}}\right) + \left(S_{oL} - n^2\frac{u_A|u_A|}{R_A^{4/3}}\right)\right] + \frac{\Delta t}{2}\left[\frac{u_L c_L}{B_L}\left(\frac{\partial B}{\partial x}\right)_L + \frac{u_A c_A}{B_A}\left(\frac{\partial B}{\partial x}\right)_L\right] = 0,$$

and:

$$(C.4): \quad F_2(u_A, h_A) = u_A - 2c_A - u_R + 2c_R - g\frac{\Delta t}{2}\left[\left(S_{oR} - n^2\frac{u_R|u_R|}{R_R^{4/3}}\right) + \left(S_{oR} - n^2\frac{u_A|u_A|}{R_A^{4/3}}\right)\right] - \frac{\Delta t}{2}\left[\frac{u_R c_R}{B_R}\left(\frac{\partial B}{\partial x}\right)_R + \frac{u_A c_A}{B_A}\left(\frac{\partial B}{\partial x}\right)_R\right] = 0.$$

The functions F_1 and F_2 at the m+1-st iteration level are now expanded in a Taylor series of first-order around the previous iteration level (m):

$$(C.5): \quad F_1^{(m+1)} = F_1^{(m)} + \left.\frac{\partial F_1}{\partial u_A}\right|_m \Delta u_A + \left.\frac{\partial F_1}{\partial h_A}\right|_m \Delta h_A = 0,$$

and:

$$(C.6): \quad F_2^{(m+1)} = F_2^{(m)} + \left.\frac{\partial F_2}{\partial u_A}\right|_m \Delta u_A + \left.\frac{\partial F_2}{\partial h_A}\right|_m \Delta h_A = 0.$$

where $\partial F_1/\partial u_A|_m$ and $\partial F_1/\partial h_A|_m$ are the partial derivatives evaluated at the "known" m-th iteration, and Δh_A and Δu_A are incremental corrections of the variables u_A and h_A :

(C.7): $\Delta h_A = h_A^{(m+1)} - h_A^{(m)}$ and $\Delta u_A = u_A^{(m+1)} - u_A^{(m)}$.

After the notation is introduced:

(C.8):
$$\begin{cases} A = \left.\dfrac{\partial F_1}{\partial u_A}\right|_m, \quad B = \left.\dfrac{\partial F_1}{\partial h_A}\right|_m, \quad G = -F_1^{(m)}, \\ A' = \left.\dfrac{\partial F_2}{\partial u_A}\right|_m, \quad B' = \left.\dfrac{\partial F_2}{\partial h_A}\right|_m, \quad G' = -F_2^{(m)}, \end{cases}$$

the linear system of Eqs.(C.5 and C.6) is solved for the corrections Δh_A and Δu_A:

(C.9):
$$\Delta u_A = \frac{GB' - G'B}{AB' - A'B},$$
$$\Delta h_A = \frac{G'A - GA'}{AB' - A'B},$$

from which the values for the new iteration are obtained.

For the initial, zero-th, iteration the first-order approximation (integration) of the compatibility conditions is used:

$$(C.10): \qquad u_A+2c_A = u_L+2c_L+g\Delta t\left(S_{oL}-n^2\frac{u_L|u_L|}{R_L^{4/3}}\right)-\Delta t\frac{u_Lc_L}{B_L}\left(\frac{\partial B}{\partial x}\right)_L,$$

$$(C.11): \qquad u_A-2c_A = u_R-2c_R+g\Delta t\left(S_{oR}-n^2\frac{u_R|u_R|}{R_R^{4/3}}\right)+\Delta t\frac{u_Rc_R}{B_R}\left(\frac{\partial B}{\partial x}\right)_R,$$

whereupon the initial iterations $u_A^{(0)}$ and $h_A^{(0)}$ can be easily obtained.

It remains, now, to obtain the expressions for the partial derivatives of Eq.(C.8) for use in the Newton-Raphson iterations:

$$(C.12): \qquad A = \frac{\partial F_1}{\partial u_A} = 1+g\Delta t\frac{n^2|u_A|}{R_A^{4/3}}+\frac{\Delta t}{2}\frac{c_A}{B_A}\left(\frac{\partial B}{\partial x}\right)_1,$$

(C.13): $$B = \frac{\partial F_1}{\partial h_A} = \left[1 + \frac{\Delta t}{4}\frac{u_A}{B_A}\left(\frac{\partial B}{\partial x}\right)_L\right]\sqrt{\frac{g}{h_A}} - \frac{2}{3}9\Delta t\frac{n^2 u_A|u_A|}{R_A^{1/3}h_A^2},$$

(C.14): $$A' = \frac{\partial F_2}{\partial u_A} = 1 + g\Delta t\frac{n^2|u_A|}{R_A^{4/3}} - \frac{\Delta t}{2}\frac{c_A}{B_A}\left(\frac{\partial B}{\partial x}\right)_I,$$

(C.15): $$B' = \frac{\partial F_2}{\partial h_A} = -\left[1 + \frac{\Delta t}{4}\frac{u_A}{B_A}\left(\frac{\partial B}{\partial x}\right)_R\right]\sqrt{\frac{g}{h_A}} - \frac{2}{3}9\Delta t\frac{n^2 u_A|u_A|}{R_A^{1/3}h_A^2}.$$